

Copyright is owned by the Author of the thesis. Permission is given for a copy to be downloaded by an individual for the purpose of research and private study only. The thesis may not be reproduced elsewhere without the permission of the Author.

Travelling Wave Solutions of Multisymplectic Discretisations of Wave Equations

A thesis presented in partial fulfillment of the requirements for the degree of

Doctor of Philosophy

in

Mathematics

at Massey University, Manawatu,
New Zealand.

Fleur Cordelia McDonald

2013

Abstract

Symplectic integrators for Hamiltonian ODEs have been well studied over the years and a lot is known about these integrators. They preserve the symplecticity of the system which automatically ensures the preservation of other geometric properties of the system, such as a nearby Hamiltonian and periodic and quasiperiodic orbits.

It is then natural to ask how this situation generalises to Hamiltonian PDEs, which leads us to the concept of multisymplectic integration. In this thesis we study the question of how well multisymplectic integrators capture the long-time dynamics of multi-Hamiltonian PDEs. We approach this question in two ways—numerically and through backward error analysis (BEA). As multi-Hamiltonian PDEs possess travelling wave solutions, we wish to see how well multisymplectic integrators preserve these types of solutions.

We mainly use the leapfrog method applied to the nonlinear wave equation as our test problem and look for the preservation of periodic travelling waves. We call the resulting equation the *discrete travelling wave equation*. It cannot be solved exactly. Therefore, our analysis begins with numerically solving the discrete travelling wave equation for simplified nonlinearities.

Next, we move on to analysing periodic solution for a smooth nonlinearity. This results in the presence of resonances in the solutions for certain combinations of the parameters. Finally, we use backward error analysis to compare and back up our results from numerical analysis.

Acknowledgements

My biggest thanks goes to my supervisor Professor Robert McLachlan. Thank you for taking me on for the past few years and giving me the chance to learn something new. You have been great at steering me in the right direction throughout my research. Thanks for your enthusiasm and perseverance with me. Not only have you helped me with my research but you have helped me grow in other ways by encouraging me to attend many conferences and workshops within and outside of New Zealand. I would not have gone to any of these without your encouragement, but I am very glad that I did. They gave me confidence in presenting, the chance to work with others, and the opportunity to meet many people within the mathematical community. I appreciate all the opportunities you have given to me.

Thanks also to the Marsden Fund of the Royal Society of New Zealand for funding my PhD. I would have not been able to continue my studies without this funding.

I largely have Associate Professor Brian Moore to thank for the topic of my research. Brian came to visit Massey University in early 2010 from Florida. He was working on travelling waves and while he was here we looked at travelling waves for a semi-discrete semi-linear wave equation using the McKean caricature. We moved on to looking at the fully discrete system with Brian and when he left Robert and I continued on with our study of discrete travelling waves by varying the nonlinearity. Thanks Brian more for giving us the idea for such an interesting topic.

Next, I would like to thank Professor Reinout Quispel. It has been good to meet you at various conferences in New Zealand and Australia throughout the years. You always seemed quite interested in our research and were very happy to give your ideas on these. I remember you visiting Massey University soon after Robert found our equation was like a multistep method. It was then that you gave us the idea of applying backward error analysis (BEA) to our equation. I am very grateful for your input over the last few years.

Next, I would like to thank my two co-supervisors, Associate Professor

Matt Perlmutter and Associate Professor Bruce van Brunt. Thanks Matt for being my co-supervisor for the first part of my PhD until you had to move overseas. I know we did not get a chance to talk much while you were my co-supervisor, but thanks for the discussions we had when we met again at a conference down south and then back in Palmerston North. I enjoyed getting to know you during this time. Thank you Bruce for being my co-supervisor throughout the remainder of my studies. You are always very approachable and happy to discuss anything with me.

Next, I would like to thank Professor Brynjulf Owren, Professor Elena Celledoni and their students. It was so good to meet you all and spend time with you when you all came to New Zealand in 2012. Thank you all for all the research discussions and social catch-ups we had.

Finally, I would you like to thank my family, close friends, and my treasured animal friends Coco, Tammy, Tortie, Stripes, Muzbie, Toby, Jake, Ferghus and Flynn, for always supporting me and bringing happiness to my life throughout my many years of university study.

Contents

1	Geometric Integration of Ordinary Differential Equations	1
1.1	Introduction to Ordinary Differential Equations (ODEs)	1
1.1.1	Flow Map	3
1.2	Numerical Solutions of ODEs	4
1.2.1	Errors in Numerical Methods	5
1.2.2	Other One-Step Methods	7
1.2.3	Runge–Kutta Methods	7
1.2.4	Errors for Runge–Kutta Methods	9
1.2.5	Splitting and Composition Methods	17
1.3	Hamiltonian Systems	18
1.3.1	N -Body Newtonian Gravitational Problem	19
1.3.2	Molecular Dynamics	19
1.3.3	Poisson Systems	21
1.4	Symplecticity	22
1.5	Conserved Quantities	27
1.6	Symmetries	28
1.7	Reversible Differential Equations	30
1.8	Geometric Integrators	31
1.8.1	Symplectic Integrators	32
1.8.2	Preserving First Integrals	37
1.8.3	Symmetric and Time-Reversible Integrators	38
1.9	N -Body Simulations Using a Symplectic Integrator	40

1.9.1	The Leapfrog Method Applied to the Lennard–Jones Potential	40
1.9.2	The Outer Solar System	44
1.10	Conservation Laws	47
1.11	Backward Error Analysis (BEA)	48
1.11.1	Introduction	49
1.11.2	The Modified Differential Equation (MDE)	51
1.11.3	Geometric Properties and the Modified Differential Equation	54
1.11.4	Long-Time Energy Conservation	58
2	Multisymplectic Integration of Partial Differential Equations	59
2.1	Introduction to Partial Differential Equations (PDEs)	59
2.2	Hamiltonian PDEs	60
2.3	Multi-Hamiltonian PDEs	62
2.3.1	Conservation Laws	64
2.4	Solving PDEs Numerically	67
2.5	Multisymplectic Integrators	69
2.5.1	The Preissman Box Scheme	73
2.6	Constructions of Multisymplectic integrators	75
2.6.1	Discrete Lagrangian Approach	76
2.6.2	Gaussian Runge–Kutta Methods	76
2.6.3	Partitioned Runge–Kutta methods	77
2.7	Behaviour of Multisymplectic Integrators	79
2.7.1	The Dispersion Relation	79
2.7.2	Numerical Experiments	80
2.8	Case Study: Numerical Solution of Burgers’ Equation	82
2.8.1	Burgers’ Equation	82
2.8.2	A Multisymplectic Scheme for Burgers’ Equation	83
2.8.3	Solutions to the 8-Point Burgers’ Scheme (2.26)	86

3	Introduction to Travelling Waves	89
3.1	Travelling Waves	89
3.1.1	Travelling Wave Solutions for the Multi-Hamiltonian Formulation	95
3.1.2	Travelling Wave Solutions for the Nonlinear Wave Equation	96
3.2	Travelling Wave Solutions in the Literature	98
3.2.1	Lattice Dynamical Systems (LDSs)	98
3.2.2	Coupled Map Lattices (CMLs)	105
4	Travelling Wave Solutions for Multisymplectic Discretisations of Wave Equations with Simplified Nonlinearities	107
4.1	A Multisymplectic Discretisation of the Nonlinear Wave Equation (3.4)	108
4.1.1	The Discrete Travelling Wave Equation	108
4.2	Discrete Travelling Wave Equation with McKean Nonlinearity .	111
4.2.1	The Continuous Case	112
4.2.2	Symmetric PDEs and Symmetric Methods: An Example	119
4.2.3	The Semi-Discrete Case	122
4.2.4	The Discrete Case	124
4.2.5	Summary of Results	128
4.2.6	Periodic Travelling Wave Solutions	130
4.3	Discrete Travelling Wave Equation with Sawtooth Nonlinearity .	135
4.3.1	Analytic Solution	137
4.3.2	Discrete Solution	142
5	Numerical Solution of the Discrete Travelling Wave Equation with Smooth Nonlinearity	147
5.1	The sine-Gordon equation	148
5.2	Numerical Method for Periodic Travelling Wave Solutions	149
5.2.1	Checking our Numerical Solution	153
5.3	Resonance	155

5.4	Resonances in the Discrete Travelling Wave Equation	156
5.4.1	Initial Results	157
5.4.2	Measuring the Size of the Resonances	160
5.4.3	Resonance Results	161
6	Backward Error Analysis of the Discrete Travelling Wave Equation	171
6.1	Multistep Methods	171
6.1.1	Linear Multistep Methods for First Order Systems	172
6.1.2	Example of the Behaviour of Multistep methods	174
6.2	Multistep Methods for Second Order Equations	177
6.3	The Underlying One-Step Method	181
6.3.1	Non-Symplecticity of the Underlying One-Step Method	184
6.4	Backward Error Analysis for Multistep Methods for Second Order Differential Equations	185
6.4.1	The (Principal) Modified Equation	185
6.4.2	The Parasitic Modified Equation	188
6.4.3	Conservation Properties from the Underlying One-Step Method	190
6.5	The Discrete Travelling Wave Equation as a Multistep Method .	191
6.6	Backward Error Analysis of the Discrete Travelling Wave Equation	198
6.6.1	Numerical Validation of the BEA	202
6.6.2	The Modified Hamiltonian of the Discrete Travelling Wave Equation	208
6.7	Backward Error Analysis for Multisymplectic Integrations of Multi-Hamiltonian PDEs	214
7	Summary and Conclusions	227

List of Figures

1.1	First step in the formation of the rooted tree for the elementary differential $f'f''(f, f)$	11
1.2	Second step in the formation of the rooted tree for the elementary differential $f'f''(f, f)$	11
1.3	Final step in the formation of the rooted tree for the elementary differential $f'f''(f, f)$	12
1.4	Illustration of lower and upper vertices in a rooted tree.	12
1.5	Illustration showing the leaves of rooted trees.	13
1.6	Labeling of a rooted tree τ for the related polynomial $\phi(\tau)$	13
1.7	Labeling of a rooted tree τ for the related polynomial $\phi(\tau)$, with factors assigned to each label.	14
1.8	Labeling of a rooted tree τ for the related polynomial $\phi(\tau)$, with factors assigned to each label and leaf.	14
1.9	Labeling of the leaves of a rooted tree τ for the related polynomial $\gamma(\tau)$	15
1.10	Labeling of the leaves and other vertices of a rooted tree τ for the related polynomial $\gamma(\tau)$	16
1.11	Flow of a Hamiltonian system, (the Pendulum), showing preservation of areas. This figure is reproduced from [53].	25
1.12	The 2-form ω for $d = 1$	26

1.13	Exact solution of the harmonic oscillator (left), compared with two numerical solutions, the Euler method - solution spirals out clockwise from the centre (middle) and a symplectic integrator (right).	34
1.14	Energy error of the Euler method (left) and a symplectic integrator (right) when applied to the harmonic oscillator.	35
1.15	The attractive and repulsive forces of the Lennard–Jones potential.	41
1.16	Results of the simulation: Snapshots of the dynamics of the two-dimensional Lennard–Jones system.	43
1.17	Energy error of the two-dimensional Lennard–Jones system. . .	44
1.18	The initial position of the outer planets relative to the sun. . .	45
1.19	Orbits of the outer solar system.	46
1.20	The energy error of the outer solar system after 10000 time steps.	46
1.21	The energy error of the outer solar system after 1000000 time steps.	47
1.22	The MDE as the exact solution of a perturbed problem. This diagram is reproduced from [37].	50
1.23	Comparison of truncated solutions of the modified differential equation (1.34) and the numerical solution from Euler’s method (red) of the equation $\dot{y} = y^2$, $y(0) = 1$. The blue curve gives the truncation after the 1st term (or the exact solution), the green curve the truncation after the 2nd term, and the yellow curve the truncation after the 3rd term.	55
1.24	Solution of the pendulum and its modified Hamiltonian for the symplectic Euler method.	57
2.1	Snapshots in time of the leapfrog method applied to the semi-discretisation of the sine-Gordon equation.	70
2.2	Energy error for 50000 time steps of the leapfrog method applied to the sine-Gordon equation.	70

2.3	Uniform grid for multisymplectic discretisations.	71
2.4	The dispersion relation of the linearised wave equation.	80
2.5	Solution to Burgers' equation at different points in time for $\nu = 1$, $\Delta x = 0.01$, and $\Delta t = 0.005$	86
2.6	Solution to Burgers' equation at time $t = 0.3$ for $\nu = 0.0001$, $\Delta x = 0.01$, and $\Delta t = 0.0001$	87
3.1	Solitary wave corresponding to a homoclinic orbit.	90
3.2	Solitary waves corresponding to heteroclinic orbits.	91
3.3	A homoclinic orbit.	92
3.4	A heteroclinic orbit	92
3.5	FitzHugh-Nagumo travelling wave solutions reproduced from [48].	93
3.6	Combustion travelling wave solutions.	93
3.7	Periodic travelling wave.	94
3.8	Periodic orbit.	94
3.9	Phase portrait of the travelling wave equation of the sine-Gordon equation.	97
3.10	Propagation failure for different values of parameters: a versus c for different values of σ , where $a \in (0, 1)$ and c is the wave speed. This figure is reproduced from [25].	102
3.11	Left: A single pulse solution. Right: Zoom on the oscillatory tail from the solution on the left. This figure is reproduced from [49].	104
4.1	The five-point stenci used in the leapfrog method.	108
4.2	Grid points of the discrete travelling wave equation (4.4) with spacing κ (red) and σ (blue).	110
4.3	McKean nonlinearity: $V'(u) = u - h(u - a)$	112
4.4	Phase portrait of the travelling wave equation of the nonlinear wave equation with McKean nonlinearity.	113

4.5	Expected travelling wave solution of the nonlinear wave equation with McKean nonlinearity.	114
4.6	The singularities of equation (4.18).	117
4.7	Contour in the upper half plane.	118
4.8	Travelling wave solution (4.19) of (4.6) with $c = 0.1$ and $\xi^* = 0$	119
4.9	The phase portrait of the symmetric PDE (4.20).	120
4.10	Exact solution of the symmetric PDE (4.20).	121
4.11	Numerical solution of the symmetric PDE (4.20) with a symmetric method.	121
4.12	The zeros of $R_{\text{Semi}}(s)$ with a 4th order cosine approximation on the left and an 8th order cosine approximation on the right.	124
4.13	The solution of (4.25) for $c = 0$: $\kappa = 0.1$ left, $\kappa = 0.2$ right.	126
4.14	The solution of (4.25) for $\sigma = \kappa$: $c = 0.2$ left, $c = 0.9$ right.	127
4.15	Zeros of $R_{\text{Disc}}(s)$ for $\sigma = 2\kappa$ and their periodic images.	127
4.16	Solution from a real pole for $\frac{\kappa}{\sigma} = \frac{1}{2}$ and $\kappa = 0.2$, and $c = 0.2$	128
4.17	Solution from an imaginary pole for $\frac{\kappa}{\sigma} = \frac{1}{2}$ and $\kappa = 0.2$, and $c = 0.2$	129
4.18	Solution of the discrete travelling wave equation with McKean nonlinearity for $\sigma = 2\kappa$	129
4.19	Expected periodic travelling wave solution of the nonlinear wave equation with McKean nonlinearity.	131
4.20	Periodic travelling wave solution of the discrete differential-difference equation (4.25) for parameters $\tau = 30$, $\sigma = 2\kappa$, $\kappa = 0.01$, and $c = 0.5$	133
4.21	Zoom of Figure 4.20 showing the occurrence of wiggles.	134
4.22	Zoom of solution for irrational $r = \frac{1}{\sqrt{2}}$ showing the occurrence of wiggles.	134
4.23	Wiggles in the periodic travelling wave solution of the nonlinear wave equation with McKean nonlinearity.	135
4.24	Sawtooth function (4.30).	136

4.25	Phase portrait of the travelling wave equation of the nonlinear wave equation with sawtooth nonlinearity.	137
4.26	Phase portrait and expected solution of the nonlinear wave equation with sawtooth nonlinearity.	138
4.27	Exact solutions of the nonlinear wave equation with sawtooth nonlinearity.	141
4.28	Comparison of the analytic solution and the discrete solution of the nonlinear wave equation with sawtooth nonlinearity, for fixed periods and fixed c , for rational values of $\frac{\sigma}{\kappa}$	144
4.29	Comparison of the analytic solution and the discrete solution of the nonlinear wave equation with sawtooth nonlinearity, for fixed periods and fixed c , for irrational values of $\frac{\sigma}{\kappa}$	145
5.1	Phase portrait of the travelling wave equation of the nonlinear wave equation with smooth nonlinearity.	148
5.2	Numerical solution $\varphi(\xi)$ of the discrete travelling wave equation (5.3). ξ is on the x -axis and φ on the y -axis.	152
5.3	Two cases for numerical solutions of the discrete travelling wave equation. ξ is on the x -axis and φ on the y -axis. (5.3)	153
5.4	Left: An orbit for the leapfrog method applied to the reduced ODE (5.2), and, Right: the corresponding solution in red, with the numerical solution of the discrete travelling wave equation (5.3) for $\sigma = \kappa = 0.5$ superimposed in blue.	154
5.5	Left: An orbit for the leapfrog method applied to the reduced ODE (5.2), and, Right: the corresponding solution in red, with the numerical solution of the discrete travelling wave equation (5.3) for $\sigma = \kappa = 0.8$ superimposed in blue.	155
5.6	Continuation in T starting with $T = 2\pi$ for $\sigma = 1$, $\kappa = \frac{1}{\sqrt{2}}$, $c = 1.3$	158
5.7	Continuation in T starting with $T = 2\pi$ for $\sigma = 1$, $\kappa = \frac{1}{\sqrt{2}}$, $c = 1.3$	159
5.8	A chosen section of the solution φ	161

5.9	A short continuation simulation showing one major resonance peak. The y -axis gives the size of the resonance defined by (5.6).	161
5.10	Comparison of the resonances for a rational ratio of $\frac{\sigma}{\kappa}$ and an irrational one. The y -axis gives the size of the resonance defined by (5.6).	162
5.11	Continuation in T starting with $T = 2\pi$ for different rational values of $\frac{\sigma}{\kappa}$. The y -axis gives the size of the resonance defined by (5.6).	163
5.12	Continuation simulation for $\sigma = 2\kappa$: resonances plotted against T and $\frac{T}{2\kappa}$. The y -axis gives the size of the resonance defined by (5.6).	164
5.13	Continuation in T starting with $T = 2\pi$ for different rational values of $\frac{\sigma}{\kappa}$. The y -axis gives the size of the resonance defined by (5.6).	165
5.14	The left plot shows the resonances for $\frac{\sigma}{\kappa} = \frac{m}{n}$ for the case $n = 1$ and $m = 1, 2, 3, 4$ and the plot on the right shows the case $n = 2$ and $m = 3, 5, 7$. The y -axis gives the size of the resonance defined by (5.6).	166
5.15	Continuation in T starting with $T = 2\pi$ for fixed rational values of $\frac{\sigma}{\kappa}$ for different values of σ . The y -axis gives the size of the resonance defined by (5.6).	167
5.16	Continuation in T tending to infinity starting with $T = 2\pi$. The y -axis gives the size of the resonance defined by (5.6).	169
5.17	Continuation in T tending to infinity starting with $T = 2\pi$. The y -axis gives the size of the resonance defined by (5.6).	170
6.1	The explicit Adams method with step size $h = 0.5$, initial value $(q_0, p_0) = (0.7, 0)$ and the explicit midpoint rule with $h = 0.4$, initial value $(q_0, p_0) = (0, 1.1)$, applied to the pendulum.	175
6.2	Energy error for three different linear multistep methods applied to the Kepler problem, reproduced from [37]. The x -axis gives the number of periods, and the y -axis gives the energy error.	182

6.3	The solution of the 2-step symmetric explicit midpoint rule plotted with the MDE. The blue solution curve corresponds to the same orbit of the numerical solution (also in blue).	189
6.4	Relabeling of the five grid points in (6.15) to match that of a multistep method (6.6) for $\sigma = 2\kappa$. The grid points are given as red dots with the spacing between each equal to κ . The labels of the grid points of (6.15) are in blue and those of (6.6) are in green.	192
6.5	Roots of the characteristic polynomial of the discrete travelling wave equation for $c = 1.3$ —Case 1.	195
6.6	Roots of the characteristic polynomial of the discrete travelling wave equation for $c = 0.5$ —Case 3. and 4.	196
6.7	Roots of the characteristic polynomial of the discrete travelling wave equation for $c = 0$ —Case 2.	197
6.8	Phase portraits of the solution of the modified differential equation of the discrete travelling wave equation (6.23).	203
6.9	Left: Orbits of fixed period $T = 2\pi$, for increasing $\kappa = \sigma$. The blue orbit has very small value of $\sigma = 0$ and the black orbit has a large value of $\sigma = 1.5$. The curves in between these have increasing values of σ from the blue orbit to the black orbit. Right: Orbits of fixed amplitude equal to 1.6, for increasing $\kappa = \sigma$. The blue orbit has very small value of $\sigma = 0$ and the orange orbit has a large value of $\sigma = 1.8$. The curves in between these have increasing values of σ from the blue orbit to the orange orbit.	204
6.10	Truncated solutions of the modified differential equation for the discrete travelling wave equation: y_1 is the green curve, y_2 , the red curve, and y_3 the orange curve. The numerical solution is given by the blue curve.	205

6.11	On the left we show the error (the difference between the numerical solution and the solution of the modified equation) of the three truncations of the modified equation for the discrete travelling wave equation: y_1 -green, y_2 -red, y_3 -orange. On the right is a zoom of the graph on the left.	206
6.12	Resonances of the numerical solution from Chapter 5 given by the blue curve. Resonances of the modified differential equation for the discrete travelling wave equation given by the red curve.	207
6.13	Contour plot of the resonances for $T = 2\pi$ and $c = 1.3$. The lighter the shading the bigger the resonances are.	207
6.14	On the left is the modified Hamiltonian with small values of σ and κ and on the right the modified Hamiltonian with large values of σ and κ	211
6.15	Modified Hamiltonian of the 1st order nonlinear wave system with change of coordinates.	223
6.16	Modified Hamiltonians of the leapfrog method applied to the nonlinear wave equation as a 1st order system for small σ and κ on the left and large σ and κ on the right.	225
6.17	Modified Hamiltonians of the Preissman box scheme applied to the nonlinear wave equation as a 1st order system for small σ and κ on the left and large σ and κ on the right.	226

List of Tables

1.1	Trees of order 3 with their elementary differentials and coefficients.	17
2.1	Conservation laws for ODEs and PDEs.	68

Chapter 1

Geometric Integration of Ordinary Differential Equations

This chapter begins with an introduction to ordinary differential equations and then moves on to the numerical solution of ordinary differential equations. Next we look at a type of ODE known as a Hamiltonian system. We then look at the idea of symplecticity, which is a property inherent to all Hamiltonian ordinary differential equations. The chapter continues by exploring other types of geometric properties that an ordinary differential equation may possess and how methods are constructed to preserve such properties. Next, we look at some numerical experiments using symplectic integrators. Finally, we begin an introduction to backward error analysis for ordinary differential equations.

1.1 Introduction to Ordinary Differential Equations (ODEs)

Differential equations are often formed to describe some physical phenomenon. An ordinary differential equation (ODE) contains only ordinary derivatives [102] of one or more dependent variables with respect to a single independent

variable. For example,

$$\frac{d^2x}{dt^2} + 16x = 0$$

is an ODE with one dependent variable, x , and one independent variable, t .

Our differential equations will generally be of the form

$$\frac{dy}{dt} = f(t, y) \text{ and } \frac{d^2y}{dt^2} = f(t, y, y') \quad (1.1)$$

and are called evolution equations, and represent physical systems. They are called evolution equations because they contain time t as the independent variable and so the derivatives are taken with respect to time. A solution then evolves as time goes by. We seek a solution $y(t)$ of the above equations (1.1). Some analytical methods are known, but quite often an ODE cannot be solved exactly and this is when we turn to numerical methods.

A system of ODEs contains two or more equations involving two or more dependent variables with respect to a single independent variable. For example,

$$\begin{aligned} \frac{du}{dt} &= f(t, u, v) \\ \frac{dv}{dt} &= g(t, u, v) \end{aligned} \quad (1.2)$$

is a system of first order differential equations with dependent variables, u and v , and independent variable, t .

We will generally be talking about systems of equations and these can be written more compactly as

$$\dot{y} = f(t, y), \quad (1.3)$$

where y is a vector in \mathbb{R}^N representing a point in phase space, \dot{y} is the derivative of the dependent variables with respect to t , and $f(t, y)$ is a vector-valued function representing a vector field. In the above system, (1.2), $y = (u, v)$, and is a point in the phase plane \mathbb{R}^2 .

Normally, we impose some condition or conditions on the solution $y(t)$ of (1.1) or its derivatives. When these side conditions are given we seek the solution of an initial value problem (IVP). Imposing initial conditions on equations

(1.1) respectively, we get

$$\begin{aligned}\frac{dy}{dt} &= f(t, y), & y(t_0) &= y_0 \\ \frac{d^2y}{dt^2} &= f(t, y, y'), & y(t_0) &= y_0, \quad y'(t_0) = y_1\end{aligned}$$

where $y(t_0) = y_0$ represents the position of an object at some initial time t_0 , and $y'(t_0) = y_1$ the velocity at t_0 .

Autonomous differential equations have no explicit dependence on the independent variable. That is, the vector field f does not depend on t . Equation (1.3) can be written as an autonomous first order system of differential equations:

$$\frac{dy}{dt} = f(y).$$

Any non-autonomous equation (1.3) can be converted to an autonomous system by raising the dimension by 1 and introducing an additional y -component whose derivative always equals 1. For (1.3) we get the $(N + 1)$ -dimensional autonomous system,

$$\begin{aligned}\frac{dy}{dt} &= f(y_{N+1}, y) \\ \frac{dy_{N+1}}{dt} &= 1\end{aligned}$$

1.1.1 Flow Map

The flow map of an ODE is a mapping which takes initial data to later points along trajectories. That is, the flow map takes any initial point y_0 in phase space and associates the value $y(t)$ of the solution. The map is denoted by φ_t and therefore defined by,

$$\varphi_t(y_0) = y(t),$$

where $y(0) = y_0$.

1.2 Numerical Solutions of ODEs

Even if it can be shown that a solution of an ODE exists, it might be difficult or even impossible to find the solution analytically. Therefore, we often have to be satisfied with finding an approximate solution by a numerical method or an “integrator”.

This section begins to introduce one-step methods using the Euler method as an example. The general form of a one-step method is then given, followed by a brief discussion on multistep methods. Next, an introduction to the types of errors involved in using a numerical method is given. The Euler method is then used to show how the truncation error of a method is calculated using a Taylor series expansion. Next, other examples of one-step methods are given, followed by a class of one-step methods known as Runge–Kutta integrators. The errors in Runge–Kutta methods are then described using rooted trees. Finally, splitting and composition methods are discussed briefly.

The simplest example of a numerical method is Euler’s method. It uses the idea of approximating values of a function using tangent lines. Euler’s method for a first order initial value problem $y' = f(t, y)$, $y(t_0) = y_0$, is

$$y_{n+1} = y_n + hf(t_n, y_n),$$

where h is called the step size and $t_n = t_0 + nh$, $n = 0, 1, 2, \dots$.

The repeated use of Euler’s formula for $n = 0, 1, 2, \dots$ produces the y -coordinates y_1, y_2, y_3, \dots of points on successive tangent lines to the solution curve at t_1, t_2, t_3, \dots .

If the system is autonomous then Euler’s method simplifies slightly to

$$y_{n+1} = y_n + hf(y_n). \tag{1.4}$$

Euler’s method is an explicit one-step method. It is explicit since all information to find the next approximation is known, and it is a one-step method since only one previous value is needed to determine the current value. General one-step methods are written in the following form,

$$y_{n+1} = \Phi_h(y_n),$$

for some mapping $\Phi_h : \mathbb{R}^N \rightarrow \mathbb{R}^N$.

Implicit methods require solving a system of equations by some iterative method. An example of an implicit method, for an autonomous system, is the implicit Euler method,

$$y_{n+1} = y_n + hf(y_{n+1}). \quad (1.5)$$

In (1.5), we see that to find the next approximation y_{n+1} , the function needs to be evaluated at y_{n+1} . Therefore, the approximation y_{n+1} is defined implicitly and is found by solving a system of nonlinear equations.

Hence, one step of an implicit method tends to be more computationally expensive than one step of an explicit method. Despite this, implicit methods are sometimes preferred because the time step can be larger (for so-called ‘stiff’ systems) and they can have different geometric properties than explicit methods.

Multistep methods can also be explicit or implicit, but instead of using the value from one previous step to obtain the current value, they use the values from several computed steps. This is done in attempt to achieve greater accuracy. The following are examples of explicit and implicit multistep methods respectively,

$$y_{n+2} = y_n + 2hf(y_{n+1}), \quad (1.6)$$

$$y_{n+2} = \frac{4}{3}y_{n+1} - \frac{1}{3}y_n + \frac{2}{3}hf(y_{n+2}). \quad (1.7)$$

Both equations, (1.6) and (1.7), give 2-step methods since the next value, y_{n+2} , depends on two previous values, y_n and y_{n+1} . Equation (1.6) is an explicit method because the function f is only evaluated at previous time values (y_{n+1}) that are already computed. On the other hand, (1.7) is implicit since the function evaluation contains the time value (y_{n+2}) that is currently being computed.

1.2.1 Errors in Numerical Methods

When using a numerical method we must be aware of the different types of errors that can be introduced. Accumulation of error could reduce the accuracy

of the solution we are trying to approximate.

Round-off error [102] is the error due to the calculations being done by a calculator or computer that can only calculate up to a finite number of digits. This type of error can be reduced by reducing the number of calculations to be made.

The other type of error involved comes from using the numerical method itself to approximate values of the solution. This is called the local truncation error or sometimes also called the discretisation error, and is introduced at each step of the method. Using Euler's method as an example, we can derive the local truncation error using Taylor's formula with remainder.

Say we are given an equation,

$$\dot{y} = f(t, y), \quad y(t_0) = y_0,$$

and want to solve this using Euler's method,

$$y_{n+1} = y_n + hf(t_n, y_n).$$

Taylor's formula with remainder is given below,

$$y(t) = y(a) + y'(a)\frac{t-a}{1!} + \cdots + y^{(k)}(a)\frac{(t-a)^k}{k!} + y^{(k+1)}(c)\frac{(t-a)^{k+1}}{(k+1)!}$$

where c is some point between a and t .

If we set $k = 1$, $a = t_n$, and $t = t_{n+1} = t_n + h$, we get

$$\begin{aligned} y(t_{n+1}) &= y(t_n) + y'(t_n)\frac{h}{1!} + y''(c)\frac{h^2}{2!} \\ \text{or } y(t_{n+1}) &= \underbrace{y_n + hf(t_n, y_n)}_{y_{n+1}} + y''(c)\frac{h^2}{2!} \quad (\text{since } y' = f(t, y)) \\ \Rightarrow y_{n+1} &= y_{n+1} + y''(c)\frac{h^2}{2!}. \end{aligned}$$

Therefore, the local truncation error in y_{n+1} for Euler's method is $y''(c)\frac{h^2}{2!}$, where $t_n < c < t_{n+1}$.

The value of c exists only theoretically and therefore the exact error cannot be calculated, but an upper bound on the absolute value of the error is $\frac{Mh^2}{2!}$, where $M = \max_{t_n < t < t_{n+1}} |y''(t)|$.

Using the Landau ‘big O’ notation, the local truncation error of Euler’s method, a first order method, is $O(h^2)$. The global error of Euler’s method is $O(h)$. In general, if the error in the numerical method is of order h^n and h is halved, the error is reduced by a factor of about $\frac{1}{2^n}$. This means that methods with higher order do better for a small value of h .

1.2.2 Other One-Step Methods

The implicit Euler method is similar to the explicit Euler method, except that the function evaluation is done at the value we are trying to estimate. For $\dot{y} = f(y)$, implicit Euler is,

$$y_{n+1} = y_n + hf(y_{n+1}).$$

The Trapezoidal Rule takes the average of the function evaluation at the previous value (y_n) and current value (y_{n+1}),

$$y_{n+1} = y_n + \frac{h}{2}(f(y_n) + f(y_{n+1})). \quad (1.8)$$

The implicit midpoint rule averages the function evaluation over the previous value (y_n) and current value (y_{n+1}),

$$y_{n+1} = y_n + hf\left(\frac{y_n + y_{n+1}}{2}\right). \quad (1.9)$$

1.2.3 Runge–Kutta Methods

Runge–Kutta (RK) methods are also one-step methods which basically [102] generalise the Euler method. The slope function f of the Euler method is replaced in a Runge–Kutta method by a weighted average of slopes over the interval $t_n \leq t \leq t_{n+1}$. That is, a Runge–Kutta method is of the form,

$$y_{n+1} = y_n + h \underbrace{(b_1k_1 + b_2k_2 + \cdots + b_mk_m)}_{\text{Weighted Average}},$$

where b_i , $i = 1, 2, \dots, m$, are constants that satisfy $b_1 + b_2 + \cdots + b_m = 1$, and each k_i is a function evaluation of f at a selected point.

By taking $m = 1$, $b_1 = 1$, and $k_1 = f(t_n, y_n)$, we get the Euler formula,
 $y_{n+1} = y_n + hf(t_n, y_n)$.

Let s be an integer [36] and $a_{21}, a_{31}, a_{32}, \dots, a_{s1}, a_{s2}, \dots, a_{s,s-1}, b_1, \dots, b_s, c_2, \dots, c_s$ be real coefficients. Then the method

$$\begin{aligned} k_1 &= f(t_0, y_0) \\ k_2 &= f(t_0 + c_2h, y_0 + ha_{21}k_1) \\ k_3 &= f(t_0 + c_3h, y_0 + h(a_{31}k_1 + a_{32}k_2)) \\ &\dots \\ k_s &= f(t_0 + c_sh, y_0 + h(a_{s1}k_1 + \dots + a_{s,s-1}k_{s-1})) \\ y_1 &= y_0 + h(b_1k_1 + \dots + b_sk_s), \end{aligned}$$

is called an s -stage explicit Runge–Kutta method (ERK) for $\dot{y} = f(t, y)$,
 $y(t_0) = y_0$.

Usually, the c_i satisfy the conditions

$$c_i = \sum_{j=1}^{i-1} a_{ij}. \quad (1.10)$$

The above method can be written in tableau form

0					
c_2	a_{21}				
c_3	a_{31}	a_{32}			
\vdots	\vdots	\vdots	\ddots		
c_s	a_{s1}	a_{s2}	\dots	$a_{s,s-1}$	
	b_1	b_2	\dots	b_{s-1}	b_s

Let $b_i, a_{ij}, (i, j = 1, \dots, s)$ be real numbers and let $c_i = \sum_{j=1}^s a_{ij}$ be defined as above. The method

$$Y_i = y_n + h \sum_{j=1}^s a_{ij} f(Y_j), \quad (1.11)$$

$$y_{n+1} = y_n + h \sum_{i=1}^s b_i f(Y_i), \quad (1.12)$$

is called an s -stage Runge–Kutta method. The constant coefficients $\{b_i\}$ and $\{a_{ij}\}$ completely describe a Runge–Kutta method. When $a_{ij} = 0$ for $i \leq j$ we have an explicit (ERK) method. If $a_{ij} = 0$ for $i < j$ and at least one $a_{ii} \neq 0$, we have a diagonally-implicit Runge–Kutta method (DIRK). If in addition all diagonal elements are identical we have a singly-diagonally-implicit (SDIRK) method. In all other cases we have an implicit Runge–Kutta method (IRK).

The coefficients for Implicit Runge–Kutta methods can also be displayed in a tableau, known as a Butcher tableau after its founder.

$$\begin{array}{c|ccc} c_1 & a_{11} & \dots & a_{1s} \\ \vdots & \vdots & \vdots & \ddots \\ c_s & a_{s1} & \dots & a_{ss} \\ \hline & b_1 & \dots & b_s \end{array}.$$

1.2.4 Errors for Runge–Kutta Methods

In the years 1963–72 Butcher developed a nice way of analysing the error and finding the order conditions for Runge–Kutta methods (see [11]) using rooted trees. The order conditions are derived by comparing successive terms in the Taylor series expansions of the exact (1.13) and numerical solutions. For the autonomous problem,

$$\dot{y} = f(y), \quad y(t_0) = y_0, \quad (1.13)$$

where $f : \mathbb{R}^N \rightarrow \mathbb{R}^N$ is sufficiently differentiable, we firstly compute the higher derivatives of the solution y at the initial point t_0 . This is done by repeated differentiation of the differential equation. Using the chain rule we find that

$$\ddot{y} = \frac{d}{dt}f(y) = f'(y)\dot{y}.$$

Note that $f'(y) = \frac{\partial}{\partial y}f(y)$ and $\dot{y} = \frac{d}{dt}y$.

Continuing in this way, and also using the product rule and symmetry of partial

derivatives, we get,

$$\begin{aligned}
\dot{y} &= f(y) \\
\ddot{y} &= f'(y)\dot{y} \\
y^{(3)} &= f''(y)(\dot{y}, \dot{y}) + f'(y)\ddot{y} \\
y^{(4)} &= f'''(y)(\dot{y}, \dot{y}, \dot{y}) + 3f''(y)(\ddot{y}, \dot{y}) + f'(y)y^{(3)} \\
y^{(5)} &= f^{(4)}(y)(\dot{y}, \dot{y}, \dot{y}, \dot{y}) + 6f'''(y)(\ddot{y}, \dot{y}, \dot{y}) \\
&\quad + 4f''(y)(y^{(3)}, \dot{y}) + 3f''(y)(\ddot{y}, \ddot{y}) + f'(y)y^{(4)},
\end{aligned}$$

and so on.

Next we insert \dot{y}, \ddot{y}, \dots recursively into the above equations, remembering $f = f(y)$, to get,

$$\begin{aligned}
\dot{y} &= f \\
\ddot{y} &= f'f \\
y^{(3)} &= f''(f, f) + f'f'f \\
y^{(4)} &= f'''(f, f, f) + 3f''(f'f, f) + f'f''(f, f) + f'f'f'f,
\end{aligned}$$

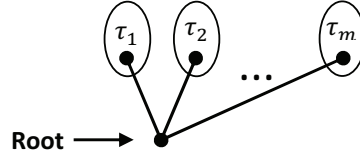
and so on.

The expressions on the right hand side of the above formulas are called elementary differentials and can be represented as rooted trees. A tree is a connected graph which does not contain any cycles. A rooted tree specifies one of the vertices as the root. Following standard practice the root is placed at the bottom of the tree.

Definition 1.2.1. (*Rooted Trees*). The set T of rooted trees τ [37] is defined recursively as:

- , the graph with only one vertex is in T

If $\tau_1, \dots, \tau_m \in T$ then $\tau = [\tau_1, \dots, \tau_m] \in T$, where τ is the graph obtained by grafting the roots of τ_1, \dots, τ_m to a new vertex.



To represent each elementary differential as a rooted tree, each k th derivative $f^{(k)}$ becomes a vertex with k branches and f becomes a single vertex. For example the rooted tree of the elementary differential $f'f''(f, f)$ is constructed by first noting that f' is a vertex with one branch (see Figure 1.1).



Figure 1.1: First step in the formation of the rooted tree for the elementary differential $f'f''(f, f)$.

Next, we have the rooted tree for f'' , which is a vertex with two branches (see Figure 1.2).



Figure 1.2: Second step in the formation of the rooted tree for the elementary differential $f'f''(f, f)$.

Finally, we add a vertex to each branch for (f, f) to get the final rooted tree for $f'f''(f, f)$ (see Figure 1.3).

The order of τ , the number of vertices, is denoted by $|\tau|$. The coefficients in front of the elementary differentials in the derivative equations are denoted by $\alpha(\tau)$.

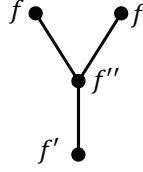


Figure 1.3: Final step in the formation of the rooted tree for the elementary differential $f'f''(f, f)$.

Definition 1.2.2. (*Elementary Differentials*). For a tree [37] $\tau \in T$ the elementary differential is a mapping $F(\tau) : \mathbb{R}^N \rightarrow \mathbb{R}^N$, defined recursively by

$$F(\bullet)(y) = f(y), \text{ and}$$

$$F(\tau)(y) = f^{(m)}(y) (F(\tau_1)(y), \dots, F(\tau_m)(y))$$

where $\tau = [\tau_1, \dots, \tau_m]$.

Theorem 1.2.1. [37]. The q th derivative of the exact solution is given by

$$y^{(q)}(t_0) = \sum_{|\tau|=q} \alpha(\tau) F(\tau)(y_0),$$

where $\alpha(\tau)$ are positive integer coefficients (of the elementary differentials).

Let v be a vertex in a tree τ . Say v has a downward, or inward, directed branch; then the branch is connected to a vertex w of τ called a parent of v . Similarly, if v has an upward, or outward, directed branch then the branch is connected to a vertex x of τ called a child of v . For example, in the tree in Figure 1.4, vertex v has one parent w and two children x and y .

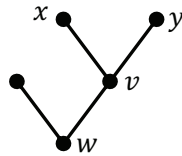


Figure 1.4: Illustration of lower and upper vertices in a rooted tree.

Also, we call some of the vertices leaves. If the order of a tree $|\tau| > 1$, then a vertex, excluding the root, is a leaf if it has no children. The root is the vertex without a parent. The leaves are labeled in Figure 1.5 for two trees.

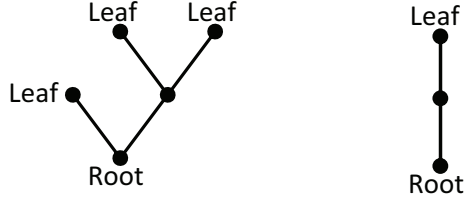


Figure 1.5: Illustration showing the leaves of rooted trees.

For every tree τ there is a related polynomial denoted by $\phi(\tau)$ and a constant denoted by $\gamma(\tau)$.

To write out the polynomial $\phi(\tau)$ we firstly assign labels to each vertex. The root is labeled i and every other vertex which is not a leaf is given a label j, k, \dots . For example, a given tree is labeled in Figure 1.6.

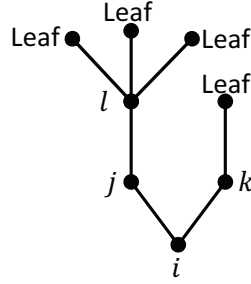


Figure 1.6: Labeling of a rooted tree τ for the related polynomial $\phi(\tau)$.

Next, we start from the bottom of the tree and work our way up giving each label a factor. Starting at the root, we assign i the factor b_i . For every other label at a vertex we assign the factor a_{jk} where j is a parent of k . For the same tree above see Figure 1.7.

Finally, for each leaf we assign the factor c_j where j is a parent of the leaf (see Figure 1.8).

We now form the product,

$$b_i \left(\prod a_{jk} \right) \left(\prod c_j \right),$$

then sum this product over i, j, k, \dots from 1 to s .

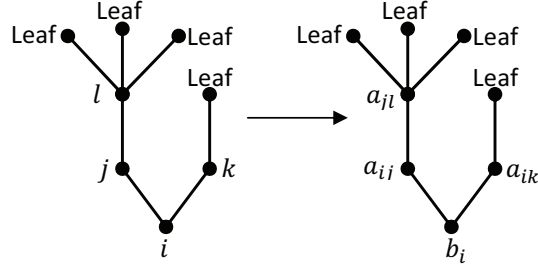


Figure 1.7: Labeling of a rooted tree τ for the related polynomial $\phi(\tau)$, with factors assigned to each label.

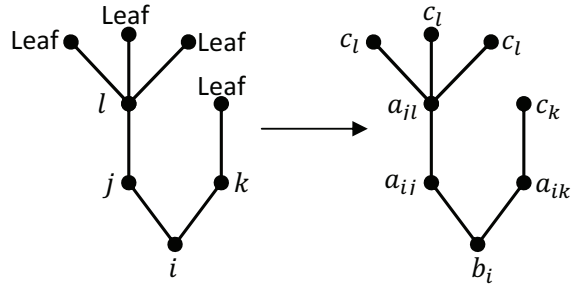


Figure 1.8: Labeling of a rooted tree τ for the related polynomial $\phi(\tau)$, with factors assigned to each label and leaf.

For the above tree, we get,

$$\sum b_i a_{ij} a_{jl} a_{ik} c_l^3 c_k.$$

Using coefficients from the specific Runge–Kutta method, this gives a series of order conditions, the set of algebraic conditions on the coefficients of the method that must be satisfied for the method to be of order p .

In contrast to $\phi(\tau)$ we form $\gamma(\tau)$ for a particular τ by working from the top of the tree, the leaves, to the bottom of the tree, the root. First, we assign each leaf the value 1. Using the same tree as was used in the previous example, we get the labeling given in Figure 1.9.

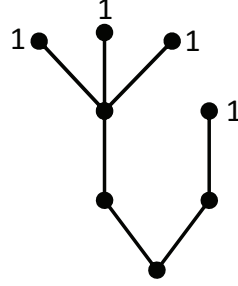


Figure 1.9: Labeling of the leaves of a rooted tree τ for the related polynomial $\gamma(\tau)$.

Working downwards to the next set of vertices, we assign these with the sum of the values of the children plus 1. We continue down the tree to the root until all vertices are given a value (See Figure 1.10).

We now multiply all the values of the vertices to get $\gamma(\tau)$. For the above tree, we have,

$$\gamma = 8.5.4.2.1.1.1.1 = 320.$$

By expanding the Runge–Kutta method in a Taylor series and comparing this term by term with the expansion of the exact solution we get conditions for the coefficient of each elementary differential of order $< p$ to be zero. These conditions are polynomial equations in the Runge–Kutta coefficients a_{ij} , b_i and c_i and will ensure that the method has order p .

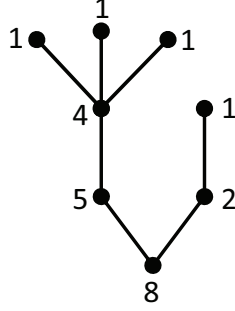


Figure 1.10: Labeling of the leaves and other vertices of a rooted tree τ for the related polynomial $\gamma(\tau)$.

Expansion of the method is more complicated than the exact solution. Details can be found in [37], [11], and [12]. After finding this expansion we get the following theorem.

Theorem 1.2.2. [37]. *The derivatives with respect to h at $h = 0$ of the numerical solution of a Runge–Kutta method are given by*

$$y_1^{(q)}|_{h=0} = \sum_{|\tau|=q} \gamma(\tau) \cdot \phi(\tau) \cdot \alpha(\tau) F(\tau)(y_0),$$

where $\alpha(\tau)$ and $F(\tau)$ are the same as in Theorem 1.2.1 and the coefficients $\gamma(\tau)$ and the elementary weights $\phi(\tau)$ are obtained from the tree τ as described earlier.

Comparing this with the exact solution in Theorem 1.2.1 we get the following theorem.

Theorem 1.2.3. *The Runge–Kutta method has order p if and only if*

$$\varphi(\tau) = \frac{1}{\gamma(\tau)} \quad \text{for } |\tau| \leq p.$$

We give an example of the elementary differentials and the coefficients for the trees of order three in Table 1.1.



Graph	$F(\tau)$	$\alpha(\tau)$	$\gamma(\tau)$	$\sigma(\tau)$	$\phi(\tau)$
	$f''(f, f)$	1	3	2	$\sum_{ijk} b_i a_{ij} a_{ik}$
	$f' f' f$	1	6	1	$\sum_{ijk} b_i a_{ij} a_{jk}$

Table 1.1: Trees of order 3 with their elementary differentials and coefficients.

1.2.5 Splitting and Composition Methods

For an ODE $\dot{y} = f(y)$, $y \in \mathbb{R}^N$, there are three main steps involved in a splitting method. First, the vector field f is split up into a sum of vector fields f_i ,

$$f(y) = \sum_{i=1}^n f_i(y).$$

Next, each f_i is integrated either exactly or approximately. Finally, the solutions are combined to form an integrator for f . This last step is known as composition. We give the standard 1st and 2nd order compositions as an example to clarify the last step.

For these examples, suppose that the vector field f is split into two parts,

$$f(y) = f_1(y) + f_2(y).$$

Let us also say that both $f_1(y)$ and $f_2(y)$ can be integrated exactly to give the exact flows $\varphi_{f_1}(t)$ and $\varphi_{f_2}(t)$ of the systems $\dot{y} = f_1(y)$ and $\dot{y} = f_2(y)$ respectively.

Combining these solutions by composition we form the following 1st order integrator for $f(y)$,

$$\Phi_h = \varphi_{h,f_1} \circ \varphi_{h,f_2}.$$

Composing the solutions in a slightly different way, we get the 2nd order integrator,

$$\Phi_h = \varphi_{\frac{h}{2},f_1} \circ \varphi_{h,f_2} \circ \varphi_{\frac{h}{2},f_1}.$$

The advantages of splitting methods are that they are usually simple and explicit, and can also preserve a variety of structures. On the other hand,

higher order splitting methods tend to be costly to implement. Also, the splitting may sometimes break up an important property that we may want to preserve.

A couple of examples of Hamiltonian splitting are given in Section 1.8.1.

1.3 Hamiltonian Systems

Hamiltonian systems [46] are common in many branches of applied mathematics and physical sciences and possess some important structures or geometric properties [100]. These include symplecticity (see Section 1.4), conservation laws (see Section 1.5), preservation of Poisson brackets (see Section 1.3.3), and symmetries (see Sections 1.6 and 1.7). These properties are usually destroyed when a numerical method is applied to the system, but special numerical methods can be found to solve such systems while preserving these properties. These numerical methods are known as geometric integrators. More detail on geometric integrators is given in Section 1.8.

Hamiltonian systems are of the form

$$\dot{q} = H_p(q, p), \quad \dot{p} = -H_q(q, p),$$

where the Hamiltonian $H = H(q_1, \dots, q_d, p_1, \dots, p_d) : \mathbb{R}^N \times \mathbb{R}^N \rightarrow \mathbb{R}$ represents the total energy of the system; q_i , ($q \in \mathbb{R}^N$), are the position coordinates, and p_i , ($p \in \mathbb{R}^N$), the momenta for $i = 1, \dots, N$, with N the number of degrees of freedom; $H_p = (\frac{\partial H}{\partial p})^T$ and $H_q = (\frac{\partial H}{\partial q})^T$ are column vectors of partial derivatives. The Hamiltonian function $H(q, p)$ is a first integral or conserved quantity (see Section 1.5) of the system.

It is often convenient to use the shorthand notation,

$$\dot{\mathbf{z}} = J \nabla_{\mathbf{z}} H(\mathbf{z}), \tag{1.14}$$

where $\mathbf{z} = (q, p)^T$, $q, p \in \mathbb{R}^N$, $z \in \mathbb{R}^{2N}$, and J is the $2N \times 2N$ canonical structure matrix,

$$J = \begin{pmatrix} 0 & I_{N \times N} \\ -I_{N \times N} & 0 \end{pmatrix}.$$

Often the Hamiltonian H of a system can be written in the form,

$$H(q, p) = T(q, p) + V(q),$$

where T is the kinetic energy and V is the potential energy. Systems written in this way can be solved by special methods. References [86, 46] give a good introduction to Hamiltonian systems and numerical methods for such systems such as splitting methods. This is shown in Section 1.8.1.

1.3.1 N -Body Newtonian Gravitational Problem

N -body problems involve finding the motion of N bodies in time, given their initial positions, masses, and velocities. Each body interacts with all other bodies and the motions are then determined by classical mechanics. The motion can be cast into a Hamiltonian system: for Newtonian gravitational forces,

$$\dot{q}_i = \frac{1}{m_i} p_i, \quad \dot{p}_i = -G \sum_{j=1, j \neq i}^N \frac{m_i m_j}{\|q_i - q_j\|^3} (q_i - q_j), \quad i = 1, 2, \dots, N$$

with Hamiltonian,

$$H(p, q) = \frac{1}{2} \sum_{i=1}^N \frac{1}{m_i} p_i^T p_i - G \sum_{i=2}^N \sum_{j=1}^{i-1} \frac{m_i m_j}{\|q_i - q_j\|},$$

where p_i and q_i are the position and momenta vectors of the i th body respectively, G is the gravitational constant, and m_i is the mass of the i th body.

1.3.2 Molecular Dynamics

Molecular Dynamics, “in its simplest form”, [53] requires the solution of Hamiltonian systems, where the total energy is given by,

$$H(p, q) = \frac{1}{2} \sum_{i=1}^N \frac{1}{m_i} p_i^T p_i + \sum_{i=2}^N \sum_{j=1}^{i-1} V(r_{ij}),$$

with $r_{ij} = \|q_i - q_j\|$ and $V(r)$ a given potential function, that is, the interaction potential between the i th and j th particle.

The N particles interact [36] pairwise with potential forces depending on the distances of the particles.

The equations of motion are

$$\dot{q}_i = \frac{1}{m_i} p_i, \quad \dot{p}_i = - \sum_{j=1}^N \frac{V'(r_{ij})}{r_{ij}} (q_i - q_j), \quad i = 1, 2, \dots, N,$$

where $r_{ij} = \|q_i - q_j\|$.

Molecular dynamics simulations are important in the areas of chemistry, physics, bio-science and engineering. N -body problems, as described in Section 1.3.1, are an example of molecular dynamics. The idea is to construct a model approximating the trajectories and to use this to obtain knowledge about how the molecules evolve in time.

Molecular systems generally contain very rapid oscillatory motions and because of this very small time steps are usually needed. Therefore, molecular simulations tend to need to be run for extremely long times to gain any information about the motion of the particles in time. It is not only the case of needing small time steps that require the simulations in molecular dynamics to be run for long times, but the molecules themselves can take a very long time to thermalise. Thermalisation occurs when the particles reach thermal equilibrium. They can also exhibit different behaviour on different time scales. An example where small time steps and long thermalisation time occur is protein folding, which can take milliseconds (10^{-3} seconds) to reach thermalisation with a very small time step of a few femtoseconds (10^{-15} seconds). In addition, the force evaluations at each time step are generally complicated and can therefore slow down the simulation process.

To start the simulation process, arbitrary initial positions and velocities are chosen. The system is then evolved in time to reach thermalisation. The positions and velocities are then taken at this stage to be the initial data and the simulation run again, ignoring the initial simulation that was performed.

The results of simulations are generally gathered over long runs and sometimes also over many initial conditions. These results are then used to study processes such as conformational changes of large molecules.

1.3.3 Poisson Systems

Poisson systems are a generalisation of Hamiltonian systems. To motivate this generalisation we first introduce the canonical Poisson bracket. In a Poisson system J is replaced with a non constant matrix $B(z)$.

The derivative of a function $F(p, q)$ along the flow of a Hamiltonian system,

$$\dot{p} = -\frac{\partial H}{\partial q}(p, q), \quad \dot{q} = \frac{\partial H}{\partial p}(p, q), \quad (1.15)$$

is given by,

$$\frac{d}{dt}F(p(t), q(t)) = \sum_{i=1}^d \left(\frac{\partial F}{\partial p_i} \dot{p}_i + \frac{\partial F}{\partial q_i} \dot{q}_i \right) = \sum_{i=1}^d \left(\frac{\partial F}{\partial q_i} \frac{\partial H}{\partial p_i} - \frac{\partial F}{\partial p_i} \frac{\partial H}{\partial q_i} \right). \quad (1.16)$$

This very symmetric equation motivates the following definition.

Definition 1.3.1. *The (canonical) Poisson bracket of 2 smooth functions $F(q, p)$ and $G(q, p)$ is the function*

$$\{F, G\} = \sum_{i=1}^d \left(\frac{\partial F}{\partial q_i} \frac{\partial G}{\partial p_i} - \frac{\partial F}{\partial p_i} \frac{\partial G}{\partial q_i} \right), \quad (1.17)$$

or in vector notation

$$\{F, G\}(z) = \nabla F(z)^T J \nabla G(z),$$

where $\mathbf{z} = (q, p)$ and $J = \begin{pmatrix} 0 & I \\ -I & 0 \end{pmatrix}$.

This Poisson bracket is bilinear, skew-symmetric ($\{F, G\} = -\{G, F\}$), and satisfies the Jacobi identity,

$$\{\{F, G\}, H\} + \{\{G, H\}, F\} + \{\{H, F\}, G\} = 0,$$

and Leibniz's rule,

$$\{F \cdot G, H\} = F \cdot \{G, H\} + G \cdot \{F, H\}.$$

With this notation, the Lie derivative (1.16) becomes

$$\frac{d}{dt}F(z(t)) = \{F, H\}(z(t)).$$

If we take [37] $F(z) = z_i$, the mapping that selects the i th component of z , we see that the Hamiltonian system (1.15) or $\dot{z} = J\nabla H(z)$ can be written as,

$$\dot{z}_i = \{z_i, H\}, \quad i = 1, \dots, 2d.$$

The general Poisson bracket in vector notation is given by,

$$\{F, G\}(z) = \nabla F(z)^T B(z) \nabla G(z).$$

It is bilinear and is skew-symmetric if $B(z) = -B(z)^T$. If it also satisfies the Jacobi identity then it is called a Poisson bracket and the corresponding system

$$\dot{z} = B(z) \nabla H(z)$$

is known as a Poisson system.

The Euler rigid body equations are an example of a Poisson system in \mathbb{R}^3 and are given by

$$\begin{bmatrix} \dot{z}_1 \\ \dot{z}_2 \\ \dot{z}_3 \end{bmatrix} = \begin{bmatrix} 0 & -z_3 & z_2 \\ z_3 & 0 & -z_1 \\ -z_2 & z_1 & 0 \end{bmatrix} \begin{bmatrix} \frac{z_1}{I_1} \\ \frac{z_2}{I_2} \\ \frac{z_3}{I_3} \end{bmatrix},$$

where I_1 , I_2 , and I_3 are the principal moments of inertia, and

$$H = \frac{1}{2} \left(\frac{z_1^2}{I_1} + \frac{z_2^2}{I_2} + \frac{z_3^2}{I_3} \right).$$

Functions [68] $C : \mathbb{R}^{2N} \rightarrow \mathbb{R}$, which are preserved for arbitrary Hamiltonians H , that is, $\dot{C} = \{C, H\} = 0$, $\forall H$, are called Casimir functions. For the rigid body bracket, $C = z_1^2 + z_2^2 + z_3^2$ is a Casimir.

Solutions of Poisson systems are confined to a level set of the Casimirs, and each such level set is an example of what is called a symplectic manifold. Thus, Poisson dynamics look essentially like Hamiltonian dynamics in a nonlinear space.

1.4 Symplecticity

This section begins with the definition of a symplectic map and that of a simplified version, a symplectic linear transformation. A geometric interpre-

tation of symplecticity for 2-dimensional systems is then given. Next we give the proof that the flow map of a Hamiltonian system is symplectic. Finally, we introduce the concept of symplecticity in terms of the wedge product of 2-forms.

Definition 1.4.1. *A smooth map $\psi : \mathbb{R}^{2N} \rightarrow \mathbb{R}^{2N}$ is called symplectic, with respect to the canonical structure matrix J , if its Jacobian $\psi'(\mathbf{z})$ satisfies,*

$$\psi'(\mathbf{z})^T J^{-1} \psi'(\mathbf{z}) = J^{-1}, \quad (1.18)$$

where J was given by (1.3) and the Jacobian is a matrix given by,

$$\psi'_{ij}(\mathbf{z}) = \frac{\partial \psi_i}{\partial z_j}.$$

For a linear [53] transformation $\psi = Az$, the condition of symplecticity reduces to,

$$A^T J^{-1} A = J^{-1},$$

where A is known as a symplectic matrix.

Equation (1.18) is related to the conservation of areas in phase space. For systems with one degree of freedom, for example $\mathbf{z} = (q, p) \in \mathbb{R}^2$, symplecticity corresponds to preservation of area in the (q, p) -plane. We can show this by taking,

$$\psi'(\mathbf{z}) = \begin{bmatrix} a & b \\ c & d \end{bmatrix},$$

whose determinant is given by $|\psi'(\mathbf{z})| = ad - bc$.

We now substitute this matrix into (1.18) to get,

$$\begin{bmatrix} 0 & ad - bc \\ bc - ad & 0 \end{bmatrix} = \begin{bmatrix} 0 & 1 \\ -1 & 0 \end{bmatrix}$$

which gives the equivalent conditions $ad - bc = 1$ and $bc - ad = -1$. Hence the determinant of the Jacobian is one, so a symplectic map is equivalent to preservation of area for systems with one degree of freedom.

In words, taking the area of sets of initial conditions then applying the flow results in a shape that becomes distorted from the initial sets but whose area

remains constant. Figure 1.11 demonstrates this. In the background is the phase portrait of the pendulum and on the left at position A we have a set of initial conditions forming the shape of a cat face. The cat face A is then integrated and follows the heteroclinic orbit (see Section 3.1 for a definition). As the face traces out this orbit it becomes more and more distorted but its area remains the same as the original cat face at A. Similarly, the cat face at B follows a periodic orbit, with the cat face areas remaining the same. For higher dimensions, the flow preserves [23] the sum of the oriented areas projected onto the (q_i, p_i) -coordinate planes.

This can be explained in more detail using the differential geometry view of symplecticity, given below.

Theorem 1.4.1. *The flow map $\varphi(t) : \mathbb{R}^{2N} \rightarrow \mathbb{R}^{2N}$ of a Hamiltonian system, $\dot{\mathbf{z}} = J\nabla_{\mathbf{z}}H(\mathbf{z})$, is symplectic.*

Proof. Let $A(t) = \varphi'(t) \in \mathbb{R}^{N \times N}$ be the Jacobian of the flow map and note that $A(t)$ satisfies the variational equation,

$$\frac{d}{dt}A(t) = JH_{zz}(z)A(t),$$

where $H_{zz}(z)$ is the symmetric Hessian matrix of H .

$A(0)$ is the identity map, so we get,

$$A^T(0)J^{-1}A(0) = IJ^{-1}I = J^{-1}.$$

Hence the theorem is true for $t = 0$ and therefore only need to show that $\frac{d}{dt}(A^T(t)J^{-1}A(t)) = 0$.

$$\begin{aligned} \frac{d}{dt}(A^T(t)J^{-1}A(t)) &= \frac{d}{dt}(A^T(t))J^{-1}A(t) + A^T(t)J^{-1}\frac{d}{dt}(A(t)) \\ &= A^T(t)H_{zz}J^TJ^{-1}A(t) + A^T(t)J^{-1}JH_{zz}A(t) \\ &= -A^T(t)H_{zz}A(t) + A^T(t)H_{zz}A(t), \text{ (since } J^T = -J) \\ &= 0. \end{aligned}$$

□

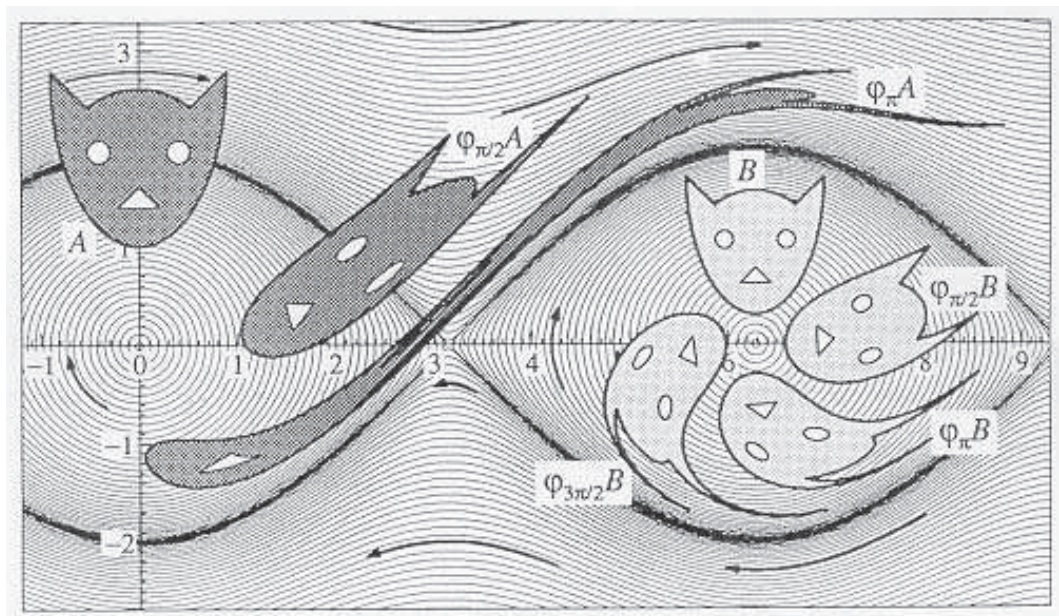


Figure 1.11: Flow of a Hamiltonian system, (the Pendulum), showing preservation of areas. This figure is reproduced from [53].

Symplecticity can also be introduced using the language of differential forms, an approach which is both a convenient form of calculation and also offers a geometric insight into the meaning of symplecticity. We will now briefly sketch this approach.

Definition 1.4.2. A 2-form on \mathbb{R}^{2N} is a skew-symmetric bilinear function $\omega(\xi, \eta)$, where $\xi, \eta \in \mathbb{R}^{2N}$. Bilinearity means that ω is linear in each of its arguments ξ and η . Skew-symmetry means

$$\omega(\xi, \eta) = -\omega(\eta, \xi), \quad \forall \xi, \eta.$$

For an introduction to differential forms and their derivatives see [1].

The canonical structure matrix J (1.3) introduces the symplectic 2-form [53] ω on the phase plane \mathbb{R}^{2N} . The symplectic 2-form is defined as,

$$\omega(\xi, \eta) = \xi^T J^{-1} \eta,$$

where $\xi, \eta \in \mathbb{R}^{2d}$.

As stated earlier, symplecticity is related to preservation of areas in phase space. Also, the 2-form ω , is geometrically interpreted in this way. For $N = 1$, $\omega(\xi, \eta)$ is the oriented area of the parallelogram spanned by $\xi, \eta \in \mathbb{R}^2$. See Figure 1.12.

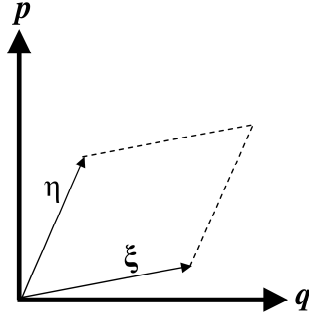


Figure 1.12: The 2-form ω for $d = 1$.

For $N > 1$, $\xi, \eta \in \mathbb{R}^{2N}$ are projected down onto the (q_i, p_i) -planes with corresponding vectors $\xi^{(i)}, \eta^{(i)} \in \mathbb{R}^2$, where $i = 1, \dots, N$. Then $\omega(\xi, \eta)$ is the sum of the oriented areas of the parallelograms spanned by $\xi^{(i)}$ and $\eta^{(i)}$.

If we now apply a transformation, $\psi : \mathbb{R}^{2N} \rightarrow \mathbb{R}^{2N}$, to the symplectic 2-form ω , then the transformation ψ is symplectic if

$$\psi^*\omega(\xi, \eta) = \omega(\psi_z(z)\xi, \psi_z(z)\eta) = \omega(\xi, \eta).$$

That is, the symplectic 2-form is invariant under a symplectic map. Introducing the wedge product of two differentials df and dg as

$$(df \wedge dg)(\xi, \eta) = dg(\xi)df(\eta) - df(\xi)dg(\eta),$$

we can express the 2-form ω as,

$$\omega = \sum_i dp_i \wedge dq_i.$$

Or, we can use the following shorthand notation,

$$\omega = dp \wedge dq.$$

Under the transformation

$$\begin{aligned}\hat{p} &= \psi^1(p, q), \\ \hat{q} &= \psi^2(p, q),\end{aligned}$$

symplecticity now becomes,

$$d\hat{p} \wedge d\hat{q} = dp \wedge dq.$$

1.5 Conserved Quantities

A non-constant function [38] $I(y)$ is a first integral, also known as conserved quantity, constant of motion, or invariant, of the differential equation $\dot{y} = f(y)$ if $I(y(t))$ is constant along every solution, or equivalently, if

$$\nabla I(y)^T \dot{y} = 0 \quad \forall y \tag{1.19}$$

$$\Rightarrow \nabla I(y)^T f(y) = 0. \tag{1.20}$$

Having a first integral is a ‘geometric property’ [53] of a system because its existence implies that the solutions are to some extent described by the geometry of the lower dimensional manifolds $\{y \in \mathbb{R}^{2N} : I(y) = \text{constant}\}$.

The Hamiltonian of any Hamiltonian system is an example of a first integral.

For a Hamiltonian system $\dot{p} = -H_q(q, p)$, $\dot{q} = H_p(q, p)$, we get

$$\begin{aligned} \frac{d}{dt}H(q, p) &= H_p(q, p)^T \dot{p} + H_q(q, p)^T \dot{q} \\ &= -H_p(q, p)^T H_q(q, p) + H_q^T(q, p) H_p(q, p) \\ &= 0. \end{aligned}$$

Hence $H(q, p)$ is constant along any solution $\mathbf{z} = (q, p)$.

In Poisson bracket notation $I(q, p)$ is a first integral of a Hamiltonian system with Hamiltonian H if and only if $\{I, H\} = 0$.

1.6 Symmetries

Consider the ODE $\dot{y} = f(y)$, $y \in \mathbb{R}^N$. A diffeomorphism S is a symmetry of f if

$$S'f(y) = f(y) \circ S. \tag{1.21}$$

The significance of symmetries for the dynamics includes:

- symmetries map solutions to solutions;
- the fixed set of a symmetry is invariant, which can be useful for finding special (“symmetric”) solutions; and
- when the system is Hamiltonian and has a symplectic symmetry S , the system has a lot of other special properties as well.

The linear or affine symmetries of an ODE are those for which the function S in (1.21) is linear or affine. An example of such a symmetry is given using the

pendulum,

$$\dot{q} = p, \tag{1.22}$$

$$\dot{p} = -\sin(q). \tag{1.23}$$

Setting

$$y = \begin{bmatrix} q \\ p \end{bmatrix},$$

then $S(y) = -y$ is a symmetry of the pendulum equation (1.22).

To see that S is a symmetry of the pendulum we write the mapping out in full,

$$\begin{bmatrix} q \\ p \end{bmatrix} \mapsto \begin{bmatrix} -q \\ -p \end{bmatrix}.$$

The pendulum (1.22) becomes,

$$-\dot{q} = -p,$$

$$-\dot{p} = -\sin(-q),$$

and multiplying both sides of each equation by -1 we get,

$$\dot{q} = p,$$

$$\dot{p} = \sin(-q) = -\sin(q), \quad (\text{since } \sin(q) \text{ is an odd function}),$$

which is just the equations of the original system. In geometric terms, the symmetry S in this example is just a rotation of the phase space by π . This can be seen from looking at phase portrait of the pendulum in Figure 1.11 or more easily seen from the exact solution of the pendulum in Figure 1.24. Also we notice that the phase portrait is symmetric about the lines $q = 0$ and $p = 0$. These reflection symmetries are described in Section 1.7. A composition of these two reflections gives the π rotation symmetry.

1.7 Reversible Differential Equations

An ODE $\dot{y} = f(y)$, $y \in \mathbb{R}^N$ possesses the time-reversal symmetry R , where R is a diffeomorphism, if it is invariant under

$$\begin{cases} y & \rightarrow R(y) \\ t & \rightarrow -t \end{cases}.$$

For example, for conservative mechanical systems [36], such as Hamiltonian systems, this means that inverting the direction of the velocity vector and keeping the initial position the same does not change the solution trajectory, but only inverts the direction of motion.

All second order differential equations $\ddot{u} = g(u)$ written as a first order system, $\dot{u} = v$, $\dot{v} = g(u)$ are reversible.

It was mentioned in Section 1.6 that the pendulum has two other obvious symmetries, other than that of the example given in that section. These reflection symmetries are time-reversing symmetries. We show that one of these reflections is a time-reversing symmetry for the pendulum (1.22). If we have the mapping

$$\begin{bmatrix} q(t) \\ p(t) \end{bmatrix} \mapsto \begin{bmatrix} q(-t) \\ -p(-t) \end{bmatrix},$$

the pendulum, (by the chain rule), becomes,

$$\begin{aligned} -\dot{q}(-t) &= -p(-t), \\ \dot{p}(-t) &= -\sin(q(-t)), \end{aligned}$$

and multiplying the first equation by -1 , we get

$$\begin{aligned} \dot{q}(-t) &= p(-t), \\ \dot{p}(-t) &= -\sin(q(-t)). \end{aligned}$$

This symmetry corresponds to an up-down flip of the phase portrait. The left-right flip of the phase portrait can similarly be shown to be a time-reversing symmetry.

As seen from the examples in this section and the previous one, a system may possess more than one symmetry or time-reversing symmetry. The combined set of all symmetries and reversing symmetries of a system is called its reversing symmetry group. The reversing symmetry group of the pendulum is a four-element group, the Vierergruppe

$$\left\{ Id, S \left(\begin{bmatrix} q \\ p \end{bmatrix} \right) = \begin{bmatrix} -q \\ -p \end{bmatrix}, R_1 \left(\begin{bmatrix} q \\ p \end{bmatrix} \right) = \begin{bmatrix} q \\ -p \end{bmatrix}, R_2 \left(\begin{bmatrix} q \\ p \end{bmatrix} \right) = \begin{bmatrix} -q \\ p \end{bmatrix} \right\}.$$

1.8 Geometric Integrators

We have seen that ODEs often have geometric properties such as symplecticity, first integrals, and (reversing) symmetries. All the ODEs with a particular set of such properties form a class, and may share dynamical features that are not shared by ODEs not in the class. It is therefore natural to ask, when solving such a system, whether or not these intrinsic properties are preserved by the numerical method. This question has been greatly addressed over the last decade, and methods by which structural properties are preserved now come under the title of ‘geometric integrators’. Other properties of interest, not already mentioned include, but are not limited to, preservation of phase space volume, energy, momentum, and dissipation.

Geometric integrators fall into two main categories [65]. There are integrators which happen to preserve a property when present in any system and integrators which are intentionally designed to preserve a specific property or properties common to special classes of systems. For example, the implicit midpoint rule automatically preserves all quadratic integrals.

More and more interest has grown in methods [80] that are custom-built to preserve qualitative features of systems of ODEs. This has led to symplectic integrators for Hamiltonian systems, volume-preserving integrators for divergence free ODEs, integral-preserving integrators for systems containing first integrals, or constants of motion, as they are sometimes known, and integrators that preserve both symmetries and time-reversing symmetries. See [37, 66, 10, 68] for an introduction to geometric integrators.

Preservation of these geometric properties is important for the long-term stability of dynamical systems. For general methods, that may not preserve geometric properties, the small errors tend to accumulate which can lead to qualitatively wrong results. For example, bounded orbits may become unbounded, or dissipation could be introduced. By using special purpose methods we reduce these errors producing more accurate results.

1.8.1 Symplectic Integrators

A numerical method is called symplectic if [38] the Jacobian of the numerical flow $\Phi_h(p_n, q_n) = (p_{n+1}, q_{n+1})$ satisfies,

$$\Phi'_h(p, q)^T J^{-1} \Phi'_h(p, q) = J^{-1}.$$

Or, in wedge product notation,

$$dp_{n+1} \wedge dq_{n+1} = dp_n \wedge dq_n$$

is preserved exactly. In other words, the wedge product at one step of the method is equal to the wedge product at the previous step.

As was previously stated, the flow map of a Hamiltonian system is symplectic. Therefore, when solving such a system, we choose to use a symplectic integrator, thereby preserving the symplectic structure and improving the qualitative solution compared with a general method. The papers [58, 87] give introductions to symplecticity and give some examples of symplectic integrators.

The condition for being symplectic is more general than the condition for being a Hamiltonian flow map. There exist symplectic maps that are not the flow of any Hamiltonian system. Although this is the case, symplectic methods impose conditions so restrictive that some integrals of the flow may also be preserved. For example, symplectic methods [23] exactly conserve a nearby Hamiltonian and this ensures long-time approximate conservation of energy, a first integral of a Hamiltonian system. A more detailed explanation for this is given in Section 1.11.1. Symplectic integrators generally only show this

desirable behaviour when using fixed step size implementation. The paper [38] gives an example of symplectic integration using the leapfrog method.

To compare the qualitative results of a symplectic integrator and a non-symplectic integrator we use the harmonic oscillator as an example. The Hamiltonian is $H(q, p) = \frac{1}{2} (p^2 + q^2)$, and the equations of motion are,

$$\dot{p} = -q, \quad \dot{q} = p.$$

In Figure 1.13 we plot the exact solution of the system, along with the solution from a non-symplectic integrator and a symplectic integrator. The exact solution (left graph) gives a series of closed or periodic orbits. Comparing the non-symplectic integrator solution (middle graph) with this exact solution (left graph), it can be seen that it gives completely wrong behaviour. The exact solution gives a series of level curves which are periodic, whereas the Euler method gives a solution which spirals out clockwise from the centre. In this case, it would be expected that the energy error from this method would grow very fast and become unbounded. The graph on the left in Figure 1.14 confirms this, showing exponential energy error. Now, comparing the symplectic integrator solution with the exact solution, it can be seen that they both give a solution with a series of periodic solutions. The symplectic method does not exactly lie on the orbits of the exact solution, but at least it gives the right qualitative behaviour. Here, it would be expected that the energy error is bounded. This is confirmed in the left graph of Figure 1.14, showing approximate conservation of the energy or Hamiltonian of the system, as expected for symplectic integrators for Hamiltonian ODEs.

One way of constructing symplectic methods for Hamiltonian systems is by splitting the Hamiltonian into a sum of simpler Hamiltonians,

$$H(\mathbf{z}) = \sum_{i=1}^k H_i(\mathbf{z}),$$

such that each Hamiltonian vector field $\dot{\mathbf{z}} = J\nabla_{\mathbf{z}}H_i(\mathbf{z})$ is explicitly solvable. A symplectic integrator can then be derived by an appropriate composition of the flow maps. The method is symplectic since the flow map is symplectic and a composition of symplectic flow maps, produces a symplectic map.

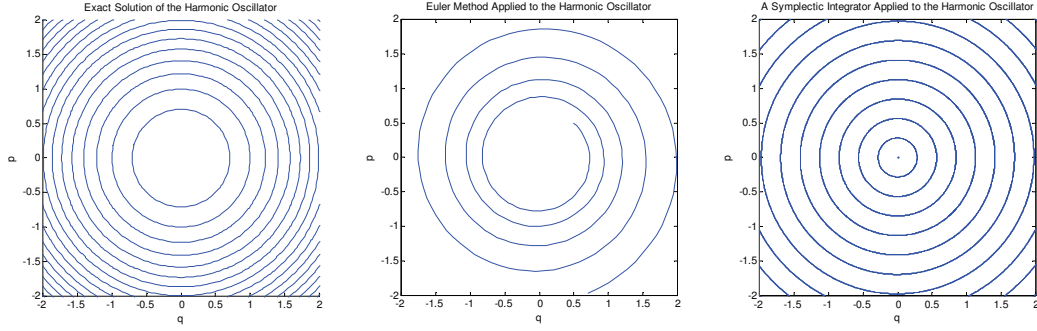


Figure 1.13: Exact solution of the harmonic oscillator (left), compared with two numerical solutions, the Euler method - solution spirals out clockwise from the centre (middle) and a symplectic integrator (right).

Using the harmonic oscillator with Hamiltonian $H(q, p) = \frac{1}{2} (p^2 + q^2)$ as an example again, the energy H can be split into its kinetic and potential terms,

$$H = H_1 + H_2, \quad H_1 = \frac{1}{2}p^2, \quad H_2 = \frac{1}{2}q^2.$$

Now, H_1 and H_2 are exactly integrable. The equations of motion for H_1 are

$$\begin{aligned} \dot{p} &= -\frac{\partial H_1}{\partial q} = 0 \\ \dot{q} &= \frac{\partial H_1}{\partial p} = p, \end{aligned}$$

which has flow map,

$$\varphi_{t, H_1} \left[\begin{pmatrix} p \\ q \end{pmatrix} \right] = \begin{pmatrix} p \\ q + tp \end{pmatrix}.$$

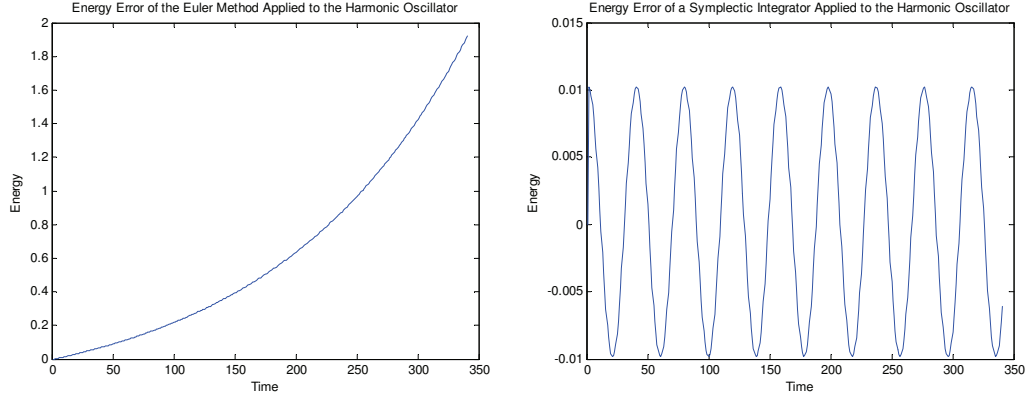


Figure 1.14: Energy error of the Euler method (left) and a symplectic integrator (right) when applied to the harmonic oscillator.

Similarly, the equations of motion of H_2 are

$$\begin{aligned}\dot{p} &= -\frac{\partial H_1}{\partial q} = -q \\ \dot{q} &= \frac{\partial H_1}{\partial p} = 0.\end{aligned}$$

So, H_2 has flow map,

$$\varphi_{t,H_2} \left[\begin{pmatrix} p \\ q \end{pmatrix} \right] = \begin{pmatrix} p - tq \\ q \end{pmatrix}.$$

Since each map is the flow map of a Hamiltonian system, each is symplectic.

Therefore the map,

$$\Phi_h = \varphi_{h,H_1} \circ \varphi_{h,H_2},$$

is symplectic.

This type of splitting into explicitly solvable subproblems may not always be possible. If it is not possible, but the system still possesses some kind of partitioning then an effective scheme may still be able to be constructed by

substituting a symplectic method for the exact flow at some stage. If splitting is not possible, then symplectic Runge–Kutta and symplectic partitioned Runge–Kutta methods can be constructed.

The splitting derived above can be used on all systems with a separable Hamiltonian of the form,

$$H(q, p) = T(p) + V(q),$$

where $T(p)$ is the kinetic energy and $V(q)$ the potential energy of the system.

Following the example for the harmonic oscillator, we naturally split the Hamiltonian into its kinetic and potential parts,

$$H_1(p) = T(p), \quad H_2(q) = V(q).$$

The equations of motion for H_1 , the kinetic term, are

$$\begin{aligned} \dot{p} &= \mathbf{0}, \\ \dot{q} &= \nabla_p T(p). \end{aligned}$$

Since p is constant along solutions and q varies linearly in time, the above equations are completely integrable. The flow map is

$$\varphi_{t,V}(p, q) = \begin{pmatrix} p \\ q + t\nabla_p T(p) \end{pmatrix}.$$

Similarly, for the potential term, H_2 , the equations of motion are

$$\begin{aligned} \dot{p} &= -\nabla_q V(q), \\ \dot{q} &= \mathbf{0} \end{aligned}$$

and the flow map is,

$$\varphi_{t,T}(p, q) = \begin{pmatrix} p - t\nabla_q V(q) \\ q \end{pmatrix}.$$

Now, the composition of these two maps,

$$\Phi_h = \varphi_{h,T} \circ \varphi_{h,V},$$

where $t = h$, is a symplectic map.

The splitting methods given above are first order symplectic methods. A second order symplectic method can also be constructed by the following splitting,

$$H = H_1 + H_2 + H_3,$$

with,

$$H_1 = T(p)$$

$$H_2 = V(q)$$

$$H_3 = T(p).$$

Taking the composition,

$$\Phi_h = \varphi_{\frac{1}{2}h, T} \circ \varphi_{h, V} \circ \varphi_{\frac{1}{2}h, T},$$

and simplifying we get the well known leapfrog method,

$$\begin{aligned} q_{n+\frac{1}{2}} &= q_n + \frac{1}{2}h\nabla_p T(p_n) \\ p_{n+1} &= p_n - h\nabla_q V(q_{n+\frac{1}{2}}) \\ q_{n+1} &= q_{n+\frac{1}{2}} + \frac{1}{2}h\nabla_p T(p_{n+1}). \end{aligned}$$

Higher order splitting methods are constructed in [98].

1.8.2 Preserving First Integrals

Numerical integrators used for preserving first integrals tend to be quite costly, as they are generally implicit, and do not typically give a qualitative solution as accurate as using simpler and more easily implemented symplectic methods. However, there are still good reasons for preserving some integrals of a system. Preserving first integrals [79] is important because of their physical relevance and also because they can ensure long-term stabilising effects. They also play a significant role in determining which bifurcations generically occur. In particular, it is important that a first integral be preserved if the dimension of the

system is low, if the integration time is very long, or if the integral-surface is compact.

All methods that are of practical use, such as all explicit and implicit Runge–Kutta methods, exactly conserve linear invariants, and a specific class of Runge–Kutta methods exactly conserve quadratic invariants.

Conservation laws for Hamiltonian systems with symmetry [31] are usually destroyed by a numerical integrator in time. This could possibly lead to physically impossible solutions or numerical instability. Therefore, for Hamiltonian systems with symmetry it is important that physically consequential integrals are preserved when applying a numerical integrator. Integrators that do this are usually called conserving integrators.

1.8.3 Symmetric and Time-Reversible Integrators

The flow φ_t of an ODE $\dot{y} = f(y)$, $y(t_0) = y_0$ satisfies

$$\varphi_{-t}^{-1} = \varphi_t.$$

Generally, the map Φ_h of a numerical integrator [36] does not share this property. Those that do are called symmetric integrators. We will see below that symmetric integrators are useful for constructing integrators that preserve reversing symmetries.

It is important to preserve symmetries because non-generic bifurcations can become generic in the presence of symmetries, and vice versa. In addition, reversing symmetries give rise to the existence of invariant tori and invariant cylinders. The adjoint method is important in understanding the concept of symmetry.

Definition 1.8.1. *The adjoint method Φ_h^* of an integrator Φ_h is defined as*

$$\Phi_h^* = \Phi_{-h}^{-1}.$$

In words, the adjoint method is the inverse map of the original method with reversed time step.

A method which satisfies

$$\Phi_h^* = \Phi_h$$

is called symmetric.

The adjoint method has the same order and same absolute value of the leading error term as the original method. As an example, the implicit midpoint (1.9) and the trapezoidal (1.8) method are symmetric methods, whereas the implicit Euler and the explicit Euler method are not symmetric methods. We show that the implicit midpoint rule is symmetric and the explicit Euler method is not symmetric.

For the implicit midpoint method $\Phi_h = y_n + hf(\frac{1}{2}(y_n + y_{n+1}))$. The inverse Φ_h^{-1} is obtained by swapping y_n and y_{n+1} , so the adjoint method Φ_{-h}^{-1} is,

$$\begin{aligned} y_n &= y_{n+1} - hf(\frac{1}{2}(y_{n+1} + y_n)) \\ \Rightarrow y_{n+1} &= y_n + hf(\frac{1}{2}(y_n + y_{n+1})), \end{aligned}$$

which is the implicit midpoint method. Hence it is symmetric.

For the explicit Euler method $\Phi_h = y_n + hf(y_n)$, the adjoint method Φ_{-h}^{-1} is

$$\begin{aligned} y_n &= y_{n+1} - hf(y_{n+1}) \\ \Rightarrow y_{n+1} &= y_n + hf(y_{n+1}), \end{aligned}$$

which is the implicit Euler method, so the explicit Euler method is not symmetric; neither is the implicit Euler method. But the explicit Euler and implicit Euler method are adjoint methods of each other.

If a method is not symmetric, a symmetric method can easily be constructed by composing a half step of the method with a half step of its adjoint method. The method

$$\hat{\Phi}_h = \Phi_{\frac{1}{2}h}^* \circ \Phi_{\frac{1}{2}h}, \tag{1.24}$$

is symmetric. We illustrate this by taking Φ_h as the implicit Euler method

and Φ_h^* as the explicit Euler method then (1.24) becomes,

$$\begin{aligned}y_{n+\frac{1}{2}} &= y_n + \frac{1}{2}hf(y_n) \\y_{n+1} &= y_{n+\frac{1}{2}} + \frac{1}{2}hf(y_{n+1}).\end{aligned}$$

Substituting the first equation into the second equation we get,

$$\begin{aligned}y_{n+1} &= y_n + \frac{1}{2}hf(y_n) + \frac{1}{2}hf(y_{n+1}) \\&= y_n + \frac{1}{2}h(f(y_n) + f(y_{n+1}))\end{aligned}$$

which is the implicit midpoint rule. We showed this was a symmetric method earlier, so the composition of the implicit Euler and the explicit Euler gives the symmetric implicit midpoint method.

Linear or affine symmetries are preserved by all Runge–Kutta methods, and linear or affine time-reversing symmetries are preserved by all symmetric Runge–Kutta methods.

1.9 *N*-Body Simulations Using a Symplectic Integrator

Any numerical experiment performed should be reproducible. As an introduction to symplectic integration the following two sections contain reproductions of simulations from the literature.

1.9.1 The Leapfrog Method Applied to the Lennard–Jones Potential

In this numerical experiment we simulate a molecular dynamics system using the Lennard–Jones potential.

The Lennard–Jones Potential

The Lennard–Jones potential was developed in 1924 to model pairs of uncharged atoms or molecules. A pair of neutral atoms is subject to two distinct

forces. At close range two atoms will be strongly repulsive, and at a distance from each other the two atoms will possess a weak attractive force. As a consequence of the strong repulsive force we would expect that the particles never collide with each other, since once two particles get close enough to each other the forces will take over and the particles will repel each other before they get a chance to touch.

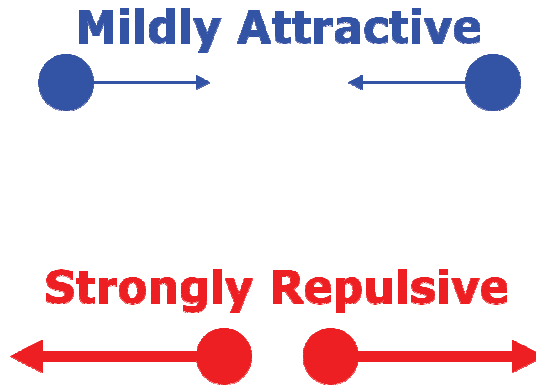


Figure 1.15: The attractive and repulsive forces of the Lennard–Jones potential.

The Lennard–Jones potential is given by

$$\varphi_{\text{L.J.}}(r) = \epsilon \left[\left(\frac{\bar{r}}{r} \right)^{12} - 2 \left(\frac{\bar{r}}{r} \right)^6 \right], \quad (1.25)$$

where:

- φ is the intermolecular pair potential between two particles;
- r is the atomic separation between two particles;
- ϵ is the well depth (or energy); and
- \bar{r} is the equilibrium atomic separation (the value of r at which $\varphi'(r) = 0$).

The $\left(\frac{\bar{r}}{r} \right)^{12}$ term in (1.25) is the repulsive term and the term $\left(\frac{\bar{r}}{r} \right)^6$ is the attractive term.

The Simulation

In this experiment, we aim to replicate the two-dimensional Lennard–Jones experiment given in [53] and study the rearrangement of particles over time. N is the number of particles to be studied.

The equations of motion for a two-dimensional Lennard–Jones system with Lennard–Jones potential (1.25) is a molecular dynamics problem given by,

$$\begin{aligned}\dot{q}_i &= p_i, \\ \dot{p}_i &= - \sum_{i \neq j} \frac{\varphi'_{\text{L.J.}}(r_{ij})}{r_{ij}} (q_i - q_j), \quad i = 1, 2, \dots, N,\end{aligned}$$

where $r_{ij} = \|q_i - q_j\|$.

In our simulation we take $\epsilon = 1$ and $\bar{r} = 1$, so we get,

$$\varphi_{\text{L.J.}}(r_{ij}) = r_{ij}^{-12} - 2r_{ij}^{-6},$$

and,

$$\varphi'_{\text{L.J.}}(r_{ij}) = -12r_{ij}^{-13} + 12r_{ij}^{-7}.$$

The leapfrog method was used to simulate a simplified molecular system consisting of N equal mass particles interacting via a Lennard–Jones potential. The particles were placed on a regular Cartesian lattice, with each particle perturbed slightly from its exact lattice position. This was the initial configuration of the particles for the simulation. Next, the simulation was run using the leapfrog method.

Conclusions

Figure 1.16 gives snapshots of the dynamics of the system with $N = 169$ particles at various times during the simulation. After 1 step we see the particles in their almost lattice positions. By 150 steps we see that the corners of the lattice are starting to change shape and the four particles in each corner tend to be forming a more diamond-shaped configuration than a square one. By the time 200–250 steps have been taken we see triangles forming in the once

Cartesian lattice and by 400 steps a triangular lattice takes over the most part of the original Cartesian lattice.

Once formed, the particles tend to stay at this triangular lattice configuration. We also notice that the triangular lattice configuration is not entirely uniform with gaps forming amongst particles in the configuration. At 400 and 600 steps we see some of these gaps separating the triangular lattice.

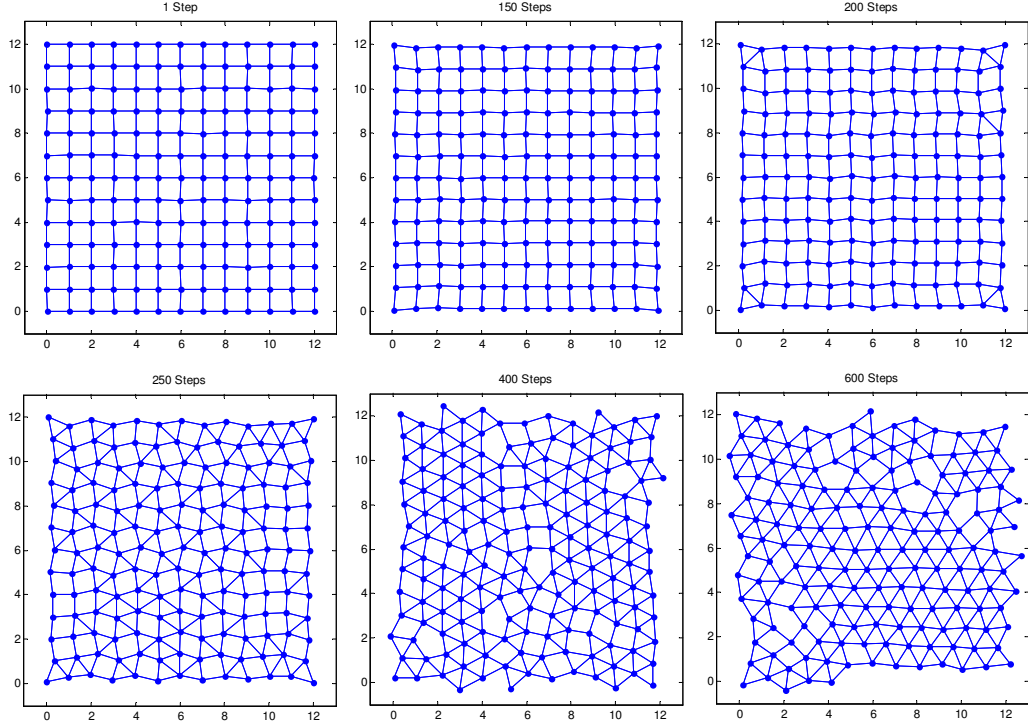


Figure 1.16: Results of the simulation: Snapshots of the dynamics of the two-dimensional Lennard–Jones system.

As can be seen from the snapshots of the simulation in Figure 1.16, the Cartesian lattice is not a stable equilibrium structure for the Lennard–Jones system. If it were we would expect the particles to oscillate chaotically about their lattice sites, but instead the system rearranges itself into a more favourable configuration which is near a triangular lattice. At this energy level, the particles are mostly held together by the attractive effect of the Lennard–Jones potential, although it is possible for particles to be ejected occasionally from

the group.

The energy error for 50000 time steps is plotted in 1.17. The error is bounded so we expect that our numerical solution is giving good long-time behaviour.

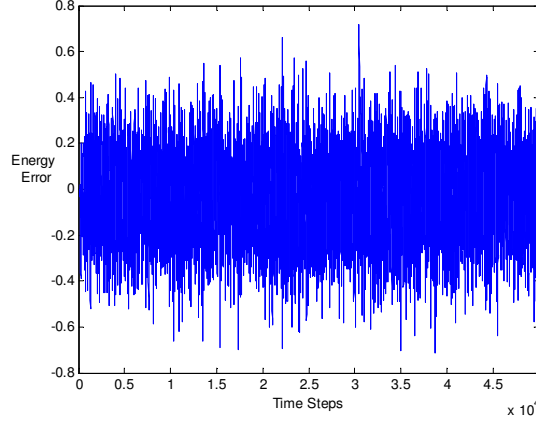


Figure 1.17: Energy error of the two-dimensional Lennard–Jones system.

1.9.2 The Outer Solar System

The outer solar system is modeled as an N -body problem using data from [37]. The model used is based on 6 bodies: The sun and the five outer planets, Jupiter, Saturn, Uranus, Neptune, and Pluto. See Figure 1.18 for a diagram of the initial position of the planets. The entire system orbits around the centre of mass of the system.

The equations of motion of the solar system are

$$\begin{aligned}\dot{q}_i &= \frac{p_i}{m_i}, \\ \dot{p}_i &= - \sum_{j=1, j \neq i}^{10} \frac{Gm_i m_j (q_i - q_j)}{\|q_i - q_j\|^3}, \quad i = 1, 2, \dots, N,\end{aligned}$$

with Hamiltonian,

$$H(p, q) = \frac{1}{2} \sum_{i=1}^6 \frac{1}{m_i} p_i^T p_i - G \sum_{i=1}^5 \sum_{j=i+1}^6 \frac{m_i m_j}{\|q_i - q_j\|},$$

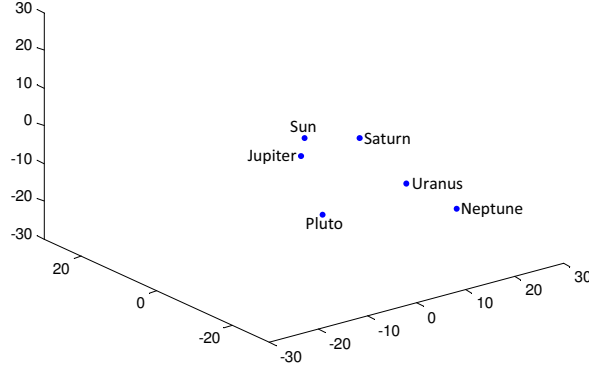


Figure 1.18: The initial position of the outer planets relative to the sun.

where $q_i \in \mathbb{R}^3$ are the positions coordinates of body i , $p_i \in \mathbb{R}^3$ are the momenta, m_i are the masses of each body i , and $G = 2.95912208286 \times 10^{-4}$ is the gravitational constant (values from [37]).

The masses of the planets are given relative to the mass of the sun, so that the sun has mass 1. However, in this simulation the mass of the sun is very slightly greater than 1 to account for the inner planets, which are not included in the simulation. The initial position for the sun is $q_1(0) = (0, 0, 0)^T$ and the initial velocity is $\dot{q}_1(0) = (0, 0, 0)^T$. The initial data for the planets is given in the table in [37]. For the simulation the velocities are converted to momenta. See Figure 1.19 for the orbits of the planets after the simulation has been run with a step size of $h = 20$ days.

When doing any numerical experiment it is important to calculate the energy in order to determine whether or not the simulation gives qualitatively correct behaviour. Figure 1.20 gives the energy error for the simulation of 10000 steps. It appears that the energy fluctuates but is bounded, which is good for our results. In order to confirm that the energy error remains bounded and does not grow with time, we plot the energy error for a million steps in Figure 1.21. In this figure we see that the energy does remain bounded within a narrow band. The total energy of the system in this simulation is 2.2075×10^{-5} .

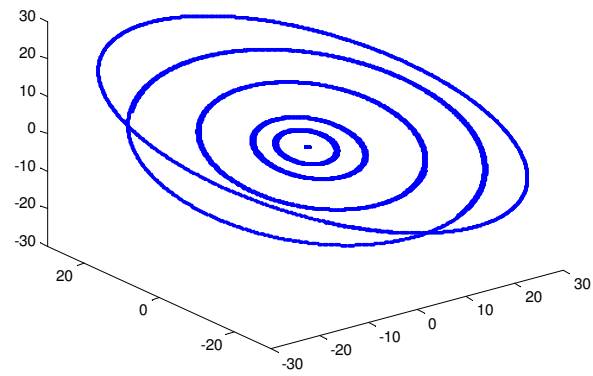


Figure 1.19: Orbits of the outer solar system.

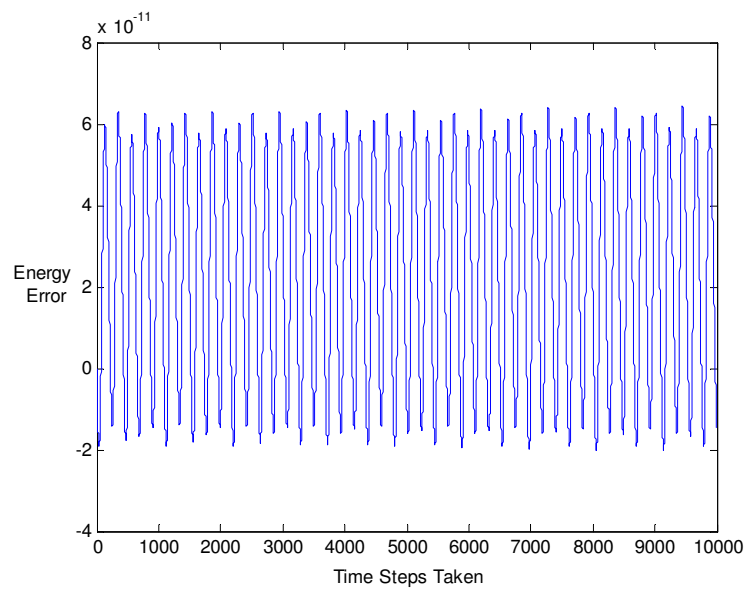


Figure 1.20: The energy error of the outer solar system after 10000 time steps.

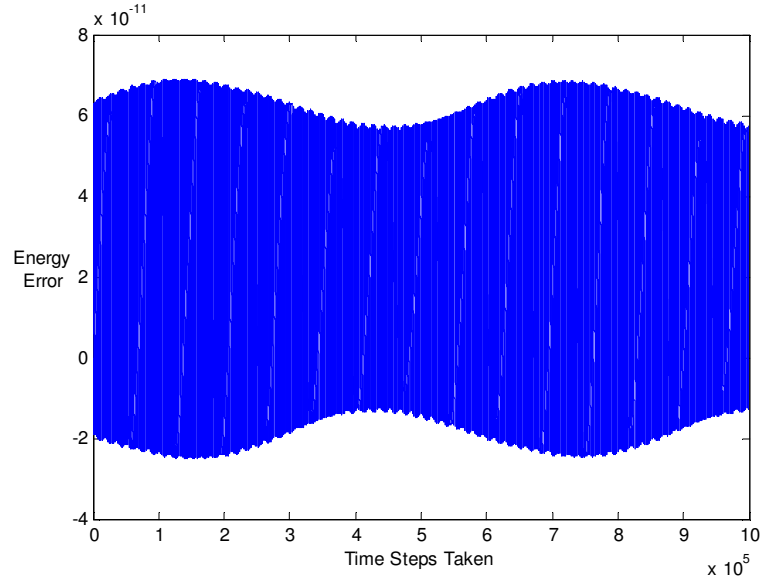


Figure 1.21: The energy error of the outer solar system after 1000000 time steps.

We expect the planets to travel around the sun in bounded, close-to-elliptical orbits as occurs in “real world”. In Figure 1.19 we see that our simulation does orbit the sun in close to elliptical orbits.

1.10 Conservation Laws

First integrals and symplecticity can both be regarded as types of conservation laws for ODEs. These laws can be distinguished by where the law is evaluated. The first type of conservation law, or first integral, is evaluated on solutions to the system and can be written as

$$H_t = 0. \quad (1.26)$$

For Hamiltonian systems (1.26) is conservation of energy where H is the Hamiltonian. This was already proved in 1.5.

The second conservation law, symplecticity, for an ODE is the differential conservation law and is evaluated on solutions to the first variation of the

system. For an ODE the differential conservation law has the form

$$\omega_t = 0, \tag{1.27}$$

where ω is the usual 2-form.

For Hamiltonian ODEs (1.27) is simply conservation of symplecticity, which is inherent to all Hamiltonian systems. A symplectic method will satisfy a discrete version of (1.27).

In general, any integrator that preserves a discrete analogue of any of the conservation laws is said to preserve the same property as the conservation law. For example, if the conservation law is conservation of energy and energy is preserved by a numerical method then the method is known as an energy preserving integrator.

In Section 2.3.1 the analogues of the energy and differential conservation laws for PDEs will be discussed.

1.11 Backward Error Analysis (BEA)

In this section we introduce backward error analysis for ODEs by first discussing its beginnings in numerical linear algebra and then make the extension to numerical integrators. Next, we introduce the form of the modified differential equation and truncation of the modified equations, which are needed to begin a formal analysis. We then give an example of a simple ODE integrated by the explicit Euler method and find the modified equation, displaying the solution of the modified differential equation at different order truncations. Finally, we look at the relationship between geometric properties of the ODE and the modified differential equation. In particular, we look at the modified Hamiltonian of symplectic integrators for Hamiltonian systems, and give an example using the symplectic Euler method applied to the pendulum.

1.11.1 Introduction

Backward error analysis (BEA) is a tool used to analyse the long-time behaviour of numerical integrators. The idea began in the field of numerical linear algebra, with Wilkinson [97] in 1960, and was extended to numerical integration in the late 80s and early 90s [33, 28, 85, 24, 99].

In numerical linear algebra backward error analysis is used as a way to calculate the accumulation of rounding errors in a variety of matrix algorithms.

An example of this is Gaussian elimination for solving a linear system of equations

$$A\mathbf{x} = \mathbf{b},$$

where A is an $N \times N$ invertible matrix of the coefficients of the unknown variables, $\mathbf{x} \in \mathbb{R}^N$ is a vector of the unknown variables, and $\mathbf{b} \in \mathbb{R}^N$ is known.

Quite often “real world” problems have real coefficients, which are expressed as decimal approximations. In this case, the problem being solved is only an approximation to the actual problem. That is, A and \mathbf{b} themselves have small measurement errors even before any calculations have been performed.

If the exact problem is being solved and all calculations are performed exactly then the Gaussian elimination method will produce exact solutions, but if finite digit arithmetic is used at each step of the Gaussian elimination method a rounding error is introduced at each step.

Then the resulting solution is the exact solution of a nearby system of equations.

The idea of backward error analysis can be extended to numerical integrators, whereby a linear system of equations is replaced by a system of differential equations. Instead of rounding errors in the linear algebra setting, we now get truncation errors introduced at each step of the method. And the solution obtained by a numerical method is the exact solution of a nearby system of differential equations. This nearby system is called the modified differential equation (MDE). This can be summarised in Figure 1.22, motivated by [37], where $\dot{y} = f(y)$ is an ODE with initial value $y(t_0) = y_0$, $\varphi_t(y_0)$ is the flow map of

the ODE, $\Phi_h(y)$ is a numerical method producing approximations y_0, y_1, y_2, \dots with step size h , and $\dot{y} = \tilde{f}_h(y)$ is the modified differential equation.

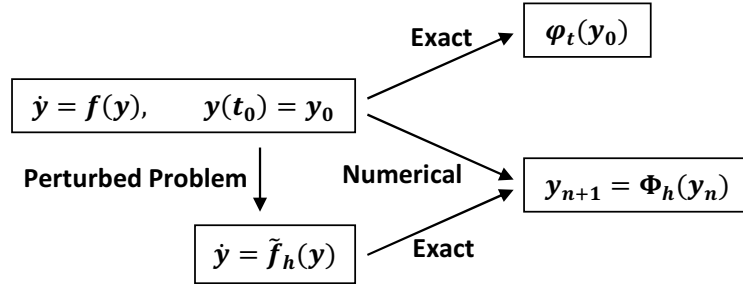


Figure 1.22: The MDE as the exact solution of a perturbed problem. This diagram is reproduced from [37].

If a geometric integrator is used, then the numerical solution is the exact solution of a perturbed system of differential equations satisfying the same geometric properties. For example, in Section 1.8.1, we said that when a symplectic integrator is applied to a Hamiltonian system we get long-time approximate conservation of energy (or the Hamiltonian). This approximate conservation of energy comes from the fact that we are applying a symplectic integrator to a Hamiltonian system, which itself is symplectic and hence the solution obtained from the method will be the exact solution of a nearby Hamiltonian system. Since this nearby system is Hamiltonian, then this system will have its own Hamiltonian or energy which will be conserved, giving approximate conservation of the original Hamiltonian system. The Hamiltonian of the nearby system is known as the modified Hamiltonian.

Backward error analysis is helpful when studying the qualitative behaviour of numerical methods and the consequences for long-time simulations. It is also useful for comparing the value of different methods.

The following sections involve initial value problems for ODEs and their numerical integrations.

1.11.2 The Modified Differential Equation (MDE)

The modified differential equation $\dot{y} = \tilde{f}_h(y)$ is a formal series in powers of the step size h and has the form,

$$\dot{y} = f(y) + hf_2(y) + h^2f_3(y) + \dots, \quad (1.28)$$

where $f(y)$ is the original vector field in the ODE and $f_2(y), f_3(y), \dots$ are functions to be determined.

Equation (1.28) is generally a divergent infinite series and needs to be truncated before any analysis can be made. Error is introduced by the truncation of this series, but this can be made exponentially small by ‘optimal truncation’. The optimal truncation index is found by putting bounds on the coefficient functions $f_j(y)$. The theorem for the existence of an optimal truncation is given in Theorem 1.11.1. A series possessing these properties is known as an asymptotic series.

Theorem 1.11.1. *Let $\dot{y} = \tilde{F}_N(y)$ where $\tilde{F}_N(y)$ is the $N - 1$ order truncation of the modified differential equation (1.28) given by,*

$$\tilde{F}_N(y) = f(y) + hf_2(y) + h^2f_3(y) + \dots + h^{N-1}f_N(y),$$

then there exists an $N = N(h)$ such that the difference between the numerical solution $y_1 = \Phi_h(y_0)$ and the exact solution of the truncated modified differential equation $\tilde{\varphi}_{N,h}(y_0)$ satisfy,

$$\|\Phi_h(y_0) - \tilde{\varphi}_{N,h}(y_0)\| \leq hc_1e^{c_2/h}$$

where $c_1, c_2 > 0$ are appropriate constants.

The proof and details are given in [37].

Note that for a finite truncation of the modified differential equation, as the number of terms increases in the truncation, the solution of the modified equation gets closer and closer to the numerical solution, up to the ‘optimal truncation’.

A formal backward error analysis begins with the construction and truncation of the modified differential equation and then a study of its properties in comparison to the original ODE.

To find the unknown functions $f_i(y)$, $i = 2, 3, \dots$ in the modified equation (1.28), the following steps are used.

1. $y(t + h)$ is expanded in a Taylor series.
2. The modified equation (1.28) and its derivatives are substituted into the expansion of $y(t + h)$.
3. Coefficients of like powers of h (from the previous step) are compared to the numerical method $\Phi_h(y)$ to find $f_i(y)$, $i = 2, 3, \dots$

Using the above steps, we get

1.

$$y(t + h) = y + h\dot{y} + \frac{h^2}{2!}\ddot{y} + \frac{h^3}{3!}y^{(3)} + \dots$$

2.

$$\begin{aligned} y(t + h) &= y + h\dot{y} + \frac{h^2}{2!}\ddot{y} + \frac{h^3}{3!}y^{(3)} + \dots \\ &= y + h(f(y) + hf_2(y) + \dots) + \frac{h^2}{2!}(f'(y)(f(y) + hf_2(y) + \dots) \\ &\quad + hf'_2(y)(f(y) + hf_2(y) + \dots)) \\ &= y + h(f(y) + hf_2(y) + \dots) \\ &\quad + \frac{h^2}{2!}(f(y) + hf_2(y) + \dots)(f'(y) + hf'_2(y) + \dots) + \dots \end{aligned} \tag{1.29}$$

3. Assume that the numerical method is some expansion of the form,

$$\Phi_h(y) = y + hf(y) + h^2d_2(y) + h^3d_3(y) + \dots \tag{1.30}$$

The functions $d_i(y)$ are usually made up of $f(y)$ and its derivatives. For the explicit Euler method we simply have $d_i(y) = 0$ for all $i \geq 2$.

Comparing coefficients of like powers in h in (1.30) and (1.29), we get from the h terms $f_2(y) = f'(y)$. This always occurs for consistent methods. We get $f_2(y)$ from the h^2 terms, $f_3(y)$ from the h^3 terms, and so on. The first two functions are given below.

$$f_2(y) = d_2(y) - \frac{1}{2!} f' f(y) \quad (1.31)$$

$$f_3(y) = d_3(y) - \frac{1}{3!} (f''(f, f)(y) + f' f' f(y)) - \frac{1}{2!} (f' f_2(y) + f_2' f(y)). \quad (1.32)$$

Notice that $f_2(y)$ appears in the formula for $f_3(y)$, so that the function $f_i(y)$, $i = 2, 3, \dots$ are defined recursively.

Using the definition of the Lie derivative,

$$(D_i g)(y) = g'(y) f_i(y), \quad (1.33)$$

where $f_1(y) = f(y)$ a general formula for all $f_i(y)$ can be defined. By using the Lie derivative (1.33), equations (1.31) and (1.32) can be rewritten as

$$\begin{aligned} f_2(y) &= d_2(y) - \frac{1}{2!} (D_1 f_1)(y) \\ f_3(y) &= d_3(y) - \frac{1}{3!} (D_1^2 f_1)(y) - \frac{1}{2!} (D_2 f_1 + D_1 f_2)(y). \end{aligned}$$

Lemma 1.11.1. *If the numerical method has an expansion of the form $\Phi_h(y) = y + hf(y) + h^2 d_2(y) + h^3 d_3(y) + \dots$ then the functions $f_i(y)$, $i = 2, 3, 4, \dots$ of the modified differential equation (1.28) satisfy*

$$f_i(y) = d_i(y) - \sum_{j=2}^i \frac{1}{j!} \sum_{k_1 + \dots + k_j = i} (D_{k_1} \dots D_{k_{j-1}} f_{k_j})(y),$$

where $k_m \geq 1 \ \forall m$. Notice the right hand side involves only $f_k(y)$ where $k < j$.

A proof can be found in [37].

As a simple example we calculate the modified equation for a specific ODE, $\dot{y} = y^2$, $y(0) = 1$, using the explicit Euler method, $\Phi_h(y) = y + hf(y)$, with step size $h = 0.02$. The steps are the same as the above, for the general case,

except in step 3, we can use the equations (1.2) and (1.3) to find $f_2(y)$ and $f_3(y)$ and put $d_2(y) = 0$ and $d_3(y) = 0$ and substitute $f(y) = y^2$ from the ODE given. We get

$$\begin{aligned} f_2(y) &= -y^3 \\ f_3(y) &= -y^4 - \frac{1}{3}(2yf_2(y) + f_2'(y)y^2), \end{aligned}$$

where $f_3(y)$ is defined recursively, but can be written out explicitly by substituting in $f_2(y)$ and its derivative, to get

$$f_3(y) = \frac{3}{2}y^4.$$

Therefore the modified equation for the explicit Euler method applied to $\dot{y} = y^2$ is,

$$\dot{y} = y^2 - hy^3 + h^2\frac{3}{2}y^4 + \dots \quad (1.34)$$

The solution of the truncated modified equation (1.34) can now be compared with the numerical solution. This is shown in Figure 1.23 for different truncations of (1.34). As expected, the solutions of the truncated modified equation (1.34) get closer to the solution of the Euler method as the number of terms in the truncation increases. The blue curve gives the truncation after one term, which is equivalent to the exact solution. The blue curve is far away from the red curve, which gives Euler's method. The green curve gives the truncation after two terms of (1.34) and is much closer to the numerical solution (red curve) than the blue curve. Truncation after three terms gives the solution corresponding to the yellow curve, which lies almost exactly on the numerical solution.

1.11.3 Geometric Properties and the Modified Differential Equation

All proofs for the following theorems can be found in [37].

Theorem 1.11.2 (Modified Equations of Symmetric Methods). *The coefficient functions of the modified equation of a symmetric method satisfy $f_i(y) = 0$*

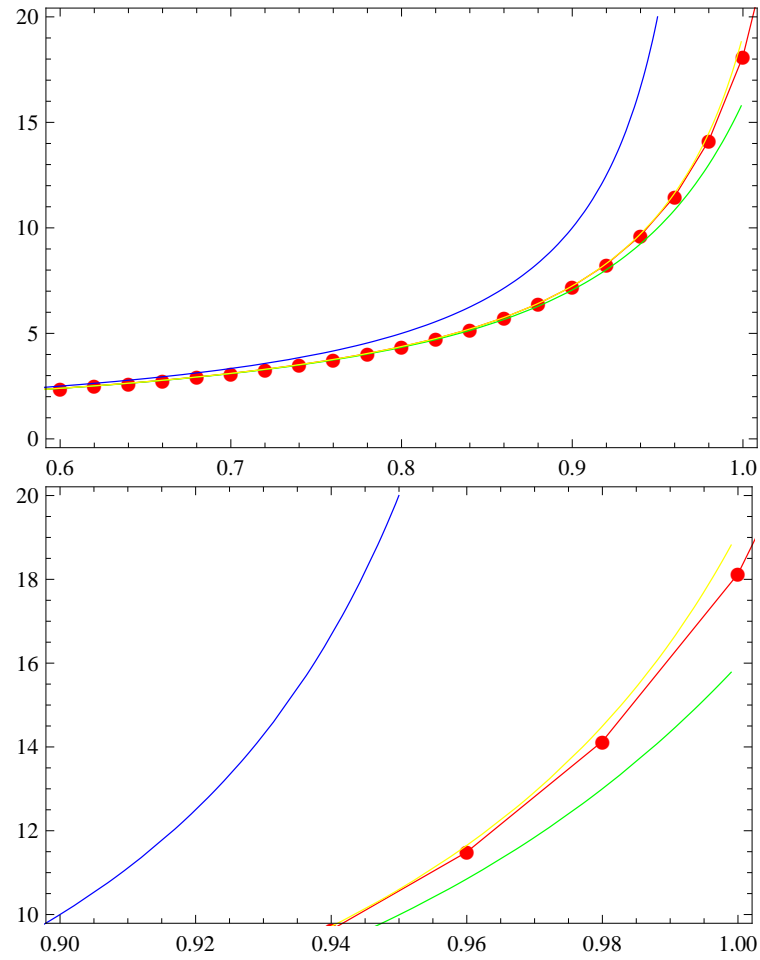


Figure 1.23: Comparison of truncated solutions of the modified differential equation (1.34) and the numerical solution from Euler's method (red) of the equation $\dot{y} = y^2$, $y(0) = 1$. The blue curve gives the truncation after the 1st term (or the exact solution), the green curve the truncation after the 2nd term, and the yellow curve the truncation after the 3rd term.

whenever i is even, so that the modified differential equation (1.28) has an expansion in even powers of h .

Theorem 1.11.3 (Modified Equations of Reversible Methods). *Let $\dot{y} = f(y)$ be a ρ -reversible differential equation and $\Phi_h(y)$ a ρ -reversible method. Then every truncation of the modified differential equation (1.28) is ρ -reversible.*

Theorem 1.11.4 (Modified Equations of Symplectic Methods). *If a symplectic method $\Phi_h(y)$ is applied to a Hamiltonian system with a smooth Hamiltonian $H : \mathbb{R}^{2N} \rightarrow \mathbb{R}$, then the modified equation (1.28) is also Hamiltonian. That is, there exist smooth functions $H_i : \mathbb{R}^{2N} \rightarrow \mathbb{R}$, $i = 2, 3, \dots$, such that $f_i(y) = J^{-1}\nabla H_i(y)$.*

So for numerical methods applied to Hamiltonian systems $\dot{y} = J^{-1}\nabla H(y)$ the corresponding modified differential equation is also Hamiltonian and its Hamiltonian has the form

$$\tilde{H}(y) = H(y) + hH_2(y) + h^2H_3(y) + \dots$$

Figure 1.24 gives the exact solution of the pendulum and its modified Hamiltonian, truncated up to order h^2 , for the symplectic Euler Method for different values of the step size h . The phase portraits are given by the coloured lines and the symplectic Euler method in black. It is well known that for sufficiently small step sizes, a symplectic integrator for a Hamiltonian ODE gives good long-time behaviour. The figure on the top left gives the phase portrait of the exact Hamiltonian of the pendulum. On the top right is the phase portrait of the modified Hamiltonian for small step size $h = 0.1$. Here the solution is almost exactly the same as that for the exact Hamiltonian and the symplectic Euler method almost matched the modified Hamiltonian. Moving down to the bottom left, we have the symplectic Euler method and phase portrait of the modified Hamiltonian for a relatively large step size $h = 0.7$. Here the symplectic Euler method is starting to show chaos at the fixed points $(q, p) = (-\pi, 0)$ and $(q, p) = (\pi, 0)$. Other than that, the method and the modified Hamiltonian almost match up showing a solution which is getting

distorted, but still giving the correct qualitative behaviour. Finally, the figure in the bottom right gives the phase portrait of the modified Hamiltonian and the symplectic Euler method for large step size $h = 1$. Here, the method shows chaos, but the modified Hamiltonian still seems to show the correct qualitative behaviour. Therefore, the modified Hamiltonian seems to converge for some values, but not where the numerical method is chaotic.

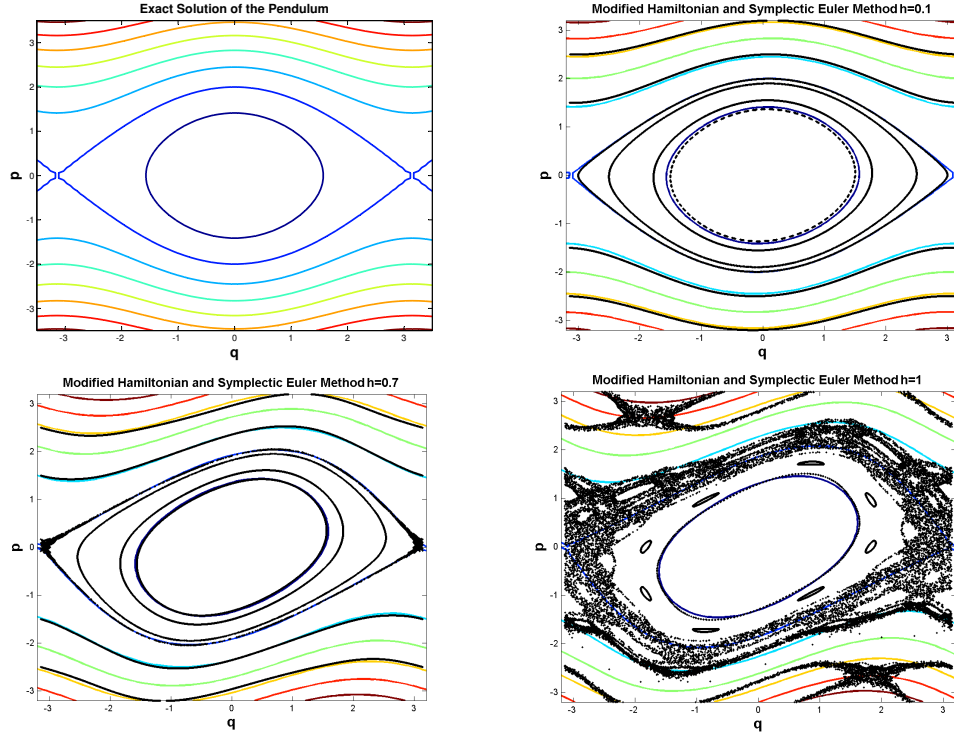


Figure 1.24: Solution of the pendulum and its modified Hamiltonian for the symplectic Euler method.

Theorem 1.11.5 (Modified Equations of First Integrals). *Let $\dot{y} = f(y)$ be a differential equation with first integral $I(y)$, i.e., $\nabla I(y)^T f(y) = 0$ for all y . If the numerical method also preserves this first integral, then every truncation of the modified equation (1.28) has $I(y)$ as a first integral.*

The converse is also true. That is, if $I(y)$ is a first integral of the differential equation $\dot{y} = f(y)$ and every truncation of the modified equation (1.28) has $I(y)$ as a first integral, then the numerical method preserves $I(y)$ exactly.

See [40] for a thorough discussion of geometric properties of modified equations.

1.11.4 Long-Time Energy Conservation

The basis for thorough statements concerning the long-time behaviour of numerical solutions involves estimating the difference between the numerical solution and the exact solution of the modified differential equation.

We can look at this idea through the study of the long-time energy conservation of symplectic methods applied to Hamiltonian systems $\dot{y} = J^{-1}\nabla H(y)$. We get $\tilde{H}(y_n) = \tilde{H}(y_0) + O(e^{\frac{-h_0}{2h}})$ and $H(y_n) = H(y_0) + O(h^p)$ over exponentially long times. The drift in energy \tilde{H} remains exponentially small over exponentially long-time intervals.

Chapter 2

Multisymplectic Integration of Partial Differential Equations

In the previous chapter we talked about symplectic integrators for Hamiltonian ODEs and how symplectic integrators give good long-time behaviour. We want to see how these ideas generalise to Hamiltonian PDEs and multisymplectic integrators. Before looking at these ideas, an introduction to PDEs in general is given. Further on in this chapter the construction and behaviour of multisymplectic integrators is discussed, followed by a case study of Burgers' equation.

2.1 Introduction to Partial Differential Equations (PDEs)

Partial differential equations (PDEs) contain one or more dependent variables, say u , and their partial derivatives with respect to the independent variables. An ODE contains only one independent variable, whereas a PDE contains two or more independent variables. An example of a PDE is the wave equation,

$$\frac{\partial^2 u}{\partial t^2} = a^2 \frac{\partial^2 u}{\partial x^2} \tag{2.1}$$

or

$$u_{tt} = a^2 u_{xx}.$$

Here u is the dependent variable and x and t are the independent variables, and $u = u(x, t)$ is a solution satisfying the equation for some values of the independent variables x , the spatial variable, and t , the time variable. The space-time domain of (x, t) and suitable initial/boundary conditions, and function space in which a solution is sought may also be specified. Zill and Cullen [102] give an introduction to PDEs and numerical methods for solving them.

Many physical processes not only evolve continuously in time but also in space, and can be described by PDEs. Also, many fundamental laws of physics, such as [53] quantum mechanics, electrodynamics, and ideal continuum mechanics, can be extended to the Hamiltonian PDE (see Section 2.2) framework.

Very often, initial value problems for PDEs [36] can be conveniently transformed into a system of ODEs by discretising the spatial derivatives. By using finite difference approximations in the variable x , (the spatial variable), equation (2.1) becomes,

$$\frac{d^2 u_i}{dt^2} = \frac{a^2}{\Delta x^2} (u_{i+1} - 2u_i + u_{i-1}),$$

where $u_i(t) \approx u(t, x_i)$. This procedure is called the method of lines or method of semi-discretisation in space.

2.2 Hamiltonian PDEs

In this section we introduce one form of Hamiltonian PDEs and give a few examples of PDEs written in this form.

A Hamiltonian PDE can be written [21] as,

$$u_t = \mathcal{D} \frac{\delta \mathcal{H}}{\delta u}, \tag{2.2}$$

where $\mathcal{H}[u]$ is the Hamiltonian functional, u is a function, and $\frac{\delta \mathcal{H}}{\delta u}$ is the variational derivative. A functional is a mapping from a function, or set of functions, to a real value and the variational derivative of a functional measures

how much the functional changes if its argument, the function, changes by an infinitesimal amount. \mathcal{D} is a skew-symmetric operator, that is, \mathcal{D} satisfies

$$\langle \mathcal{D}v, w \rangle = -\langle v, \mathcal{D}w \rangle.$$

This generalises the ODE framework, where the analogous Hamiltonian ODE system was given in (1.14). We give some examples of Hamiltonian PDEs written in this way. The KdV equation is given by

$$u_t + 6uu_x + u_{xxx} = 0$$

and can be put into the form (2.2) in two different ways, showing that the operator \mathcal{D} is not unique. We get,

KdV I:

$$\mathcal{D}_1 = \frac{\partial}{\partial x}, \quad \mathcal{H}_1 = \int_{-\infty}^{\infty} \left(\frac{1}{2}u_x^2 - u^3 \right) dx.$$

KdV II:

$$\mathcal{D}_2 = u \frac{\partial}{\partial x} + \frac{\partial}{\partial x} u + \frac{1}{6} \partial_{xxx}, \quad \mathcal{H}_2 = - \int_{-\infty}^{\infty} \frac{1}{2} u^2 dx.$$

The canonical infinite-dimensional Hamiltonian system is,

$$u_t = \frac{\delta \mathcal{H}}{\delta v}, \quad v_t = -\frac{\delta \mathcal{H}}{\delta u}, \quad (2.3)$$

where if written in the form (2.2) we have,

$$\mathcal{D} = \begin{bmatrix} 0 & 1 \\ -1 & 0 \end{bmatrix}.$$

The nonlinear wave equation is

$$u_{tt} - u_{xx} = -V'(u), \quad (2.4)$$

where $V(u)$ is some [7] smooth function and u is scalar valued.

We can rewrite the nonlinear wave equation in canonical form (2.3) by defining a new variable

$$v = u_t.$$

The wave equation (2.4) now becomes

$$v_t - u_{xx} = -V'(u) \Rightarrow v_t = u_{xx} - V'(u)$$

so that the canonical infinite-dimensional Hamiltonian system for (2.4) is

$$u_t = \frac{\delta \mathcal{H}}{\delta v} = v \tag{2.5}$$

$$v_t = -\frac{\delta \mathcal{H}}{\delta u} = u_{xx} - V'(u), \tag{2.6}$$

where \mathcal{D} is the canonical structure matrix given above and the Hamiltonian functional is given by

$$\mathcal{H} = \int_{-\infty}^{\infty} \left(\frac{1}{2}v^2 + \frac{1}{2}u_x^2 + V(u) \right) dx.$$

For a Hamiltonian PDE [83] energy is no longer represented by a single function. Instead, we have two functions, $E(z)$, describing the local energy density, and $F(z)$, describing the local energy flux, in the system. Together, the energy density and energy flux describe how the distribution of energy in a PDE varies over time. The energy density and energy flux are described in more detail in Section 2.3.1.

2.3 Multi-Hamiltonian PDEs

In this section we introduce multi-Hamiltonian PDEs as a direct extension of Hamiltonian ODEs and give an example of a PDE in this form. We then discuss conservation laws of multi-Hamiltonian PDEs and also the multisymplectic conservation law.

For comparison later in this section, we rewrite the Hamiltonian ODE (1.14) as,

$$\mathbf{K}\mathbf{z}_t = \nabla_{\mathbf{z}}S(\mathbf{z}) \tag{2.7}$$

where \mathbf{K} is some invertible skew-symmetric matrix and S is the Hamiltonian of the system. If (2.7) is the canonical Hamiltonian ODE then \mathbf{K} is just the inverse of the canonical structure matrix J , given in 1.3.

When a PDE is transformed to its canonical form, the resulting equations contain only first order derivatives in time, but the space derivatives can be of any order. By rewriting a Hamiltonian PDE as a system of equations containing only first order derivatives in space and time we obtain the general multi-Hamiltonian form

$$\mathbf{K}\mathbf{z}_t + \mathbf{L}\mathbf{z}_x = \nabla_{\mathbf{z}}S(\mathbf{z}) \quad (2.8)$$

where $\mathbf{z} \in \mathbb{R}^N$ is the state variable, $\mathbf{K}, \mathbf{L} \in \mathbb{R}^{N \times N}$ are two (constant) skew-symmetric matrices, $S : \mathbb{R}^N \rightarrow \mathbb{R}$ is a smooth function, and $\nabla_{\mathbf{z}}$ is the standard gradient in \mathbb{R}^N .

Comparing (2.8) to the Hamiltonian ODE form (2.7), we see that this multi-Hamiltonian form is a direct extension, where instead of just first order derivatives with respect to time we also have first order spatial derivatives. The spatial derivatives introduce a second skew-symmetric matrix \mathbf{L} . But, as we will see in Section 2.3.1, S is no longer represents the Hamiltonian of the system as it did in the ODE case.

Using the example in the previous section, we can rewrite the wave equation, (2.4), as a system containing only first order derivatives in space and time. We define

$$u_t = v, \quad u_x = w,$$

and the wave equation becomes the first order system,

$$u_t = v \quad (2.9)$$

$$u_x = w \quad (2.10)$$

$$v_t - w_x = -V'(u). \quad (2.11)$$

Taking,

$$\mathbf{z} = \begin{bmatrix} u \\ v \\ w \end{bmatrix}, \quad \mathbf{K} = \begin{bmatrix} 0 & 1 & 0 \\ -1 & 0 & 0 \\ 0 & 0 & 0 \end{bmatrix}, \quad \mathbf{L} = \begin{bmatrix} 0 & 0 & -1 \\ 0 & 0 & 0 \\ 1 & 0 & 0 \end{bmatrix},$$

and $S(\mathbf{z}) = -V(u) + \frac{1}{2}(w^2 - v^2)$, we get a multi-Hamiltonian form for the wave equation (2.4). A Hamiltonian PDE written in this way is called a multi-Hamiltonian PDE.

Currently, there is no general method for putting a Hamiltonian PDE into its multi-Hamiltonian form, although the multi-Hamiltonian forms for many conservative PDEs are known. These include PDEs for [68] nonlinear wave equations, shallow-water equations, atmospheric flows, fluid-structure interaction and water waves.

2.3.1 Conservation Laws

As was the case for ODEs, PDEs also have two types of conservation law depending on where the law is evaluated. A conservation law evaluated on solutions to the system has the form

$$E(\mathbf{z})_t + F(\mathbf{z})_x = 0. \quad (2.12)$$

When (2.12) describes an energy conservation law, the functions E and F are the energy density and energy flux functions respectively as described in Section 2.2. The momentum conservation law for PDEs also has the form of (2.12).

For multi-Hamiltonian PDEs, when $S(\mathbf{z})$ does not depend explicitly on x or t there are two fundamental conservation laws. Conservation of energy is associated with translation invariance in time and conservation of momentum is associated with translation invariance in space. In contrast to Hamiltonian ODEs, the Hamiltonian function $S(\mathbf{z})$ associated with the multi-Hamiltonian system will not be conserved in any sense.

The total energy of the system is no longer represented by a single function, but two functions $E(\mathbf{z})$ and $F(\mathbf{z})$. Together, they describe how the distribution of energy in a PDE varies over time. Individually, $E(\mathbf{z})$ describes the local energy density, and $F(\mathbf{z})$, the local energy flux of the system.

The energy and momentum conservation laws are local, which means the conservation properties do not depend on a specific domain or on the boundary

conditions of the PDE.

Theorem 2.3.1. *The energy conservation law for a multi-Hamiltonian PDE is given by,*

$$E(\mathbf{z})_t + F(\mathbf{z})_x = 0$$

where

$$\begin{aligned} E(\mathbf{z}) &= S(\mathbf{z}) + \frac{1}{2} \langle \mathbf{z}_x, \mathbf{Lz} \rangle, \text{ and} \\ F(\mathbf{z}) &= -\frac{1}{2} \langle \mathbf{z}_t, \mathbf{Lz} \rangle. \end{aligned}$$

Proof. We take the inner product of \mathbf{z}_t with the multi-Hamiltonian PDE (2.8),

$$\begin{aligned} \langle \mathbf{z}_t, \mathbf{Kz}_t + \mathbf{Lz}_x \rangle &= \langle \mathbf{z}_t, \nabla_{\mathbf{z}} S(\mathbf{z}) \rangle \\ \Rightarrow \langle \mathbf{z}_t, \mathbf{Kz}_t \rangle + \langle \mathbf{z}_t, \mathbf{Lz}_x \rangle &= \langle \mathbf{z}_t, \nabla_{\mathbf{z}} S(\mathbf{z}) \rangle \\ \Rightarrow \langle \mathbf{z}_t, \mathbf{Lz}_x \rangle &= \langle \mathbf{z}_t, \nabla_{\mathbf{z}} S(\mathbf{z}) \rangle, \\ &\text{(due to the skew-symmetry of } \mathbf{K}, \text{ we have } \langle \mathbf{z}_t, \mathbf{Kz}_t \rangle = 0) \\ \Rightarrow \frac{1}{2} \langle \mathbf{z}_t, \mathbf{Lz}_x \rangle + \frac{1}{2} \langle \mathbf{z}_t, \mathbf{Lz}_x \rangle &= S(\mathbf{z})_t \\ \Rightarrow \frac{1}{2} \langle \mathbf{z}_t, \mathbf{Lz}_x \rangle - \frac{1}{2} \langle \mathbf{z}_x, \mathbf{Lz}_t \rangle &= S(\mathbf{z})_t \\ \Rightarrow \frac{1}{2} \langle \mathbf{z}_t, \mathbf{Lz} \rangle_x - \frac{1}{2} \langle \mathbf{z}_{tx}, \mathbf{Lz} \rangle - \frac{1}{2} \langle \mathbf{z}_x, \mathbf{Lz} \rangle_t + \frac{1}{2} \langle \mathbf{z}_{xt}, \mathbf{Lz} \rangle &= S(\mathbf{z})_t \\ \Rightarrow \frac{1}{2} \langle \mathbf{z}_t, \mathbf{Lz} \rangle_x - \frac{1}{2} \langle \mathbf{z}_x, \mathbf{Lz} \rangle_t &= S(\mathbf{z})_t \\ \Rightarrow S(\mathbf{z})_t + \frac{1}{2} \langle \mathbf{z}_x, \mathbf{Lz} \rangle_t - \frac{1}{2} \langle \mathbf{z}_t, \mathbf{Lz} \rangle_x &= 0. \end{aligned}$$

Setting

$$\begin{aligned} E(\mathbf{z})_t &= \left(S(\mathbf{z}) + \frac{1}{2} \langle \mathbf{z}_x, \mathbf{Lz} \rangle \right)_t \text{ and} \\ F(\mathbf{z})_x &= -\frac{1}{2} \langle \mathbf{z}_t, \mathbf{Lz} \rangle_x, \end{aligned}$$

we obtain the energy conservation law. □

Theorem 2.3.2. *The momentum conservation law for a multi-Hamiltonian PDE is given by*

$$I(\mathbf{z})_t + G(\mathbf{z})_x = 0$$

where

$$I(\mathbf{z}) = -\frac{1}{2} \langle \mathbf{z}_x, \mathbf{Kz} \rangle, \text{ and}$$

$$G(\mathbf{z}) = S(\mathbf{z}) + \frac{1}{2} \langle \mathbf{z}_t, \mathbf{Kz} \rangle.$$

Proof. Similar to proof of Theorem 2.3.1 but take the inner product of \mathbf{z}_x with $\mathbf{Kz}_t + \mathbf{Lz}_x = \nabla_{\mathbf{z}} S(\mathbf{z})$ instead. \square

A differential conservation law, which is evaluated on first variations to the solutions of the system, is given for a PDE by

$$\omega_t + \kappa_x = 0 \tag{2.13}$$

where ω and κ are 2-forms defined below for multi-Hamiltonian PDEs.

For Hamiltonian PDEs, the differential conservation law (2.13) is called the multisymplectic conservation law and is a geometric property of the system.

Every multi-Hamiltonian PDE, a Hamiltonian PDE written in the form of equation (2.8), where the Hamiltonian has space and time translational invariance, has conservation laws of energy, momentum, and symplecticity. For multi-Hamiltonian PDEs symplecticity may vary from position to position and from time to time. Therefore, multisymplectic conservation laws describe the conservation of the amount of multisymplecticity at each point in time and correspond to the local conservation of some quantity, which is evaluated on solutions to the first variation of the system.

In comparison to Hamiltonian ODEs where a symplectic form ω was defined, Hamiltonian PDEs have two pre-symplectic forms,

$$\omega = \frac{1}{2} d\mathbf{z} \wedge \mathbf{K}d\mathbf{z}, \quad \kappa = \frac{1}{2} d\mathbf{z} \wedge \mathbf{L}d\mathbf{z}. \tag{2.14}$$

By taking the partial derivatives of these pre-symplectic forms with respect to t and x respectively and combining these, we obtain the multisymplectic conservation law.

Theorem 2.3.3. *The multisymplectic conservation law is given by,*

$$\omega_t + \kappa_x = 0$$

where ω and κ are defined in (2.14).

Proof. We take the first variation of the system (2.8) to get

$$\mathbf{K}d\mathbf{z}_t + \mathbf{L}d\mathbf{z}_x = S''(\mathbf{z})d\mathbf{z} \quad (2.15)$$

where $S''(\mathbf{z})$ is the Hessian of $S(\mathbf{z})$.

Now, we take the wedge product of $d\mathbf{z}$ with (2.15),

$$\begin{aligned} d\mathbf{z} \wedge (\mathbf{K}d\mathbf{z}_t + \mathbf{L}d\mathbf{z}_x) &= d\mathbf{z} \wedge S''(\mathbf{z})d\mathbf{z} \\ \Rightarrow d\mathbf{z} \wedge \mathbf{K}d\mathbf{z}_t + d\mathbf{z} \wedge \mathbf{L}d\mathbf{z}_x &= 0 \quad (\text{since } S''(\mathbf{z}) \text{ is symmetric}) \\ \Rightarrow \frac{1}{2}d\mathbf{z} \wedge \mathbf{K}d\mathbf{z}_t + \frac{1}{2}d\mathbf{z} \wedge \mathbf{K}d\mathbf{z}_t + \frac{1}{2}d\mathbf{z} \wedge \mathbf{L}d\mathbf{z}_x + \frac{1}{2}d\mathbf{z} \wedge \mathbf{L}d\mathbf{z}_x &= 0 \\ \Rightarrow \frac{1}{2}d\mathbf{z} \wedge \mathbf{K}d\mathbf{z}_t - \frac{1}{2}\mathbf{K}d\mathbf{z} \wedge d\mathbf{z}_t + \frac{1}{2}d\mathbf{z} \wedge \mathbf{L}d\mathbf{z}_x - \frac{1}{2}\mathbf{L}d\mathbf{z} \wedge d\mathbf{z}_x &= 0 \\ \Rightarrow \frac{1}{2}d\mathbf{z} \wedge \mathbf{K}d\mathbf{z}_t + \frac{1}{2}d\mathbf{z}_t \wedge \mathbf{K}d\mathbf{z} + \frac{1}{2}d\mathbf{z} \wedge \mathbf{L}d\mathbf{z}_x + \frac{1}{2}d\mathbf{z}_x \wedge \mathbf{L}d\mathbf{z} &= 0 \\ \Rightarrow \frac{1}{2}(d\mathbf{z} \wedge \mathbf{K}d\mathbf{z})_t + \frac{1}{2}(d\mathbf{z} \wedge \mathbf{L}d\mathbf{z})_x &= 0 \\ \Rightarrow \omega_t + \kappa_x &= 0. \end{aligned}$$

□

Note that by local we mean that such conservation properties do not depend on the specific domain or boundary conditions of the PDE. A local multisymplectic conservation law can be made global by integrating over the spatial boundary conditions. This reduces the multisymplectic conservation law to a symplectic conservation law, as for Hamiltonian ODEs in Section 1.10.

A table of the different conservation laws for ODEs and PDEs is summarised in 2.1 and will be discussed in more detail in Section 2.5.

2.4 Solving PDEs Numerically

In Section 1.1 we saw that initial conditions were imposed on the ODE. These initial conditions were needed if the ODE was to be solved by some numerical method. Extending this to PDEs, where we now have at least two independent

	ODEs	PDEs
Conservation law	$H_t = 0$	$E_t + F_x = 0$
Differential conservation law	$\omega_t = 0$	$\omega_t + \kappa_x = 0$

Table 2.1: Conservation laws for ODEs and PDEs.

variables, say x and t , then for PDEs modeling dynamical processes we not only have initial conditions in time t , but we also need boundary conditions in space x . This gives us an example of boundary conditions for which this problem is known as an initial-boundary value problem. The added spatial condition on the PDE can completely change the numerical characteristics of any method, so much so that it may not be well defined.

As stated in Section 2.1, PDEs can be transformed into a system of ODEs by discretising the spatial derivatives. Time, t , will now be the only independent variable. We can then solve the PDE by integrating the system of ODEs numerically.

If the PDEs are of the Hamiltonian [86] type, we may want to preserve this Hamiltonian structure, and therefore the space discretisation should be carried out in such a way that the resulting system of ODEs is Hamiltonian. For symplectic discretisation methods [53] we then solve the system of finite-dimensional Hamiltonian ODEs using an appropriate symplectic integrator.

Example

In Section 2.2 we defined (2.6) the canonical Hamiltonian PDE for the non-linear wave equation. The spatial derivative can now be discretised using a

central finite difference approximation to give the system of ODEs

$$\frac{d}{dt}u_i = v_i \quad (2.16)$$

$$\frac{d}{dt}v_i = \frac{u_{i-1} - 2u_i + u_{i+1}}{\Delta x^2} - V'(u_i). \quad (2.17)$$

This system of ODEs turns out to be automatically Hamiltonian with

$$H = \sum_i \frac{1}{2}v_i^2 - \frac{1}{2} \left(\frac{u_{i+1} - u_i}{\Delta x} \right)^2 + V(u_i).$$

If we take the nonlinearity $V'(u) = \sin(u)$, we get the sine-Gordon equation,

$$u_{tt} = u_{xx} - \sin(u) \quad (2.18)$$

and semi-discretisation,

$$\begin{aligned} \frac{d}{dt}u_i &= v_i \\ \frac{d}{dt}v_i &= \frac{u_{i-1} - 2u_i + u_{i+1}}{\Delta x^2} - \sin(u_i). \end{aligned}$$

This system can now be solved by a symplectic integrator, such as the leapfrog method, to produce a symplectic discretisation of (2.18). Figure 2.1 gives some snapshots of the solution to (2.18).

Plotting the energy error of the simulation (Figure 2.2) we see that it is bounded, which is what we expect of a symplectic integrator.

A better method of symplectic discretisation is to discretise \mathcal{H} and then form Hamilton's equations. This ensures that (2.16) is Hamiltonian. This is the approach discussed in [62].

2.5 Multisymplectic Integrators

Multisymplecticity is a geometric property of Hamiltonian PDEs, and therefore when looking for a numerical method to solve such a system we naturally try to find a discretisation that reflects this property. Based on this idea, Bridges and Reich [7], and also Marsden and Shkoller [60], introduced the concept of a multisymplectic integrator.

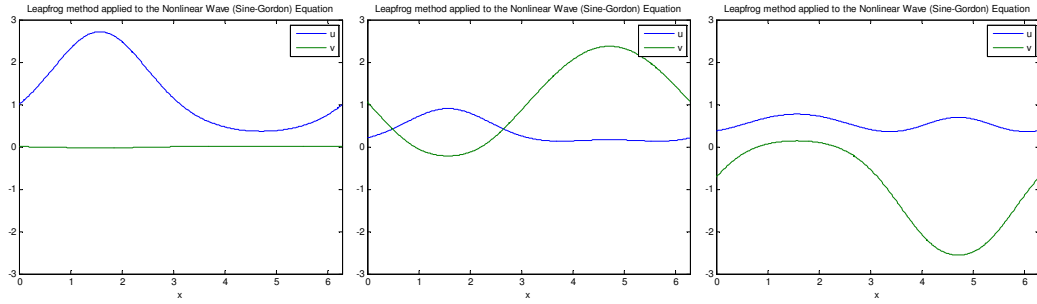


Figure 2.1: Snapshots in time of the leapfrog method applied to the semi-discretisation of the sine-Gordon equation.

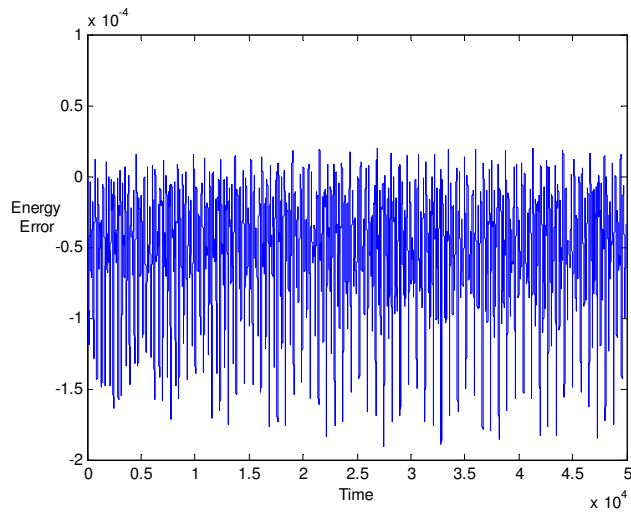


Figure 2.2: Energy error for 50000 time steps of the leapfrog method applied to the sine-Gordon equation.

A multisymplectic integrator is one which preserves a discrete version of the multisymplectic conservation law (2.13). This conservation law can be preserved by applying symplectic discretisations, such as leapfrog or symplectic Runge–Kutta methods, in space x and time t . Here discretisations applied in space and time are treated on an equal footing. In contrast, in Section 2.4 where we formed a symplectic integrator for a PDE, space and time were treated separately, with time only being explicitly treated by a symplectic method.

Discretisations are made on a uniform grid $\{(x_i, t_n)\} \in \mathbb{R}^2$, with mesh length Δt in the t direction and mesh length Δx in the x direction. See Figure 2.3 for a visual representation of the grid. A numerical discretisation of (2.8) can be written as

$$\mathbf{K}\partial_t \mathbf{z}_i^n + \mathbf{L}\partial_x \mathbf{z}_i^n = \nabla_{\mathbf{z}} S(\mathbf{z}_i^n)$$

where $\mathbf{z}_i^n = \mathbf{z}(x_i, t_n)$, and $\partial_t \mathbf{z}_i^n$ and $\partial_x \mathbf{z}_i^n$ are discrete approximations to \mathbf{z}_t and \mathbf{z}_x respectively. Here x_i makes reference to a specific point on the spatial grid and t_n to a specific point in time.

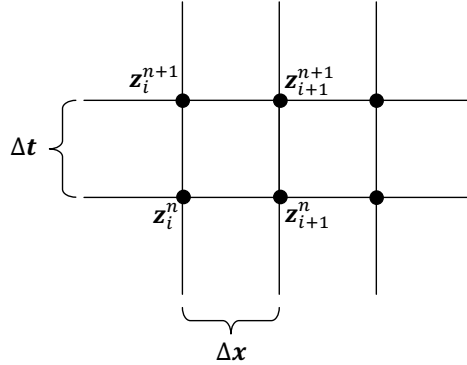


Figure 2.3: Uniform grid for multisymplectic discretisations.

A discrete version of the multisymplectic conservation law is

$$\frac{\omega_i^{n+1} - \omega_i^n}{\Delta t} + \frac{\kappa_{i+1}^n - \kappa_i^n}{\Delta x} = 0 \quad (2.19)$$

A numerical scheme of the form (2.5) is called a multisymplectic integrator if it satisfies some version of (2.19). Bridges and Reich [7] gives a good introduction to the multi-Hamiltonian form and multisymplectic integration.

Table 2.1, in Section 2.3.1, summarizes the different conservation laws for ODEs and PDEs. For ODEs we saw that if a method satisfies a discrete version of the ODE differential conservation law then it is called a symplectic integrator. Methods which preserve a discrete version of the ordinary conservation law where H is the total energy of the system are known as energy preserving methods. For ODEs the most common method for good long-time behaviour is a symplectic one. A numerical method cannot be both symplectic and energy preserving.

On the other hand, for PDEs, methods preserving an ordinary conservation law are the most popular. The paper [30] is an example using this point of view.

Many well known symplectic integrators, such as the leapfrog method, are also multisymplectic when applied to a Hamiltonian PDE. For Hamiltonian ODEs it was found that integration by a symplectic method produces good energy preservation; energy is not exactly preserved, but the energy error is bounded, giving good long-time behaviour of the method. So we have a relationship between methods that give good long-time behaviour and discrete preservation of the symplectic conservation law (1.26). We want to see how these ideas generalise to multisymplectic methods for Hamiltonian PDEs. For Hamiltonian PDEs it is not known if preserving a discrete version of the multisymplectic conservation law provides better qualitative preservation of the dynamics. It has been shown that over long-time integration, multisymplectic schemes show excellent local conservation of energy and momentum. Bridges and Reich [9] gives an introduction to symplectic and multisymplectic integrators for Hamiltonian PDEs. So we look at this question by looking at preservation of travelling wave solutions of multisymplectic integrators.

2.5.1 The Preissman Box Scheme

In this section we present an example of a multisymplectic integrator, the Preissman box scheme. In [2], Ascher and McLachlan use this scheme and compare it with other methods for the KdV equation. They find that where other methods develop small wiggles, the Preissman scheme stays smooth.

The Preissman box scheme is formed by concatenating a pair of midpoint discretisations, one in the t -direction and one in the x -direction. First, we define the following finite difference and average operators,

$$D_x \mathbf{z}_i^n = \frac{\mathbf{z}_{i+1}^n - \mathbf{z}_i^n}{\Delta x}, \quad D_t \mathbf{z}_i^n = \frac{\mathbf{z}_i^{n+1} - \mathbf{z}_i^n}{\Delta t}, \quad (2.20)$$

$$M_x \mathbf{z}_i^n = \frac{\mathbf{z}_i^n + \mathbf{z}_{i+1}^n}{2}, \quad M_t \mathbf{z}_i^n = \frac{\mathbf{z}_i^n + \mathbf{z}_i^{n+1}}{2}. \quad (2.21)$$

By applying finite difference and averages to (2.8) in time first, we get

$$\mathbf{K} D_t \mathbf{z}_i^n + \mathbf{L} M_t \mathbf{z}_i^n = \nabla_{\mathbf{z}} S(M_t \mathbf{z}_i^n).$$

Next, we apply finite difference and averages in space, giving

$$\mathbf{K} M_x D_t \mathbf{z}_i^n + \mathbf{L} D_x M_t \mathbf{z}_i^n = \nabla_{\mathbf{z}} S(M_x M_t \mathbf{z}_i^n). \quad (2.22)$$

This is known as the Preissman box or multisymplectic box scheme. Writing the first step out in full we get

$$\frac{1}{\Delta t} \mathbf{K}(\mathbf{z}_i^{n+1} - \mathbf{z}_i^n) + \frac{1}{2} \mathbf{L}(\mathbf{z}_i^n + \mathbf{z}_i^{n+1}) = \nabla_{\mathbf{z}} S\left(\frac{1}{2}(\mathbf{z}_i^n + \mathbf{z}_i^{n+1})\right).$$

The second step gives

$$\begin{aligned} & \frac{1}{\Delta t} \mathbf{K} M_x(\mathbf{z}_i^{n+1} - \mathbf{z}_i^n) + \frac{1}{2} \mathbf{L} D_x(\mathbf{z}_i^n + \mathbf{z}_i^{n+1}) = \nabla_{\mathbf{z}} S\left(\frac{1}{2} M_x(\mathbf{z}_i^n + \mathbf{z}_i^{n+1})\right) \\ \Rightarrow & \frac{1}{2\Delta t} \mathbf{K}(\mathbf{z}_i^{n+1} + \mathbf{z}_{i+1}^{n+1} - \mathbf{z}_i^n - \mathbf{z}_{i+1}^n) + \frac{1}{2\Delta x} \mathbf{L}(\mathbf{z}_{i+1}^n - \mathbf{z}_i^n + \mathbf{z}_{i+1}^{n+1} - \mathbf{z}_i^{n+1}) \\ & = \nabla_{\mathbf{z}} S\left(\frac{1}{4}(\mathbf{z}_i^n + \mathbf{z}_{i+1}^n + \mathbf{z}_i^{n+1} + \mathbf{z}_{i+1}^{n+1})\right). \end{aligned}$$

Using stencil notation we get

$$\frac{1}{2\Delta t} \mathbf{K} \begin{bmatrix} 1 & 1 \\ -1 & -1 \end{bmatrix} \mathbf{z} + \frac{1}{2\Delta x} \mathbf{L} \begin{bmatrix} -1 & 1 \\ -1 & 1 \end{bmatrix} \mathbf{z} = \nabla_{\mathbf{z}} S\left(\frac{1}{4} \begin{bmatrix} 1 & 1 \\ 1 & 1 \end{bmatrix} \mathbf{z}\right).$$

Finally, the variables that were introduced to write the PDE in its multisymplectic form (2.8) can be eliminated to get a stencil in terms of the original PDE.

For example, using the multisymplectic form of the nonlinear wave equation (2.9) and applying the above box scheme we get,

$$\begin{aligned} v_t - w_x &= -V'(u), & M_x M_t v - D_x M_t w &= -V'(M_x M_t u) \\ -u_t &= -v, & -M_x D_t u &= -M_x M_t v \\ u_x &= w, & D_x M_t u &= M_x M_t w. \end{aligned}$$

Now, eliminating the variables v and w we get,

$$M_x^2 D_t^2 u = D_x^2 M_t^2 u - M_x M_t V'(M_x M_t u). \quad (2.23)$$

Expanding this out and putting it into stencil notation, we get the following multisymplectic box scheme for the nonlinear wave equation (2.9)

$$\begin{aligned} \frac{1}{4(\Delta t)^2} \begin{bmatrix} 1 & 2 & 1 \\ -2 & -4 & -2 \\ 1 & 2 & 1 \end{bmatrix} u &= -\frac{1}{4} \begin{bmatrix} 1 & 1 \\ 1 & 1 \end{bmatrix} V' \left(\frac{1}{4} \begin{bmatrix} 1 & 1 \\ 1 & 1 \end{bmatrix} u \right) \\ &+ \frac{1}{4(\Delta x)^2} \begin{bmatrix} 1 & -2 & 1 \\ 2 & -4 & 2 \\ 1 & -2 & 1 \end{bmatrix} u. \end{aligned}$$

We now prove that the Preissman box scheme (2.22) satisfies the discrete multisymplectic conservation law

$$\frac{\omega_{i+\frac{1}{2}}^{n+1} - \omega_{i+\frac{1}{2}}^n}{\Delta t} + \frac{\kappa_{i+1}^{n+\frac{1}{2}} - \kappa_i^{n+\frac{1}{2}}}{\Delta x} = 0. \quad (2.24)$$

First, we take exterior derivatives of both sides of (2.22) to get,

$$\mathbf{K} M_x D_t d\mathbf{z}_i^n + \mathbf{L} D_x M_t d\mathbf{z}_i^n = S''(M_x M_t \mathbf{z}_i^n) M_x M_t d\mathbf{z}_i^n.$$

Next, we take the wedge products of both sides with $M_x M_t d\mathbf{z}_i^n$ to annihilate the nonlinear term of the right hand side. This gives

$$M_x M_t d\mathbf{z}_i^n \wedge \mathbf{K} M_x D_t d\mathbf{z}_i^n + M_x M_t d\mathbf{z}_i^n \wedge \mathbf{L} D_x M_t d\mathbf{z}_i^n = 0. \quad (2.25)$$

We need to rearrange this to show that it takes the form of a discrete conservation law. First note that

$$d\mathbf{a} \wedge \mathbf{K}d\mathbf{b} = -d\mathbf{a} \wedge \mathbf{K}^T d\mathbf{b} = -\mathbf{K}d\mathbf{a} \wedge d\mathbf{b} = d\mathbf{b} \wedge \mathbf{K}d\mathbf{a},$$

which shows that 8 of the 16 terms obtained by expanding the first term in (2.25) cancel, leaving,

$$\begin{aligned} M_x M_t d\mathbf{z}_i^n \wedge \mathbf{K} M_x D_t d\mathbf{z}_i^n &= \frac{1}{4\Delta t} (d\mathbf{z}_i^{n+1} \wedge \mathbf{K} d\mathbf{z}_i^{n+1} + 2d\mathbf{z}_i^{n+1} \wedge \mathbf{K} d\mathbf{z}_{i+1}^{n+1} \\ &\quad + d\mathbf{z}_{i+1}^{n+1} \wedge \mathbf{K} d\mathbf{z}_{i+1}^{n+1} - d\mathbf{z}_i^n \wedge \mathbf{K} d\mathbf{z}_i^n - 2d\mathbf{z}_i^n \wedge \mathbf{K} d\mathbf{z}_{i+1}^n - d\mathbf{z}_{i+1}^n \wedge \mathbf{K} d\mathbf{z}_{i+1}^n) \\ &= \frac{1}{4\Delta t} ((d\mathbf{z}_i^{n+1} + d\mathbf{z}_{i+1}^{n+1}) \wedge \mathbf{K}(d\mathbf{z}_i^{n+1} + d\mathbf{z}_{i+1}^{n+1}) \\ &\quad - (d\mathbf{z}_i^n + d\mathbf{z}_{i+1}^n) \wedge \mathbf{K}(d\mathbf{z}_i^n + d\mathbf{z}_{i+1}^n)) \\ &= D_t(M_x d\mathbf{z}_i^n \wedge \mathbf{K} M_x d\mathbf{z}_i^n). \end{aligned}$$

Similarly, by the expanding the 2nd term in (2.25) we get

$$M_x M_t d\mathbf{z}_i^n \wedge \mathbf{L} D_x M_t d\mathbf{z}_i^n = D_x(M_t d\mathbf{z}_i^n \wedge \mathbf{L} M_t d\mathbf{z}_i^n).$$

Combining these results we get (2.24). Hence the Preissman box scheme is multisymplectic.

Notice that a multisymplectic method satisfies ‘a’ discrete version of the multisymplectic conservation law. This implies that there is not a unique discrete multisymplectic law that has to be satisfied by a multisymplectic integrator. This is in contrast to Hamiltonian ODEs where there is a specific symplectic conservation law which must be satisfied for a method to be symplectic. The Preissman box scheme satisfies the above multisymplectic conservation law (2.24), but other schemes may satisfy a different version of the discrete multisymplectic conservation law (2.19).

2.6 Constructions of Multisymplectic integrators

Construction of multisymplectic integrators is not as well understood as that of symplectic integrators, with most studies using the simplest methods such

as the box scheme and the leapfrog method. The following subsections give different approaches to constructing multisymplectic integrators.

2.6.1 Discrete Lagrangian Approach

The discrete Lagrangian approach to constructing multisymplectic integrators uses multisymplectic geometry. See [32, 60, 59] for a review of multisymplectic geometry in its Lagrangian form. The paper [59] shows that the existence of geometric structures and their preservation along solutions can be obtained directly from the variational principle using multisymplectic geometry. This paper [59] develops the geometric foundations for multisymplectic momentum integrators for variational PDEs. Veselov [92, 93] gives a new approach to symplectic integration where he develops a discrete mechanics based on a discretisation of Hamilton's principle. In the paper [59] Veselov's idea is extended to discretisations for PDEs in the variational form. This leads naturally to multisymplectic momentum integrators. This approach cannot in general preserve the Hamiltonian exactly, but under appropriate circumstances conserves a nearby Hamiltonian up to exponentially small errors, assuming small time steps.

2.6.2 Gaussian Runge–Kutta Methods

Many higher order Runge–Kutta (RK) methods are based on the concept of collocation. The idea of collocation is to choose a finite-dimensional space of candidate solutions and a number of points in the domain. The candidate solutions are generally polynomials up to a certain degree and the points are called collocation points. The solution which satisfies the given equation at the collocation points is then chosen. For ODEs the coefficients in the RK method are determined by a collocation polynomial, which passes through the nodes y_n of (1.11) and has derivatives matching the ODE at a number of quadrature points. An r -stage Gaussian RK (GRK) method has quadrature points that

are the zeros of the shifted Legendre polynomial of degree r ,

$$P_r(x) = \frac{1}{r!} \frac{d^r}{dx^r} (x^r (x-1)^r)$$

which are in the range $(0, 1)$. GRK methods have order $2r$ in time.

In [82] Reich introduces GRK methods in this context and applies them to the nonlinear wave equation (2.4). The paper looks at whether or not symplectic methods for canonical Hamiltonian ODEs can be generalised to multi-Hamiltonian PDEs. It was shown that applying GRK methods in space and time to a multi-Hamiltonian PDE results in a system of equations that satisfy a discrete multisymplectic conservation law. In [83] Ryland further investigates discretisations of multi-Hamiltonian PDEs by GRK methods and shows the GRK methods do not in general lead to useful methods. Not only must a method satisfy a discrete multisymplectic conservation law to be a multisymplectic integrator, but the system of discrete equations produced by a method must form a well-defined integrator. This is the basis of [83]. The system of equations produced from the Preissman box scheme with periodic boundary conditions typically only have a solution when the number of grid points is odd. In addition, Ryland [83] showed that the number of stages also has to be odd for the discrete equations to have a solution. Therefore, forming a useful integrator when the number of grid points and number of stages is odd. For GRK it is shown that there are many things that could go wrong and cause the system of equations to not be well-defined, resulting in an integrator that is not yet very useful for multi-Hamiltonian PDEs.

2.6.3 Partitioned Runge–Kutta methods

Systems of the form

$$\begin{aligned}\dot{q} &= f(q, p) = \frac{\partial H}{\partial p} \\ \dot{p} &= g(q, p) = -\frac{\partial H}{\partial q}\end{aligned}$$

can be solved by partitioned Runge–Kutta (PRK) methods

$$\begin{aligned}
Q_i &= q_0 + h \sum_{j=1}^s a_{ij} f(Q_j, P_j) \\
P_i &= p_0 + h \sum_{j=1}^s \hat{a}_{ij} g(Q_j, P_j) \\
q_1 &= q_0 + h \sum_{j=1}^s b_j f(Q_j, P_j) \\
p_1 &= p_0 + h \sum_{j=1}^s \hat{b}_j g(Q_j, P_j)
\end{aligned}$$

where $q \in \mathbb{R}^N$, $p \in \mathbb{R}^N$.

As with Runge–Kutta methods, such as the GRK method in the previous section, PRK methods can be used to discretise multi-Hamiltonian PDEs in space and time. In [43] it was shown that discretisation of a multi-Hamiltonian PDE in space and time by symplectic PRK methods gives a system of equations that satisfy a discrete multisymplectic conservation law. As for RK methods, the equations from the discretisation by a PRK may not form a well-defined integrator. But Ryland, in [83, 84], gives conditions on the coefficients of PRK methods such that they give a well-defined integrator when applied to a multi-Hamiltonian PDE, and gives conditions for when a PRK method is multisymplectic. For a certain class of multi-Hamiltonian PDEs, the idea is to apply an explicit symplectic PRK discretisation in each dimension, obtaining a fully explicit, fully discrete system. (Since symplectic RK methods are implicit the approach cannot be applied to methods such as Gaussian Runge–Kutta methods, considered previously). The Lobatto IIIA–IIIB class of PRK methods, of which the leapfrog method is an example, is used to explore this approach for symplectic PRK methods. The algorithm is then used on various well-known multi-Hamiltonian PDEs. The paper [69] uses the generalised leapfrog method, a Lobatto IIIA–IIIB method with 2 stages, as a multisymplectic PRK method and studies the linear stability of this method.

2.7 Behaviour of Multisymplectic Integrators

Many numerical experiments have been performed on multi-Hamiltonian PDEs to test the behaviour of multisymplectic integrators. The behaviour of multisymplectic integrators can be explored by examining the discrete dispersion relation or looking for the preservation of travelling wave solutions. Most of the experiments test the behaviour by considering the propagation of a solitary wave solution or the collision of two or three solitons, which does not give us very much insight into the overall behaviour of multisymplectic integrators.

2.7.1 The Dispersion Relation

Any time-dependent scalar, linear PDE with constant coefficients on an unbounded space domain possesses plane wave solutions

$$u(x, t) = e^{i(\xi x + \omega t)}, \quad \xi \in \mathbb{R}$$

where ξ is the wave number and ω is the wave frequency.

The dispersion relation describes how the frequencies ω in time are related to the wave numbers ξ in space of a plane wave solution to a linear PDE. Therefore, for a nonlinear PDE the behaviour of the PDE will only be determined by the dispersion relation in regions where the linearised PDE is a suitable approximation to the nonlinear PDE. Fortunately, these are the regions that we are generally interested in.

A discrete dispersion relation may also be calculated for a numerical integrator. This is an approximation to the continuous dispersion relation over a finite set of wave numbers. Properties of the numerical solution of PDEs, such as the stability, conservation of the sign of the wave group velocity, and existence of spurious waves, may be determined by comparing the dispersion relation of the continuous PDE with that of the numerical integrator.

The behaviour of linear PDEs can be well understood from dispersion analysis. Research into the dispersion relation for multisymplectic integrators applied to the linearised nonlinear wave equation shows that for higher order

schemes there is a break in the curve. Figure 2.4 shows the break in the curve for a 3-stage Lobatto method, which suggests only the bottom half of the frequencies are handled reliably.

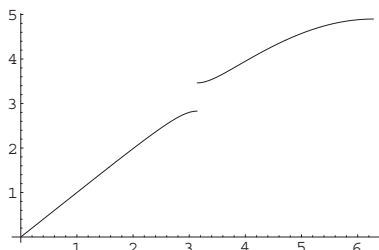


Figure 2.4: The dispersion relation of the linearised wave equation.

All Lobatto methods have a similar dispersion relation as that given in Figure 2.4. That is, they only conditionally preserve part of the dispersion relation. But the solutions from Lobatto methods contain no parasitic waves. Parasitic solutions give false behaviours, such as oscillations. Gauss methods unconditionally preserve the entire dispersion relation with no parasitic waves.

2.7.2 Numerical Experiments

Below are some of the numerical experiments that have been performed:

- The Preissman box scheme is applied to the nonlinear Schrödinger and the sine-Gordon equations and the behaviour of the scheme is analysed by looking for solitary wave solutions [72].
- The box scheme is derived and applied to the KdV equation and it is found that the box scheme preserves the dispersion relation [2, 3]. Following on from this result, in [29] it is shown that there are no spurious reflections.
- The formulation of a six point box scheme is derived for a coupled 1D nonlinear Schrödinger equation. The behaviour of the method is examined by considering the interaction of two solitary waves and the energy error from the simulation [90].

- Various multisymplectic methods are derived for Klein–Gordon equation and the collision of two solitons is considered. The behaviour of the multisymplectic integrator is compared with that of an energy preserving method [95]. Here the multisymplectic integrator performs better than the energy-preserving method.
- A six point multisymplectic scheme is derived for the nonlinear Schrödinger equation [17]. The collision of two and three solitons is considered, along with the propagation of one soliton, for the multisymplectic scheme and a symplectic scheme. For one and two solitons the multisymplectic method performs better than the symplectic integrator. For three solitons both methods perform well. The results are based on how well the integrators preserve local conservation of energy.
- A 10-point multisymplectic scheme is derived for the regularised long-wave equations from its multi-Hamiltonian form [14]. To examine the behaviour of the integrator numerical experiments are performed for the motion of a single solitary wave and for the interaction of two and three solitary waves. The L_2 and L_∞ error norms are used to determine the accuracy of the motion of a single solitary wave. For the accuracy of the interaction of two or three solitons the analytical invariant values are used. The results are acceptable in all three cases.
- A 16-point multisymplectic scheme is derived for the Kadomtsev-Petviashvili equation and tested on one soliton and a lump-type solitary wave.

The energy and momentum conservation laws are not preserved by multisymplectic integrators and it is not known if backward error analysis can be applied to find corresponding modified conservation laws. In [71] Moore and Reich show that for semi-discretised multi-Hamiltonian PDEs the corresponding modified semi-discrete conservation laws of energy and momentum exist. A multi-Hamiltonian PDE discretised in space yields a semi-discrete energy

conservation law which is preserved exactly, and that discretised in time yields a semi-discrete momentum conservation law. Also, no results are known that use the discrete multisymplectic conservation law directly. The main question of our research is, does preservation of a discrete multisymplectic conservation law provide better qualitative preservation of the dynamics? We propose to look at this question by studying preservation of travelling waves in multi-Hamiltonian PDEs. We analyse this numerically and also from a backward error analysis point of view, finding modified equations and the corresponding modified Hamiltonians.

2.8 Case Study: Numerical Solution of Burgers' Equation

In this section we present a numerical experiment inspired by [91]. They derive a multisymplectic scheme for Burgers' even though the equation is not Hamiltonian. They then claim that that the method could cope with shocks developed from the PDE. This seemed odd so the paper was studied and it was firstly found to contain a mistake in the derivation of the scheme. Secondly, they only tested their method for $u_x = O(\nu)$, in which there are no shocks. We wish to test our correct scheme for ν very small to see whether or not it can cope with the formation of shocks.

2.8.1 Burgers' Equation

The general form of Burgers' equation is

$$u_t = -uu_x + \nu u_{xx} = -V'(u)_x + \nu u_{xx}, \quad V(u) = \frac{u^3}{6},$$

where ν is the viscosity. When $\nu \neq 0$ Burgers' equation is a nonlinear second order parabolic equation. On the other hand, when $\nu = 0$ Burgers' equation becomes

$$u_t + uu_x = 0,$$

a first order hyperbolic equation known as the inviscid Burgers' equation. In this situation discontinuous solutions called shocks develop.

Burgers' equation is used in fluid dynamics and in engineering as a simplified model for turbulence, shock wave formation, and mass transport. These properties make Burgers' equation a good model for testing numerical algorithms in flows where severe gradients or shocks are anticipated.

2.8.2 A Multisymplectic Scheme for Burgers' Equation

Following the work done by Ascher and McLachlan [2] on multisymplectic schemes for the KdV equation, we find the multisymplectic formulation of Burgers' equation. The KdV equation is given by,

$$u_t = V'(u)_x + \nu u_{xxx},$$

where $V(u) = \frac{\alpha}{3}u^3 + \frac{\rho}{2}u^2$.

While KdV is Hamiltonian, Burgers' is not, but we still wish to apply the multisymplectic box scheme to determine if it will produce good results for non-Hamiltonian PDEs also.

Apart from the reasons in Section 2.8.1 Burgers' is also a good choice as a follow on from KdV since when $|\nu| \ll 1$ the dispersion limit for KdV is the same as that of Burgers' [3]. Burgers' equation can have shocks, whereas the solution to KdV is always smooth.

The multisymplectic scheme for Burgers' has been incorrectly formulated in [91]. The writers do not go through the steps in their formulation and only give the stencils for the 8-point and 12-point box schemes. Here we give the correct formulation in full. Our aim is to write Burgers' equation (2.8.1) in the multisymplectic form (2.8). Firstly, we define the following finite difference

and average operators,

$$\begin{aligned} D_x u_i^n &= \frac{u_{i+1}^n - u_i^n}{\Delta x}, \\ D_t u_i^n &= \frac{u_i^{n+1} - u_i^n}{\Delta t}, \\ M_x u_i^n &= \frac{u_i^n + u_{i+1}^n}{2}, \\ M_t u_i^n &= \frac{u_i^n + u_i^{n+1}}{2}. \end{aligned}$$

Next, we introduce new variables to get the following system for Burgers' equation (2.8.1)

$$\begin{aligned} \phi_x &= u, \\ u_x &= -\frac{1}{\nu}v, \\ \frac{1}{2}\phi_t &= w - V'(u) - v, \\ w_x + \frac{1}{2}u_t &= 0. \end{aligned}$$

Applying the box scheme

$$\mathbf{K}D_x M_t z + \mathbf{L}D_t M_x z = \nabla S(M_t M_x z)$$

we get the discretisation

$$\begin{aligned} D_x M_t \phi &= M_t M_x u, \\ D_x M_t u &= -\frac{1}{\nu}M_t M_x v, \\ \frac{1}{2}D_t M_x \phi &= M_t M_x w - V'(M_t M_x u) - M_t M_x v, \\ D_x M_t w + \frac{1}{2}D_t M_x u &= 0. \end{aligned}$$

Eliminating v , w , and ϕ from the above discretisation, then adding another space average operator to each side of the resulting equation we get,

$$D_t M_x^3 u = -D_x M_x V'(M_t M_x u) + \nu D_x^2 M_x M_t u.$$

Thus, the 8-point box scheme for (2.8.1) written in stencil notation is

$$\begin{aligned} \frac{1}{8(\Delta t)} \begin{bmatrix} 1 & 3 & 3 & 1 \\ -1 & -3 & -3 & -1 \end{bmatrix} u = -\frac{1}{2\Delta x} \begin{bmatrix} -1 & 0 & 1 \end{bmatrix} V' \left(\frac{1}{4} \begin{bmatrix} 1 & 1 \\ 1 & 1 \end{bmatrix} u \right) \\ + \frac{\nu}{4(\Delta x)^2} \begin{bmatrix} 1 & -1 & -1 & 1 \\ 1 & -1 & -1 & 1 \end{bmatrix} u. \end{aligned} \quad (2.26)$$

We can also derive a 12-point scheme for (2.8.1),

$$D_t M_x^3 M_t u = -D_x M_x M_t V'(M_t M_x u) + \nu D_x^2 M_x M_t^2 u,$$

and in stencil notation,

$$\begin{aligned} \frac{1}{16(\Delta t)} \begin{bmatrix} 1 & 3 & 3 & 1 \\ 0 & 0 & 0 & 0 \\ -1 & -3 & -3 & -1 \end{bmatrix} u = -\frac{1}{4\Delta x} \begin{bmatrix} -1 & 0 & 1 \\ -1 & 0 & 1 \end{bmatrix} V' \left(\frac{1}{4} \begin{bmatrix} 1 & 1 \\ 1 & 1 \end{bmatrix} u \right) \\ + \frac{\nu}{8(\Delta x)^2} \begin{bmatrix} 1 & -1 & -1 & 1 \\ 2 & -2 & -2 & 2 \\ 1 & -1 & -1 & 1 \end{bmatrix} u. \end{aligned}$$

The 8-point and 12-point box scheme stencils for Burgers' are given incorrectly in [91] as,

$$\begin{aligned} \frac{1}{8(\Delta t)} \begin{bmatrix} 1 & 3 & 3 & 1 \\ -1 & -3 & -3 & -1 \end{bmatrix} u = -\frac{1}{2\Delta x} \begin{bmatrix} -1 & 0 & 1 \end{bmatrix} V' \left(\frac{1}{4} \begin{bmatrix} 1 & 1 \\ 1 & 1 \end{bmatrix} u \right) \\ + \frac{1}{2(\Delta x)^2} \begin{bmatrix} 1 & -2 & 1 \\ 1 & -2 & 1 \end{bmatrix} u \end{aligned}$$

and,

$$\begin{aligned} \frac{1}{16(\Delta t)} \begin{bmatrix} 1 & 3 & 3 & 1 \\ 0 & 0 & 0 & 0 \\ -1 & -3 & -3 & -1 \end{bmatrix} u = -\frac{1}{4\Delta x} \begin{bmatrix} -1 & 0 & 1 \\ -1 & 0 & 1 \end{bmatrix} V' \left(\frac{1}{4} \begin{bmatrix} 1 & 1 \\ 1 & 1 \end{bmatrix} u \right) \\ + \frac{1}{4(\Delta x)^2} \begin{bmatrix} 1 & -2 & 1 \\ 2 & -4 & 2 \\ 1 & -2 & 1 \end{bmatrix} u \end{aligned}$$

respectively. We see that the last term in both the 8-point and 12-point scheme are wrong. Firstly, they do not include the viscosity ν , or else $\nu = 2$ is fixed. Secondly, both stencils for the last terms are only 3 grid points wide, but should be 4.

2.8.3 Solutions to the 8-Point Burgers' Scheme (2.26)

Figure 2.5 gives snapshots of the solution to the 8-Point Burgers' scheme for $\nu = 1$. This is a relatively large value of the viscosity and we see that the solution does not develop shocks but gradually decays to 1.

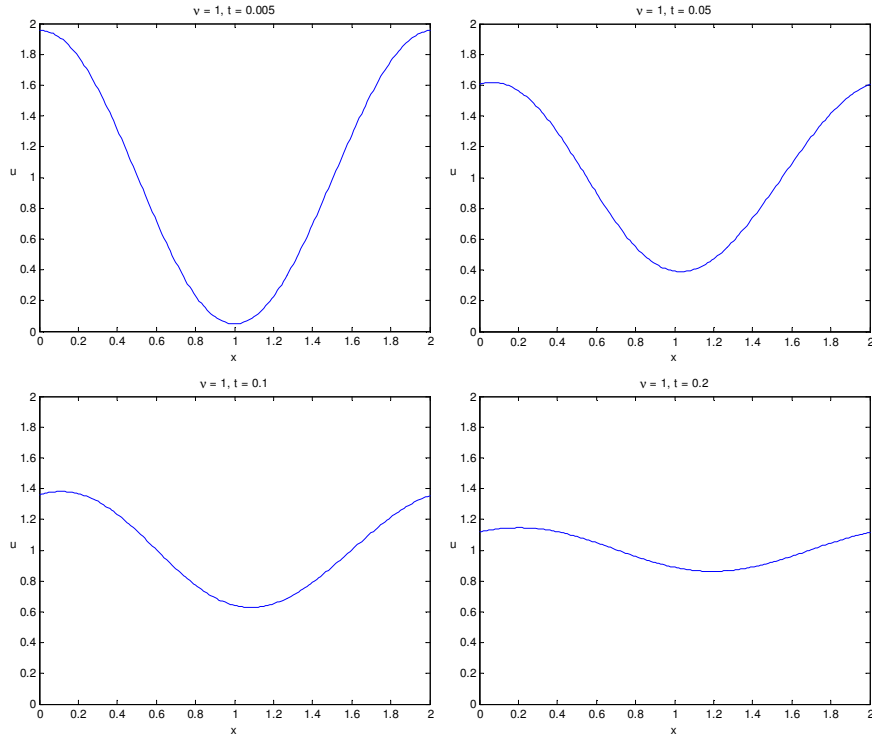


Figure 2.5: Solution to Burgers' equation at different points in time for $\nu = 1$, $\Delta x = 0.01$, and $\Delta t = 0.005$.

As we decrease the value of the viscosity ν we would expect to see shocks developing. For $\nu = 0.0001$ we plot the solution, in Figure 2.6, and see the formation of a shock wave. As this shock wave forms we see that wiggles in

the solution also develop. If the solution is run for a longer length of time the wiggles become very large. This shows that the scheme cannot cope with the shock as [91] incorrectly stated.

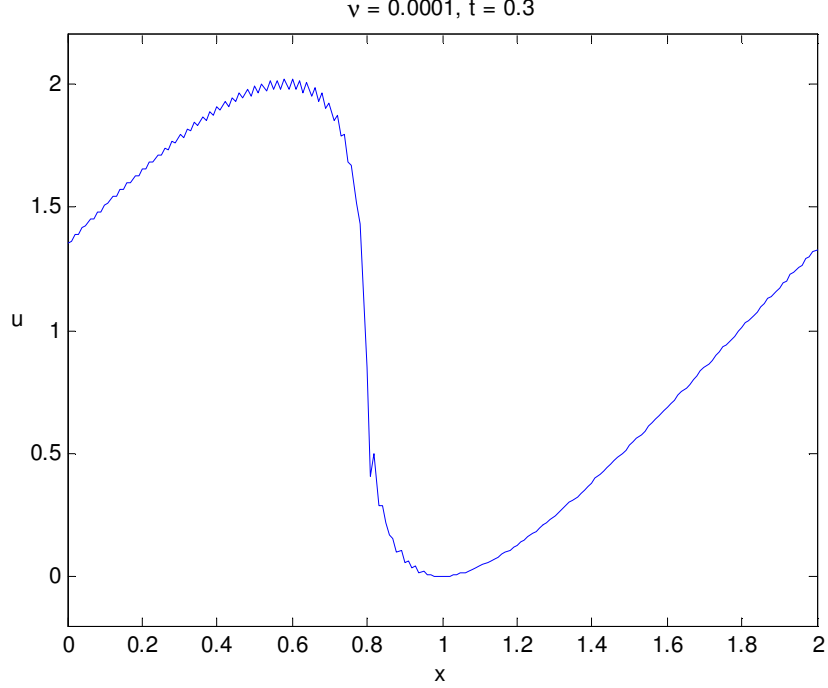


Figure 2.6: Solution to Burgers' equation at time $t = 0.3$ for $\nu = 0.0001$, $\Delta x = 0.01$, and $\Delta t = 0.0001$.

For very small values of ν the method will not work unless the time step Δt is also very small. More analysis needs to be done on the impact that the interaction between ν , Δt , and Δx has on the performance of the method. Preferably, there would be some critical value of $\frac{\nu \Delta t}{\Delta x}$ in which the method fails to produce good results.

Error analysis needs to still be performed. We also want to see if there is a critical ratio of Δx and Δt for the formation of wiggles. The same analysis also needs to be applied to other non-Hamiltonian PDEs to see whether multisymplectic methods give good qualitative behaviour for these types of PDEs

as well as Hamiltonian PDEs.

This experiment shows that the multisymplectic conservation law does not help keep the wiggles small.

Chapter 3

Introduction to Travelling Waves

In this chapter we introduce travelling waves and give a description of the different types of travelling waves that exist. We also introduce travelling waves in semi-discrete and fully discrete systems and give some examples and properties of these from the literature.

3.1 Travelling Waves

Travelling waves are a type of wave that travels at a constant speed $c \neq 0$ without changing shape. The most commonly observed type of travelling wave is that of an ocean wave. They are described mathematically by a smooth function φ . If $u(x, t)$ is a solution to a PDE, then a travelling wave solution satisfies,

$$u(x, t) = \varphi(x - ct) = \varphi(\xi). \quad (3.1)$$

From (3.1) it can be seen that by using travelling wave coordinates, we condense our independent variables x and t in the PDE to one variable $\xi = x - ct$, where c is the wave speed.

There are 3 types of travelling wave solution depending on the solution of the reduced equation for φ :

- Solitary waves (which may exist when the spatial domain is $-\infty < x < \infty$)
 - Homoclinic orbits (see Figure 3.1)
 - Heteroclinic orbits (see Figure 3.2)
- Periodic travelling waves (see Figure 3.7) (which may exist when the domain is infinite or finite with periodic boundary conditions).

A travelling wave solution $\varphi(\xi)$ is called a solitary wave solution if the boundary conditions $\varphi'(\xi)(\pm\infty) = 0$ are satisfied. In other words, $\varphi(\xi)$ approaches some constant value at the boundaries $\xi \rightarrow \pm\infty$. In Figure 3.1, we see that $\varphi(\xi)$ approaches the same value as $\xi \rightarrow +\infty$ and $\xi \rightarrow -\infty$, and in Figure 3.2, $\varphi(\xi)$ approaches a different value at each boundary. This determines whether or not the solitary solution corresponds to a homoclinic or heteroclinic orbit.

A homoclinic and heteroclinic orbit are plotted in Figures 3.3 and 3.4 respectively. We see that a homoclinic orbit is an orbit which travels from a fixed point back to that same fixed point. This is equivalent to the values at the boundaries being the same, that is $\lim_{\xi \rightarrow -\infty} \varphi(\xi) = \lim_{\xi \rightarrow \infty} \varphi(\xi)$, so a homoclinic orbit in the phase portrait corresponds to a solitary wave solution that approaches the same constant value at the boundaries (see Figure 3.1). This type of travelling wave is also sometimes called a pulse, but we will call it a homoclinic travelling wave.

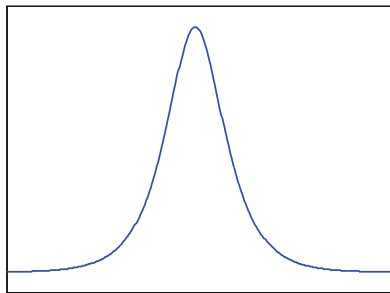


Figure 3.1: Solitary wave corresponding to a homoclinic orbit.

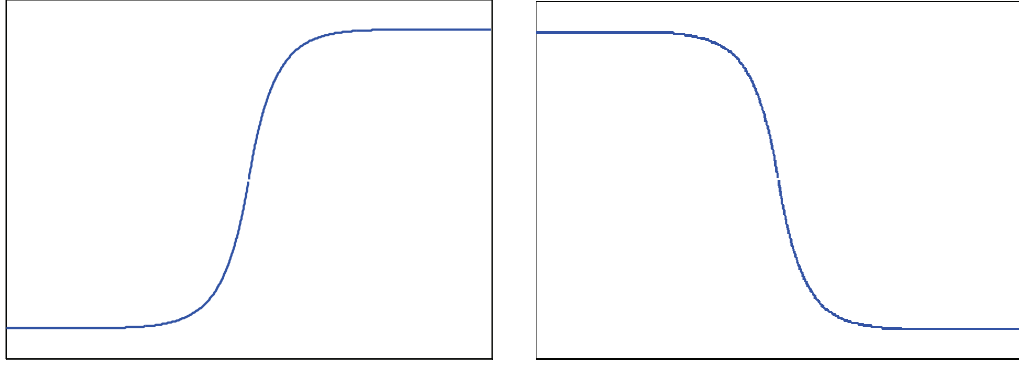


Figure 3.2: Solitary waves corresponding to heteroclinic orbits.

Figure 3.4 for the heteroclinic orbit shows that this type of orbit travels from a fixed point to a different fixed point. This is equivalent to the values at the boundaries being different, that is $\lim_{\xi \rightarrow -\infty} \varphi(\xi) \neq \lim_{\xi \rightarrow \infty} \varphi(\xi)$, so a heteroclinic orbit in the phase portrait corresponds to a solitary wave solution that approaches different constant values at the boundaries (see Figure 3.2). This type of wave is also sometimes called a wave front, kink, or anti-kink solution, but we will refer to it as a heteroclinic travelling wave.

Any orbit of these types gives rise to a (not necessarily stable) soliton solution for the nonlinear PDE (3.2) given in Section 3.1.1.

There are many mathematical models that produce these two types of solitary waves. There are two famous models that produce homoclinic travelling wave solutions. These models are the Hodgkin–Huxley model [41] and the FitzHugh–Nagumo models [61, 19] which both explore excitable cells and nerve impulses.

The Hodgkin–Huxley model is a set of nonlinear PDEs that approximates the electrical features of excitable cells, such as neurons and cells in heart tissue. Hodgkin and Huxley described the model in 1952 [41] to explain the underlying ionic mechanisms essential for the initiation and propagation of action potentials in the squid giant axon. The trouble with their solution was that only projections of the model’s 4-dimensional phase space could be observed.

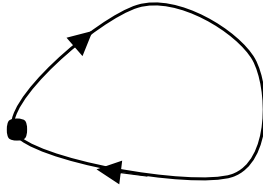


Figure 3.3: A homoclinic orbit.

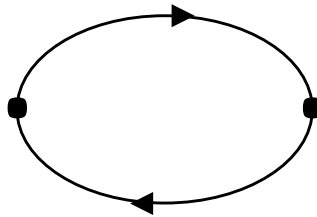


Figure 3.4: A heteroclinic orbit

To eliminate this problem, FitzHugh and Nagumo proposed a simpler 2-dimensional model,

$$u_t = u_{xx} + f(u) - w, \quad w_t = \epsilon(u - \gamma w).$$

The motivation for this simplified model was to theoretically separate the mathematical properties of excitation and propagation from the electrochemical properties of sodium and potassium ion flow. Also, the simplicity of the model allows the entire solution to be viewed at once. In addition, the model is analytic, and therefore many important properties of travelling waves can be obtained without numerical simulation. Figure 3.5 shows some solutions of the FitzHugh–Nagumo equation, both of which can be seen to be homoclinic travelling waves.

Heteroclinic travelling waves are found in chemical kinetics and combustion. Combustion waves are of practical and scientific interest. They represent simple models for the spread of a reaction in space. Chemical kinetics is the study of rates of chemical processes. This includes constructing mathematical models that can describe the features of a chemical reaction. Waves in chemical kinetics are found in frontal polymerisation, concentration reactions,

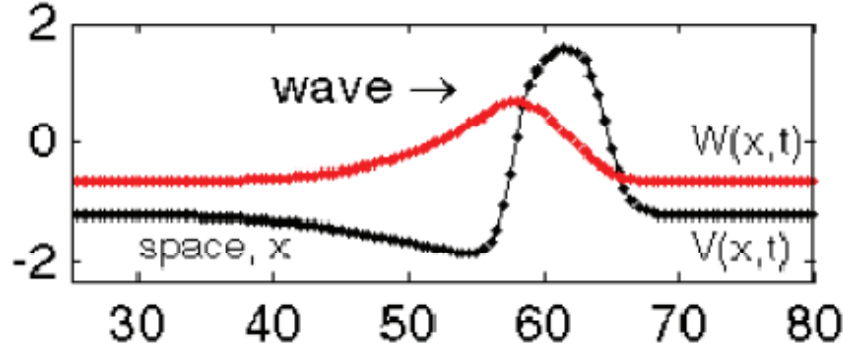


Figure 3.5: FitzHugh-Nagumo travelling wave solutions reproduced from [48].

cold flames, and so on. Figure 3.6 gives some solutions of different 2- and 3-dimensional combustion waves, which are all heteroclinic waves.

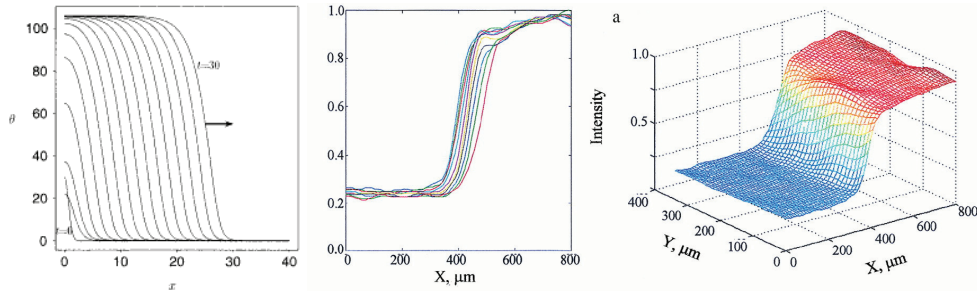


Figure 3.6: Combustion travelling wave solutions.

A periodic travelling wave has periodic boundary conditions (see Figure 3.7) and corresponds to a periodic orbit (see Figure 3.8) of the travelling wave equation phase portrait. That is, a periodic travelling wave will have the same value at the initial point and after one period T , that is $\varphi(0) = \varphi(T)$. A periodic orbit is an orbit the returns to the same point and in the 2-dimensional

case circulates a fixed point at its centre.

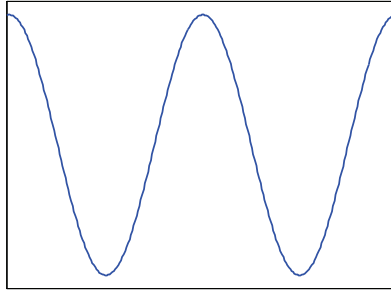


Figure 3.7: Periodic travelling wave.

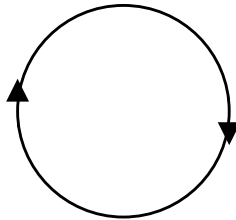


Figure 3.8: Periodic orbit.

An example of a periodic travelling wave is given by the PDE,

$$u_{tt} = u_{xx} - u.$$

Substituting travelling wave coordinates (3.1) into the above PDE and rearranging we get the ODE,

$$(c^2 - 1)\varphi'' = -\varphi,$$

which is the harmonic oscillator. We plotted the solution of the harmonic oscillator in Figure 1.13 and saw that it contained only periodic solutions. Hence, all travelling waves of this PDE are periodic.

3.1.1 Travelling Wave Solutions for the Multi-Hamiltonian Formulation

In this section we give the travelling wave solution of a PDE written in its multi-Hamiltonian form.

The multi-Hamiltonian form of a PDE given previously in Section 2.3 is,

$$\mathbf{K}\mathbf{z}_t + \mathbf{L}\mathbf{z}_x = \nabla_{\mathbf{z}}S(\mathbf{z}) \quad (3.2)$$

where \mathbf{K} and \mathbf{L} are constant skew-symmetric matrices, $S(\mathbf{z})$ is a smooth function, and $\mathbf{z} = \mathbf{z}(x, t)$ is a vector of state variables. For travelling wave solutions, we introduce the travelling wave coordinates,

$$\mathbf{z}(x, t) = \varphi(x - ct) = \varphi(\xi) \quad (3.3)$$

where $\xi = x - ct$ and c is the wave speed.

It follows that solutions of the form (3.3) satisfy

$$\mathbf{z}_t = -c\varphi'(\xi), \text{ and } \mathbf{z}_x = \varphi'(\xi).$$

Substituting the above and (3.3) into (3.2) we get the ODE

$$\begin{aligned} -c\mathbf{K}\varphi'(\xi) + \mathbf{L}\varphi'(\xi) &= \nabla S(\varphi(\xi)) \\ \Rightarrow (\mathbf{L} - c\mathbf{K})\varphi'(\xi) &= \nabla S(\varphi(\xi)). \end{aligned}$$

Therefore, by considering travelling wave solutions we reduce a PDE to an ODE problem. If the skew-symmetric matrix $\mathbf{L} - c\mathbf{K}$ is nonsingular then the ODE will be Hamiltonian. If $\mathbf{L} - c\mathbf{K} = \mathbf{0}$ then we get a system of N equations with N unknowns where N is the size of the square matrix \mathbf{K} (and \mathbf{L}). The system of equations is given by

$$\nabla S(\varphi(\xi)) = \mathbf{0}.$$

We hope that this will reduce the multisymplectic conservation law from the PDE type law, $\omega_t + \kappa_x = 0$, to that of an ODE type law, $(\kappa - c\omega)_\xi = 0$.

3.1.2 Travelling Wave Solutions for the Nonlinear Wave Equation

We use the nonlinear wave equation as our test problem for studying preservation of travelling waves in multisymplectic discretisations.

For now we look at the PDE in its original form, rather than putting it into its multi-Hamiltonian form (3.2).

The nonlinear wave equation is given by

$$u_{tt} = u_{xx} - V'(u) \quad (3.4)$$

where $V'(u)$ is some nonlinearity.

Substituting (3.3) into the nonlinear wave equation (3.4) we get

$$\begin{aligned} c^2 \varphi''(\xi) &= \varphi''(\xi) - V'(\varphi(\xi)) \\ \Rightarrow (c^2 - 1) \varphi''(\xi) &= -V'(\varphi(\xi)). \end{aligned}$$

This is a Hamiltonian ODE which usually possesses travelling wave solutions. Therefore, we wish to look for travelling wave solutions for multisymplectic discretisations of the nonlinear wave equation. Since this is a second order ODE, we can write it as a first order system to find the Hamiltonian. The phase portrait can then be drawn and the types of travelling waves the equation possesses can be determined from the orbits of the phase portrait.

The reduced ODE

$$(c^2 - 1) \varphi''(\xi) = -V'(\varphi(\xi)) \quad (3.5)$$

can be written as a first order system by letting

$$\psi(\xi) = (c^2 - 1) \varphi'(\xi).$$

Rearranging we get the first order Hamiltonian system,

$$\begin{aligned} \varphi'(\xi) &= \frac{\psi}{c^2 - 1} \\ \psi'(\xi) &= -V'(\varphi(\xi)) \end{aligned}$$

with Hamiltonian,

$$H = \frac{\psi^2}{2(c^2 - 1)} + V(\varphi).$$

We can now plot the Hamiltonian, as it is a function of 2 variables, and by looking at the different types of orbits in the solution we can determine what types of travelling waves are present in the original PDE. If we choose $V(\varphi) = \sin(\varphi)$ then we get the following phase portrait given by Figure 3.9. It can be seen that the nonlinear wave equation with sine nonlinearity contains periodic travelling waves and heteroclinic travelling waves.

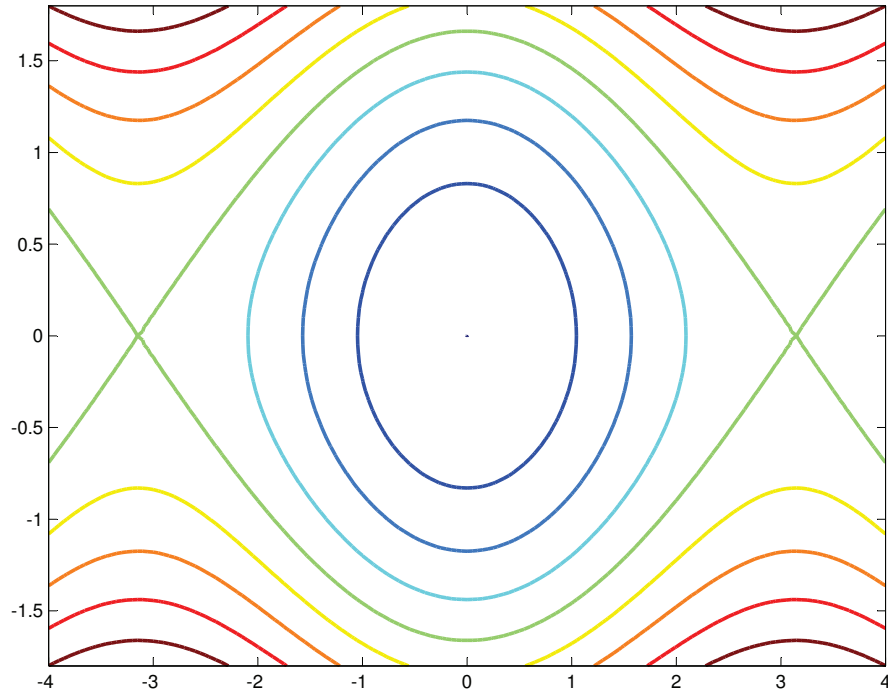


Figure 3.9: Phase portrait of the travelling wave equation of the sine-Gordon equation.

3.2 Travelling Wave Solutions in the Literature

In Section 3.1.1 we saw that by studying travelling wave solutions we reduce a PDE to a finite-dimensional ODE. Here we look at the types of equations we get by studying travelling wave solutions of discrete systems.

Most of the work on travelling wave solutions is done on systems which are discretised only in space, giving an infinite system of ODEs. These types of equations are known as lattice dynamical systems. Substitution of travelling wave coordinates into a lattice dynamical system results in a differential-difference equation, which is generally infinite-dimensional. Most of the work studying travelling waves of lattice dynamical systems looks at the values at which properties of the discrete lattice introduce behaviour that is not seen in the continuous problem.

Not as much work has been done on equations involving a discrete time component as well as a discrete spatial lattice. These types of equations are called coupled map lattices and can arise naturally or from the discretisation of PDEs in space and time. Studying travelling waves of a coupled map lattice results in a difference equation which can be finite or infinite depending on the parameters in the equation. We expect a coupled map lattice from the discretisation and substitution of travelling wave coordinates into our PDE.

3.2.1 Lattice Dynamical Systems (LDSs)

Lattice Dynamical Systems (LDSs), also sometimes called Lattice differential equations (LDEs), are systems of ordinary differential equations (ODEs) that have a discrete spatial structure. LDSs can arise from discretisations of a partial differential equation (PDE), but also occur naturally as systems in their own right. In the latter case, the system can be described as an infinite array of smaller subsystems. Here, the evolution of the subsystem at one site depends on the site itself and other sites, but the effect of sites far away is much weaker. This type of system need not be near a PDE continuum limit,

and is important in modeling many applications in which a discrete spatial structure plays a part.

A lattice Λ is a discrete subset of \mathbb{R}^N which contains finitely or infinitely many points and possesses some underlying spatial structure. More formally, LDSs are infinite systems of ODEs, indexed by points in a lattice. A LDS has the form

$$\dot{u} = g_\eta(\{u_\xi\}_{\xi \in \Lambda}), \quad \eta \in \Lambda \quad (3.6)$$

where the state vector $u = \{u_\eta\}_{\eta \in \Lambda}$ is coordinatised by the lattice Λ , and g_η is some function in these coordinates.

A solution to (3.6) is

$$u(t) = \{u_\eta(t)\}_{\eta \in \Lambda}.$$

Many LDS models are found in chemical reaction theory, image processing and pattern recognition, crystal growth and metallurgy in material science, wave propagation in excitable media in biology, and electrical circuit theory [25, 56, 18].

As with PDEs, LDSs involve dynamics with a spatial structure, but in many cases LDSs exhibit a range of phenomena not found in the associated PDEs. The following phenomena are all discussed in more detail further on. Direction dependence, the discreteness-induced Pierls–Nabarro (PN) periodic potential that can cause lattice pinning and propagation failure, and the destruction of translational invariance are a few properties introduced by the discrete lattice. The PN barrier grows exponentially fast as the natural parameter, the lattice spacing, of the problem increases. This barrier has been recognised as chiefly responsible for the resonances and eventual trapping and pinning of waves. Understanding the effect of discretisation is important when drawing conclusions from numerical simulations.

Discretisation of the n -dimensional Laplacian for $n \geq 2$ introduces directional dependence into the system. The introduction of directional dependence can be seen through an example of travelling wave solutions. Take the nonlinear wave equation with 2 spatial variables,

$$u_{tt} = u_{xx} + u_{yy} - V'(u), \quad (3.7)$$

where $u_{xx} + u_{yy}$ is the 2-dimensional Laplacian.

We introduce the travelling wave coordinates,

$$u(\mathbf{x}, t) = \varphi(\mathbf{x} \cdot \sigma - ct) = \varphi(\xi)$$

where $c \neq 0$ is the wave speed, σ is a 2-dimensional vector that determines the direction normal to the wave front and σ satisfies $\|\sigma\|^2 = 1$, and

$$\mathbf{x} = \begin{bmatrix} x \\ y \end{bmatrix}.$$

Substituting these coordinates into the nonlinear wave equation (3.7) and rearranging we get the ODE

$$\begin{aligned} (c^2 - \|\sigma\|^2)\varphi''(\xi) &= -V'(\varphi(\xi)), \text{ or} \\ (c^2 - 1)\varphi''(\xi) &= -V'(\varphi(\xi)). \end{aligned}$$

Looking at this ODE we see that it does not depend on σ , the direction vector.

On the other hand, if we discretise (3.7) in space by the leapfrog method we get a lattice ODE,

$$\ddot{u}_{ij} = \alpha(u_{i+1,j} - 2u_{ij} + u_{i-1,j}) + \beta(u_{i,j+1} - 2u_{ij} + u_{i,j-1}) - V'(u_{ij})$$

and upon substituting the travelling wave coordinates,

$$u_{ij}(t) = \varphi(\mathbf{k} \cdot \sigma - ct) = \varphi(\xi),$$

where σ is defined as above and

$$\sigma = \begin{bmatrix} \sigma_1 \\ \sigma_2 \end{bmatrix}, \quad \mathbf{k} = \begin{bmatrix} i \\ j \end{bmatrix},$$

we get the differential-difference equation

$$\begin{aligned} c^2\varphi''(\xi) &= \alpha(\varphi(\xi + \sigma_1) - 2\varphi(\xi) + \varphi(\xi - \sigma_1)) \\ &\quad + \beta(\varphi(\xi + \sigma_2) - 2\varphi(\xi) + \varphi(\xi - \sigma_2)) - V'(\varphi(\xi)) \end{aligned}$$

which now involves the variable σ and therefore depends on the direction of motion of the wave in the lattice.

The effect of spatial discretisation is most evident for wave speed c with $|c| \approx 0$.

Propagation failure is the failure of waves to move along a lattice. This is due to insufficient amount of energy to overcome the PN potential. This inability persists over an open set of parameters, that is, the wave speed c will be zero for a range of values of the parameters (see Figure 3.10). The range of propagation failure depends on the rational dependence or independence of the elements of σ . For numerical simulations the solution is piecewise constant when the elements of σ are rationally dependent. Propagation failure is more likely to occur for wavefronts with rational slopes, than with irrational slopes. Propagation failure is well studied for parabolic problems.

Conversely, in lattice pinning a wave has enough energy to get started but as it moves along the lattice it loses energy as radiation. This slows the wave down and it eventually comes to rest or ‘pins’.

Discrete models commonly break the translational invariance (TI) of their corresponding continuous system. Typically, the case for nonlinear waves is that there are two static wave configurations that are generated from the breaking of TI. One of them is centred on a lattice site (higher energy) and one is centred between two consecutive lattice sites (lower energy). The difference in energy between these two sites is the PN barrier.

The study of discrete Hamiltonian systems is focused on two areas. Firstly, the continuum approximation is studied. Here the discrete Hamiltonian reduces to a PDE, which can in turn be reduced to an ODE by studying travelling wave solutions. Mathematically, the equation resulting from substituting travelling wave coordinates into the discrete system is much more complicated than that of the equivalent ODE obtained for the continuous system. Secondly, the discrete Hamiltonian system is studied through numerical studies.

In general, no information on the global behaviour of solutions of a PDE can be derived from the study of its discrete versions even when steps of

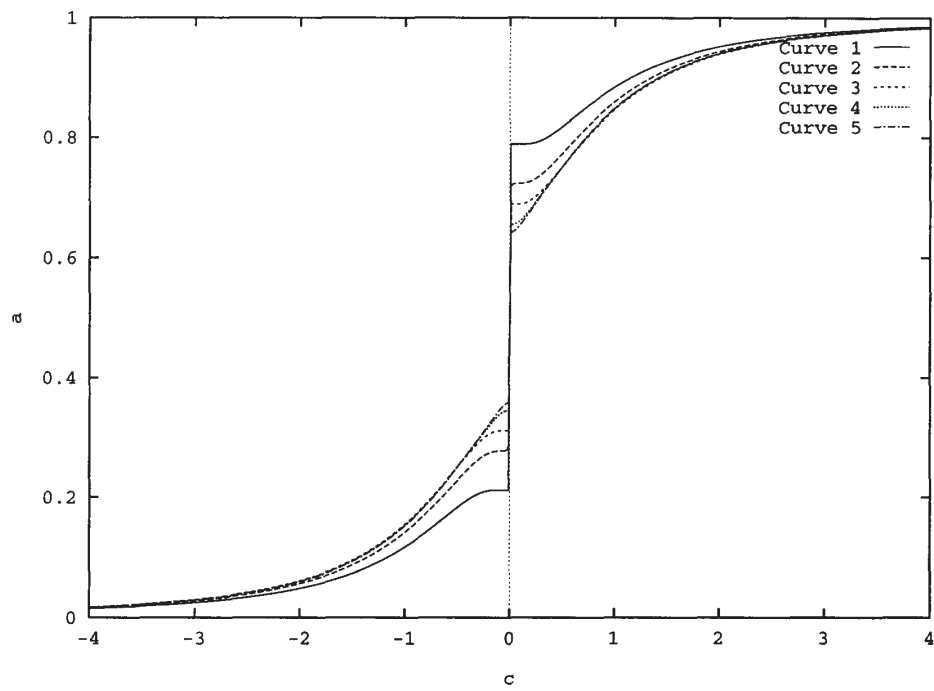


Figure 3.10: Propagation failure for different values of parameters: a versus c for different values of σ , where $a \in (0, 1)$ and c is the wave speed. This figure is reproduced from [25].

discretisation size are small.

Over the recent years there has been an increasing number of papers comparing the significant differences in the behaviour of PDEs of the continuum nonlinear field theories and their spatially discrete versions.

In [5], the continuous sine-Gordon (SG) equation is compared with its discrete version, the Frenkel–Kontorova (FK) model. Studying the continuous SG model is considered as an acceptable approximation to the system dynamics of the FK model, because, even though the discreteness introduces phenomena not exhibited by the continuous system, the main properties of kinks and their existence as topological states does not depend significantly on the discreteness of the primary model.

So far, there is no known explicit kink solution of the FK model. As described earlier, the discrete lattice introduces the existence of the PN periodic potential, and a moving kink in the FK model with not enough energy is subject to propagation failure, becoming trapped between two adjacent lattice sites, while a kink which starts off with enough speed to overcome the PN barrier is subject to lattice pinning. The translational invariance in the continuum limit of the FK model, of the kink along a chain, is broken in the discrete model, where TI occurs only for integer multiples of the size of the lattice spacing.

In numerical simulations a single-kink solution of the SG equation with some nonzero initial velocity is chosen as an initial configuration of a kink then such a construction will never evolve into a steady state. Initially, this state will transform into a kink with a modified shape and as a result, the kink will propagate through the chain not freely but with an oscillatory velocity, caused by the lattice discreteness.

Also, the discreteness of the FK model reduces the kink’s width, which in turn increases the PN barrier.

The kinks correspond to two homoclinic orbits of the standard map, the stable and unstable manifolds. In the exactly integrable SG equation these two manifolds overlap; but in the discrete FK system the manifolds are different,

being characterised by different energies.

In [49], they find solutions to the discrete Klein-Gordon (KG) system. They find single pulse solutions which consist of a non-decaying oscillatory tail. The oscillations are small with respect to the central pulse amplitude (see Figure 3.11). Solutions without an oscillatory solution may exist for exceptional values of the parameters, but this situation is not common.

In the small amplitude limit, the pulses possess an exponentially small oscillatory tail which is close to spatially localised solutions. On the other hand, in the high-amplitude regime there are good approximations of spatially localised solutions when the period tends to infinity. That is, for solutions u , with boundary conditions $\varphi_i(\xi + M) = \varphi_i(\xi)$, where M is large the solutions are good approximations.

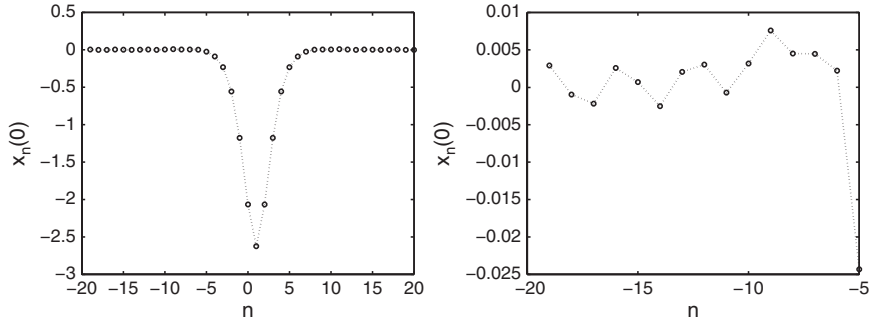


Figure 3.11: Left: A single pulse solution. Right: Zoom on the oscillatory tail from the solution on the left. This figure is reproduced from [49].

Small amplitude pulsating travelling waves in the KG lattice can be seen as trajectories of an infinite-dimensional differential equation, lying on a finite-dimensional centre manifold.

3.2.2 Coupled Map Lattices (CMLs)

While a lot of work has gone into studying LDSs, there seems to be not so much on Coupled Map Lattices (CMLs). As well as discrete space, a CML is a dynamical system that also has discrete time. A natural source of CMLs are discrete (both in space and time) versions of PDEs of evolution type and arise while modeling PDEs by computers.

The effect of temporal discretisation is most evident for large wave speeds. The shape of the solution being step-like corresponds to lurching in the interface motion and is due to either space or time discretisation. Typically, speed up of the wave is due to time discretisation only, and propagation failure is due to spatial discretisation only.

Chapter 4

Travelling Wave Solutions for Multisymplectic Discretisations of Wave Equations with Simplified Nonlinearities

In this chapter we attempt to find travelling wave solutions for the multisymplectic discretisation of the non linear wave equation. This is one way to test the behaviour of a numerical method. Solving a nonlinear equation is difficult, so we simplify our nonlinearity. The new nonlinearity still resembles the form of a nonlinear equation, but makes our problem piecewise linear. Although this makes the problem much simpler to solve, we still had difficulty in solving it. We then go on to look at a more complicated nonlinearity and finally in the next chapter a smooth nonlinearity. We begin by making a multisymplectic discretisation of the general nonlinear wave equation (3.4) and then form our discrete travelling wave equation (4.4) by the substitution of discrete travelling wave coordinates.

4.1 A Multisymplectic Discretisation of the Non-linear Wave Equation (3.4)

We choose to use the leapfrog method in space and time as our multisymplectic integrator. This produces the five-point stencil shown in Figure 4.1. The grid points across the stencil horizontally represent the leapfrog method in space with grid point spacing Δx , and those across the stencil vertically represent the leapfrog method in time with grid point spacing Δt .

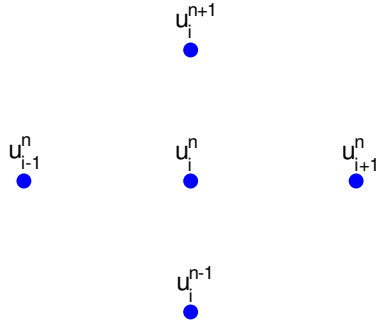


Figure 4.1: The five-point stencil used in the leapfrog method.

Discretising the nonlinear wave equation (3.4) with the leapfrog method in space and time we get

$$\frac{1}{(\Delta t)^2} (u_i^{n+1} - 2u_i^n + u_i^{n-1}) - \frac{1}{(\Delta x)^2} (u_{i+1}^n - 2u_i^n + u_{i-1}^n) = -V'(u_i^n)$$

where Δt is the time step size and Δx is the spatial step size. By setting $\kappa = c\Delta t$ and $\sigma = \Delta x$ as in Section 3.1.1 we get

$$\frac{c^2}{\kappa^2} (u_i^{n+1} - 2u_i^n + u_i^{n-1}) - \frac{1}{\sigma^2} (u_{i+1}^n - 2u_i^n + u_{i-1}^n) = -V'(u_i^n). \quad (4.1)$$

4.1.1 The Discrete Travelling Wave Equation

In this section we present what we refer to as the discrete travelling wave equation. It is the result of substituting travelling wave coordinates into the leapfrog discretisation of the nonlinear wave equation given in (4.1).

We want to look for travelling wave solutions of the discretisation (4.1) so we define discrete travelling wave coordinates. For a discrete solution $\mathbf{z}(x_i, t_n)$ we seek travelling wave solutions of the form

$$\begin{aligned}\mathbf{z}(x_i, t_n) &= \varphi(x_i - ct_n) \\ &= \varphi(i\Delta x - cn\Delta t).\end{aligned}$$

We now let

$$\sigma = \Delta x, \quad \kappa = c\Delta t.$$

That is, we are seeking solutions of the form

$$\begin{aligned}\mathbf{z}(x_i, t_n) &= \varphi(i\Delta x - cn\Delta t) \\ &= \varphi(i\sigma - n\kappa)\end{aligned}\tag{4.2}$$

The ratio $\frac{\sigma}{\kappa}$ becomes important later on in this chapter.

We substitute the discrete travelling wave coordinates,

$$u_i^n = \varphi(i\sigma - n\kappa) = \varphi(\xi)\tag{4.3}$$

into (4.1) to produce what we call the discrete travelling wave equation

$$\begin{aligned}\frac{c^2}{\kappa^2} (\varphi(\xi + \kappa) - 2\varphi(\xi) + \varphi(\xi - \kappa)) \\ - \frac{1}{\sigma^2} (\varphi(\xi + \sigma) - 2\varphi(\xi) + \varphi(\xi - \sigma)) = -V'(\varphi(\xi)), \quad \xi \in \mathbb{R}.\end{aligned}\tag{4.4}$$

Here ξ is a real variable, so we have five grid points, $\varphi(\xi - \sigma)$, $\varphi(\xi - \kappa)$, $\varphi(\xi)$, $\varphi(\xi + \kappa)$, $\varphi(\xi + \sigma)$, which have to be evaluated at all real values. Therefore, this equation is really infinite-dimensional, which makes it very difficult to solve and analyse.

Also, there are two different cases that need to be considered depending on whether the ratio of κ and σ is rational or irrational. When $\frac{\sigma}{\kappa}$ is rational and we move the grid points along the length of the grid, at some stage the points will match up with each other. On the other hand, if $\frac{\sigma}{\kappa}$ is irrational the grid points will never match up. To demonstrate this see Figure 4.2. Here, the top part of each ratio shows the five grid points and the bottom part has red dots

with size κ spacing and blue dots for size σ spacing. For the top two (rational) ratios we see that the red and blue dots match up at some stage along the grid points, but for the bottom (irrational) ratio the red and blue dots do not match up at any point (except the centre grid point) and never will.

Therefore, when $\frac{\sigma}{\kappa} = \frac{m}{n}$, where m and n are positive integers, the discrete travelling wave equation can be thought of as a finite (possibly high) dimensional map. The resulting map will be $2m$ -dimensional and will have a corresponding finite-dimensional symplectic conservation law. Otherwise, the discrete travelling wave equation will be truly infinite-dimensional, with an infinite-dimensional symplectic conservation law. When $\frac{\sigma}{\kappa}$ is rational the discrete travelling wave equation (4.4) corresponds to a symmetric multistep method of degree $2m$. Section 6.5 gives more detail on the discrete travelling wave as a symmetric multistep method.

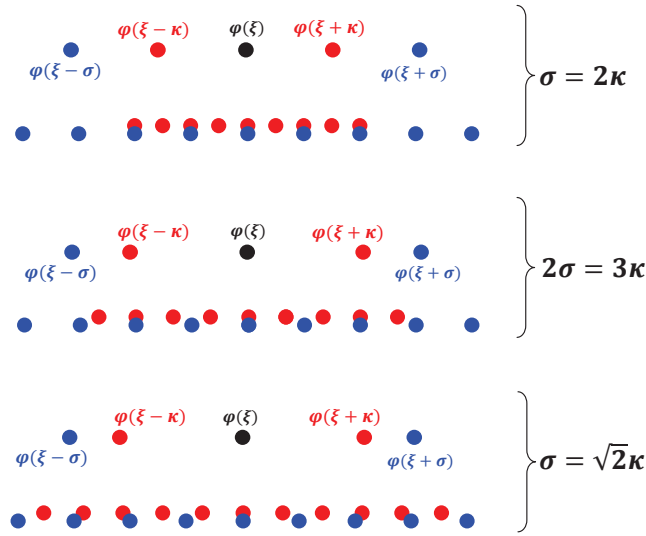


Figure 4.2: Grid points of the discrete travelling wave equation (4.4) with spacing κ (red) and σ (blue).

Note $\sigma \geq \kappa$ for stability.

Boundary conditions can be imposed on the discrete travelling wave equation corresponding to each type of orbit in the phase portrait,

- Homoclinic: $\varphi(\pm\infty) = \varphi_0$;
- Heteroclinic: $\varphi(+\infty) = \varphi_+$, $\varphi(-\infty) = \varphi_-$;
- Periodic: $\varphi(T) = \varphi(0)$.

We begin our study of the discrete travelling wave equation by choosing a very simple nonlinearity, the McKean caricature.

4.2 Discrete Travelling Wave Equation with McKean Nonlinearity

In this section we begin by introducing the McKean caricature and model. We then use this as the nonlinearity in the nonlinear wave equation and solve this continuous case for a heteroclinic travelling wave. Next, we briefly discuss the dynamics of symmetric methods using an example. As we are interested in the dynamics of the discrete case we next move onto the semi-discrete case and finally the fully discrete case. After making some conclusions on the discrete case we look at periodic travelling wave solutions of the discrete travelling wave equation with McKean nonlinearity.

The McKean caricature (cubic) is a very simplified version of a cubic function and is given by the formula,

$$f(x) = -x + h(x - a) \tag{4.5}$$

where $0 < a < 1$ is a threshold and h is the Heaviside function. It is piecewise linear function with a discontinuity at $x = a$. McKean, in 1970 [61], used this function originally in the McKean model for studying nerve conduction. The McKean model is given by

$$\begin{aligned} \dot{x} &= f(x) - y + I \\ \dot{y} &= b(x - cy) \end{aligned}$$

where $f(x)$ is given in (4.5), x is the membrane potential, y is a recovery variable and a, c are constants.

This model is a piecewise linear caricature of the FitzHugh–Nagumo equations, which we discussed in Section 3.1. Taking a piecewise nonlinearity allowed McKean to perform explicit calculations, while still preserving the essential features of neuronal behaviour. Note that the McKean model is dissipative, whereas the nonlinear wave equation is non-dissipative.

If we use the McKean caricature for the nonlinearity in the nonlinear wave equation (3.4) (see Figure 4.3) we get a piecewise linear wave equation (with discontinuity at $u = a$)

$$u_{tt} = u_{xx} - u + h(u - a) \quad (4.6)$$

where $a \in (0, 1)$ and

$$h(u) = \begin{cases} 0 & \text{if } u < 0 \\ 1 & \text{if } u > 0. \end{cases} \quad (4.7)$$

Hence,

$$h(u - a) = \begin{cases} 0 & \text{if } u < a \\ 1 & \text{if } u > a. \end{cases} \quad (4.8)$$

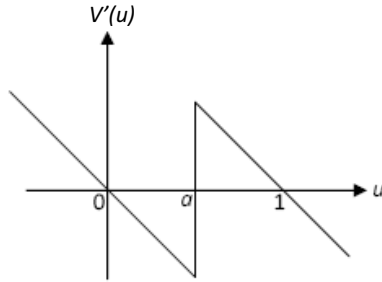


Figure 4.3: McKean nonlinearity: $V'(u) = u - h(u - a)$.

4.2.1 The Continuous Case

Firstly, we consider the continuous case with travelling wave solution

$$u(x, t) = \varphi(x - ct) = \varphi(\xi) \quad (4.9)$$

where $\xi = x - ct$ and $0 \leq |c| < 1$.

Upon substituting (4.9) into (4.6) and rearranging, the wave equation becomes

$$(c^2 - 1)\varphi''(\xi) = -\varphi(\xi) + h(\varphi(\xi) - a) \quad (4.10)$$

where

$$h(\varphi(\xi) - a) = \begin{cases} 0 & \text{if } \varphi(\xi) < a \\ 1 & \text{if } \varphi(\xi) > a. \end{cases} \quad (4.11)$$

Now we have an ODE and can plot the phase portrait (see Figure 4.4) to determine what types of travelling waves are present in the equation. From Figure 4.4, we see that (4.10) possesses periodic and heteroclinic travelling waves. We wish to look at the travelling waves corresponding to a heteroclinic orbit so we impose the following boundary conditions,

$$\lim_{\xi \rightarrow -\infty} \varphi(\xi) = 0, \quad \lim_{\xi \rightarrow \infty} \varphi(\xi) = 1. \quad (4.12)$$

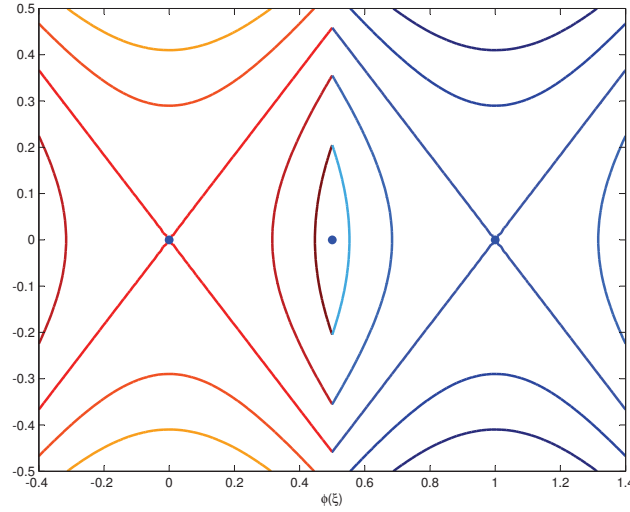


Figure 4.4: Phase portrait of the travelling wave equation of the nonlinear wave equation with McKean nonlinearity.

Figure 4.5 gives a travelling wave solution which satisfies the boundary conditions (4.12). This is what we expect our analytic solution to look like.

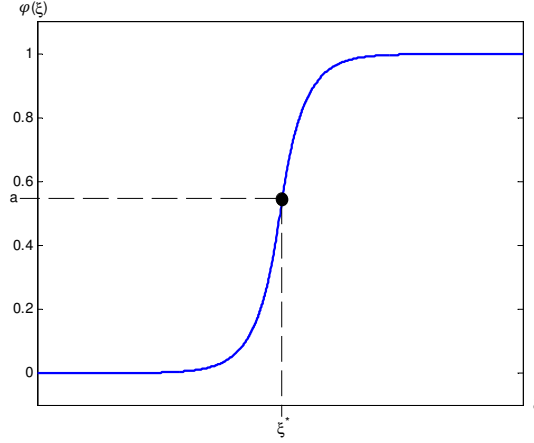


Figure 4.5: Expected travelling wave solution of the nonlinear wave equation with McKean nonlinearity.

Given that $a \in (0, 1)$ and the limits in the boundary conditions (4.12), there must be a value ξ for which $\varphi(\xi) = a$. If we choose this value to be ξ^* , then we get

$$\varphi(\xi^*) = a.$$

It is easy to see from Figure 4.5 that if we have any value of ξ less than ξ^* then $\varphi(\xi)$ will be less than $\varphi(\xi^*) = a$, and for any value of ξ greater than ξ^* then $\varphi(\xi)$ will be greater than $\varphi(\xi^*) = a$. Thus, we get

$$\begin{aligned} \varphi(\xi) &< a & \text{for } \xi < \xi^* \\ \varphi(\xi) &> a & \text{for } \xi > \xi^*. \end{aligned} \tag{4.13}$$

Substituting (4.13) into the (4.11) we get

$$h(\varphi(\xi) - a) = \begin{cases} 0 & \text{if } \xi < \xi^* \\ 1 & \text{if } \xi > \xi^*. \end{cases}$$

Hence,

$$h(\varphi(\xi) - a) = h(\xi - \xi^*).$$

Note that due to translational invariance we can take $\xi^* = 0$ without loss of generality. Then $h(\varphi(\xi) - a) = h(\xi)$ for $\xi \neq 0$.

The continuous problem (4.10) now becomes,

$$(c^2 - 1)\varphi''(\xi) = -\varphi(\xi) + h(\xi - \xi^*). \quad (4.14)$$

Because of the special form of h , the nonlinear travelling wave equation (4.10) has become, for the form of heteroclinic travelling waves considered here (see Figure 4.5), the linear equation (4.14). This is the essential reason for considering the McKean nonlinearity.

We need a preliminary result, before going further, to justify the use of the Fourier transform to solve the equation.

Lemma 4.2.1. *There exists an $\epsilon > 0$ such that*

$$|\varphi(\xi)| \leq Ke^{\epsilon\xi} \quad \text{for } \xi \leq 0$$

for some $K > 0$.

Proof. See Lemma 4.1 of [13] for the proof. □

We seek a solution for equation (4.14), and, based on Lemma 4.2.1, we apply the change of variables

$$\varphi_\epsilon(\xi) = e^{-\epsilon\xi}\varphi(\xi) \quad (4.15)$$

where $\epsilon > 0$ is sufficiently small. Noting that

$$\begin{aligned} \varphi(\xi) &= e^{\epsilon\xi}\varphi_\epsilon(\xi) \\ \varphi'(\xi) &= e^{\epsilon\xi}(\epsilon\varphi_\epsilon(\xi) + \varphi'_\epsilon(\xi)) \\ \varphi''(\xi) &= e^{\epsilon\xi}(\epsilon^2\varphi_\epsilon(\xi) + 2\epsilon\varphi'_\epsilon(\xi) + \varphi''_\epsilon(\xi)) \end{aligned}$$

we get

$$(c^2 - 1)e^{\epsilon\xi}(\epsilon^2\varphi_\epsilon(\xi) + 2\epsilon\varphi'_\epsilon(\xi) + \varphi''_\epsilon(\xi)) = -e^{\epsilon\xi}\varphi_\epsilon(\xi) + h(\xi - \xi^*)$$

which simplifies to

$$(c^2 - 1)(2\epsilon\varphi'_\epsilon(\xi) + \varphi''_\epsilon(\xi)) + \varphi_\epsilon(\xi)(1 + \epsilon^2(c^2 - 1)) = e^{-\epsilon\xi}h(\xi - \xi^*).$$

Applying the Fourier transform,

$$\hat{\varphi}_\epsilon(s) = \int_{-\infty}^{\infty} e^{-is\xi} \varphi_\epsilon(\xi) d\xi \quad (4.16)$$

and using the properties of Fourier transforms, we get

$$(c^2 - 1)(2\epsilon is \hat{\varphi}_\epsilon(s) - s^2 \hat{\varphi}_\epsilon(s)) + \hat{\varphi}_\epsilon(s)(1 + \epsilon^2(c^2 - 1)) = \frac{e^{-(is+\epsilon)\xi^*}}{is + \epsilon}$$

which simplifies to

$$\hat{\varphi}_\epsilon(s) = \frac{e^{-(is+\epsilon)\xi^*}}{(is + \epsilon)R(s - i\epsilon)}$$

where $R_{\text{Cont}}(s) = 1 - c^2 s^2 + s^2$.

Next, we take the inverse Fourier transform,

$$\varphi_\epsilon(\xi) = \frac{1}{2\pi} \int_{-\infty}^{\infty} e^{is\xi} \hat{\varphi}_\epsilon(s) ds, \quad (4.17)$$

and remembering the change of variables we applied,

$$\varphi(\xi) = e^{\epsilon\xi} \varphi_\epsilon(\xi),$$

we get a formula for the solution in the original variables,

$$\begin{aligned} \varphi(\xi) &= \frac{1}{2\pi} \int_{-\infty}^{\infty} e^{\epsilon\xi} e^{is\xi} \hat{\varphi}_\epsilon(s) ds \\ &= \frac{1}{2\pi} \int_{-\infty}^{\infty} e^{(is+\epsilon)\xi} \hat{\varphi}_\epsilon(s) ds \\ &= \frac{1}{2\pi} \int_{-\infty}^{\infty} \frac{e^{(is+\epsilon)\xi} e^{-(is+\epsilon)\xi^*}}{(is + \epsilon)R(s - i\epsilon)} ds. \end{aligned}$$

Taking the limit as $\epsilon \rightarrow 0$ and changing the limits of integration we get

$$\begin{aligned} \varphi(\xi) &= \frac{1}{2\pi} \int_{-i\epsilon-\infty}^{-i\epsilon+\infty} \frac{e^{is(\xi-\xi^*)}}{is R_{\text{Cont}}(s)} ds \\ &= \frac{1}{2\pi i} \int_{-i\epsilon-\infty}^{-i\epsilon+\infty} \frac{e^{is(\xi-\xi^*)}}{s R_{\text{Cont}}(s)} ds \end{aligned}$$

where $R_{\text{Cont}}(s) = 1 - c^2 s^2 + s^2$.

The domain of integration is changed slightly in order that residue theory can be applied to evaluate the improper integral.

We can factorise $R_{\text{Cont}}(s)$ to get,

$$R_{\text{Cont}}(s) = (1 - c^2) \left(s - \frac{i}{\sqrt{1 - c^2}} \right) \left(s + \frac{i}{\sqrt{1 - c^2}} \right).$$

Now, we have to evaluate the integral

$$\frac{1}{2\pi i} \int_{-i\epsilon - \infty}^{-i\epsilon + \infty} \frac{e^{is(\xi - \xi^*)}}{(1 - c^2) s \left(s - \frac{i}{\sqrt{1 - c^2}} \right) \left(s + \frac{i}{\sqrt{1 - c^2}} \right)} ds$$

which we do by residue theory. Firstly, let

$$f(s) = \frac{1}{2\pi i} \frac{e^{is(\xi - \xi^*)}}{(1 - c^2) s \left(s - \frac{i}{\sqrt{1 - c^2}} \right) \left(s + \frac{i}{\sqrt{1 - c^2}} \right)} \quad (4.18)$$

where $s \in \mathbb{C}$.

Here $f(s)$ has 3 singularities,

$$s_0 = 0, \quad s_1 = \frac{i}{\sqrt{1 - c^2}}, \quad s_2 = -\frac{i}{\sqrt{1 - c^2}}.$$

These singularities are plotted in Figure 4.6 for $0 \leq c < 1$.

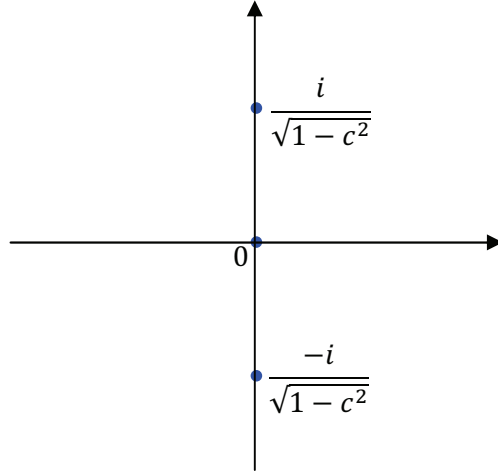


Figure 4.6: The singularities of equation (4.18).

Now, we close the top half plane with a semi-circular region taking the real axis to at $-i\epsilon$. See Figure 4.7. The singularities enclosed by this region are s_0 and s_1 .

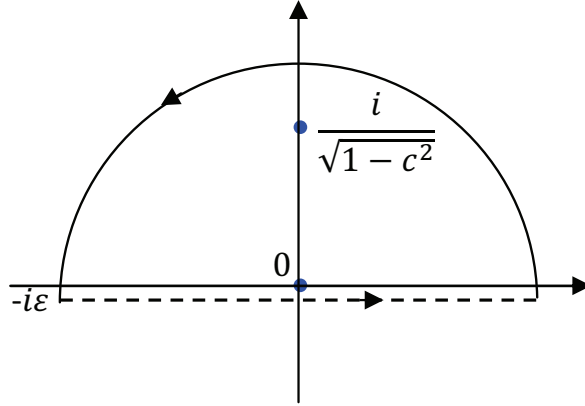


Figure 4.7: Contour in the upper half plane.

Using the fact that

$$\int_{-\infty}^{\infty} f(s)ds = 2\pi i \sum_{k=0}^n \text{Res}_{s=s_k} f(s),$$

we get the solution

$$\varphi(\xi) = 1 - \frac{1}{2} e^{\frac{-(\xi-\xi^*)}{\sqrt{1-c^2}}}, \quad \xi > \xi^*.$$

Similarly, if we close the bottom half plane, taking minus the sum of the residues we get,

$$\varphi(\xi) = \frac{1}{2} e^{\frac{(\xi-\xi^*)}{\sqrt{1-c^2}}}, \quad \xi < \xi^*.$$

Hence, the explicit analytic solution for the continuous case is

$$\varphi(\xi) = \begin{cases} 1 - \frac{1}{2} e^{\frac{-(\xi-\xi^*)}{\sqrt{1-c^2}}} & \text{if } \xi > \xi^* \\ \frac{1}{2} e^{\frac{(\xi-\xi^*)}{\sqrt{1-c^2}}} & \text{if } \xi < \xi^* \end{cases} \quad (4.19)$$

Graphing the solution (See Figure 4.8) for $c = 0.1$ and $\xi^* = 0$, we see that we obtain a heteroclinic travelling wave, which is what we were looking for. Hence, the continuous problem has a solitary wave solution.

Later, we want to discretise (4.6) with a multisymplectic integrator to see if we preserve this travelling wave solution in the discrete equation. However, first we look at the preservation of travelling waves of symmetric methods.

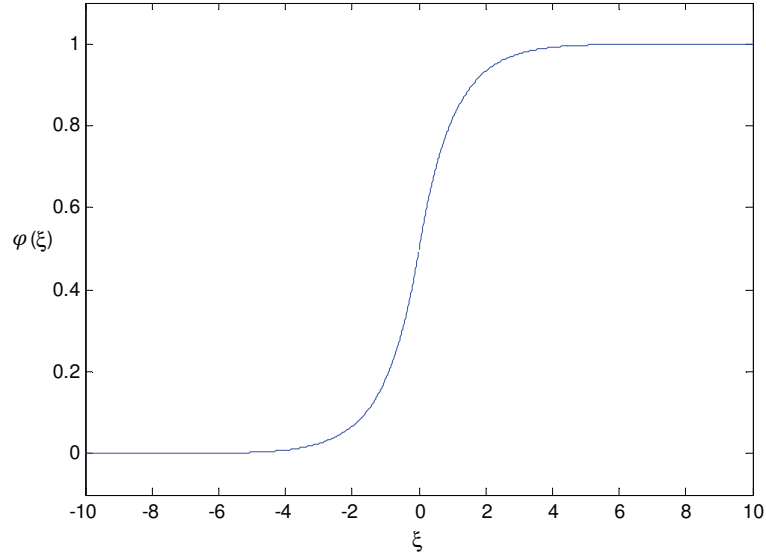


Figure 4.8: Travelling wave solution (4.19) of (4.6) with $c = 0.1$ and $\xi^* = 0$.

4.2.2 Symmetric PDEs and Symmetric Methods: An Example

Symmetric methods tend to give good long-time behaviour. Here we will show that for the preservation of travelling wave solutions this is not always true. Symmetric methods only preserve symmetric waves. This is important because the conventional wisdom is that it is sufficient to preserve the symmetry of differential operators to get qualitatively good results. We chose the symmetric nonlinear wave equation,

$$u_{tt} = u_{xx} - \sin(u) - \frac{2}{5} \cos(2u) \quad (4.20)$$

to demonstrate this.

The model ODE,

$$u_{tt} = -\sin(u) - \frac{2}{5} \cos(2u),$$

was used by in [37] to study non-conservation of energy by symmetric integrators. This ODE is time-reversible, but has non-symmetric orbits. In the pendulum, $u_{tt} = -\sin(u)$, almost all orbits are symmetric with respect to the

reversing symmetry $u \rightarrow -u$. It is necessary to break this symmetry to see the influence of non-symmetric orbits.

Eq. (4.20) has the phase portrait given in Figure 4.9. From this we see that the continuous solution contains periodic and heteroclinic travelling waves.

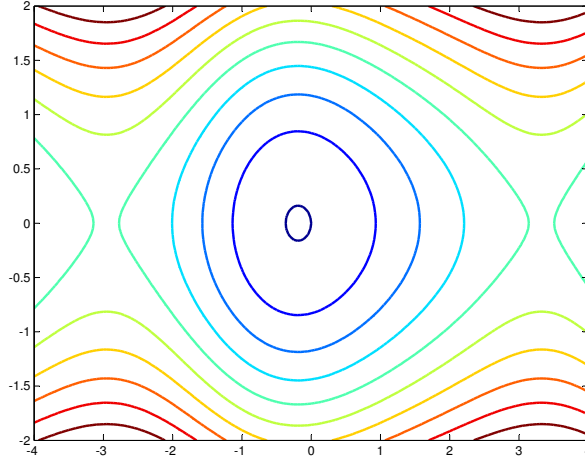


Figure 4.9: The phase portrait of the symmetric PDE (4.20).

We chose one of the heteroclinic orbits and plot the corresponding solution in Figure 4.10. Note the exact solution giving a heteroclinic travelling wave here is non-symmetric under $x \mapsto -x$ and the exact solution contains no homoclinic travelling waves.

The 3-stage Lobatto IIIA method is applied to the symmetric PDE (4.20). This Runge–Kutta method is symmetric, non-symplectic, 4th order in time and 2nd order in space. We look for travelling waves in the simplest setting $\sigma/\kappa = 1$. The results from this method are plotted in Figure 4.11 and shows that the method has no heteroclinic travelling waves for any Δx , but it does have homoclinic travelling waves. These are formed by gluing together a heteroclinic wave and its reflection a distance $\log(\Delta x)$ apart. To conclude, the symmetric method has a qualitatively wrong travelling wave structure for all Δx .

We hope that a multisymplectic integrator performs better than a symmetric method in the preservation of travelling waves.

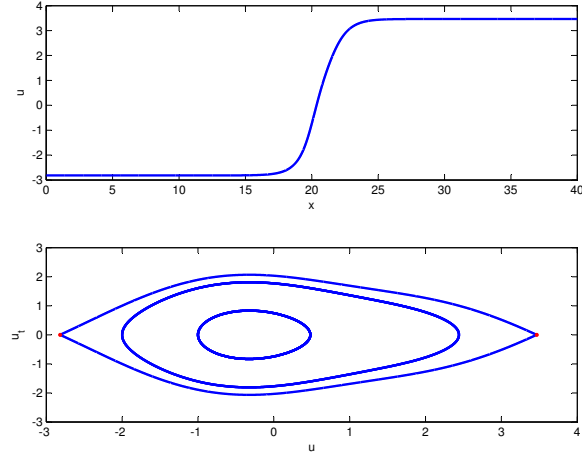


Figure 4.10: Exact solution of the symmetric PDE (4.20).

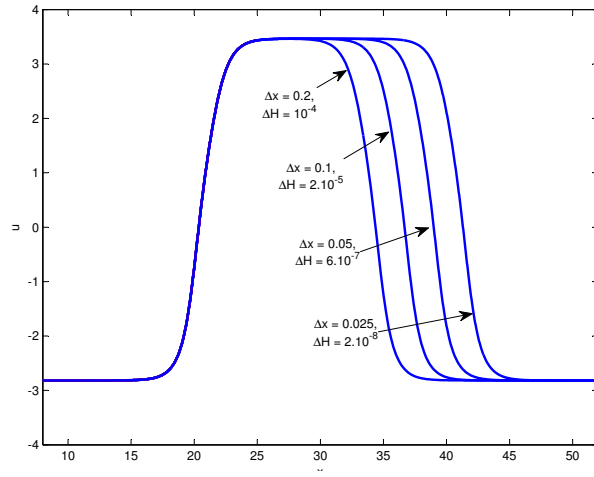


Figure 4.11: Numerical solution of the symmetric PDE (4.20) with a symmetric method.

4.2.3 The Semi-Discrete Case

Discretising equation (4.6) in the x direction using the symplectic leapfrog method we get a lattice dynamical system, the infinite system of ODEs

$$u_{tt} = \frac{u_{i+1}^n - 2u_i^n + u_{i-1}^n}{\sigma^2} - u_i^n + h(u_i^n - a). \quad (4.21)$$

For a travelling wave solution we substitute

$$u_i(t) = \varphi(i\sigma - ct) = \varphi(\xi) \quad (4.22)$$

into (4.21) to obtain the differential-difference equation,

$$c^2 \varphi''(\xi) = \frac{1}{\sigma^2} (\varphi(\xi + \sigma) - 2\varphi(\xi) + \varphi(\xi - \sigma)) - \varphi(\xi) + h(\xi - \xi^*).$$

Now, applying the change of variables (4.15), as was done in the continuous case, we get

$$\begin{aligned} c^2 (\varphi_\epsilon''(\xi) + 2\epsilon \varphi_\epsilon'(\xi)) &= \frac{1}{\sigma^2} (e^{\epsilon\sigma} \varphi_\epsilon(\xi + \sigma) - 2\varphi_\epsilon(\xi) + e^{-\epsilon\sigma} \varphi_\epsilon(\xi - \sigma)) \\ &\quad - (1 + c^2 \epsilon^2) \varphi_\epsilon(\xi) + e^{-\epsilon\xi} h(\xi - \xi^*). \end{aligned}$$

Applying the Fourier transform (4.16) we get,

$$\hat{\varphi}_\epsilon(s) = \frac{e^{-(is+\epsilon)\xi^*}}{(is + \epsilon)R(s - i\epsilon)}$$

where

$$R_{\text{Semi}}(s) = 1 - c^2 s^2 + \frac{2}{\sigma^2} (1 - \cos(\sigma s)). \quad (4.23)$$

Taking the inverse Fourier transform (4.17), we get the solution

$$\varphi(\xi) = \frac{1}{2\pi i} \int_{-i\epsilon-\infty}^{-i\epsilon+\infty} \frac{e^{is(\xi-\xi^*)}}{sR_{\text{Semi}}(s)} ds \quad (4.24)$$

where $R_{\text{Semi}}(s)$ is given in (4.23).

If this integral exists then the semi-discrete case has an explicit solution.

The integral (4.24) is difficult to evaluate as the zeros of $R_{\text{Semi}}(s)$ need to be found. But these zeros cannot be found algebraically. So an explicit solution φ was not found in this case. Instead we take a Taylor series approximation of the

cosine function in $R_{\text{Semi}}(s)$ and then use residue theory, as for the continuous case, to give an approximate solution for $\varphi(\xi)$.

Taking a second order Taylor series approximation we get,

$$\begin{aligned} R_{\text{Semi}}(s) &= 1 - c^2 s^2 + \frac{2}{\sigma^2} \left(1 - \left(1 - \frac{(\sigma s)^2}{2} + \frac{(\sigma s)^4}{24} + \dots \right) \right) \\ &\approx 1 - c^2 s^2 + \frac{2}{\sigma^2} \left(\frac{\sigma^2 s^2}{2} \right) \\ &= 1 - c^2 s^2 + s^2. \end{aligned}$$

So, in this semi-discrete case,

$$R_{\text{Semi}}(s) \approx 1 - c^2 s^2 + s^2,$$

which is the same as $R_{\text{Cont}}(s)$ which we found in the continuous case. Therefore, an approximation of the semi-discrete solution gives a travelling wave solution equivalent to the continuous case. To get an idea if this approximation to the semi-discrete solution is close to the actual solution of this system, we can take increasingly higher order approximations to the cosine function in $R_{\text{Semi}}(s)$ and apply residue theory by finding the zeros. But as higher order approximations are taken the number of zeros of $R_{\text{Semi}}(s)$ increases and so the difficulty of finding them becomes increasingly more difficult, so we are almost back to square one.

We now look at an example of $R_{\text{Semi}}(s)$ which has a fourth order approximation of the cosine function,

$$R_{\text{Semi}}(s) \approx 1 - c^2 s^2 + s^2 - \frac{\sigma^2 s^4}{12}.$$

We plot the roots of this approximation for $c = 0.7$ and $\sigma = 0.5$ in Figure 4.12 on the left. We see that as well as pure imaginary roots we have roots on the real line. In Section 4.2.4 we see that roots on the real line produce wiggles in the solution. On the right of Figure 4.12 the roots of $R_{\text{Semi}}(s)$ are plotted for an 8th order approximation of the cosine term for $c = 0.7$ and $\sigma = 0.5$.

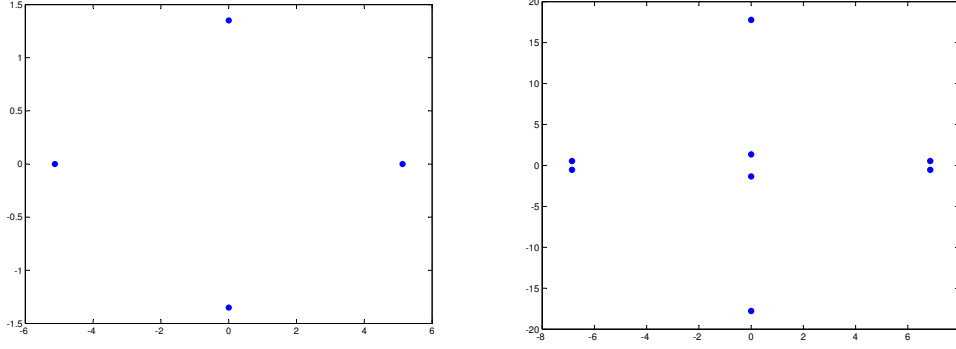


Figure 4.12: The zeros of $R_{\text{Semi}}(s)$ with a 4th order cosine approximation on the left and an 8th order cosine approximation on the right.

4.2.4 The Discrete Case

Our eventual goal is to study travelling wave solutions for multisymplectic discretisations of the nonlinear wave equation (3.4) with smooth nonlinearity. For a multisymplectic integration we use the leapfrog method in space and time and first apply this to our simplified nonlinearity, the McKean cubic. From (4.4), we get our discrete travelling wave equation with McKean nonlinearity to be

$$\begin{aligned} \frac{c^2}{\kappa^2} (\varphi(\xi + \kappa) - 2\varphi(\xi) + \varphi(\xi - \kappa)) \\ - \frac{1}{\sigma^2} (\varphi(\xi + \sigma) - 2\varphi(\xi) + \varphi(\xi - \sigma)) = -\varphi(\xi) + h(\xi - \xi^*). \end{aligned} \quad (4.25)$$

We have the same difficulties in solving this equation as were discussed in Section 4.1.1, but hope that the simplified nonlinearity will make this problem slightly easier to solve, with it now being a linear problem rather than a fully nonlinear one. We give results for 3 cases in particular: $c = 0$, $\sigma = \kappa$, and $\sigma = 2\kappa$.

Using the same procedure as we did for the continuous and semi-discrete case, we get the solution

$$\varphi(\xi) = \frac{1}{2\pi i} \int_{-\infty}^{\infty} \frac{e^{is(\xi - \xi^*)}}{s R_{\text{Disc}}(s)} ds \quad (4.26)$$

where the function $R_{\text{Disc}}(s)$ is now

$$R_{\text{Disc}}(s) = 1 - \frac{2c^2}{\kappa^2} (1 - \cos(\kappa s)) + \frac{2}{\sigma^2} (1 - \cos(\sigma s)). \quad (4.27)$$

Finding the explicit solution $\varphi(\xi)$ for this discrete case all comes down to analysing the function $R_{\text{Disc}}(s)$. Surprisingly, we are actually able to calculate the zeros of the function $R_{\text{Disc}}(s)$ directly for rational values of $\frac{\sigma}{\kappa}$, rather than making approximations with Taylor series expansions, even though the function looks more complicated than that for the semi-discrete case.

Case $c = 0$

First, we can look at, what would seem, a simpler case of $R_{\text{Disc}}(s)$ by considering the steady state solution, $c = 0$. This is the solution of a travelling wave with zero velocity. Putting $c = 0$ in (4.27), we get,

$$R_{\text{Disc}}(s) = 1 + \frac{2}{\sigma^2} (1 - \cos(\sigma s)).$$

Setting this $R_{\text{Disc}}(s) = 0$ we get two zeros lying on the imaginary axis, (which are complex conjugates), and all their periodic images. These are given by

$$s = \frac{\pm \arccos(1 + \frac{1}{2}\sigma^2) \pm 2n\pi}{\sigma}$$

where $n = 1, 2, 3, \dots$.

We also get a zero at $s = 0$ from the denominator of the solution (4.26). The residues are calculated in Mathematica and an explicit solution of (4.25) is plotted in Figure 4.13. The solution on the left is for $\sigma = 0.1$ and the one on the right is for $\sigma = 0.2$. We see that in both cases the solution is monotonic and piecewise constant. Note that the tail at each end of the solution does not contain any wiggles.

Case $\sigma = \kappa$

The next simplest thing to do is set $\sigma = \kappa$. This reduces the discrete travelling wave equation (4.4) to the symplectic leapfrog method applied to the reduced

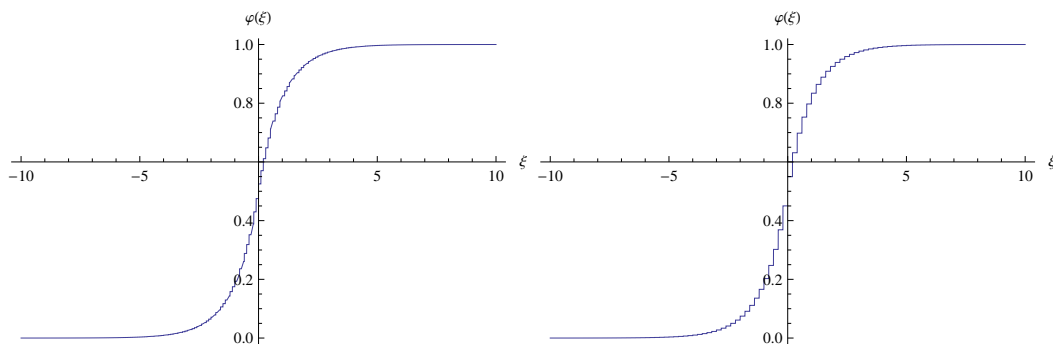


Figure 4.13: The solution of (4.25) for $c = 0$: $\kappa = 0.1$ left, $\kappa = 0.2$ right.

ODE (3.5). Putting $\sigma = \kappa$ in (4.27) we get,

$$R_{\text{Disc}}(s) = 1 + \frac{2}{\kappa^2} (1 - \cos(\kappa s)) (1 - c^2).$$

Setting, $R_{\text{Disc}}(s) = 0$ for the above equation we get two zeros lying on the imaginary axis as in the previous case for $c = 0$. The periodic images of these zeros are also zeros of $R_{\text{Disc}}(s)$ for $\sigma = \kappa$. The complete set of zeros of $R_{\text{Disc}}(s)$ for $\sigma = \kappa$ is given by,

$$s = \frac{\pm \arccos\left(1 + \frac{\kappa^2}{2(1-c^2)}\right) \pm 2n\pi}{\kappa}$$

where $n = 1, 2, 3, \dots$.

We also get the zero $s = 0$ from the denominator of the solution (4.26) as was for the case $c = 0$. The residues are calculated in Mathematica and an explicit solution of (4.25) is plotted in Figure 4.14 for fixed κ and two different value of c . The solution on the left is for $c = 0.2$ and the one on the right is for $c = 0.9$. We see that in both cases the solution is monotonic and piecewise constant. Note that the tail at each end of the solution does not contain any wiggles. Also, notice that as c increases the solution becomes steeper.

Case $\sigma = 2\kappa$

The next simplest thing to do is set $\sigma = 2\kappa$, giving the ratio $\frac{\kappa}{\sigma} = \frac{1}{2}$. We now get,

$$R_{\text{Disc}}(s) = 1 - \frac{2c^2}{\kappa^2} (1 - \cos(\kappa s)) + \frac{1}{2\kappa^2} (1 - \cos(2\kappa s)).$$

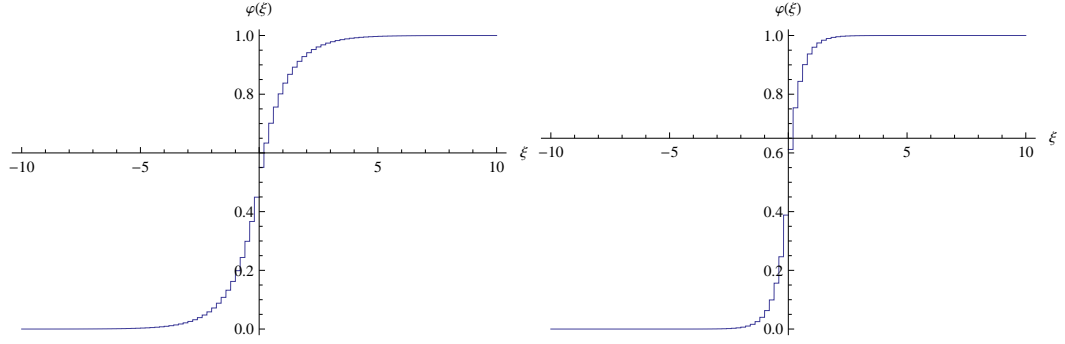


Figure 4.14: The solution of (4.25) for $\sigma = \kappa$: $c = 0.2$ left, $c = 0.9$ right.

As was said earlier, the poles of $R_{\text{Disc}}(s)$ can be found using Matlab or Mathematica without making any Taylor series approximations for the cosine terms. For this case, we get two complex roots and two real roots, plus their periodic images, see Figure 4.15. The residues are calculated by Mathematica and an explicit formula for the solutions in terms of Hypergeometric functions, ${}_2F_1(a, b; c; z)$ is found.

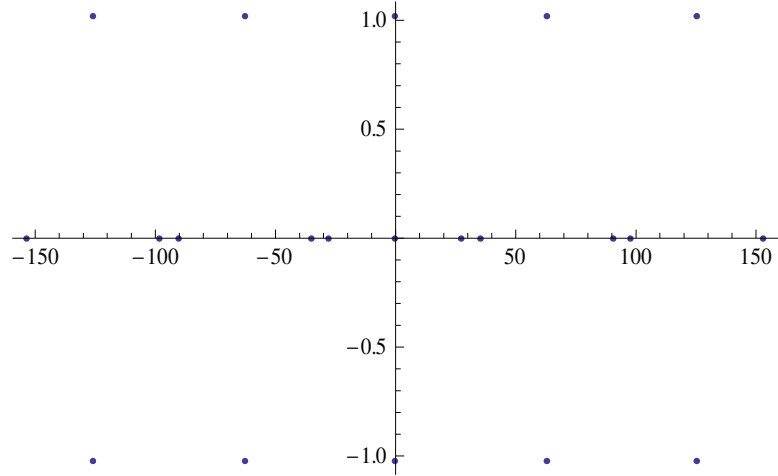


Figure 4.15: Zeros of $R_{\text{Disc}}(s)$ for $\sigma = 2\kappa$ and their periodic images.

Definition 4.2.1 (Hypergeometric Function). *The hypergeometric function ${}_2F_1(a, b; c; z)$ is a function represented by the hypergeometric series. For $|z| < 1$*

the function is defined by the series

$${}_2F_1(a, b; c; z) = \sum_{n=0}^{\infty} \frac{(a)_n (b)_n}{(c)_n} \frac{z^n}{n!}$$

where $c \neq 0, -1, -2, \dots$ and $(a)_n = a(a+1)(a+2)\dots(a+n-1)$, $(a)_0 = 1$. $(a)_n$ is called the Pochhammer symbol.

Before plotting the full solution, we give a plot of the sum of the residues for a real pole and its periodic images in Figure 4.16, and a plot of the sum of the residues for an imaginary pole and its periodic images in Figure 4.17. From these plots we see that the wiggles at the boundaries or tails come from the real poles.

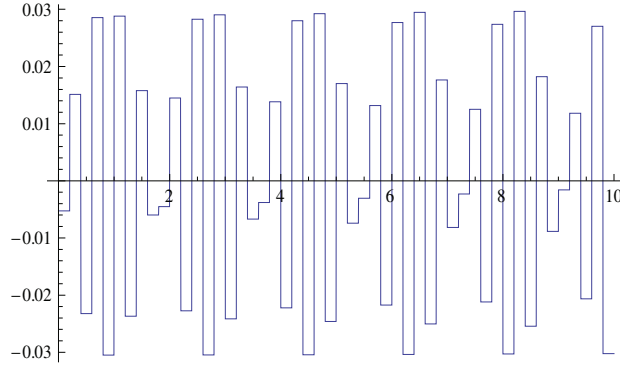


Figure 4.16: Solution from a real pole for $\frac{\kappa}{\sigma} = \frac{1}{2}$ and $\kappa = 0.2$, and $c = 0.2$.

We get the final solution by combining the solution for all the real and imaginary poles. This function is given in Figure 4.18. Notice, that we get a piecewise constant solution with wiggles at the tails.

4.2.5 Summary of Results

The solutions in Figure 4.13, Figure 4.14 and Figure 4.18 all have the general shape of a solitary solution corresponding to a heteroclinic orbit, but contain wiggles. The solutions are piecewise constant including the wiggles, which are of order κ^2 (or σ^2 when $c = 0$). This is a good sign because as the step size

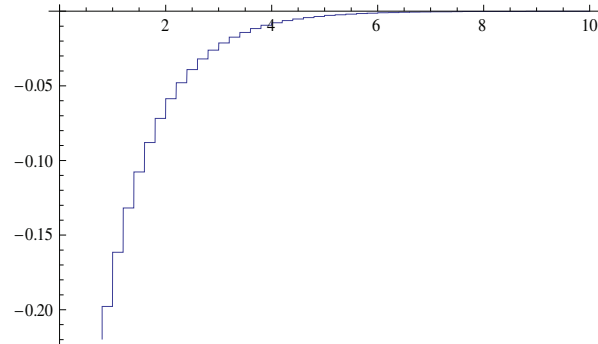


Figure 4.17: Solution from an imaginary pole for $\frac{\kappa}{\sigma} = \frac{1}{2}$ and $\kappa = 0.2$, and $c = 0.2$.

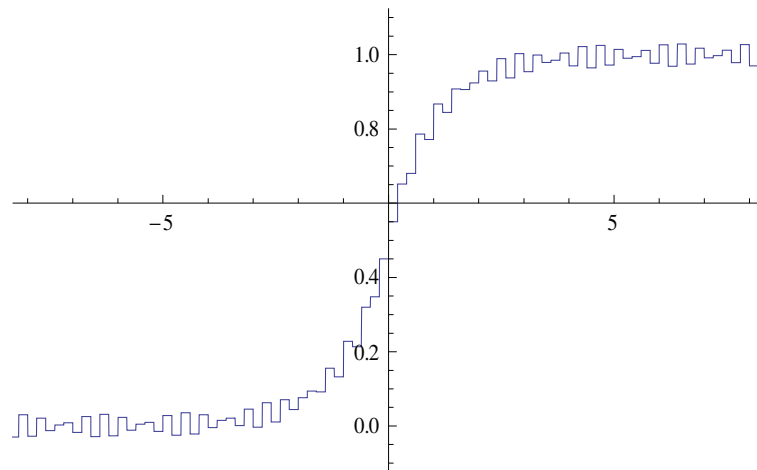


Figure 4.18: Solution of the discrete travelling wave equation with McKean nonlinearity for $\sigma = 2\kappa$.

κ is reduced and tends to zero, the size of the wiggles also tends to zero, but at a faster rate. The wiggles at the boundaries of the solution come from the residues of the real poles. Since we do not have any real poles, (except for the pole at $s = 0$), for the cases $c = 0$ and $\sigma = \kappa$ these wiggles do not appear in these solutions. Instead we just get a piecewise constant solution with the shape of a heteroclinic travelling wave.

Our solution from the discretisation of a multisymplectic integrator is better than that of a discretisation with a non-multisymplectic integrator. With a non-multisymplectic integrator we will not preserve travelling wave solutions at all, but here we at least get the shape of the travelling wave solution. Even symmetric methods applied to symmetric PDEs need not preserve travelling wave solutions as we saw in Section 4.2.2.

Further work can be done on this problem, which includes testing the approach out on other rational values of $\frac{\kappa}{\sigma}$ to see if similar results are obtained, and also, use the approach to find the solution for a set of rational values of $\frac{\kappa}{\sigma}$ tending to an irrational.

4.2.6 Periodic Travelling Wave Solutions

In this section we look at periodic travelling wave solutions of the discrete travelling wave equation with McKean nonlinearity (4.25).

Discrete periodic travelling waves can be sought of by taking the Fourier series of the discrete difference equation (4.25). We will see that, instead of an explicit solution in terms of an infinite integral, as occurred for the heteroclinic travelling wave, the periodic case produces an explicit formula in terms of a Fourier series. We expect our travelling wave solutions to look similar to the wave shown in Figure 4.19.

First, we set $\xi \in [0, 2\tau)$ so our function $h(\xi)$ becomes,

$$h(\xi) = \begin{cases} 0 & \text{if } \xi \in [0, \tau) \\ 1 & \text{if } \xi \in (\tau, 2\tau). \end{cases}$$

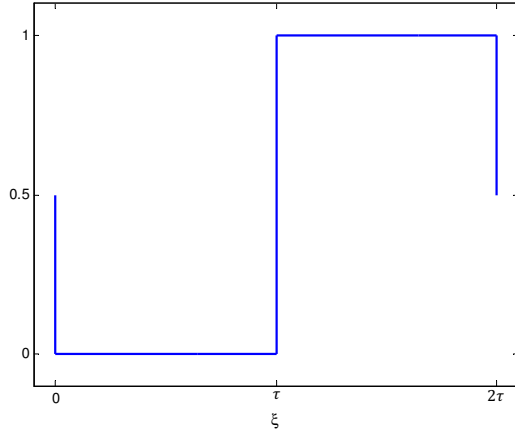


Figure 4.19: Expected periodic travelling wave solution of the nonlinear wave equation with McKean nonlinearity.

Taking the Fourier Series

$$\varphi(\xi) = \sum_{n=-\infty}^{\infty} \tilde{\varphi}_n e^{in\frac{\pi}{\tau}\xi} \quad (4.28)$$

and

$$h(\xi) = \sum_{n=-\infty}^{\infty} \tilde{h}_n e^{in\frac{\pi}{\tau}\xi}$$

and substituting into the discrete difference equation (4.25) we get,

$$\begin{aligned} & \frac{c^2}{\kappa^2} \left(\sum_{n=-\infty}^{\infty} \tilde{\varphi}_n e^{in\frac{\pi}{\tau}(\xi+\kappa)} - 2 \sum_{n=-\infty}^{\infty} \tilde{\varphi}_n e^{in\frac{\pi}{\tau}\xi} + \sum_{n=-\infty}^{\infty} \tilde{\varphi}_n e^{in\frac{\pi}{\tau}(\xi-\kappa)} \right) \\ & - \frac{1}{\sigma^2} \left(\sum_{n=-\infty}^{\infty} \tilde{\varphi}_n e^{in\frac{\pi}{\tau}(\xi+\sigma)} - 2 \sum_{n=-\infty}^{\infty} \tilde{\varphi}_n e^{in\frac{\pi}{\tau}\xi} + \sum_{n=-\infty}^{\infty} \tilde{\varphi}_n e^{in\frac{\pi}{\tau}(\xi-\sigma)} \right) \\ & = - \sum_{n=-\infty}^{\infty} \tilde{\varphi}_n e^{in\frac{\pi}{\tau}\xi} + \sum_{n=-\infty}^{\infty} \tilde{h}_n e^{in\frac{\pi}{\tau}\xi}. \end{aligned}$$

Collecting like terms we get,

$$\begin{aligned}
& \frac{c^2}{\kappa^2} \sum_{n=-\infty}^{\infty} \tilde{\varphi}_n e^{in\frac{\pi}{\tau}\xi} \left(e^{in\frac{\pi}{\tau}\kappa} - 2 + e^{-in\frac{\pi}{\tau}\kappa} \right) \\
& - \frac{1}{\sigma^2} \sum_{n=-\infty}^{\infty} \tilde{\varphi}_n e^{in\frac{\pi}{\tau}\xi} \left(e^{in\frac{\pi}{\tau}\sigma} - 2 + e^{-in\frac{\pi}{\tau}\sigma} \right) + \sum_{n=-\infty}^{\infty} \tilde{\varphi}_n e^{in\frac{\pi}{\tau}\xi} \\
& = \sum_{n=-\infty}^{\infty} \tilde{h}_n e^{in\frac{\pi}{\tau}\xi}.
\end{aligned}$$

Dividing by $e^{in\frac{\pi}{\tau}\xi}$ we get,

$$\begin{aligned}
& \sum_{n=-\infty}^{\infty} \tilde{\varphi}_n \left(\frac{c^2}{\kappa^2} \left(e^{in\frac{\pi}{\tau}\kappa} + e^{-in\frac{\pi}{\tau}\kappa} - 2 \right) - \frac{1}{\sigma^2} \left(e^{in\frac{\pi}{\tau}\sigma} + e^{-in\frac{\pi}{\tau}\sigma} - 2 \right) + 1 \right) \\
& = \sum_{n=-\infty}^{\infty} \tilde{h}_n.
\end{aligned}$$

Substituting the exponentials for cosine terms we get the explicit formula,

$$\sum_{n=-\infty}^{\infty} \tilde{\varphi}_n \left(\frac{2c^2}{\kappa^2} \left(\cos\left(\frac{n\pi\kappa}{\tau}\right) - 1 \right) - \frac{2}{\sigma^2} \left(\cos\left(\frac{n\pi\sigma}{\tau}\right) - 1 \right) + 1 \right) = \sum_{n=-\infty}^{\infty} \tilde{h}_n. \quad (4.29)$$

Taking a finite truncation of the Fourier series we get,

$$\tilde{\varphi}_n = \frac{\tilde{h}_n}{1 - \frac{2c^2}{\kappa^2} \left(1 - \cos\left(\frac{n\pi\kappa}{\tau}\right) \right) + \frac{2}{\sigma^2} \left(1 - \cos\left(\frac{n\pi\sigma}{\tau}\right) \right)}.$$

The coefficients \tilde{h}_n of the Fourier Series for $h(\xi)$ can be calculated exactly,

$$\begin{aligned}
\tilde{h}_n &= \frac{1}{2\tau} \int_0^{2\tau} h(\xi) e^{-in\frac{\pi}{\tau}\xi} d\xi \\
&= \frac{1}{\tau} \int_{\tau}^{2\tau} e^{-in\frac{\pi}{\tau}\xi} d\xi \\
&= \frac{1}{2\tau} \cdot \frac{-1}{in\frac{\pi}{\tau}} e^{-in\frac{\pi}{\tau}\xi} \Big|_{\tau}^{2\tau} \\
&= \frac{-1}{in\pi} \left(e^{-in\frac{\pi}{\tau}(2\tau)} - e^{-in\frac{\pi}{\tau}\tau} \right) \\
&= \frac{1}{in\pi} \left(e^{-in\pi} - e^{-2in\pi} \right) \\
&= \frac{1}{in\pi} \left((-1)^n - 1 \right).
\end{aligned}$$

By taking a finite truncation we no longer have an explicit solution for $\varphi(\xi)$, but a numerical solution of (4.25). As n gets greater the truncation becomes closer to the explicit solution given by (4.29).

We look for the convergence of $\tilde{\varphi}_n$ as $n \rightarrow \infty$, by fixing the parameters τ , σ , κ , and c . A plot of the solution for fixed parameters is given in Figure 4.20. Here we see that we appear to get a piecewise constant solution with the shape of the periodic travelling wave form (Figure 4.19), which we expect. But if we zoom in it can be seen that there are wiggles (Figure 4.21) in our numerical solution. These wiggles are due to the Gibbs phenomenon, which occur while taking a numerical approximation of the Fourier Series of a piecewise continuously differentiable periodic function. Eventually, as $n \rightarrow \infty$ these wiggles will disappear giving a smooth solution, more like the solution we expect.

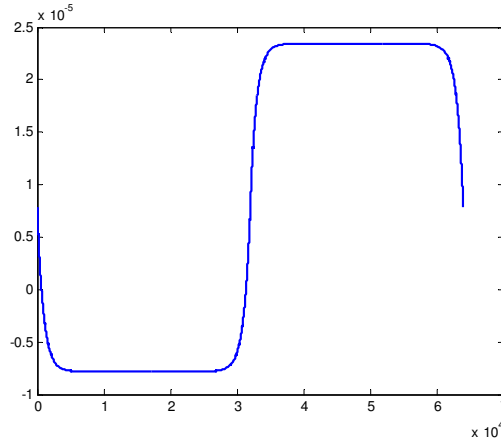


Figure 4.20: Periodic travelling wave solution of the discrete differential-difference equation (4.25) for parameters $\tau = 30$, $\sigma = 2\kappa$, $\kappa = 0.01$, and $c = 0.5$.

Even when we choose an irrational value of $\frac{\sigma}{\kappa}$, such as $\frac{\sigma}{\kappa} = \frac{1}{\sqrt{2}}$, and keep all the other parameters the same we still get a travelling wave solution the same as Figure 4.20. But, when we zoom in to look for wiggles in the solution (Figure 4.22) we see that the wiggles appear random. These wiggles are not due to the Gibbs phenomenon.

Investigating further, we found that even for some rational values of $\frac{\sigma}{\kappa}$ we

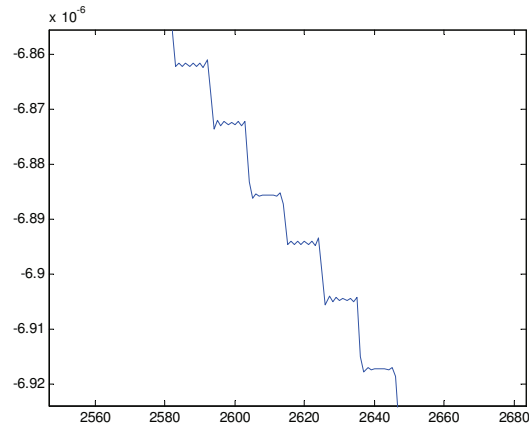


Figure 4.21: Zoom of Figure 4.20 showing the occurrence of wiggles.

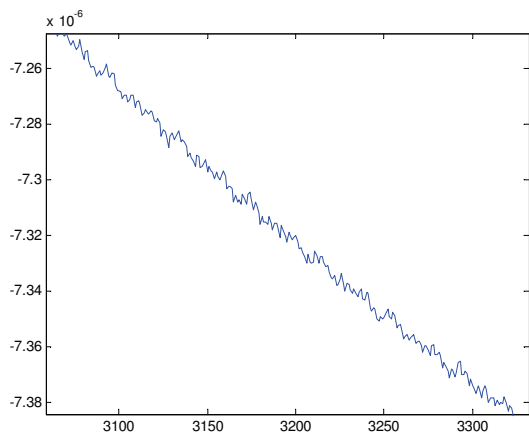


Figure 4.22: Zoom of solution for irrational $r = \frac{1}{\sqrt{2}}$ showing the occurrence of wiggles.

can get fairly large wiggles, (see Figure 4.23a), without zooming in. These wiggles also seem as though they are not due to Gibbs phenomenon. Very large wiggles can be seen for some irrational values, (see Figure 4.23b), of $\frac{\sigma}{\kappa}$.

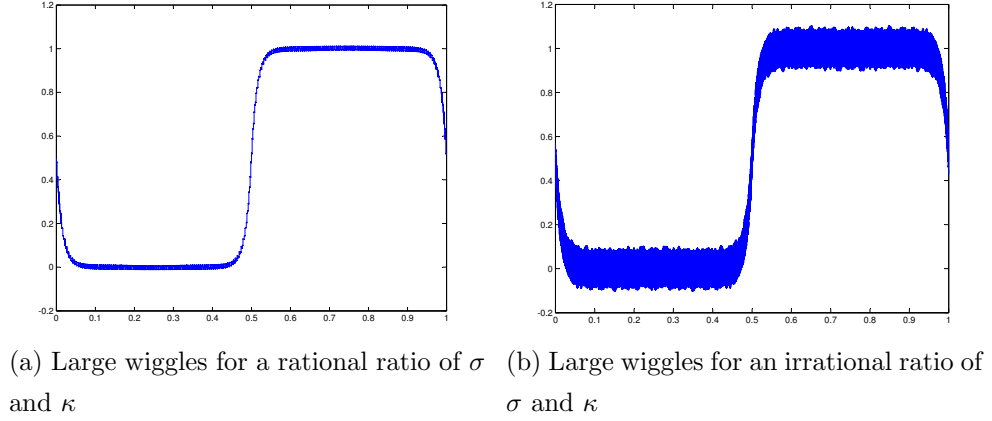


Figure 4.23: Wiggles in the periodic travelling wave solution of the nonlinear wave equation with McKean nonlinearity.

From our results we conclude that there are no true periodic travelling wave solutions of the discrete travelling wave equation with McKean nonlinearity. The McKean cubic worked well in McKean's work on nerve conduction, but did not seem to work well for results on preservation of travelling waves in the nonlinear wave equation. This could be due to the fact that our equation is non-dissipative whereas the model that McKean used was dissipative. The discontinuity at $x = a$ could be part of the problem too, so we next use a nonlinearity that is piecewise linear and continuous.

4.3 Discrete Travelling Wave Equation with Sawtooth Nonlinearity

Instead of using a discontinuous function such as the McKean cubic, we now use a piecewise linear function. We still want to approximate a cubic function,

so use a sawtooth function as our nonlinearity. We choose,

$$f(x) = \begin{cases} -x - 2, & -2 < x < -1 \\ x, & -1 < x < 1 \\ -x + 2, & 1 < x < 2 \end{cases} \quad (4.30)$$

which is plotted in Figure 4.24.

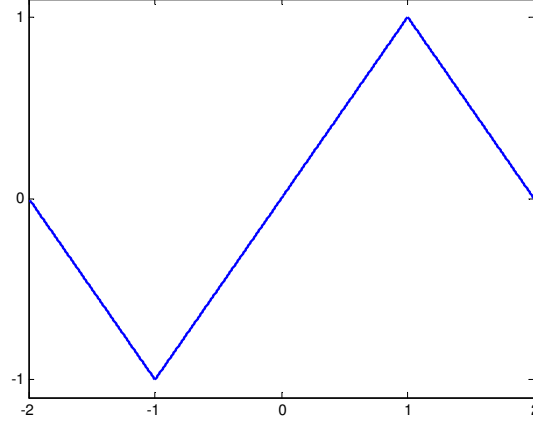


Figure 4.24: Sawtooth function (4.30).

With this nonlinearity we can now plot the phase portrait of the reduced ODE (3.5) with sawtooth nonlinearity (4.30). The phase portrait is given in Figure 4.25 and shows that the solution of this piecewise linear wave equation has heteroclinic and periodic travelling waves. We choose to concentrate on periodic travelling waves for now. But we can approach the heteroclinic travelling wave if we look at periodic travelling waves with period $T \rightarrow \infty$.

Using this sawtooth function as the nonlinearity in the discrete travelling wave equation (4.4) we get a piecewise linear discrete wave equation,

$$\begin{aligned} \frac{c^2}{\kappa^2} (\varphi(\xi + \kappa) - 2\varphi(\xi) + \varphi(\xi - \kappa)) \\ - \frac{1}{\sigma^2} (\varphi(\xi + \sigma) - 2\varphi(\xi) + \varphi(\xi - \sigma)) = \begin{cases} -\varphi(\xi) - 2, & -2 < \varphi(\xi) < -1 \\ \varphi(\xi), & -1 < \varphi(\xi) < 1 \\ -\varphi(\xi) + 2, & 1 < \varphi(\xi) < 2 \end{cases} \end{aligned} \quad (4.31)$$

where $\xi \in \mathbb{R}$.

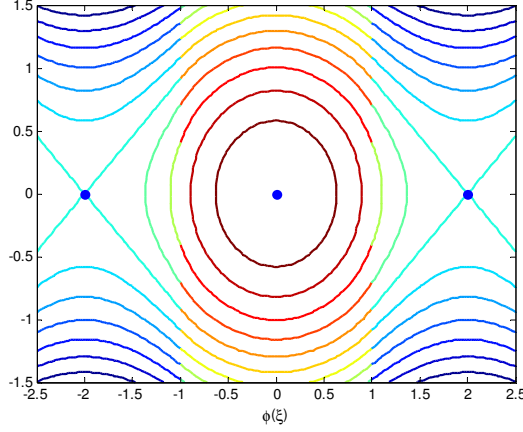


Figure 4.25: Phase portrait of the travelling wave equation of the nonlinear wave equation with sawtooth nonlinearity.

4.3.1 Analytic Solution

In this section we give the continuous periodic travelling wave solution of the nonlinear wave equation with sawtooth nonlinearity.

Recall that after substituting travelling wave coordinates the nonlinear wave equation becomes the nonlinear 2nd order Hamiltonian ODE,

$$(c^2 - 1)\varphi''(\xi) = -V'(\varphi(\xi)). \quad (4.32)$$

For $V'(\varphi(\xi))$ we now have the sawtooth function (4.30) so that the nonlinear 2nd order Hamiltonian ODE becomes a piecewise linear 2nd order Hamiltonian ODE with constant coefficients,

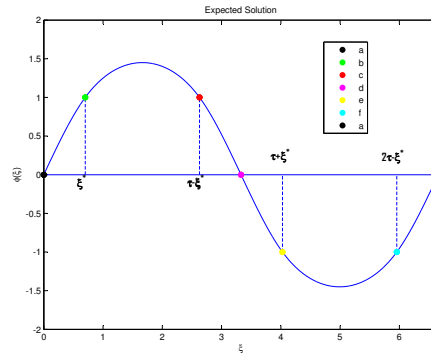
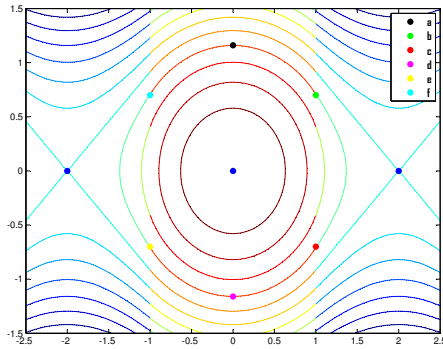
$$(c^2 - 1)\varphi''(\xi) = \begin{cases} -\varphi(\xi) - 2, & -2 < \varphi(\xi) < -1 \\ \varphi(\xi), & -1 < \varphi(\xi) < 1 \\ -\varphi(\xi) + 2, & 1 < \varphi(\xi) < 2. \end{cases} \quad (4.33)$$

For solutions with amplitude greater than one the equation (4.33) can be simplified.

The simplification is done by drawing the expected periodic solution from a periodic orbit of the phase portrait and noticing that the right hand side of (4.33) can be split into five parts instead of three. In Figure 4.26 the phase

portrait of the nonlinear wave equation with sawtooth nonlinearity and the expected solution for an orbit are plotted. Also, points on the orbit are plotted with corresponding points on the expected solution. Note that $\varphi(\xi)$ is on the x -axis for the phase portrait plot. Choosing a periodic orbit with amplitude greater than one, ($\varphi(\xi) > 1$), we trace out the orbit clockwise starting at point ‘a’ and returning back to this point. When $\varphi(\xi) = 1$ we have four points, ‘b’, ‘c’, ‘e’, and ‘f’ which correspond to critical values in the expected solution. For the first critical point we have that in the expected solution there is some value of $\xi^* \in \xi$ at which $\varphi(\xi^*) = 1$. The other values of ξ occur symmetrically along the solution, so that if the period is 2τ we have the 4 points are ξ^* , $\tau - \xi^*$, $\tau + \xi^*$ and $2\tau - \xi^*$, as labeled in the graph Figure 4.26b.

At point ‘a’ $\varphi(\xi) = 0$, travelling along the orbit to point ‘b’, $\varphi(\xi)$ increases to one, then continues to increase to its maximum value (the amplitude) then decreases again to $\varphi(\xi) = 1$ at point ‘c’. The value of φ then decreases to zero at point ‘d’, (we have travelled τ , half the period of the orbit), and continues to decrease until $\varphi(\xi) = -1$ at point ‘e’, then continues to decrease until its minimum value, where it begins to increase again to $\varphi(\xi) = -1$ at point ‘f’. We can then travel to point ‘a’ completing one period 2τ of the orbit.



(a) Phase portrait of the nonlinear wave equation with sawtooth Nonlinearity (b) Expected solution of the nonlinear wave equation with sawtooth nonlinearity

Figure 4.26: Phase portrait and expected solution of the nonlinear wave equation with sawtooth nonlinearity.

The maximum amplitude the solution can take is $\varphi(\xi) \rightarrow 2$ as the solution approaches the fixed point.

Notice, that for $0 \leq \xi \leq \xi^*$, we get $0 \leq \varphi(\xi) \leq 1$, which corresponds to $-V'(\varphi(\xi)) = \varphi(\xi)$ since $-1 < \varphi(\xi) < 1$ from (4.33). For the next interval, $\xi^* \leq \xi \leq \tau - \xi^*$, we get $1 \leq \varphi(\xi) \leq 2$, which corresponds to $-V'(\varphi(\xi)) = -\varphi(\xi) + 2$, since $1 < \varphi(\xi) < 2$ from (4.33). Doing this for all intervals up to 2τ we get the sawtooth nonlinearity written as,

$$-V'(\varphi(\xi)) = \begin{cases} \varphi(\xi), & 0 < \xi < \xi^* \\ -\varphi(\xi) + 2, & \xi^* < \xi < \tau - \xi^* \\ \varphi(\xi), & \tau - \xi^* < \xi < \tau + \xi^* \\ -\varphi(\xi) - 2, & \tau + \xi^* < \xi < 2\tau - \xi^* \\ \varphi(\xi), & 2\tau - \xi^* < \xi < 2\tau. \end{cases} \quad (4.34)$$

With (4.34) as the right hand side of (4.32) the 2nd order differential equation (4.32) can now be solved easily by looking at the roots of the auxiliary (characteristic) equation.

For the intervals, $0 < \xi < \xi^*$, $\tau - \xi^* < \xi < \tau + \xi^*$, and $2\tau - \xi^* < \xi < 2\tau$, the differential equation is

$$(c^2 - 1)\varphi''(\xi) = \varphi(\xi) \Rightarrow (c^2 - 1)\varphi''(\xi) - \varphi(\xi) = 0$$

with auxiliary equation

$$(c^2 - 1)m^2 - 1 = 0.$$

Solving, we get

$$m = \pm \frac{i}{\sqrt{1 - c^2}}.$$

Therefore, the general solution, for the intervals $0 < \xi < \xi^*$, $\tau - \xi^* < \xi < \tau + \xi^*$, $2\tau - \xi^* < \xi < 2\tau$, is

$$\varphi(\xi) = c_1 \cos\left(\frac{\xi}{\sqrt{1 - c^2}}\right) + c_2 \sin\left(\frac{\xi}{\sqrt{1 - c^2}}\right)$$

where c_1, c_2 are different constants for each interval depending on the boundary conditions at each interval.

From Figure 4.26b, we impose the boundary conditions

$$\begin{aligned} 0 < \xi < \xi^*, \quad \varphi(0) = 0, \quad \varphi(\xi^*) = 1 \\ \tau - \xi^* < \xi < \tau + \xi^*, \quad \varphi(\tau - \xi^*) = 1, \quad \varphi(\tau + \xi^*) = -1 \\ 2\tau - \xi^* < \xi < 2\tau, \quad \varphi(2\tau - \xi^*) = -1, \quad \varphi(2\tau) = 0 \end{aligned}$$

to solve for unknown constants.

For the interval $\xi^* < \xi < \tau - \xi^*$ we have

$$(c^2 - 1)\varphi''(\xi) = -\varphi(\xi) + 2 \Rightarrow (c^2 - 1)\varphi''(\xi) + \varphi(\xi) = 2$$

which is a nonhomogeneous equation. So we solve the associated homogeneous equation first. The auxiliary equation for the homogeneous equation is,

$$(c^2 - 1)m^2 + 1 = 0.$$

Solving, we get

$$m = \pm \frac{1}{\sqrt{1 - c^2}}.$$

Therefore, the general solution for the homogeneous equation is

$$\varphi(\xi) = c_3 e^{\frac{\xi}{\sqrt{1-c^2}}} + c_4 e^{\frac{-\xi}{\sqrt{1-c^2}}}$$

and the particular solution is $\varphi(\xi) = 2$.

Therefore, the general solution for the nonhomogeneous equation is,

$$\varphi(\xi) = c_3 e^{\frac{\xi}{\sqrt{1-c^2}}} + c_4 e^{\frac{-\xi}{\sqrt{1-c^2}}} + 2$$

where c_3, c_4 are constants.

From Figure 4.26b, we impose boundary conditions,

$$\xi^* < \xi < \tau - \xi^*, \quad \varphi(\xi^*) = \varphi(\tau - \xi^*) = 1$$

to solve for c_3 and c_4 .

For the interval, $\tau + \xi^* < \xi < 2\tau - \xi^*$, we have

$$(c^2 - 1)\varphi''(\xi) = -\varphi(\xi) - 2 \Rightarrow (c^2 - 1)\varphi''(\xi) + \varphi(\xi) = -2$$

which is again a nonhomogeneous equation. Solving, we get the general solution,

$$\varphi(\xi) = c_5 e^{\frac{\xi}{\sqrt{1-c^2}}} + c_6 e^{\frac{-\xi}{\sqrt{1-c^2}}} - 2$$

where c_5, c_6 are constants.

From Figure 4.26b, we impose the boundary conditions

$$\tau + \xi^* < \xi < 2\tau - \xi^*, \quad \varphi(\tau + \xi^*) = \varphi(2\tau - \xi^*) = -1$$

to solve for c_5 and c_6 .

Plotted in Figure 4.27 are solutions to the nonlinear wave equation with sawtooth nonlinearity for different values of ξ^* and fixed c .

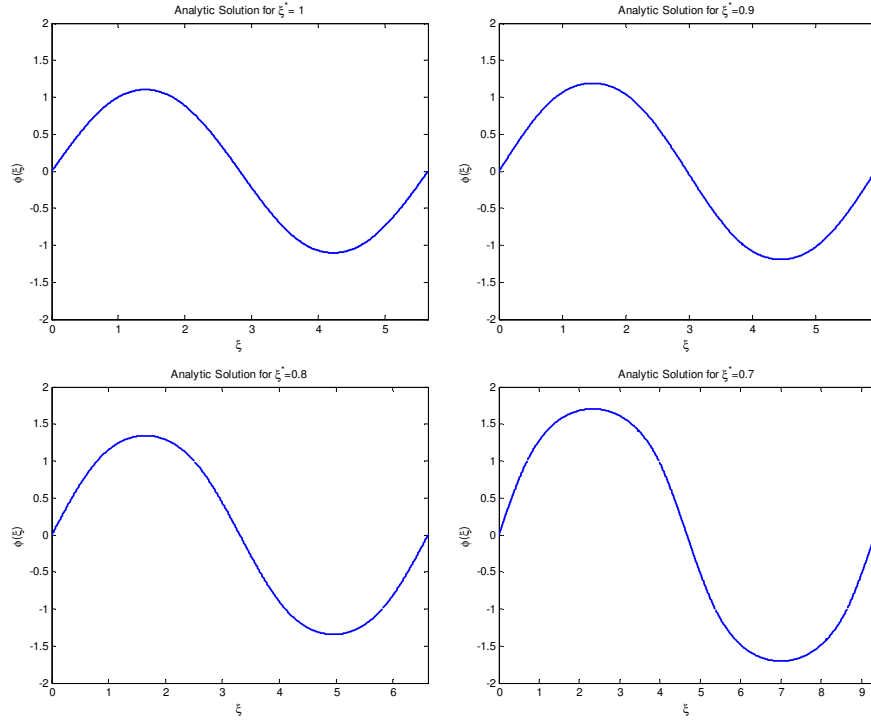


Figure 4.27: Exact solutions of the nonlinear wave equation with sawtooth nonlinearity.

We can now find the solution of the discrete travelling wave equation (4.4) for the sawtooth nonlinearity and compare the results with the analytic solution given in Figure 4.27.

4.3.2 Discrete Solution

We now move onto looking at the discrete periodic travelling wave solutions of the discrete travelling wave equation with sawtooth nonlinearity (4.25).

Let $-V'(\varphi(\xi)) = f(\varphi(\xi))$; then the discrete travelling wave equation (4.4) becomes,

$$\begin{aligned} \frac{c^2}{\kappa^2} (\varphi(\xi + \kappa) - 2\varphi(\xi) + \varphi(\xi - \kappa)) \\ - \frac{1}{\sigma^2} (\varphi(\xi + \sigma) - 2\varphi(\xi) + \varphi(\xi - \sigma)) = f(\varphi(\xi)) \end{aligned} \quad (4.35)$$

where $f(\varphi(\xi))$ is the sawtooth nonlinearity (4.34).

Following Section 4.2.6, we expand both sides of (4.35) in a Fourier series, obtaining

$$\tilde{\varphi}_n \left(\frac{2c^2}{\kappa^2} \left(\cos \left(\frac{n\pi\kappa}{\tau} \right) - 1 \right) - \frac{2}{\sigma^2} \left(\cos \left(\frac{n\pi\sigma}{\tau} \right) - 1 \right) \right) = \tilde{f}_n. \quad (4.36)$$

Since $f(\varphi(\xi))$ is a periodic function with fixed period, 2τ , for fixed c and each of the five intervals in the nonlinearity (4.34), the Fourier coefficients \tilde{f}_n can be found explicitly and are given by

$$\tilde{f}_n = \frac{1}{2\tau} \int_0^{2\tau} f(\varphi(\xi)) e^{-in\frac{\pi}{\tau}\xi} d\xi.$$

Splitting this equation up over each of the intervals in the nonlinearity (4.34), we get

$$\begin{aligned} \tilde{f}_n = \frac{1}{2\tau} \left[\int_0^{\xi^*} \varphi(\xi) e^{-in\frac{\pi}{\tau}\xi} d\xi + \int_{\xi^*}^{\tau-\xi^*} (-\varphi(\xi) + 2) e^{-in\frac{\pi}{\tau}\xi} d\xi + \right. \\ \left. \int_{\tau-\xi^*}^{\tau+\xi^*} \varphi(\xi) e^{-in\frac{\pi}{\tau}\xi} d\xi + \int_{\tau+\xi^*}^{2\tau-\xi^*} (-\varphi(\xi) - 2) e^{-in\frac{\pi}{\tau}\xi} d\xi + \int_{2\tau-\xi^*}^{2\tau} (\varphi(\xi)) e^{-in\frac{\pi}{\tau}\xi} d\xi \right]. \end{aligned}$$

Each of these integrals can be evaluated separately. Taking the first inte-

gral, and substituting in the Fourier Series, (4.28), for $\varphi(\xi)$, we get

$$\begin{aligned}
\int_0^{\xi^*} \varphi(\xi) e^{-in\frac{\pi}{\tau}\xi} d\xi &= \int_0^{\xi^*} \sum_{k=-\infty}^{\infty} \tilde{\varphi}_k e^{ik\frac{\pi}{\tau}\xi} e^{-in\frac{\pi}{\tau}\xi} d\xi \\
&= \sum_{k=-\infty}^{\infty} \int_0^{\xi^*} \tilde{\varphi}_k e^{i(k-n)\frac{\pi}{\tau}\xi} d\xi \\
&= \sum_{k=-\infty}^{\infty} \tilde{\varphi}_k \left[\frac{\tau}{i(k-n)\pi} e^{i(k-n)\frac{\pi}{\tau}\xi} \right]_0^{\xi^*} \\
&= \sum_{k=-\infty}^{\infty} \tilde{\varphi}_k \frac{\tau}{i(k-n)\pi} [e^{i(k-n)\frac{\pi}{\tau}\xi^*} - 1].
\end{aligned}$$

Evaluating the integrals for each interval we get,

$$\begin{aligned}
\tilde{f}_n &= \sum_{n=-\infty}^{\infty} \tilde{\varphi}_n \frac{1}{i(k-n)\pi} (e^{i(k-n)\frac{\pi}{\tau}\xi^*} - e^{-i(k-n)\frac{\pi}{\tau}\xi^*} + (-1)^{(k-n)} e^{i(k-n)\frac{\pi}{\tau}\xi^*} \\
&\quad - (-1)^{(k-n)} e^{-i(k-n)\frac{\pi}{\tau}\xi^*}) + \frac{1}{in\pi} (e^{-in\frac{\pi}{\tau}\xi^*} + e^{in\frac{\pi}{\tau}\xi^*} \\
&\quad - (-1)^n e^{-in\frac{\pi}{\tau}\xi^*} - (-1)^n e^{in\frac{\pi}{\tau}\xi^*}).
\end{aligned}$$

Substituting this into (4.36) and solving for $\tilde{\varphi}_n$ we get,

$$\tilde{\varphi}_n = (\mathbf{G} - \mathbf{A})^{-1} \mathbf{b} \quad (4.37)$$

where,

$$\mathbf{g} = \left(\frac{2c^2}{\kappa^2} \left(\cos \left(\frac{n\pi\kappa}{\tau} \right) - 1 \right) - \frac{2}{\sigma^2} \left(\cos \left(\frac{n\pi\sigma}{\tau} \right) - 1 \right) \right) \quad (4.38)$$

$$\mathbf{G} = \text{diag}(\mathbf{g})$$

$$\begin{aligned}
\mathbf{A} &= \frac{1}{i(k-n)\pi} (e^{i(k-n)\frac{\pi}{\tau}\xi^*} - e^{-i(k-n)\frac{\pi}{\tau}\xi^*} + \\
&\quad (-1)^{(k-n)} e^{i(k-n)\frac{\pi}{\tau}\xi^*} - (-1)^{(k-n)} e^{-i(k-n)\frac{\pi}{\tau}\xi^*})
\end{aligned} \quad (4.39)$$

$$\mathbf{b} = \frac{1}{in\pi} (e^{-in\frac{\pi}{\tau}\xi^*} + e^{in\frac{\pi}{\tau}\xi^*} - (-1)^n e^{-in\frac{\pi}{\tau}\xi^*} - (-1)^n e^{in\frac{\pi}{\tau}\xi^*}).$$

The Fourier coefficients (4.37) can be now found in Matlab by solving for ξ^* and the solution $\varphi(\xi)$ found by the taking the inverse Fourier transform. Discrete numerical solutions can now be plotted and compared with the analytic solution. These are given in Figure 4.28 and Figure 4.29.

In the figures it looks like the discrete numerical solutions are very similar to the analytic solution. This was confirmed by plotting the discrete solutions over top of the analytic solutions for fixed periods, but varying the ratios of $\frac{\sigma}{\kappa}$. In all cases tried, the discrete numerical solutions seem to match the corresponding analytic solutions. The difference in the analytic and discrete solutions was not measured as the nature of finding the analytic solution made this difficult.

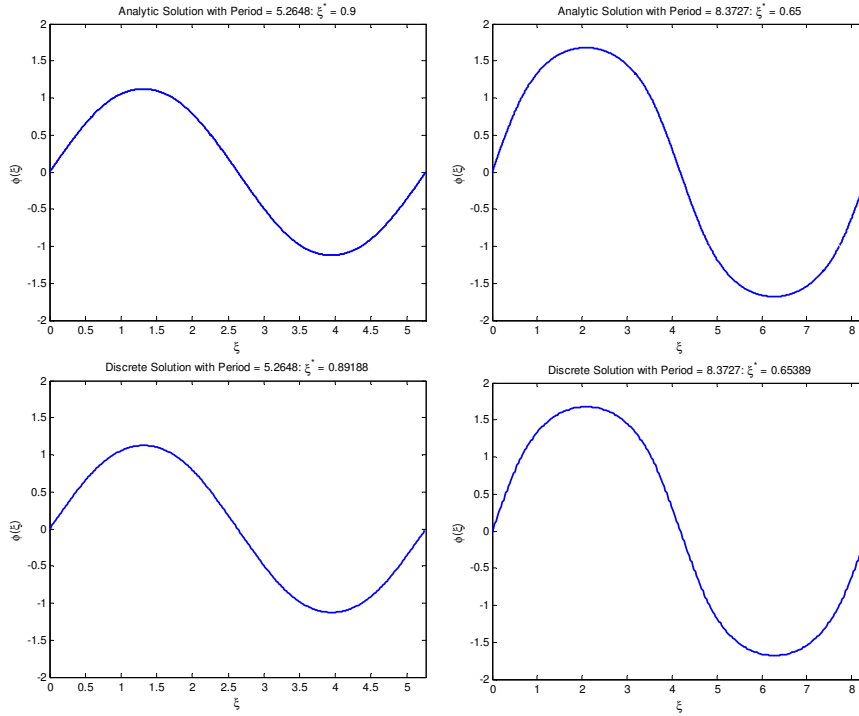


Figure 4.28: Comparison of the analytic solution and the discrete solution of the nonlinear wave equation with sawtooth nonlinearity, for fixed periods and fixed c , for rational values of $\frac{\sigma}{\kappa}$.

So, for the nonlinear wave equation with sawtooth nonlinearity it appears that discrete periodic travelling wave solutions do exist. We now want to extend this to smooth nonlinearities and say in general that multisymplectic integrators preserve travelling wave solutions.

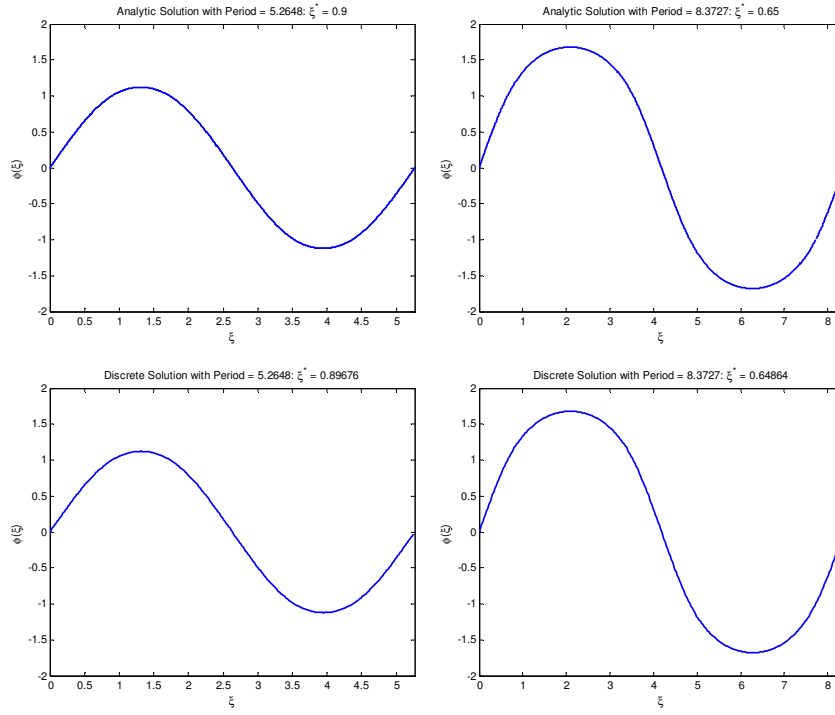


Figure 4.29: Comparison of the analytic solution and the discrete solution of the nonlinear wave equation with sawtooth nonlinearity, for fixed periods and fixed c , for irrational values of $\frac{\sigma}{\kappa}$.

Chapter 5

Numerical Solution of the Discrete Travelling Wave Equation with Smooth Nonlinearity

In this chapter we introduce the sine-Gordon equation. This is the equation which will be mostly used from now on. We then give the discrete travelling wave equation of the sine-Gordon equation, an equation resulting from applying the multisymplectic leapfrog method and discrete travelling wave coordinates to it. Because the resulting discrete travelling wave equation proved difficult to solve analytically, we will show how we solved it numerically for periodic travelling waves. The numerical solutions sometimes produce what is known as resonances. We try to predict what combination of the parameters these resonances occur and what size the resonances are. Our results from this chapter will be backed up in Chapter 6 by backward error analysis.

5.1 The sine-Gordon equation

The final choice of nonlinearity is a smooth nonlinear function. We choose the sine function, so that our nonlinear wave equation becomes the sine-Gordon equation

$$u_{tt} = u_{xx} - \sin u \quad (5.1)$$

and the ODE from travelling wave coordinate substitution is

$$(c^2 - 1)\varphi''(\xi) = -\sin(\varphi(\xi)) \quad (5.2)$$

which we can draw the phase portrait for. This is plotted in Figure 5.1. Here we can see that the solution possesses periodic and heteroclinic travelling waves.

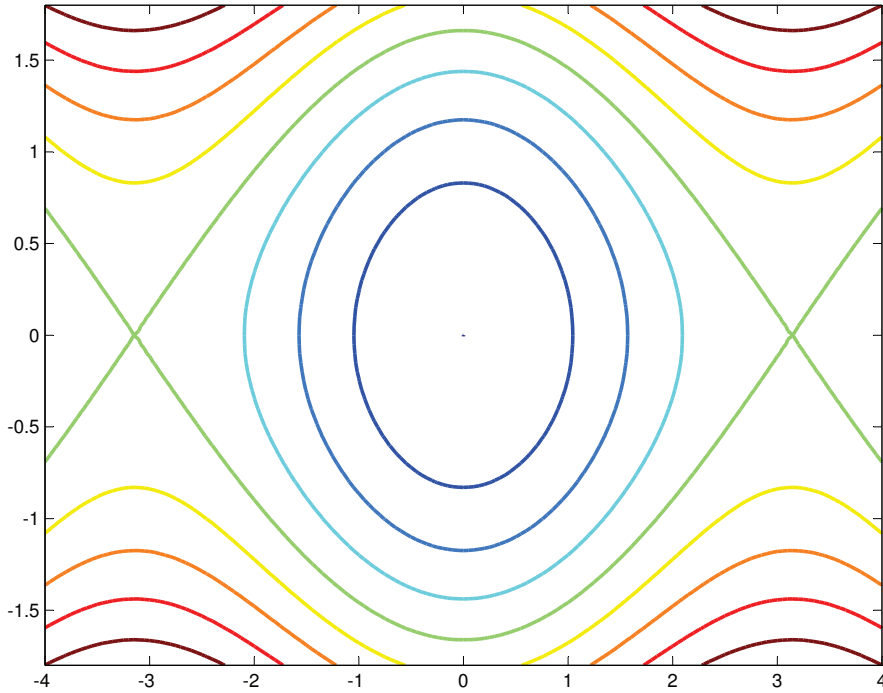


Figure 5.1: Phase portrait of the travelling wave equation of the nonlinear wave equation with smooth nonlinearity.

Figure 5.1 shows that there are fixed points at $\varphi(\xi) = 0$ and $\varphi(\xi) = \pm\pi$. So the periodic solutions will have a maximum amplitude approaching π .

The exact solution can also be found in Mathematica in terms of Jacobi Amplitude functions.

In Chapter 4 we derived the discrete travelling wave equation (4.4) for the nonlinear wave equation with a general nonlinearity $V'(u)$.

For the sine-Gordon equation we get the discrete travelling wave equation,

$$\begin{aligned} \frac{c^2}{\kappa^2} (\varphi(\xi + \kappa) - 2\varphi(\xi) + \varphi(\xi - \kappa)) \\ - \frac{1}{\sigma^2} (\varphi(\xi + \sigma) - 2\varphi(\xi) + \varphi(\xi - \sigma)) = -\sin(\varphi(\xi)), \quad \xi \in \mathbb{R}. \end{aligned} \quad (5.3)$$

As we saw in Chapter 4 the discrete travelling wave equation is difficult to solve analytically, even with simpler nonlinearities. Our sine-Gordon discrete travelling wave equation (5.3) is no different. Therefore, we will solve it numerically rather than exactly. We saw that the continuous sine-Gordon equation (5.1) (or (5.2)) contained heteroclinic and periodic travelling waves. We want to see if these travelling wave are preserved by the discrete travelling wave equation (5.3), a multisymplectic integrator. In the next section, we derive a method for numerically solving the discrete travelling wave equation (5.3) for periodic travelling wave solutions.

5.2 Numerical Method for Periodic Travelling Wave Solutions

In this section we derive a pseudospectral Newton continuation method to solve the discrete travelling wave equation (5.3) for the periodic case. In Figure 5.1 we saw that the continuous case has a family of periodic solutions each with a varying period. We assume this is also true for the discrete case and so initially fix our solution to be a specific period. Newton's method is used to solve the nonlinear part of the equation and this is combined with a continuation phase which allows us to see snapshots of the solution for increasing period. The continuation part of the method uses the solution φ at a particular parameter value as an initial estimate in Newton's method for the parameter at a slightly

different value, say slightly higher. Then by using each solution for slightly higher values of the parameter we can keep on continuing to find the solution until the desired value of the parameter is required.

We will be working in both real space and Fourier space so make the following definitions. Let $-\sin(\varphi(\xi)) = f(\varphi(\xi))$ in the discrete travelling wave equation (5.3). Then we have

$$\begin{aligned}\mathcal{F}(\varphi) &= \tilde{\varphi}_n, & \mathcal{F}^{-1}(\tilde{\varphi}_n) &= \varphi, \\ \mathcal{F}(f) &= \tilde{f}_n, & \mathcal{F}^{-1}(\tilde{f}_n) &= f,\end{aligned}$$

where \mathcal{F} is the Fourier transform.

Discrete periodic travelling waves can be sought by using the discrete Fourier series (as was done in Sections 4.2.6 and 4.3.2)

$$\varphi(\xi) = \sum_{n=-N}^N \tilde{\varphi}_n e^{in\frac{\pi}{\tau}\xi}$$

where $\tau = \frac{T}{2}$ and T is the period of the periodic solution.

To solve (5.3) numerically for φ as a discrete Fourier series, we use Newton's method and a continuation of the period T of the solution. Notice that the left hand side of (5.3) is linear, but the right hand side is nonlinear. We will not worry about the right hand side being nonlinear for now as this will be dealt with later on by Newton's method. First, we apply the discrete Fourier series to both sides of (5.3). Most of the work is already done for us as this was done for the sawtooth nonlinearity in Section 4.3.2, which gives

$$\mathbf{G}\tilde{\varphi}_n = \tilde{f}_n \tag{5.4}$$

where \mathbf{G} is given in (4.38).

Equation (5.4) is in Fourier space, but we would prefer to work in real space. By rewriting the Fourier modes in terms of Fourier transforms, equation (5.4) becomes,

$$\mathbf{G}\mathcal{F}(\varphi(\xi)) = \mathcal{F}(f(\varphi(\xi))).$$

Rearranging, we get

$$L\varphi(\xi) = f(\varphi(\xi)) \tag{5.5}$$

where $L = \mathcal{F}^{-1} \mathbf{G} \mathcal{F}$ is a linear operator.

We have reduced the discrete travelling wave equation (5.3) to a linear operator applied to $\varphi(\xi)$ on the left hand side, but the right hand side is still nonlinear.

The solution φ of the discrete travelling wave equation is a vector whose length depends on the number of Fourier modes used for solving the linear part with the discrete Fourier series.

We choose the number of Fourier modes N that we want to numerically solve for, then using Matlab we find L where we use the $N \times N$ discrete Fourier transform matrix,

$$\begin{bmatrix} 1 & 1 & 1 & 1 & \cdots & 1 \\ 1 & \omega & \omega^2 & \omega^3 & \cdots & \omega^{N-1} \\ 1 & \omega^2 & \omega^4 & \omega^6 & \cdots & \omega^{2(N-1)} \\ 1 & \omega^3 & \omega^6 & \omega^9 & \cdots & \omega^{3(N-1)} \\ \vdots & \vdots & \vdots & \vdots & \cdots & \vdots \\ 1 & \omega^{N-1} & \omega^{2(N-1)} & \omega^{3(N-1)} & \cdots & \omega^{(N-1)(N-1)} \end{bmatrix},$$

for \mathcal{F} , where $\omega = e^{\frac{-2\pi i}{N}}$.

Next, we solve the nonlinear part of (5.5) using Newton's method,

$$\varphi^{i+1} = \varphi^i - (L - \text{diag}(f'(\varphi^i)))^{-1}(L\varphi^i - f(\varphi^i)).$$

To use Newton's method we found an appropriate initial estimate of the solution φ . Next, we chose values for σ , κ and c , then chose to fix the period of the solution to $T = 2\pi$, initially. Because we are using Newton's method to solve for φ , we only get a numerical approximation to our discrete travelling wave equation (5.3), but if we have quadratic convergence of Newton's method then this numerical solution should be very close to the exact solution of the discrete travelling wave equation (5.3).

The numerical solution for the situation described above is given in Figure 5.2. We see that it is a periodic solution, resembling the sine wave, with period 2π . This solution was only for one set of values of the parameters, but we want to look at the periodic solutions for a range of all the parameters.

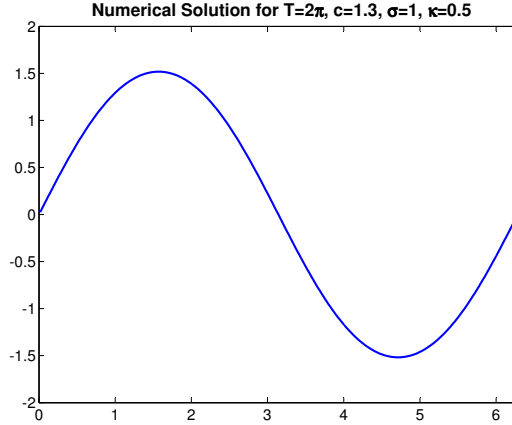


Figure 5.2: Numerical solution $\varphi(\xi)$ of the discrete travelling wave equation (5.3). ξ is on the x -axis and φ on the y -axis.

If we fix $c = 1.3$, then there are 3 parameters that need to be considered and controlled:

- T —the period of the solution;
- σ —the spatial step size; and
- κ —related to the time step ($\kappa = c\Delta t$).

Note that for this problem we have $c > 1$, compared with the wave equations with McKean and Sawtooth nonlinearity where we had $0 \leq c < 1$.

Now that we have solved for $T = 2\pi$ we can do a continuation in $\tau = \frac{T}{2}$. We keep all other parameters the same, only varying the period T . For example, we started with $\tau = \pi$ and found a solution φ . Next, we may want to find the solution for $\tau = \pi + 0.01$. To do this we use the solution φ that we found for $\tau = \pi$ as our initial guess to the solution for $\tau = \pi + 0.01$. Then for $\tau = \pi + 0.02$ we use the solution we found for $\tau = \pi + 0.01$ as our initial guess, and so on. Looking at the solutions from doing a continuation in τ , we notice two distinct types of solution, plotted in Figure 5.3. The first type appears to be smooth and is shown in Figure 5.3a. We call this the non-resonant case. While the second type possesses noticeable wiggles in the solution, shown in Figure 5.3b.

This is known as the resonant case and generally occurs when the frequency of the period resonates with the step size. Resonances will be discussed in Section 5.3.

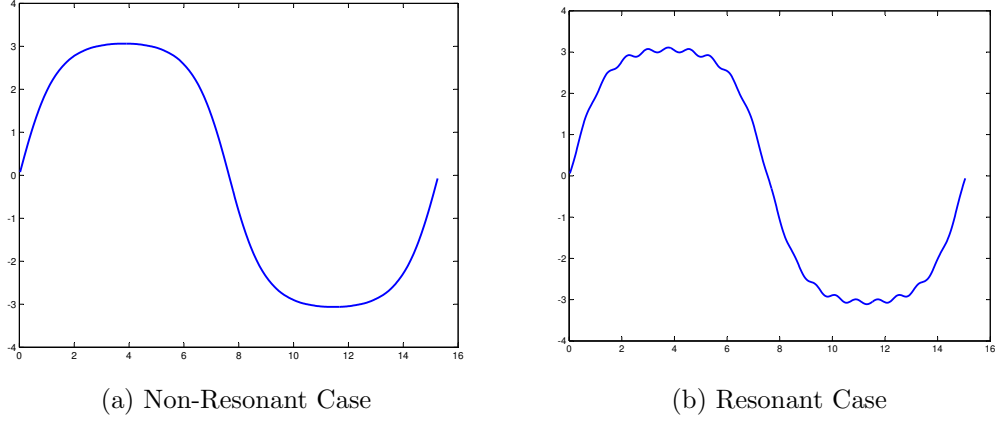


Figure 5.3: Two cases for numerical solutions of the discrete travelling wave equation. ξ is on the x -axis and φ on the y -axis. (5.3)

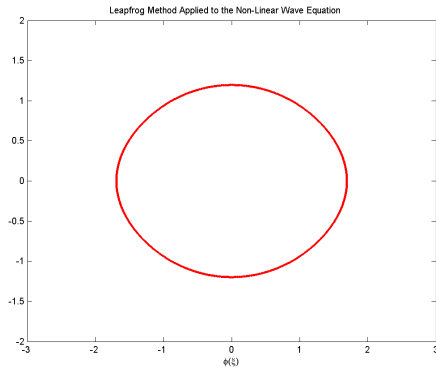
We checked the convergence of the solutions obtained from Newton's method and they all seemed to show quadratic convergence, except at the resonances, so our method is very close to giving the exact solution of the discrete travelling wave equation (5.3).

5.2.1 Checking our Numerical Solution

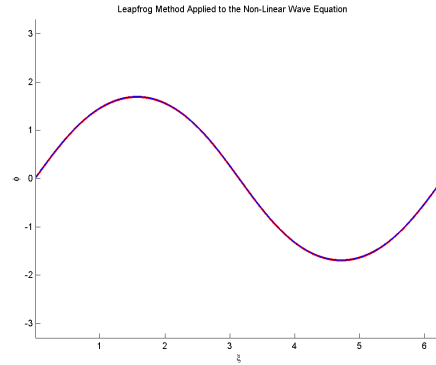
In addition to quadratic convergence, we would like another way of checking that our numerical method is giving the correct solution of the discrete travelling wave equation (5.3). This can be done for $\sigma = \kappa$, as the discrete travelling wave equation (5.3) is now equivalent to finding travelling wave solutions of the leapfrog method applied to the sine-Gordon equation. In this section we compare the solutions of the leapfrog method and those of the discrete travelling wave equation (5.3) for $\sigma = \kappa$. If these solutions are the same then we know that our pseudospectral Newton method is giving accurate solutions of the discrete travelling wave equation (5.3).

As we said above, for $\sigma = \kappa$ the discrete travelling wave equation (5.3) is equivalent to the leapfrog method applied to (5.2). The leapfrog method applied to the pendulum has been well studied. Our reduced ODE (5.2) is very similar to the pendulum equation, the only difference being the factor $c^2 - 1$. So we can apply leapfrog to our reduced ODE (5.2) and compare it with our numerical solution of the discrete travelling wave equation (5.3).

Since we are looking at periodic orbits we choose an initial condition on one of these orbits. Using our pseudospectral Newton method for $T = 2\pi$ we get a solution and find the amplitude of this solution. This is then used as our initial conditions for the leapfrog method applied to (5.2). First we choose a value of the step size in which the leapfrog method is known to give qualitatively correct results for the pendulum equation and compare the leapfrog method solution with our Newton's method solution. This is given in Figure 5.4 for $\sigma = \kappa = 0.5$ and confirms that not only does our method give solutions which accurately portray the discrete travelling wave equation (5.3) solutions but also our Matlab program is working correctly.



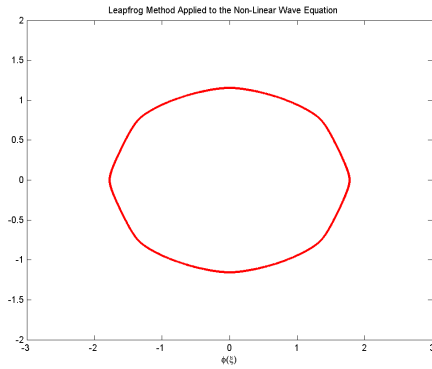
(a) Orbit of Leapfrog applied to (5.2)



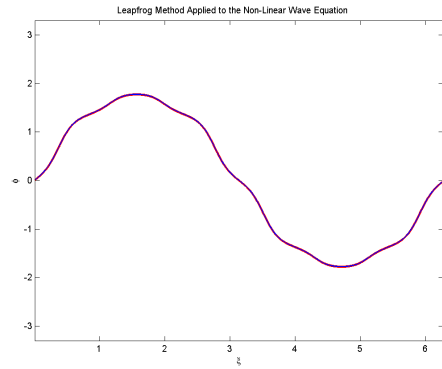
(b) Solution of Leapfrog (Red) Applied to (5.2) and numerical solution of (5.3) (Blue)

Figure 5.4: Left: An orbit for the leapfrog method applied to the reduced ODE (5.2), and, Right: the corresponding solution in red, with the numerical solution of the discrete travelling wave equation (5.3) for $\sigma = \kappa = 0.5$ superimposed in blue.

To compare the solutions of the equivalent methods more, we choose a step size in which it is known resonances occur for the leapfrog method. Resonances are discussed in Section 5.3. This comparison is given in Figure 5.5 for $\sigma = \kappa = 0.8$. Here, we see that the orbit is no longer oval shaped, but has some distortion which corresponds to wiggles in the solution. In this situation the leapfrog method and the discrete travelling wave equation solution also match up. Hence, resonances occur in our numerical solution for $\sigma = \kappa$ when they occur for the leapfrog method.



(a) Orbit of Leapfrog applied to (5.2)



(b) Solution of Leapfrog (Red) Applied to (5.2) and numerical solution of (5.3) (Blue)

Figure 5.5: Left: An orbit for the leapfrog method applied to the reduced ODE (5.2), and, Right: the corresponding solution in red, with the numerical solution of the discrete travelling wave equation (5.3) for $\sigma = \kappa = 0.8$ superimposed in blue.

5.3 Resonance

Resonances occur with all types of vibrations and waves. They come about when a system is forced at its natural frequency (resonant frequency). Even small driving forces lead to an accumulation of the amplitude of oscillation and energy. The frequencies at which resonances in a system occur are called resonant frequencies. As an example we can consider the pendulum. In the

absence of any force or friction, the pendulum will oscillate constantly with a specific frequency (natural frequency) and amplitude. If a force is applied in time with this natural frequency then the amplitude of the pendulum will continuously increase.

When the orbits of two orbiting bodies have orbital periods related by a ratio of two small integers, (we will call this rationally related or resonant), the bodies apply a regular, periodic gravitational effect on each other. This is known as an orbital resonance.

Numerical methods can introduce the concept of numerical resonance. For periodic solutions a resonance can occur, with sufficiently large step size, when the period of the solution and the step size are rationally related. That is, $\frac{T}{\Delta x} = \frac{m}{n}$, where T is the period of the solution, Δx the step size, and m and n are positive integers.

Quinlin in [77] predicts where resonances occur for symmetric multistep methods in terms of their spurious roots. See Section 6.5 for more details.

5.4 Resonances in the Discrete Travelling Wave Equation

The discrete travelling wave equation (5.3) was solved by a pseudospectral Newton method with a continuation in the period T . This produces two types of solutions, as we saw in Section 5.2, Figure 5.3a and 5.3b. The first we call the non-resonant case, the solution is a smooth periodic wave, and the second is the resonant case, where wiggles appear in the wave, or the wave becomes distorted. We would like to know when these resonances occur and whether or not they represent travelling wave solutions. In this section we investigate the resonances occurring in the solutions of the discrete travelling wave equation (5.3) and try to determine whether these occur for a certain relationship between the parameters, σ , κ and T .

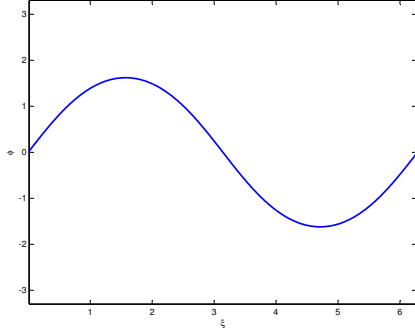
5.4.1 Initial Results

In this section we give some initial results of our pseudospectral Newton continuation method. We want to show the preservation of travelling waves through numerical work rather than actually working out theoretical proofs. But will also use backward error analysis later on to back up our numerical results. In Figure 5.6 we plot certain frames of a continuation simulation.

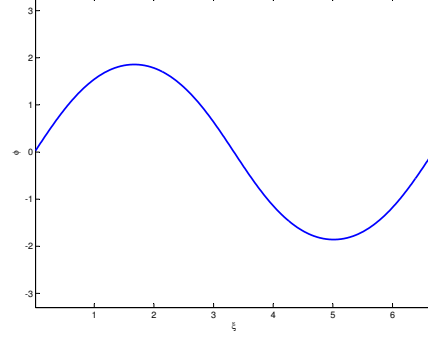
Figure 5.6 shows us that as the period increases so does the amplitude of the wave solution. This is consistent with the phase portrait (Figure 5.1) of the continuous solution (5.2). The phase portrait shows that as each periodic orbit gets closer to the heteroclinic orbit the period of the orbit increases and so does the value of $(x, 0)$. This value corresponds to the amplitude of the periodic wave solution. Figure 5.6d shows large wiggles in the solution. We want to find out why these wiggles occur for this combination of the parameters and what the relationship between the parameters is and whether or not there is a consistent relationship between the parameters where the wiggles occur. Also, we want to know the size of the wiggles in Figure 5.6d. This will also tell us whether or not any of the other frames in Figure 5.6 contain wiggles without having to zoom in on the solution. We can also run the simulation out to a longer period. This is given in Figure 5.7.

In Figure 5.7 the continuation is run out to a relatively large period. Here, as in Figure 5.6, as the period increases the amplitude increases. We also notice that at large period the amplitude of the wave approaches $\varphi = \pi$, the fixed point, which is also consistent with the phase portrait of (5.2). As the period increases and the amplitude reaches this fixed point the solution is tending to a heteroclinic travelling wave.

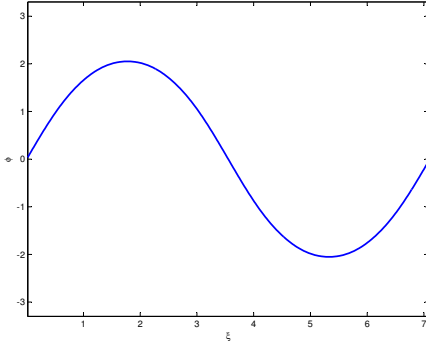
After these observations we would like to investigate further and to do this we need to be able to measure the size of the wiggles that appear in some of the solutions. We construct a way to measure the wiggles in the next section.



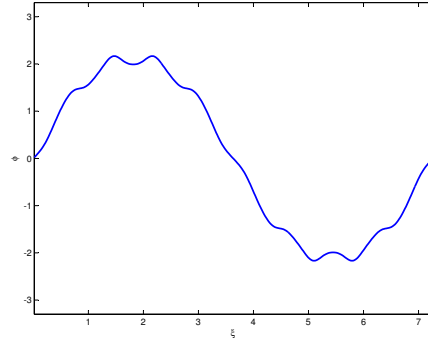
(a) $T = 2\pi = 6.2832$



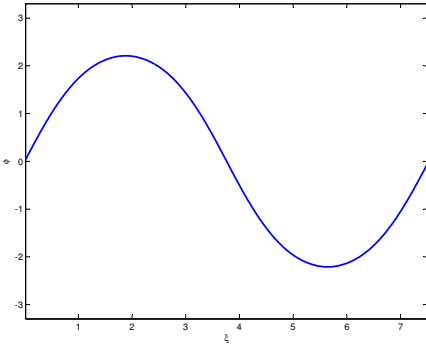
(b) $T = 2(\pi + 0.2) = 6.6832$



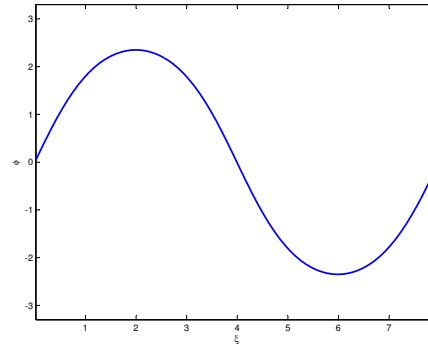
(c) $T = 2(\pi + 0.41) = 7.1032$



(d) $T = 2(\pi + 0.49) = 7.2632$

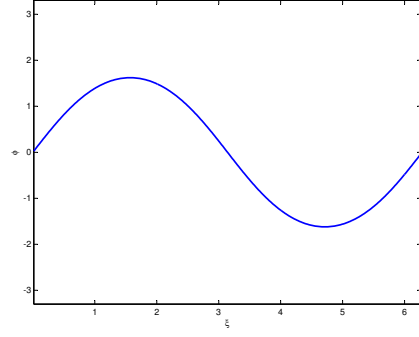


(e) $T = 2(\pi + 0.62) = 7.5232$

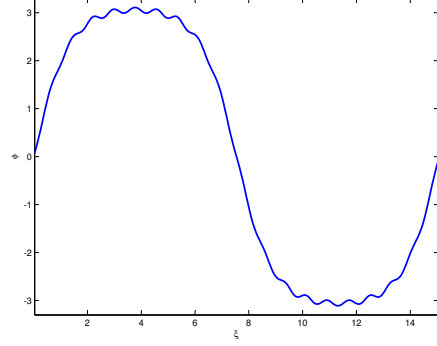


(f) $T = 2(\pi + 0.85) = 7.9832$

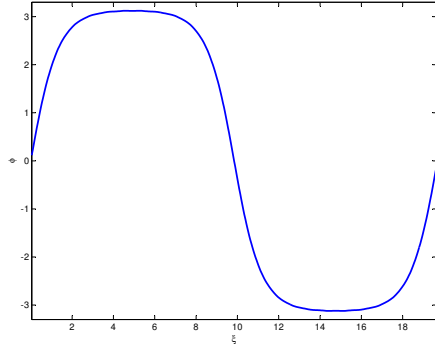
Figure 5.6: Continuation in T starting with $T = 2\pi$ for $\sigma = 1$, $\kappa = \frac{1}{\sqrt{2}}$, $c = 1.3$.



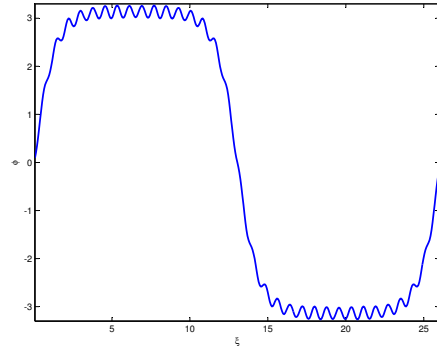
(a) $T = 2\pi = 6.2832$



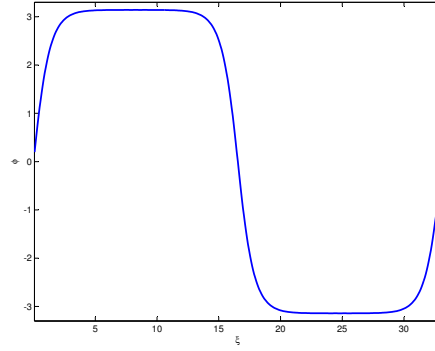
(b) $T = 2(\pi + 4.4) = 15.0832$



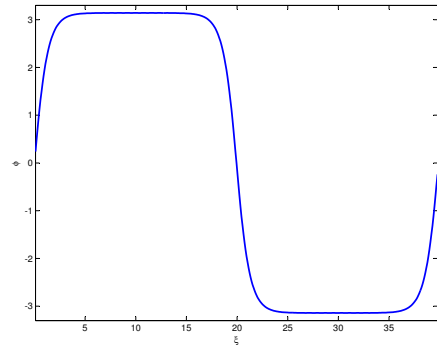
(c) $T = 2(\pi + 6.7) = 19.6832$



(d) $T = 2(\pi + 9.9) = 26.0832$



(e) $T = 2(\pi + 13.4) = 33.0832$



(f) $T = 2(\pi + 16.8) = 39.8832$

Figure 5.7: Continuation in T starting with $T = 2\pi$ for $\sigma = 1$, $\kappa = \frac{1}{\sqrt{2}}$, $c = 1.3$.

5.4.2 Measuring the Size of the Resonances

In this section we give our approach to measuring the resonances. It is based on taking a portion of the the solution vector φ then finding the difference between the maximum and minimum of the second derivative of φ over this part of the vector.

Previously, we saw that there are two types of solutions from the numerical approximation of the discrete travelling wave equation (5.3). There are smooth solutions and solutions that produce wiggles. The wiggles are clearly visible in some solutions but in others the solutions produced appear to be smooth. Upon further inspection though, by zooming in, the wiggles appear. We clearly need a way of measuring the size of these wiggles so we do not have to zoom in on every solution to see if they exist. We also want to determine whether or not they are always finite or if they tend to infinity for some parameter values. If they tend to infinity then there is definitely no travelling wave solution preserved for those particular parameters, but for the finite wiggles there could be travelling wave solutions. Finite wiggles are known as resonances and infinitely sized wiggles are known as instabilities.

To measure the size of the wiggles in the solutions we take a section of the solution φ on either side of $\frac{\tau}{2}$, see Figure 5.8. For example, if we use 400 Fourier modes to solve the discrete travelling wave equation (5.3) then the solution φ is a vector of length 400 and the period T of φ is made up of 400 points. Therefore, if we only take half the solution then the solution from $(0, \tau)$ is made up of 200 points and the solution from $(0, \frac{\tau}{2})$ is made up of 100 points, so we want to take a part of the vector which includes some elements on either side of the 100th element of φ . For $N = 400$ we took our section of the solution to be $\varphi(80 : 120)$. Letting d be this section of the solution φ then we measure the size of the wiggles by

$$\log_{10}(\max |d''| - \min |d''|). \quad (5.6)$$

We can now analyse our solutions φ of the discrete travelling wave equation (5.3) in more detail. Instead of plotting snapshots of φ for increasing periods



Figure 5.8: A chosen section of the solution φ .

as the simulation runs, we can now plot the resonance amplitude (5.6) against the period T of the solution or some other parameter.

5.4.3 Resonance Results

Now we have a way of measuring the size of the wiggles we can plot this against the period T as we run a continuation in $\frac{T}{2}$. This will help tell us where these resonances occur for certain combinations of the parameters and also how big they are.

For the simulation given in Figure 5.6 we can now plot the size of the resonance as given by (5.6) against the period of the solution. This is given in Figure 5.9b, in which the major peak showing corresponds to the solution given in Figure 5.6d and 5.9a.

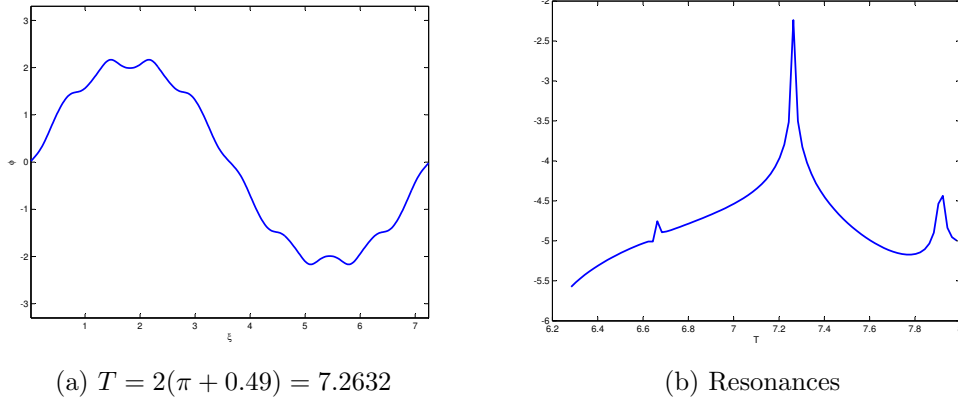


Figure 5.9: A short continuation simulation showing one major resonance peak. The y -axis gives the size of the resonance defined by (5.6).

Next, we plot the resonance for a slightly longer continuation simulation

in Figure 5.10 and compare it for a rational ratio of $\frac{\sigma}{\kappa}$ and an irrational one. From this first investigation it seems that the resonances for a rational ratio of $\frac{\sigma}{\kappa}$ are evenly spaced out over increasing value of T , but for the irrational ratio, the resonances appear to occur more randomly. From this conjecture, we would like to see how the resonances for other ratios of $\frac{\sigma}{\kappa}$ are spaced out over increasing values of T .

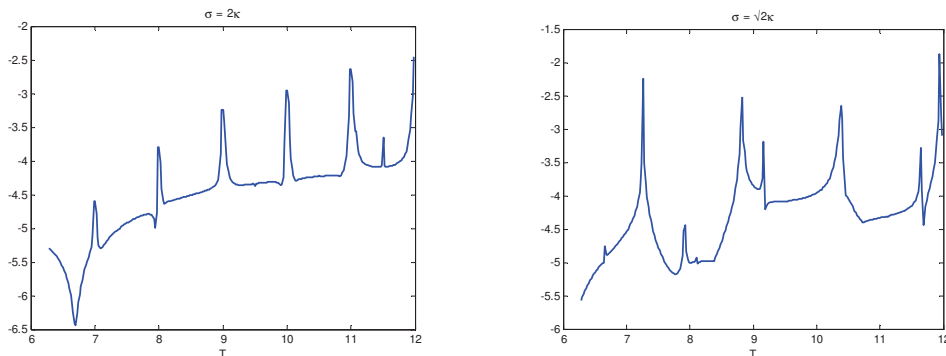
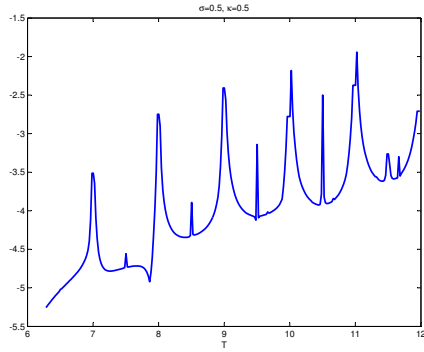


Figure 5.10: Comparison of the resonances for a rational ratio of $\frac{\sigma}{\kappa}$ and an irrational one. The y -axis gives the size of the resonance defined by (5.6).

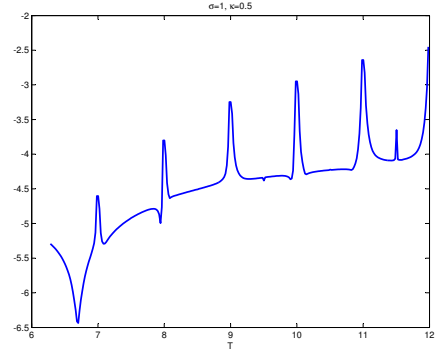
We first look at other rational values of $\frac{\sigma}{\kappa}$ and plot a continuation simulations in Figure 5.11. From this, it appears that for all rational ratios of $\frac{\sigma}{\kappa}$ the resonances are approximately equally spaced out as the period T increases. This suggests that there is some relationship between the parameters, T , σ , and κ predicting where the resonances occur.

In Figures 5.11a, 5.11b, and 5.11c a relationship between the parameters is easy to see. In all three of these plots the resonance spikes occur at integer values of the period T . The ratios of $\frac{\sigma}{\kappa}$ in these plots are $\frac{\sigma}{\kappa} = 1$, $\frac{\sigma}{\kappa} = 2$ and $\frac{\sigma}{\kappa} = 3$ respectively. Therefore, we conject that when $\frac{\sigma}{\kappa}$ is an integer value, then the resonances occur at integer values of the period.

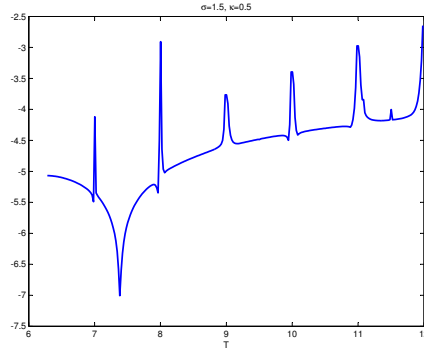
Since the above observation was only based on $\kappa = 0.5$, we use a slightly different value κ to see if what we observed is still true. We use $\sigma = 1.0567$ and $\kappa = 0.52835$, so that $\frac{\sigma}{\kappa} = 2$ and plot the results in Figure 5.12. On the left we have plotted the resonance against the period and see that the resonances do not occur at integer values of the period T , but if we plot the



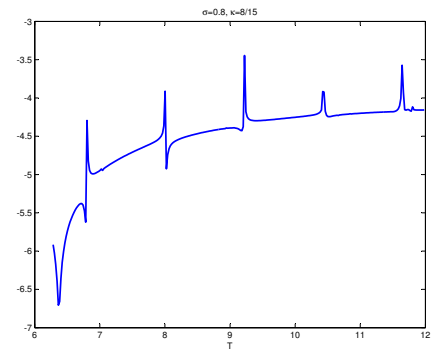
(a) $\sigma = \kappa$



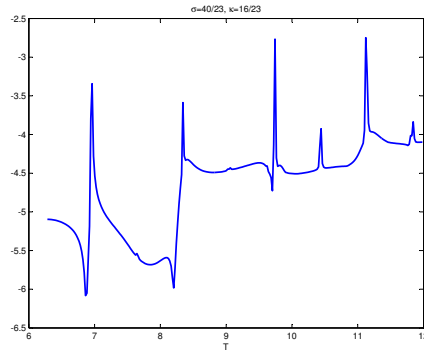
(b) $\sigma = 2\kappa$



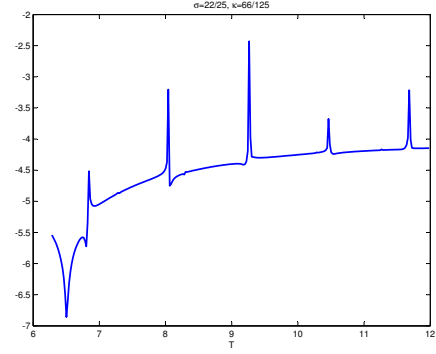
(c) $\sigma = 3\kappa$



(d) $\sigma = \frac{3}{2}\kappa$



(e) $\sigma = \frac{5}{2}\kappa$



(f) $\sigma = \frac{5}{3}\kappa$

Figure 5.11: Continuation in T starting with $T = 2\pi$ for different rational values of $\frac{\sigma}{\kappa}$. The y -axis gives the size of the resonance defined by (5.6).

resonances against $\frac{T}{2\kappa}$, as given in the right of Figure 5.12, then we do get the resonances occurring at integer values of $\frac{T}{2\kappa}$. From these observations we have the following conjecture.

Conjecture 5.4.1. *For $\frac{\sigma}{\kappa} \in \mathbb{Z}$ a resonance will occur if $\frac{T}{2\kappa} \in \mathbb{Z}$.*

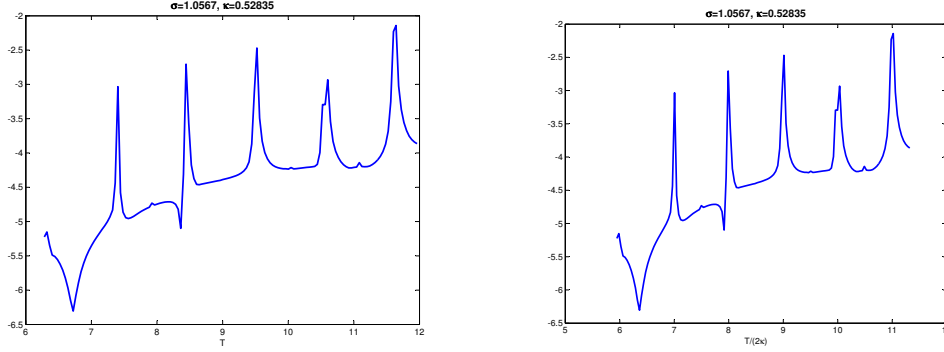


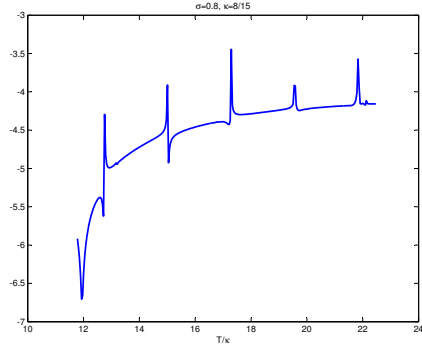
Figure 5.12: Continuation simulation for $\sigma = 2\kappa$: resonances plotted against T and $\frac{T}{2\kappa}$. The y -axis gives the size of the resonance defined by (5.6).

Following this conjecture, we plot the resonances of the remaining 3 plots of Figure 5.11, that did not have $\frac{\sigma}{\kappa} \in \mathbb{Z}$, in Figure 5.13. This time we plot the resonances against $\frac{T}{\kappa}$, instead of T , to see if the conjecture 5.4.1 can be extended to include all rational values $\frac{\sigma}{\kappa}$.

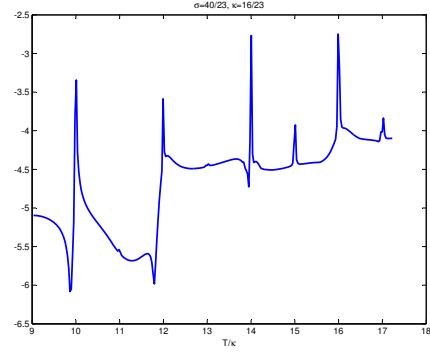
Note that we have plotted the resonances against $\frac{T}{\kappa}$ instead of $\frac{T}{2\kappa}$, as we did in Figure 5.12. The resonances will still occur at an integer value if the conjecture is correct, but instead of resonance at every integer, there will be one at every second integer.

From Figure 5.13 we see that it is not always true that $\frac{T}{2\kappa} \in \mathbb{Z}$ whenever $\frac{\sigma}{\kappa} \in \mathbb{Q}$. For Figure 5.13b it is true that $\frac{T}{2\kappa} \in \mathbb{Z}$, but for Figure 5.13a and 5.13c it is not true. After investigating to find a relationship between the parameters for rational values of $\frac{\sigma}{\kappa}$, no simple relationship could yet be found. However, there does seem to be some pattern for where the resonances occur for rational values of $\frac{\sigma}{\kappa}$.

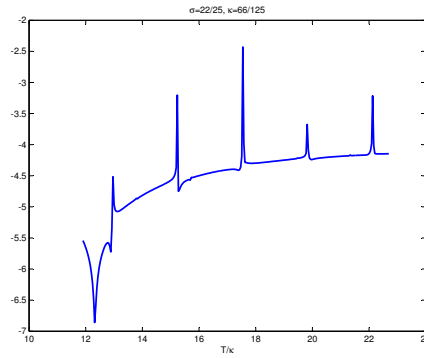
To show more clearly that our conjecture 5.4.1 does not extend to all rational values of $\frac{\sigma}{\kappa}$ we have plotted the resonances for $\frac{\sigma}{\kappa} = \frac{m}{n}$ for a fixed value



(a) $\sigma = \frac{3}{2}\kappa$



(b) $\sigma = \frac{5}{2}\kappa$



(c) $\sigma = \frac{5}{3}\kappa$

Figure 5.13: Continuation in T starting with $T = 2\pi$ for different rational values of $\frac{\sigma}{\kappa}$. The y -axis gives the size of the resonance defined by (5.6).

of n in Figure 5.14. The plot on the left gives the resonances for $n = 1$ with $m = 1, 2, 3, 4$. Here, we see that plotting against $\frac{T}{2\kappa}$ we get the resonance spikes occurring at every integer value which agrees with the conjecture 5.4.1. On the other hand for the plot on the right, for $n = 2$ and $m = 3, 5, 7$, the same does not occur. Only the red curve has resonances occurring at integer values of $\frac{T}{2\kappa}$.

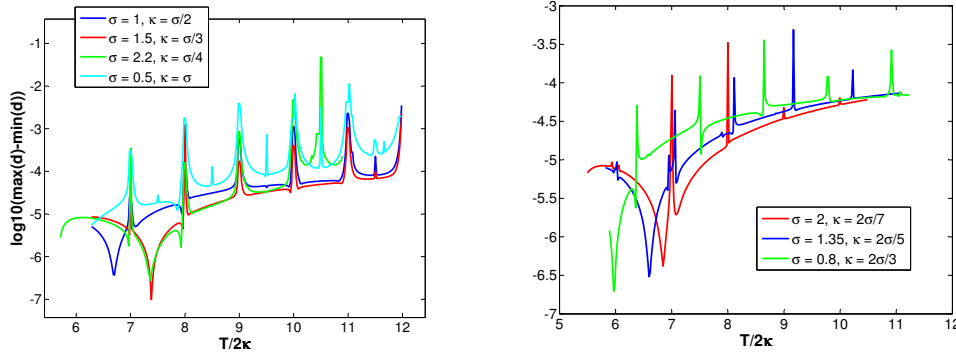


Figure 5.14: The left plot shows the resonances for $\frac{\sigma}{\kappa} = \frac{m}{n}$ for the case $n = 1$ and $m = 1, 2, 3, 4$ and the plot on the right shows the case $n = 2$ and $m = 3, 5, 7$. The y -axis gives the size of the resonance defined by (5.6).

We now take a different approach to studying the relationship between the resonances and the parameters.

We fix a ratio of $\frac{\sigma}{\kappa}$ and use different values of σ and κ with this ratio to compare the resonances. We fix $\frac{\sigma}{\kappa} = \frac{3}{5}$ and choose rational values of σ and also irrational ones to see if there is any difference. This is plotted in Figure 5.15, where the green, red, and blue curves are rational values of σ and the pink curve is an irrational value of σ . In order of decreasing values of σ are the green, pink, red, then the blue curve. As expected, generally the greater the value of σ (and hence κ) the bigger the resonance. Also, as expected, a greater value of σ produces a resonance at a slightly larger period than a smaller value of σ .

Figure 5.15 also shows that there still appears to be a relationship between where the resonances occur and the value of the parameters T , σ and κ .

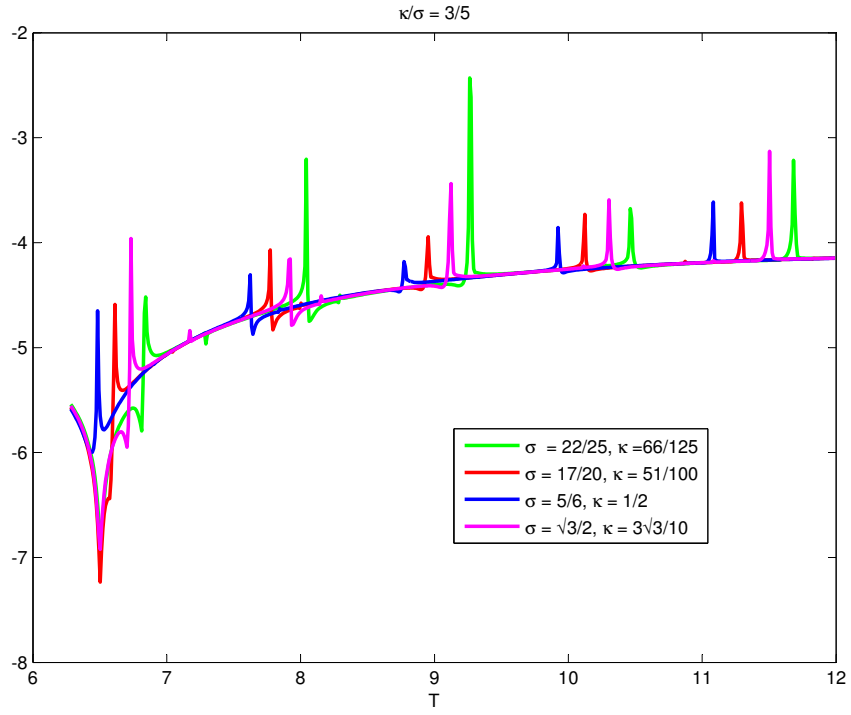


Figure 5.15: Continuation in T starting with $T = 2\pi$ for fixed rational values of $\frac{\sigma}{\kappa}$ for different values of σ . The y -axis gives the size of the resonance defined by (5.6).

We finally look at the resonances as the period tends to infinity and approaches the heteroclinic solution. We run the continuation simulation out to a very a large period to see what is happening with the pattern of resonances as the period approaches infinity. For this we plot the resonances against the logarithm of the period rather than the period itself.

In Figure 5.16 we plot the resonances from $T = 2\pi$ to $T \rightarrow \infty$ for different combinations of σ and κ . The smallest to largest values of σ (and κ) are given by the red, blue, green, cyan then pink curves. The red, blue and green curves have irrational ratios of $\frac{\sigma}{\kappa}$, while the cyan and pink curves have rational values of $\frac{\sigma}{\kappa}$, (even though σ is an irrational value—it is not important whether or not σ itself is rational or irrational, it only matters whether $\frac{\sigma}{\kappa}$ is rational or irrational). As before, the greater the value of σ (and κ) the larger the resonances. Also, notice the the base line is higher for the resonances which have higher values of σ (and κ). It seems that from these simulations that there is no difference in the ‘randomness’ of the resonances for rational and irrational ratios of $\frac{\sigma}{\kappa}$. Also, for solutions with period slightly greater than $T = 100$ the resonances suddenly decrease in size for all curves and then increase up to half way before leveling off. This suggests that as the period T of the solution tends to infinity, travelling wave solutions exist for all combinations of σ and κ .

Notice that the red and blue curves, in Figure 5.16, have the same value of σ but the red curve has a smaller value of κ than the blue curve. Even though the values of σ are the same the blue curve has a higher base line of resonances than the red curve. The case is the same for the cyan and pink curves, they have the same value of σ but the cyan curve has a smaller value of κ than the pink curve and again the pink curve has a higher base line of resonances than the cyan curve. This suggests that the value of κ has more influence on the resonances than σ . We could have have already guessed this was the case in our analysis on the resonances for $\frac{\sigma}{\kappa}$ rational, since for the cases where we found a relationship it only depended on T and κ , but not σ .

We can confirm that the value of κ has more influence on the resonances than σ by fixing the value of κ and varying the value of σ instead or vice versa.

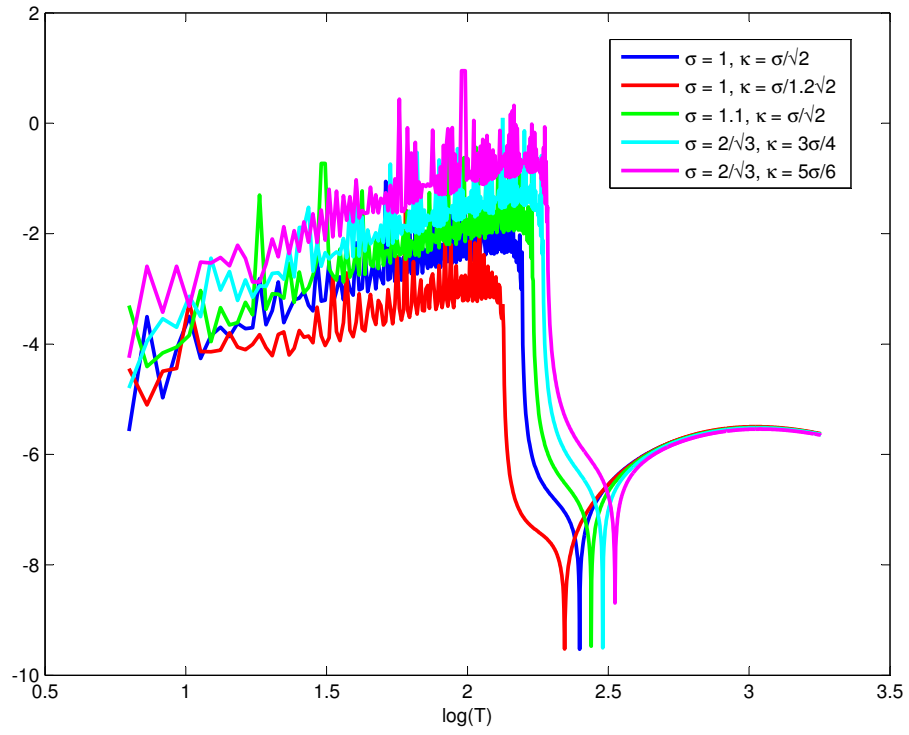


Figure 5.16: Continuation in T tending to infinity starting with $T = 2\pi$. The y -axis gives the size of the resonance defined by (5.6).

The graph for this is given in Figure 5.17, where the red and green curves have the same value of σ but different values of κ , and the blue and red curves have the same value of κ but different values of σ . For different values of κ with σ fixed, we see that the green curve with a greater value of κ has a higher base line of resonances than the red curve with a smaller value of κ . On the other hand, for different values of σ with κ fixed, we see that the base line of the resonances of the green and blue curve lie at the same level as each other, but the blue curve has slightly larger resonances overall since it has a larger value of σ than the green curve.

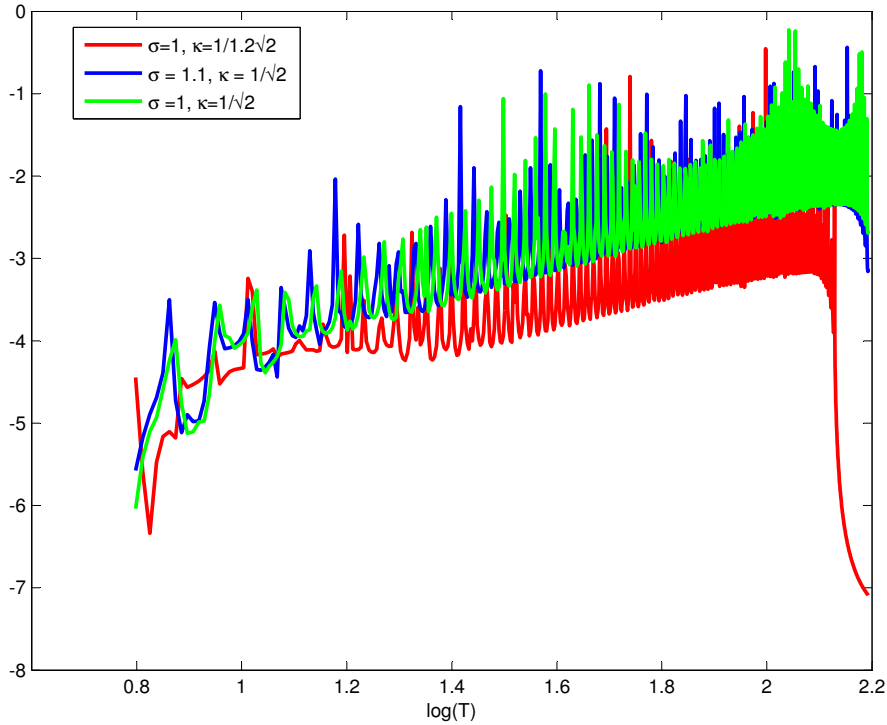


Figure 5.17: Continuation in T tending to infinity starting with $T = 2\pi$. The y -axis gives the size of the resonance defined by (5.6).

In Chapter 6 we will back up these observations, on the existence of periodic travelling wave solutions of the discrete travelling wave equation (5.3), with results from backward error analysis. We will also combine some of the results from this chapter with those of Chapter 6 and make a comparison.

Chapter 6

Backward Error Analysis of the Discrete Travelling Wave Equation

In this chapter we give an introduction to linear multistep methods for 1st order equations before moving on to multistep methods for 2nd order differential equations. This is the topic we are most interested in for our problem. Next, we give some more background information on multistep methods beginning with the underlying one-step method, then moving onto backward error analysis for multistep methods of 2nd order differential equations. Finally, we give a discussion and results from backward error analysis of the discrete travelling wave equation, then generalise this to backward error analysis for multisymplectic integrators of multi-Hamiltonian PDEs.

6.1 Multistep Methods

For one-step methods symplectic methods are known to have desirable numerical characteristics such as near energy preservation over long times and at most linear error growth for nearly integrable systems. It is these favourable features that we would also like to see in multistep methods, but the long-time

behaviour of multistep methods is generally not that great. They often behave like non-symplectic and non-symmetric one-step methods and sometimes exhibit undesired instabilities, extreme behaviour not seen in other methods, such as increasing oscillations. These types of undesired behaviours are often due to parasitic solutions.

But it has been noticed that some multistep methods for second order equations have a much better long-time behaviour. This has been investigated by various authors to see when this occurs [39, 34, 35, 20].

6.1.1 Linear Multistep Methods for First Order Systems

For a first order system of differential equations $\dot{y} = f(y)$ a linear multistep method is given by

$$\sum_{j=0}^k \alpha_j y_{n+j} = h \sum_{j=0}^k \beta_j f(y_{n+j}), \quad (6.1)$$

where α_j and β_j are real parameters, with $\alpha_k \neq 0$ and $|\alpha_0| + |\beta_0| > 0$.

The method (6.1) is said to be symmetric if coefficients satisfy

$$\alpha_{k-j} = -\alpha_j, \quad \beta_{k-j} = \beta_j, \quad \forall j. \quad (6.2)$$

See Definition 6.1.4 for an equivalent definition of symmetry.

To see how to use the formula (6.1) we expand it for the first step to get

$$\alpha_0 y_0 + \alpha_1 y_1 + \dots + \alpha_k y_k = h(\beta_0 f(y_0) + \beta_1 f(y_1) + \dots + \beta_k f(y_k)). \quad (6.3)$$

Given an initial value $y(t_0) = y_0$, we can see from (6.3) that we still need some starting procedure to find approximations for y_1, \dots, y_{k-1} . Once these are found we can find the value of y_k that we want to find, then y_n for $n > k$, (6.1) can be used recursively to find future values.

The starting procedure could be some one-step method to find values for

$$y_1, \dots, y_{k-1}.$$

Also, notice that if $\beta_k = 0$ then the method is explicit, otherwise the method will be implicit.

The generating polynomials associated with the coefficients of (6.1) are defined as

$$\rho(\zeta) = \sum_{j=0}^k \alpha_j \zeta^j = \alpha_0 + \alpha_1 \zeta + \alpha_2 \zeta^2 + \dots + \alpha_k \zeta^k, \quad (6.4)$$

$$\sigma(\zeta) = \sum_{j=0}^k \beta_j \zeta^j = \beta_0 + \beta_1 \zeta + \beta_2 \zeta^2 + \dots + \beta_k \zeta^k. \quad (6.5)$$

These polynomials are also known as the first and second characteristic polynomials respectively.

The characteristic polynomials (6.4) and (6.5) can be used to define the degree, consistency, order, stability, convergence, and symmetry of a multistep method (6.1).

Definition 6.1.1 (Degree). *A multistep method (6.1) is of degree k , where k is the number of steps needed in the method. Hence, it can also be called a k -step method.*

Definition 6.1.2 (Consistency). *The method (6.1) is consistent if the characteristic polynomials satisfy*

$$\begin{aligned} \rho(1) &= 0 \\ \rho'(1) &= \sigma(1) \neq 0. \end{aligned}$$

Theorem 6.1.1 (Order). *A linear multistep method (6.1) has order p if*

$$\rho(e^h) - h\sigma(e^h) = O(h^{p+1}), \text{ as } h \rightarrow 0.$$

Definition 6.1.3 (Stability). *A multistep method (6.1) is stable, also called zero-stable, if all the roots of $\rho(\zeta) = 0$ satisfy $|\zeta| \leq 1$, and those on the unit circle ($|\zeta| = 1$) are simple roots (roots of multiplicity 1).*

Due to the consistency condition a stable method must have a zero at $\zeta = 1$. This zero is called the principal root and all other zeros are spurious roots.

If all roots are inside the unit circle ($|\zeta| < 1$) except $\zeta = 1$ then the method is said to be strictly stable.

Theorem 6.1.2 (Convergence). *If a method (6.1) is consistent and stable of order $r \geq 1$, then it is convergent of order r for all sufficiently smooth problems.*

Definition 6.1.4 (Symmetry). *A method (6.1) is symmetric if the inverse of every zero of $\rho(\zeta)$ is also a zero of $\rho(\zeta)$. This is equivalent to condition (6.2).*

Definition 6.1.5 (Stable and Symmetric). *As a consequence of the stability and symmetry conditions above, we have that a method (6.1) is a stable symmetric method if all zeros of $\rho(\zeta)$ are simple and lie on the unit circle.*

Therefore, a symmetric multistep method cannot be strictly stable.

6.1.2 Example of the Behaviour of Multistep methods

Following an example given in [37], we consider the equations of motion of the pendulum $\dot{q} = p$, $\dot{p} = -\sin q$, and apply the 2-step explicit Adams method,

$$y_{n+2} = y_{n+1} + h \left(\frac{3}{2}f(y_{n+1}) - \frac{1}{2}f(y_n) \right),$$

and also the 2-step symmetric explicit midpoint rule,

$$y_{n+2} = y_n + 2hf(y_{n+1}).$$

We expect the explicit Adams method to behave similarly to the explicit Euler method and the symmetric midpoint rule to behave similarly to a one-step symmetric method or the implicit midpoint rule which is symplectic. Therefore we expect the second method to give good long-time behaviour.

The explicit Euler method is used to find an approximation for y_1 . The results are shown in Figure 6.1 for the first 90 steps. For both methods the phase portrait is plotted using coloured lines with the numerical solution superimposed with black points joined by lines.

In the explicit Adams method the solution spirals clockwise outwards from the centre, behaving like the explicit Euler method, as expected. On the other hand, the explicit midpoint rule exhibits unexpected behaviour. Instead of remaining close to a periodic orbit of the exact solution, as in the implicit

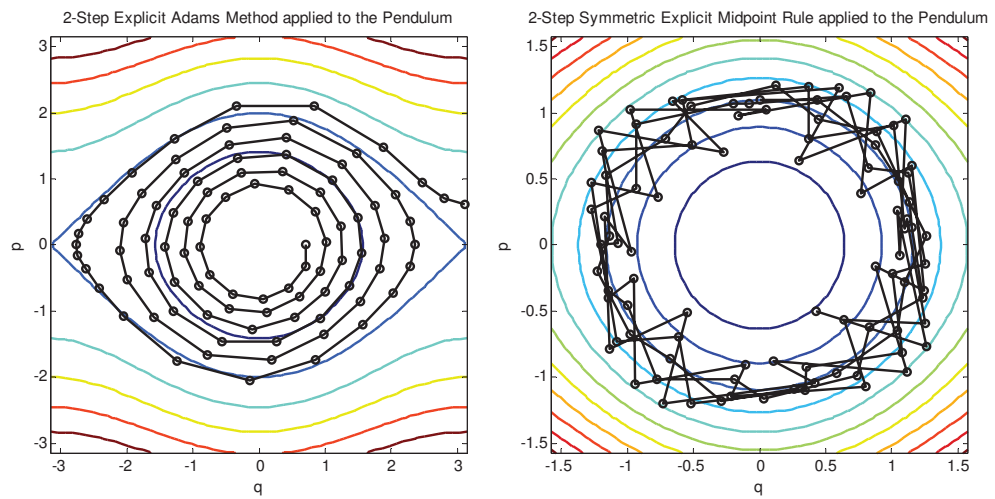


Figure 6.1: The explicit Adams method with step size $h = 0.5$, initial value $(q_0, p_0) = (0.7, 0)$ and the explicit midpoint rule with $h = 0.4$, initial value $(q_0, p_0) = (0, 1.1)$, applied to the pendulum.

midpoint rule, the solution shows increasing oscillations. These types of solutions are known as parasitic solutions.

What is the difference between these two equations? We can investigate this by first looking at the zeros of the characteristic polynomial $\rho(\zeta)$ for each method.

For the explicit Adams method, the characteristic polynomial is,

$$\rho(\zeta) = \zeta^2 - \zeta = \zeta(\zeta - 1).$$

Setting $\rho = 0$ we get the zeros of the characteristic polynomial are $\zeta = 0$ and $\zeta = 1$. So the explicit Adams method is strictly stable.

For the symmetric explicit midpoint rule, the characteristic polynomial is,

$$\rho(\zeta) = \zeta^2 - 1.$$

Setting $\rho = 0$ we get the zeros of the characteristic polynomial are $\zeta = 1$ and $\zeta = -1$. So this method is stable, but not strictly stable as expected, since no symmetric multistep method can be strictly stable.

From this example it seems that for a method to behave as expected, producing no parasitic solutions, the condition of strict stability needs to be satisfied. As was seen for the explicit symmetric method, methods that are not strictly stable have the possibility of introducing parasitic solutions. This will lead to an exponential growth in error in the solution.

In 1956, Dahlquist [22] published a paper in which he noticed that having zeros of $\rho(\zeta)$ on the unit circle can lead to an exponential error growth. So in terms of stability this fits with what we have seen. Being strictly stable means that only one zero of $\rho(\zeta)$ will be on the unit circle and all the other zeros will be inside the unit circle. On the other hand being stable, but not strictly stable, can mean that any number of zeros of $\rho(\zeta)$ can appear on the unit circle as long as they are of multiplicity one. Section 6.3 gives an explanation for this behaviour of the strictly stable method. Later on, in 1976, Lambert and Watson studied this idea in detail for multistep methods applied to a second order linear test problem; see Section 6.2 for more on this.

6.2 Multistep Methods for Second Order Equations

In this section we give an introduction to multistep methods for 2nd order equations.

For a second order differential equation $\ddot{y} = f(y)$ a multistep method is of the form

$$\sum_{j=0}^k \alpha_j y_{n+j} = h^2 \sum_{j=0}^k \beta_j f(y_{n+j}). \quad (6.6)$$

The method (6.6) is symmetric if the coefficients satisfy

$$\alpha_{k-j} = \alpha_j, \quad \beta_{k-j} = \beta_j, \quad \forall j. \quad (6.7)$$

An equivalent definition of symmetry is given by Definition 6.2.4.

The first and second characteristic polynomials $\rho(\zeta)$ and $\sigma(\zeta)$ are defined as before in (6.4) and (6.5).

The consistency, order, stability, convergence, and symmetry conditions are defined similarly to those for first order multistep methods, by using the characteristic polynomials.

Definition 6.2.1 (Degree). *A multistep method (6.6) is of degree k , where k is the number of steps needed in the method. Hence, it can also be called a k -step method.*

Definition 6.2.2 (Consistency). *A multistep method (6.6) is consistent if the characteristic polynomials satisfy*

$$\begin{aligned} \rho(1) &= \rho'(1) = 0 \\ \sigma(1) &= \frac{1}{2} \rho''(1) \neq 0. \end{aligned}$$

Theorem 6.2.1 (Order). *A multistep method (6.6) is of order p if*

$$\rho(e^h) - h^2 \sigma(e^h) = O(h^{p+2}), \text{ as } h \rightarrow 0.$$

Definition 6.2.3 (Stability). *A method (6.6) is stable, also called zero-stable, if all zeros of $\rho(\zeta)$ satisfy $|\zeta| \leq 1$ and those on the unit circle ($|\zeta| = 1$) are at most double zeros (multiplicity two).*

The method is called strictly stable if all zeros, except for $\zeta = 1$, are inside the unit circle ($|\zeta| < 1$).

Due to the consistency condition, a stable method must have a double zero at $\zeta = 1$. As with methods for first order equations, this zero is called the principal root and all other zeros are called spurious roots.

Theorem 6.2.2 (Convergence). *If a method (6.6) is consistent and stable of order $r \geq 1$, then it is convergent.*

Definition 6.2.4 (Symmetry). *If for every zero ζ of $\rho(\zeta)$, the inverse ζ^{-1} is also a zero, then the method (6.6) is said to be symmetric. See also (6.7).*

Definition 6.2.5 (Stable and Symmetric). *If all zeros of $\rho(\zeta)$ are on the unit circle and have multiplicity at most two, then (6.6) is a stable symmetric method.*

From the definition of a strictly stable method, we see that symmetric multistep methods for second order equations cannot be strictly stable, as was the case for first order methods.

Definition 6.2.6 (S-Stable). *A method (6.6) is called s-stable if all zeros of $\rho(\zeta)$ are on the unit circle, and all are simple roots except from the double root at $\zeta = 1$.*

The ‘s’ in s-stable stands for simple roots. All s-stable methods are symmetric with an extra condition posed on them, that all roots are simple except the principal root. This extra condition is known to give s-stable methods good long-time behaviour.

As was mentioned previously in Section 6.1.2, in 1976 Lambert and Watson [52] studied the idea of double zeros of $\rho(\zeta)$ on the unit and their association with parasitic solutions. They studied this in detail using the simple linear

test problem $\ddot{y} = -\omega^2 y$ (the harmonic oscillator) and found that when using symmetric methods in which the method had all zeros of $\rho(\zeta)$ on the unit circle and all roots simple except for a double root at $\zeta = 1$, then the numerical solution remained close to a periodic orbit of the exact solution. These types of methods are now called s-stable, see Definition 6.2.6. The exact solution of the harmonic oscillator was given in Figure 1.13.

In 1990, Quinlan and Tremaine [78] continued this idea in their paper studying simulations of the outer solar system. They derived high-order explicit symmetric methods appropriate for the long-time integration of planetary orbits.

Soon after this paper was published, Alar Toomre discovered a troubling aspect of the methods. When plotting the energy error, spikes in energy error occurred at certain values of the steps per period. These spikes are known as instabilities and resonances. For an instability the error grows exponentially with time. A resonance is similar to an instability but the spikes are smaller. Resonances were described in 5.3 and also appear in our numerical solution of the discrete travelling wave equation (5.3).

With this discovery, Quinlan [77], in 1999 wrote a paper giving an explanation for why the instabilities and resonances occur and also gave predictions on where they occur in terms of the spurious roots. We follow this paper in Section 6.5 to see if we can find a relationship between the resonances in our problem and the parameters.

Quinlan then goes on to say how the multistep coefficients should be chosen to reduce the instability and resonance in problems. Firstly, to avoid the instabilities the spurious roots of $\rho(\zeta)$ should be spread as evenly as possible on the unit circle. Secondly, to avoid the resonances the spurious roots of $\rho(\zeta)$ should be as far away from the principal root $\zeta = 1$ as possible. But these two conditions are conflicting: if we have the spurious roots far from $\zeta = 1$ then these roots will be bunched up close to $\zeta = -1$. So a compromise has to be made. This becomes more difficult the higher the order of the method is, because higher order methods have more spurious roots.

Using an example from [37] we can demonstrate how double zeros in the characteristic polynomial $\rho(\zeta)$ affects the error growth. We have worked through this example independently from [37], but have used their graph. The Kepler problem,

$$\ddot{q}_1 = -\frac{q_1}{(q_1^2 + q_2^2)^{3/2}}, \quad \ddot{q}_2 = -\frac{q_2}{(q_1^2 + q_2^2)^{3/2}},$$

with initial values,

$$q_1(0) = 1 - e, \quad q_2(0) = 0, \quad \dot{q}_1(0) = 0, \quad \dot{q}_2(0) = \sqrt{\frac{1+e}{1-e}},$$

and eccentricity $e = 0.2$ is used. The following three methods were applied with constant step size $h = 0.01$ for 10^5 periods:

$$\begin{aligned} \text{(A)} \quad & y_{n+4} - 2y_{n+3} + y_{n+2} = h^2 \left(\frac{7}{6}f(y_{n+3}) - \frac{5}{12}f(y_{n+2}) + \frac{1}{3}f(y_{n+1}) - \frac{1}{12}f(y_n) \right), \\ \text{(B)} \quad & y_{n+4} - 2y_{n+2} + y_n = h^2 \left(\frac{4}{3}f(y_{n+3}) - \frac{4}{3}f(y_{n+2}) + \frac{4}{3}f(y_{n+1}) \right), \\ \text{(C)} \quad & y_{n+4} - 2y_{n+3} + 2y_{n+2} - 2y_{n+1} + y_n \\ & = h^2 \left(\frac{7}{6}f(y_{n+3}) - \frac{1}{3}f(y_{n+2}) + \frac{7}{6}f(y_{n+1}) \right). \end{aligned}$$

All methods are of order 4 and the starting values y_1 , y_2 , and y_3 are all computed very accurately. We find the characteristic polynomial $\rho(\zeta)$ of each method in order to find the zeros of ρ , hence the double zeros.

For method **(A)** we get,

$$\rho(\zeta) = \zeta^4 - 2\zeta^3 + \zeta^2,$$

which has zeros at $\zeta = 1$ (multiplicity two) and $\zeta = 0$ (multiplicity two). Since $\zeta = 0$ is inside the unit circle, method **(A)** is strictly stable.

For method **(B)** we get,

$$\rho(\zeta) = \zeta^4 - 2\zeta^2 + 1,$$

which has zeros at $\zeta = 1$ (multiplicity two) and $\zeta = -1$ (multiplicity two). Since both $\zeta = 1$ and $\zeta = -1$ are their own inverses, then method **(B)** is symmetric, and cannot be strictly stable, but all zeros satisfy $|\zeta| \leq 1$ so **(B)** is a stable symmetric method.

Notice that method **(B)** has double roots other than the principal root, namely at $\zeta = -1$.

For method **(C)** we get,

$$\rho(\zeta) = \zeta^4 - 2\zeta^3 + 2\zeta^2 - 2\zeta + 1,$$

which has zeros at $\zeta = 1$ (multiplicity two), $\zeta = -i$, and $\zeta = i$. Since $\zeta = 1$ is its own inverse and $\zeta = -i$ and $\zeta = i$ are inverses of each other, then method **(C)** is also symmetric. Also, since all roots are on the unit circle and are simple except for the double principal root then method **(C)** is s-stable.

Since method **(B)** is the only method that has double roots other than $\zeta = 1$ then we expect this will be the only method that behaves unexpectedly.

Figure 6.2 is reproduced from [37] and shows the energy error for each of the three methods. To start with all methods behave well with the error bounded, but as the integration is performed for more steps, longer time period, method **(A)** begins to show linear error growth, which continues for the rest of the simulation. This is what occurs for non-symplectic and non-symmetric one-step methods, so can be expected also for multistep methods. Method **(B)** shows exponential error growth, which is expected from its double zeros. Finally, for method **(C)** the error remains bounded for the whole simulation. It is the only method which satisfies the s-stability condition.

6.3 The Underlying One-Step Method

We begin this section by giving a definition of the underlying one-step method, then discuss briefly why it is used and its disadvantage.

The underlying one-step method for a multistep method (6.1) is a mapping $y \mapsto \Phi_h(y)$ such that $y_n = \Phi_h^n(y_0)$ satisfies

$$\sum_{j=0}^k \alpha_j \Phi_h^j(y) = h \sum_{j=0}^k \beta_j f(\Phi_h^j(y)), \quad (6.8)$$

where $\Phi_h(y)$ is a one-step method.

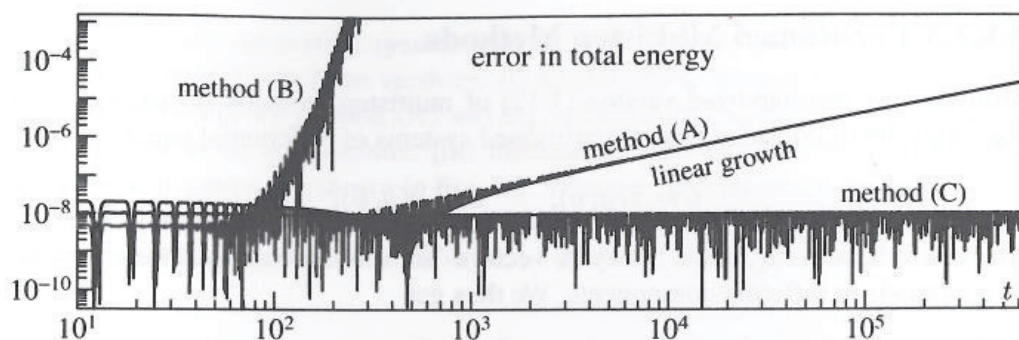


Figure 6.2: Energy error for three different linear multistep methods applied to the Kepler problem, reproduced from [37]. The x -axis gives the number of periods, and the y -axis gives the energy error.

Hence, the underlying one-step method relates a multistep method to an identical one-step method. In this way, the multistep method can now be analysed, more simply, as a one-step method. Therefore, when applying backward error analysis to the underlying one-step method a lot of good information on the conservative properties, see Section 6.4.3, of the method can be determined. The disadvantage of the underlying one-step method is that it tells us nothing about any parasitic solutions that may appear. To analyse parasitic solutions, backward error analysis will have to be directly applied to the multistep method. This method is used in Section 6.6 for our analysis of the discrete travelling wave (5.3).

In 1986 Kirchgraber [51] proved that strictly stable linear multistep methods (6.1) are basically equivalent to one-step methods. The full theorem and proof are given in [37].

By relating the numerical solution of a multistep method to a one-step method a good deal of information on the long-time behaviour of the mul-

timestep method can be extracted. We have the result that, for any starting approximations y_0, y_1, \dots, y_{k-1} which are close to the exact solution, there exists a y_0^* such that the multistep solution and the one-step solution, given by $y_{n+1}^* = \Phi_h(y_n^*)$ approach each other exponentially fast. This is known as the asymptotic phase property. Therefore, strictly stable linear multistep methods have the same long-time behaviour as one-step methods. This now explains why the explicit Adam's method in Figure 6.1 gave similar behaviour to the explicit Euler method a one-step method.

When at least one zero of $\rho(\zeta)$, different from $\zeta = 1$, is on the unit circle, the method is no longer strictly stable, so Kirchgraber's theorem and proof fail. Therefore, Kirchgraber's theorem cannot be applied to symmetric multistep methods, which are of interest to us.

Even though Kirchgraber's theorem breaks down for methods which are not strictly stable, an underlying one-step method for methods satisfying the stability condition only, called weak stability, can be found as a formal series in h . Surprisingly, this also provides a good understanding of the long-time behaviour of multistep methods, but which are weakly stable. We have the following theorem.

Theorem 6.3.1. *Consider a linear multistep method (6.1) in which $\zeta = 1$ is a single zero of $\rho(\zeta) = 0$, then there exists a one-step method of the form,*

$$\Phi_h(y) = y + hd_1(y) + h^2d_2(y) + \dots \quad (6.9)$$

that satisfies (6.8). Also, if the multistep method is of order r , then so is the underlying one-step method.

The formal series $\Phi_h(y)$ is called the underlying one-step method and does not usually converge. This theorem does not require any stability conditions and a proof can be found in [37].

Everything so far, on the underlying one-step method, can only be applied to multistep methods (6.1) for first order equations. To get similar results for multistep methods (6.6) for second order equations, an approximation for the

derivative $\dot{y} = v$ is introduced. Now, the second order equation $\ddot{y} = f(y)$ will be a system of first order equations for the variables y and v ,

$$\begin{aligned}\dot{y} &= v, \\ \dot{v} &= f(y),\end{aligned}$$

so that the results of this section can now easily be applied to each equation in the system.

Since multistep methods can now be formulated as equivalent one-step methods, the idea of backward error analysis comes to mind in the study of the method's long-time behaviour.

6.3.1 Non-Symplecticity of the Underlying One-Step Method

A natural definition of symplecticity for multistep methods is that their underlying one-step method is symplectic, which means that their truncated modified equation is Hamiltonian. But it can be shown that the underlying one-step method of a linear multistep method cannot be symplectic [37]. Even though this is the case, particular multistep methods can preserve energy over long times [39, 35].

Definition 6.3.1. *A method $\Phi_h(y)$ is called conjugate to symplectic if there exists a transformation $\chi_h(y)$ which is $O(h)$ close to the identity, such that*

$$\chi_h^{-1} \circ \Phi_h \circ \chi_h$$

is a formal symplectic transformation when $f(y)$ in (6.1) or (6.6) is a Hamiltonian vector field.

Although the underlying one-step method of a multistep method is not symplectic, it can be shown that it is conjugate to symplectic when the multistep method is symmetric [35]. This is the property that gives certain multistep methods their good long-time behaviour. They share this good long-time

behaviour with symplectic integrators because

$$(\chi_h^{-1} \circ \Phi_h \circ \chi_h)^n = \chi_h^{-1} \circ \Phi_h^n \circ \chi_h.$$

Later, Section 6.5, we will see that the discrete travelling wave equation (4.4) can be written as a multistep method for certain parameters. The discrete travelling wave equation (4.4) originates from a PDE which is reduced to a second order ordinary differential equation through the use of travelling wave coordinates (3.1), so from now on we will mainly analyse multistep methods for second order equations.

6.4 Backward Error Analysis for Multistep Methods for Second Order Differential Equations

Backward error analysis can be applied to multistep methods in two ways. Firstly, it can be applied to the underlying one-step method, which we already know, from Section 1.22, gives us a good understanding of the long-time behaviour of the method. For strictly stable methods this is all we need—the parasitic terms are quickly damped out by the asymptotic phase property. Secondly, backward error analysis can be applied directly to the multistep method (6.6) in which case the parasitic terms are not damped quickly enough and appear in the numerical solution. In this case to get a complete description of the long-time behaviour, two modified differential equations need to be analysed, the principal modified equation and the parasitic modified equation. This will be explained in more detail in Section 6.4.2.

6.4.1 The (Principal) Modified Equation

The principal modified equation, or just modified equation, for a multistep method (6.6) is found by using the multistep method directly. This avoids the use of the underlying one-step method, which does not usually converge.

Theorem 6.4.1. *Consider a consistent linear multistep method (6.6) for a second order equation $\ddot{y} = f(y)$. In the absence of derivative approximations there exists unique h -independent functions $f_i(y, \dot{y})$ such that, every solution of the modified differential equation*

$$\ddot{y} = f(y) + hf_2(y, \dot{y}) + h^2f_3(y, \dot{y}) + \dots, \quad (6.10)$$

satisfies

$$\sum_{j=0}^k \alpha_j y(t + jh) = h^2 \sum_{j=0}^k \beta_j f(y(t + jh)) \quad (6.11)$$

up to $O(h^p)$ for all p .

If the method is symmetric, then $f_i(y, \dot{y}) = 0$ for all even i , so that the modified equation (6.10) has an expansion in even powers of h only.

Proof. Equation (6.11) is of the form

$$L_1 y(t) = h^2 L_2 f(y)$$

where L_1 and L_2 are some linear operators.

To find the linear operators L_1 and L_2 we let D denote time differentiation, so that

$$\begin{aligned} D(y(t)) &= \dot{y}, \\ D(f(y(t))) &= f'(y(t))\dot{y}, \end{aligned}$$

where the dot stands for differentiation with respect to time; the $'$ stands for differentiation with respect to y , or the Jacobian derivative if f is a vector field.

Expanding $y(t + jh)$ in a Taylor series and using the derivative D we get

$$\begin{aligned} y(t + jh) &= y(t) + jh\dot{y}(t) + \frac{1}{2!}(jh)^2\ddot{y}(t) + \dots \\ &= y(t) + jhD(y(t)) + \frac{1}{2!}(jh)^2D(D(y(t))) + \dots \\ &= y(t) + jhD(y(t)) + \frac{1}{2!}(jh)^2D^2(y(t)) + \dots \\ &= (1 + jhD + \frac{1}{2!}(jhD)^2 + \dots)y(t) \\ &= e^{jhD}y(t). \end{aligned}$$

Similarly, $f(y(t + jh))$ can be expanded in a Taylor series,

$$f(y(t + jh)) = e^{jhD} f(y).$$

Now, equation (6.11) can be written as

$$\sum_{j=0}^k \alpha_j e^{jhD} y(t) = h^2 \sum_{j=0}^k \beta_j e^{jhD} f(y).$$

Note from (6.4) and (6.5) that

$$\begin{aligned} \rho(e^{hD}) &= \sum_{j=0}^k \alpha_j (e^{hD})^j = \sum_{j=0}^k \alpha_j (e^{jhD}), \\ \sigma(e^{hD}) &= \sum_{j=0}^k \beta_j (e^{hD})^j = \sum_{j=0}^k \beta_j (e^{jhD}), \end{aligned}$$

so (6.11) can be simplified even more,

$$\rho(e^{hD}) y(t) = h^2 \sigma(e^{hD}) f(y). \quad (6.12)$$

Hence $L_1 = \rho(e^{hD})$ and $L_2 = \sigma(e^{hD})$. Rearranging (6.12), we get

$$y(t) = \frac{h^2 \sigma(e^{hD})}{\rho(e^{hD})} f(y).$$

Taking the second derivative of each side we get

$$\ddot{y}(t) = \frac{(hD)^2 \sigma(e^{hD})}{\rho(e^{hD})} f(y).$$

With the expansion

$$\frac{(hD)^2 \sigma(e^{hD})}{\rho(e^{hD})} = 1 + \mu_1 hD + \mu_2 (hD)^2 + \dots,$$

the above becomes

$$\ddot{y}(t) = (1 + \mu_1 hD + \mu_2 h^2 D^2 + \dots) f(y) \quad (6.13)$$

where μ_1, μ_2, \dots are constant coefficients.

Earlier in the proof we introduced the time derivative D . This can also be used to differentiate a function of two variables by using the chain rule. That is,

$$D(f_2(y, \dot{y})) = \frac{\partial f_2(y, \dot{y})}{\partial y} \dot{y} + \frac{\partial f_2(y, \dot{y})}{\partial \dot{y}} \ddot{y}.$$

Now, a comparison in equal powers of h in (6.13) and (6.10) can be made. This uniquely defines the coefficient functions $f_i(y, \dot{y})$. \square

6.4.2 The Parasitic Modified Equation

Because we have to use a starting procedure to get approximations for y_1, \dots, y_{k-1} before we can use our multistep method, this can introduce initial values not close to the exact solution. If these initial perturbations are not damped out fast enough then solutions not close to the exact solution will be produced—parasitic solutions. It was stated in Section 6.3 that these perturbations do damp out quickly for strictly stable methods, so these methods produce behaviours expected of similar one-step methods, whether or not it is qualitatively correct.

An example of a parasitic solution occurred in Section 6.1.2 and can be used to explain the above. Here the solution from the symmetric explicit midpoint rule produced increasing oscillations. We can replot the solution given in Figure 6.1, but this time with the (principal) modified differential equation plotted in the background, instead of the exact solution. This is given in Figure 6.3.

Now, from Figure 6.3 it can be seen that the principal modified differential equation is not enough to explain the oscillating behaviour of the numerical solution. The numerical solution behaves like

$$y_n \approx \tilde{y}(nh) + (-1)^n z(nh)$$

where the term $\tilde{y}(x)$ is the solution from the truncated (principal) modified differential equation and the term $(-1)^n z(nh)$ introduces these oscillations into

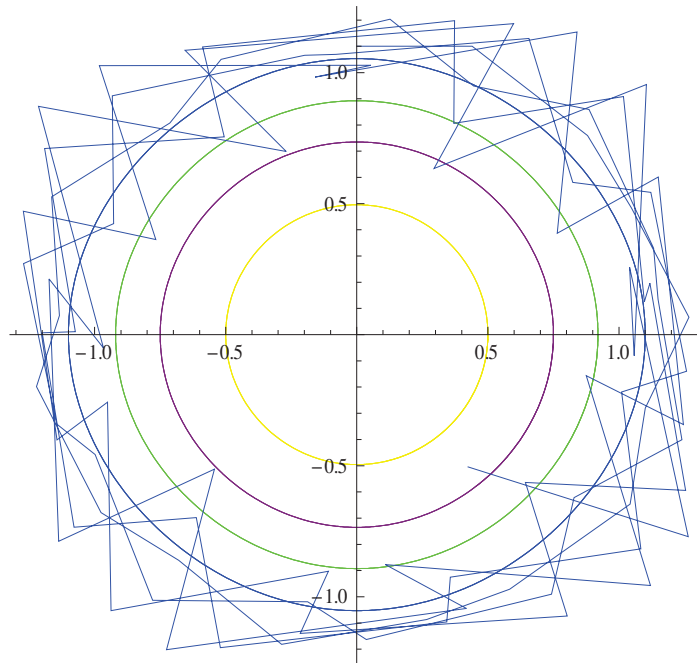


Figure 6.3: The solution of the 2-step symmetric explicit midpoint rule plotted with the MDE. The blue solution curve corresponds to the same orbit of the numerical solution (also in blue).

the numerical solution. This term is known as the solution of the parasitic modified differential equation.

Here, we do not give theorems and proofs on the parasitic modified equations because they relate to initial value problems, but these can be found in [37, 39, 34]. Whereas, our problem, in looking at the behaviour of the discrete travelling wave equation, involves boundary conditions which restricts us to travelling wave solutions only. So in this case, we do not need a starting procedure for approximations to y_0, y_1, \dots, y_{k-1} which introduce perturbations that can propagate. Without these perturbations, our problem should not produce parasitic solutions. Therefore, we only need to study the (principal) modified equations to get details of the long-time behaviour of the discrete travelling wave equation, just as was the case for strictly stable methods.

6.4.3 Conservation Properties from the Underlying One-Step Method

As was previously stated, the underlying one-step method is useful for gaining insight into the conservative properties of the method. Therefore, it is useful for statements on symplecticity, the modified Hamiltonian, and quadratic first integrals.

Theorem 6.4.2. *For a consistent symmetric linear multistep method (6.6) applied to $\ddot{y} = -\nabla U(y)$, there exists a series of the form*

$$\tilde{H}(y, \dot{y}) = \frac{1}{2} \dot{y}^T \dot{y} + U(y) + hH_2(y, \dot{y}) + h^2 H_3(y, \dot{y}) + \dots \quad (6.14)$$

which is a formal first integral of the modified equation (6.10)). $\tilde{H}(y, \dot{y})$ is called the modified Hamiltonian.

A proof of this theorem is given in [37]. A similar theorem exists for modified quadratic first integrals of multistep methods. This was first proved for one-step methods in [16]. Since the underlying one-step method is not symplectic then symmetric multistep methods do not exactly preserve quadratic first in-

tegrals, but they nearly preserve such first integrals. This is due to the fact that symmetric multistep methods are conjugate to symplectic.

6.5 The Discrete Travelling Wave Equation as a Multistep Method

In this section we show that the discrete travelling wave equation is equivalent to a multistep method when the ratio $\frac{\sigma}{\kappa}$ is rational. Next, we give a conjecture on the position of the roots of the first characteristic polynomial, $\rho(\zeta)$, of the discrete travelling wave equation relative to the unit circle.

Theorem 6.5.1. *The discrete travelling wave equation,*

$$\begin{aligned} \frac{c^2}{\kappa^2} (\varphi(\xi + \kappa) - 2\varphi(\xi) + \varphi(\xi - \kappa)) \\ - \frac{1}{\sigma^2} (\varphi(\xi + \sigma) - 2\varphi(\xi) + \varphi(\xi - \sigma)) = -V'(\varphi(\xi)), \end{aligned} \quad (6.15)$$

is equivalent to a symmetric multistep method when $\frac{\sigma}{\kappa}$ is rational.

If $\frac{\sigma}{\kappa} = \frac{m}{n}$, (m and n are integers, $n \neq 0$), is rational then the discrete travelling wave equation (6.15) is a finite (possibly high) dimensional map of dimension $2m$.

Proof. We do not give a formal proof but illustrate the proof by an example. We use $\frac{\sigma}{\kappa} = \frac{2}{1}$, so that $\sigma = 2\kappa$.

Firstly, recall that a multistep method was given for a second order differential equation of the form

$$\ddot{y} = f(y), \quad (6.16)$$

and the nonlinear wave equation upon substituting travelling wave coordinates was

$$(c^2 - 1)\ddot{\varphi} = -V'(\varphi). \quad (6.17)$$

We want our 2nd order ODE (6.17) to be in the same form as (6.16) so rearrange (6.17) to get,

$$\ddot{\varphi} = f(\varphi), \quad f(\varphi) = \frac{-V'(\varphi)}{c^2 - 1}. \quad (6.18)$$

Notice that in (6.15) we have $-V'(\varphi(\xi))$ on the right hand side, but we want this to be $f(\varphi)$ so it is equivalent to the general form of a multistep method given by (6.6). We can achieve this by dividing both sides of (4.4) by $c^2 - 1$ and get,

$$\frac{\frac{c^2}{\kappa^2} (\varphi(\xi + \kappa) - 2\varphi(\xi) + \varphi(\xi - \kappa)) - \frac{1}{\sigma^2} (\varphi(\xi + \sigma) - 2\varphi(\xi) + \varphi(\xi - \sigma))}{c^2 - 1} \quad (6.19)$$

$$= f(\varphi(\xi)).$$

Substituting $\sigma = 2\kappa$ into (6.19) and moving κ^2 to the right hand side we get,

$$\frac{c^2 (\varphi(\xi + \kappa) - 2\varphi(\xi) + \varphi(\xi - \kappa)) - \frac{1}{4} (\varphi(\xi + 2\kappa) - 2\varphi(\xi) + \varphi(\xi - 2\kappa))}{c^2 - 1} \quad (6.20)$$

$$= \kappa^2 f(\varphi(\xi)).$$



Figure 6.4: Relabeling of the five grid points in (6.15) to match that of a multistep method (6.6) for $\sigma = 2\kappa$. The grid points are given as red dots with the spacing between each equal to κ . The labels of the grid points of (6.15) are in blue and those of (6.6) are in green.

We are coupling five different grid points, which can be renamed in the form y_{n+j} to match the notation given for multistep methods (6.6). Figure 6.4

gives the original five grid points in red with the original labeling in blue and their new labels written in green. Using this new labeling in (6.20) we get

$$\frac{(c^2(y_{n+3} - 2y_{n+2} + y_{n+1}) - \frac{1}{4}(y_{n+4} - 2y_{n+2} + y_n))}{c^2 - 1} = \kappa^2 f(y_{n+2}).$$

Expanding we get,

$$\begin{aligned} -\frac{1}{4(c^2 - 1)}y_n + \frac{c^2}{c^2 - 1}y_{n+1} - \frac{4c^2 - 1}{2(c^2 - 1)}y_{n+2} + \frac{c^2}{c^2 - 1}y_{n+3} - \frac{1}{4(c^2 - 1)}y_{n+4} \\ = \kappa^2 f(y_{n+2}) \end{aligned}$$

which is degree 4 and has the same form as a multistep method (6.6) with step size κ and the symmetry condition (6.7) on the coefficients satisfied. In general, the step size will be $\frac{\kappa}{n}$. □

Note that for a multistep method which involves an odd number of grid points, symmetry simply means that the coefficient of the centre grid point of the y approximation can be any value. Then each pair of grid points on either side of the central grid point both have the same coefficient. Similarly with the coefficients of the function evaluations at grid points y_n .

This can be demonstrated using the discrete travelling wave equation (6.15). Here there are 5 grid points with the central one $\varphi(\xi)$. Since we have $\sigma \geq \kappa$ the grid points either side of the central one are $\varphi(\xi - \kappa)$ and $\varphi(\xi + \kappa)$ which have the same coefficient of $\frac{c^2}{\kappa^2}$. The grid points either side of these ones are $\varphi(\xi - \sigma)$ and $\varphi(\xi + \sigma)$ which also have the same coefficient of $\frac{-1}{\sigma^2}$. Since the function on the right hand side is only evaluated at the central grid point it does not matter what the coefficient of this function is.

For a multistep method with an even number of grid points the case is almost similar except there will be two central grid points that will have the same coefficients for a symmetric method. Then each pair of grid points on either side of the central ones will have the same coefficients; similarly for the coefficients of the function evaluations.

Conjecture 6.5.1. *A multistep method corresponding to each rational value of $\frac{\sigma}{\kappa} = \frac{m}{n}$ will be consistent, but not in general stable (it is stable for $\sigma = \kappa$). All methods have m pairs of roots, including a double principal root at $\zeta = 1$. The number of spurious roots on the unit circle depends on the value of c . We have 4 different cases,*

1. $|c| > 1$:

- n pairs of roots on the unit circle
 - 1 pair of principal roots
 - $(n - 1)$ pairs of spurious roots
- $(m - n)$ (spurious) pairs not on the unit circle

2. $c = 0$:

- m pairs of roots on the unit circle
 - 1 pair of principal roots
 - $(m - 1)$ pairs of spurious roots

3. $0 < |c| < 1$, $cm \leq n$:

- m pairs of roots on the unit circle
 - 1 pair of principal roots
 - $(m - 1)$ pairs of spurious roots

4. $0 < |c| < 1$, $cm > n$ —no general pattern found yet.

Note that when the pairs of roots are not on the unit circle, one root of the pair is inside the unit circle ($|\zeta| < 1$) and the other is outside the unit circle ($|\zeta| > 1$). Also, as $\frac{m}{n}$ approaches an irrational number the zeros of ρ approach the unit circle.

This conjecture was made from observing the results of a Matlab program which finds the roots of $\rho(\zeta)$, the first characteristic polynomial, for the discrete travelling wave equation, and plots them on the unit circle for different

combinations of the parameters c , m and n . Figures 6.5, 6.6, and 6.7 gives some examples of the roots of the discrete travelling wave equation for different parameter values.

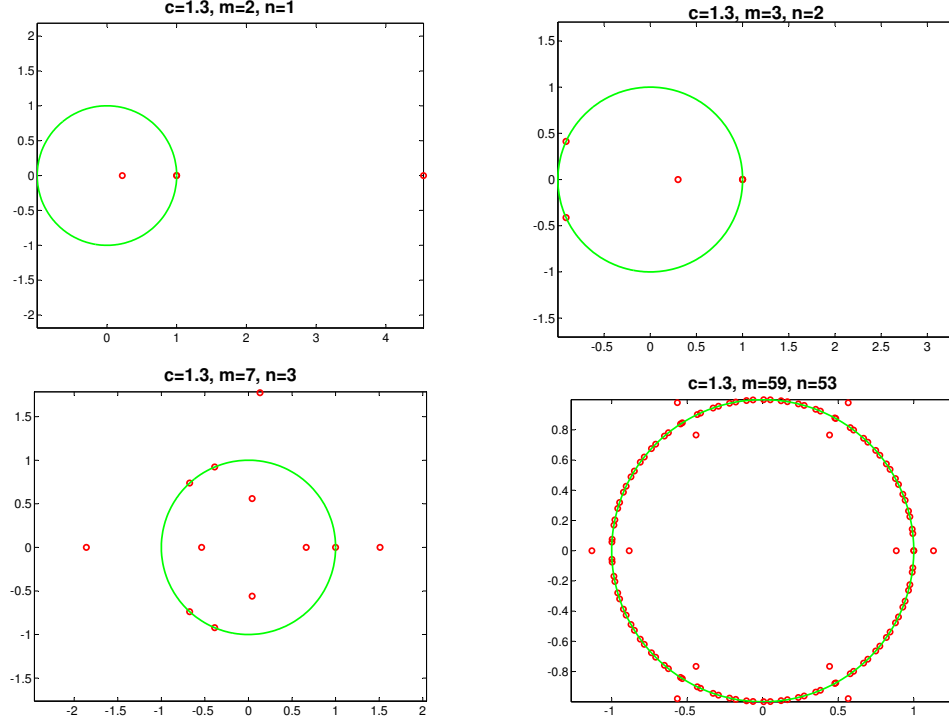


Figure 6.5: Roots of the characteristic polynomial of the discrete travelling wave equation for $c = 1.3$ —Case 1.

Recall that multistep methods for 2nd order equations are stable only if all zeros of $\rho(\zeta)$ are on the unit circle or inside the unit circle and the roots on the unit circle are at most double zeros. We proved that the discrete travelling wave equation was symmetric in Theorem 6.5.1, so, we only have a stable symmetric method when $\sigma = \kappa$, (since for $m = n = 1$ we always get a double root at 1), $c = 0$ (standing wave), and $0 < |c| < 1$ with $cm \leq n$. We generally had $c = 1.3$ fixed, which does not give a stable symmetric method. This case was plotted in Figure 6.5 where it can clearly be seen that some of the zeros lie outside the unit circle. Even though these methods are not stable in the sense of initial value problems, the periodic boundary conditions we have instead

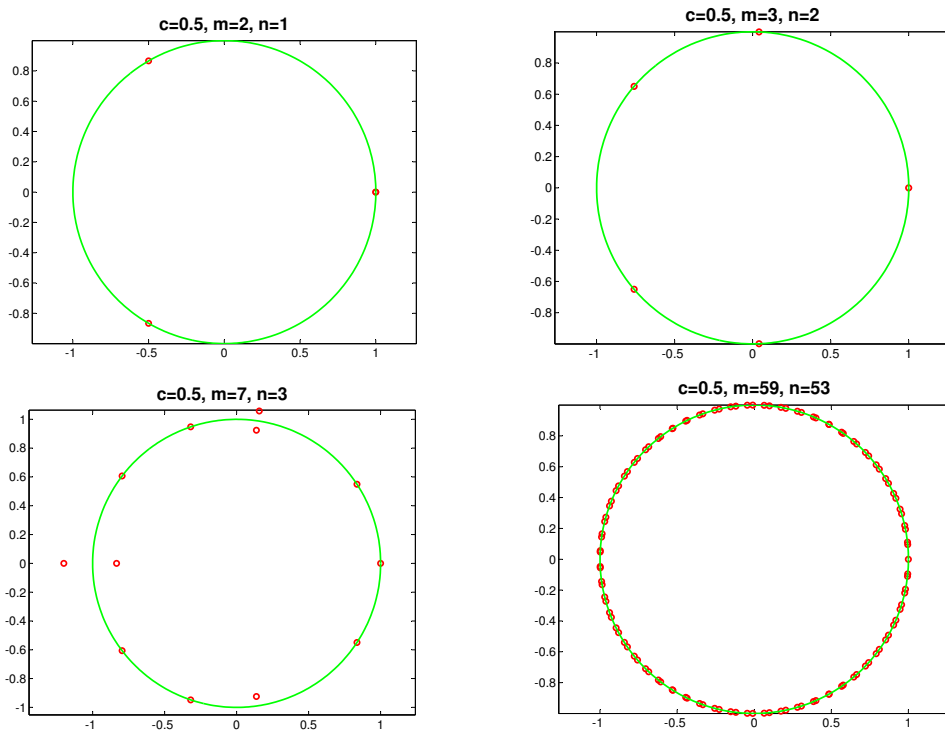


Figure 6.6: Roots of the characteristic polynomial of the discrete travelling wave equation for $c = 0.5$ —Case 3. and 4.

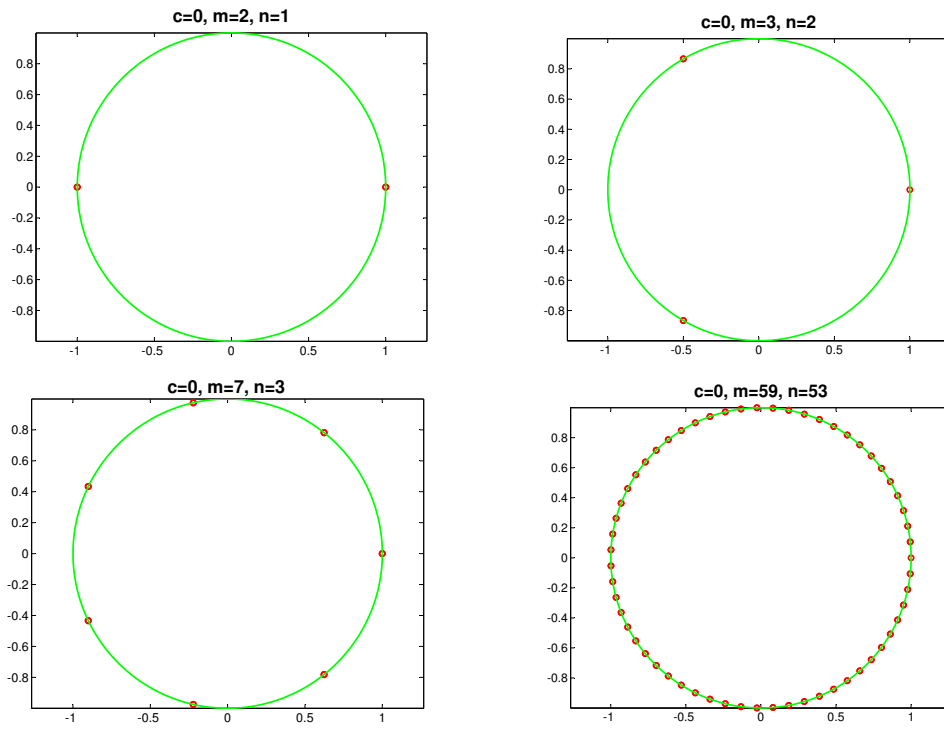


Figure 6.7: Roots of the characteristic polynomial of the discrete travelling wave equation for $c = 0$ —Case 2.

may mean that we do not have to worry about the roots outside the unit circle. These roots correspond to modes that grow exponentially in space. If they are periodic and grow exponentially, they must be identically zero. This phenomenon is exploited in the boundary value methods of Brugnano and Trigiante.

In [77] Quinlan discovered that the resonances and instabilities occurred at certain step sizes for stable symmetric multistep methods. He found formulas to predict at which step sizes these resonances would occur in terms of their spurious roots. For the resonances the prediction was quite simple:

$$N \approx \frac{2\pi q}{\theta_j}, \quad q = 1, 2, 3, \dots, \quad (6.21)$$

where N is the number of steps per period at which the resonance occurs and $z_j = \exp(i\theta_j)$ is a spurious root of $\rho(\zeta)$.

For the discrete travelling wave equation with $c = 1.3$ we tried to follow this idea of [77], ignoring the spurious roots not on the unit circle, and predict when the resonances and instabilities we observed in Sections 5.4 and 5.4.1 occur. Unfortunately, the locations of the resonances did not appear to be simply related to the prediction given in (6.21). We eventually dropped this approach in favour of the more successful backward error analysis in the next section.

6.6 Backward Error Analysis of the Discrete Travelling Wave Equation

The idea now is to apply backward error analysis to the discrete travelling wave equation (6.15). Since we can think of (6.15) as a symmetric multistep method we can find the modified differential equation by using a similar method as the proof of Theorem 6.4.1. Even though the discrete travelling wave equation is only a symmetric multistep method when $\frac{\sigma}{\kappa}$ is rational, we attempt to find the modified equations for any ratio of $\frac{\sigma}{\kappa}$. We use the form of the discrete travelling wave equation given by (6.19).

Before stating the theorem, we rename the variables; instead of $\varphi(\xi)$, we will use $y(t)$ to make it easier to follow the proof of Theorem 6.4.1. The second order ODE (6.18) becomes,

$$\ddot{y} = f(y), \quad f(y) = \frac{-V'(y)}{c^2 - 1}, \quad (6.22)$$

and the discrete travelling wave equation (6.19) becomes,

$$\frac{\frac{c^2}{\kappa^2} (y(t + \kappa) - 2y(t) + y(t - \kappa)) - \frac{1}{\sigma^2} (y(t + \sigma) - 2y(t) + y(t - \sigma))}{c^2 - 1} = f(y(t)). \quad (6.23)$$

Theorem 6.6.1. *Consider the discrete travelling wave equation (6.23) for the second order equation (6.22). There exists functions $f_i(\varphi, \dot{\varphi})$ with $(i-1)$ th order coefficients of σ and κ such that, every solution of the modified differential equation*

$$\ddot{y} = f(y) + h^2 f_3(y, \dot{y}) + h^4 f_5(y, \dot{y}) + \dots \quad (6.24)$$

satisfies

$$\begin{aligned} & \frac{c^2}{\kappa^2} (y(t + j\kappa) - 2y(t) + y(t - j\kappa)) \\ & - \frac{1}{\sigma^2} (y(t + j\sigma) - 2y(t) + y(t - j\sigma)) = -V'(y(t)) \end{aligned} \quad (6.25)$$

up to $O(h^p)$ for all p , where $f(y)$ is given in (6.22) and $h = 1$ is used as a placeholder for separating terms of different orders.

Proof. Following the proof of Theorem 6.4.1, notice that (6.23) has the form

$$L_{\kappa, \sigma} y(t) = f(y(t)) \quad (6.26)$$

where $L_{\kappa, \sigma}$ is some linear operator depending on the parameters κ and σ . Expanding $y(t + \kappa)$ and $y(t - \kappa)$ in a Taylor series we get

$$\begin{aligned} y(t + \kappa) &= e^{\kappa D} y(t) \\ y(t - \kappa) &= e^{-\kappa D} y(t), \end{aligned}$$

where D is the total derivative, the definition being given in the proof of Theorem 6.4.1. Similarly,

$$\begin{aligned}y(t + \sigma) &= e^{\sigma D} y(t) \\ y(t - \sigma) &= e^{-\sigma D} y(t).\end{aligned}$$

Substituting these into (6.23) we get

$$\frac{\frac{c^2}{\kappa^2} (e^{\kappa D} y(t) - 2y(t) + e^{-\kappa D} y(t)) - \frac{1}{\sigma^2} (e^{\sigma D} y(t) - 2y(t) + e^{-\sigma D} y(t))}{c^2 - 1} = f(y(t)).$$

Taking out the common factor $y(t)$ we get,

$$\frac{\frac{c^2}{\kappa^2} (e^{\kappa D} - 2 + e^{-\kappa D}) - \frac{1}{\sigma^2} (e^{\sigma D} - 2 + e^{-\sigma D})}{c^2 - 1} y(t) = f(y(t))$$

and now it is easy to see that our linear operator is

$$L_{\kappa, \sigma} = \frac{\frac{c^2}{\kappa^2} (e^{\kappa D} - 2 + e^{-\kappa D}) - \frac{1}{\sigma^2} (e^{\sigma D} - 2 + e^{-\sigma D})}{c^2 - 1}. \quad (6.27)$$

We will illustrate the proof by carrying out the required calculations up to the 4th order term. Firstly, we expand the linear operator (6.27) into a Taylor series up to the 4th power of h . The form (6.26) of the discrete travelling wave equation (6.23) can be rearranged and the derivative D taken twice to give

$$\ddot{y} = \frac{D^2}{L_{\kappa, \sigma}} f(y).$$

Substituting the expansion of the linear operator the above now has the form

$$\ddot{y} = (1 + \mu_2(\kappa, \sigma)h^2 D^2 + \mu_4(\kappa, \sigma)h^4 D^4) f(y). \quad (6.28)$$

Here the h^2 and h^4 terms are used as placeholders for ease of calculation and comparison. We will set $h = 1$ at the end of the comparison to the modified differential equation (6.24). The μ_i terms come from the expansion of the linear operator which involves the step size parameters σ and κ . μ_2 will involve combinations of κ and σ of order 2 and μ_4 will involve combinations of order 4. Remember that in (6.13) the μ_i s were constant coefficients.

Firstly, the derivatives $D^2f(y)$ and $D^4f(y)$ need to be calculated, as was shown in the proof of Theorem 6.4.1. This will give expressions involving $f(y)$ and its derivatives and also derivatives of y . For the second derivatives of y and greater the modified differential equation (6.24) and its derivatives are substituted. Next, these expressions are substituted back into (6.28) and finally, the coefficients of powers of h in this equation and (6.24) are compared, to give explicit equations for $f_3(y, \dot{y})$ and $f_5(y, \dot{y})$.

To show this method, we go through the process of finding $f_3(y, \dot{y})$ in detail. First, we find the second derivative of $f(y)$ and then substitute the modified equation (6.24) for \ddot{y} , giving

$$\begin{aligned} D^2f(y) &= f''(y)(\dot{y}, \dot{y}) + f'(y)\ddot{y} \\ &= f''(y)(\dot{y}, \dot{y}) + f'(y)(f(y) + h^2f_3(y, \dot{y}) + h^4f_5(y, \dot{y}) + \dots). \end{aligned}$$

Substituting this back into (6.28) we get

$$\begin{aligned} \ddot{y} &= 1 + \mu_2 h^2 (f''(y)(\dot{y}, \dot{y}) + f'(y)(f(y) + h^2f_3(y, \dot{y}) + h^4f_5(y, \dot{y}) + \dots)) \\ &\quad + \mu_4 h^4 D^4f(y) \\ &= 1 + \mu_2 h^2 f''(y)(\dot{y}, \dot{y}) + \mu_2 h^2 f'(y)f(y) + \mu_2 h^4 f'(y)f_3(y, \dot{y}) \\ &\quad + \mu_2 h^6 f'(y)f_5(y, \dot{y}) + \dots + \mu_4 h^4 D^4f(y). \end{aligned}$$

Finally, comparing the coefficients of h^2 in the above and (6.24), we get

$$\begin{aligned} f_3(y, \dot{y}) &= \mu_2 f''(y)(\dot{y}, \dot{y}) + \mu_2 f'(y)f(y) \\ &= \mu_2 (f''(y)(\dot{y}, \dot{y}) + f'(y)f(y)) \end{aligned} \tag{6.29}$$

where

$$\mu_2 = \frac{\sigma^2 - c^2 \kappa^2}{12(c^2 - 1)}.$$

Notice, that if we were also to compare the coefficients of h^4 , we would get a term involving μ_2 and $f_3(y, \dot{y})$ plus terms from $D^4f(y)$. Finding $D^4f(y)$ and comparing the coefficients of h^4 we get

$$\begin{aligned} f_5(y, \dot{y}) &= \mu_2 (f'(y)f_3(y, \dot{y})) + \mu_4 (f'(y)^2 f(y) + 3f''(y)f(y)^2 + 5f''(y)(\dot{y}, \dot{y})f'(y) \\ &\quad + 6f^{(3)}(y)(\dot{y}, \dot{y})f(y) + f^{(4)}(y)(\dot{y}, \dot{y}, \dot{y}, \dot{y})) \end{aligned}$$

where μ_2 was given above and

$$\mu_4 = \frac{3c^2\kappa^4 + 3\sigma^4 + 2c^2(\kappa^4 - 5\kappa^2\sigma^2 + \sigma^4)}{720(c^2 - 1)^2}.$$

Each f_n can be found similarly. □

6.6.1 Numerical Validation of the BEA

Before finding and plotting the modified Hamiltonian, we plot the solutions of our modified equations for the discrete travelling wave equation (6.23). These can be solved numerically using `NDSolve` in Mathematica and then the phase portraits plotted (see Figure 6.8) for different values of the parameters σ and κ . In Section 6.6.2 we plot the modified Hamiltonian, which is more accurate than the numerical solution from using `NDSolve`. For small values of σ and κ (Figure 6.8, left) the phase portrait looks similar, qualitatively, to the exact solution, as we would expect. So for σ and κ small it seems that the numerical solution, the solution of the discrete travelling wave equation, remains close to the exact solution, as expected. As σ and κ are increased the orbits of the phase portraits become distorted and stretched compared with the exact solution.

This can also be seen by plotting orbits, Figure 6.9, of constant period T and increasing σ and κ , where $\sigma = \kappa$. Plotting orbits with fixed amplitude gives a slightly more dramatic result.

Next, we begin the comparison of our numerical results with the modified differential equation. For increasing truncation index, (up to optimal truncation), we expect the solution of the truncated modified equations to get closer to the numerical solution, (the solution of the discrete travelling wave equation). First, we plot the solution of all three truncations along with our numerical result for a fixed set of parameters. Figure 6.10 gives these solutions

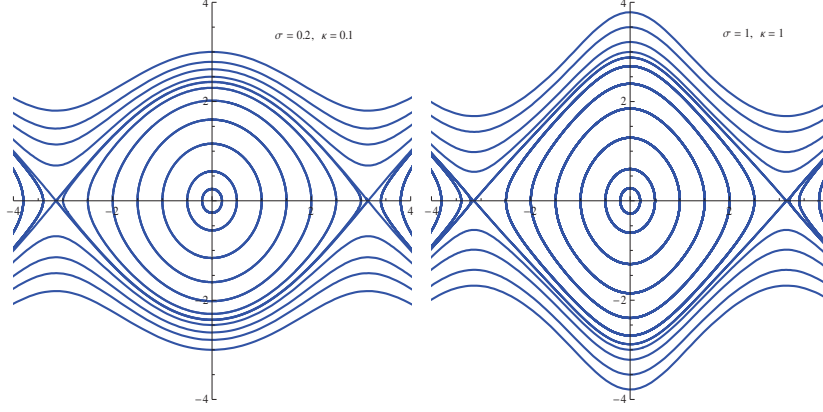


Figure 6.8: Phase portraits of the solution of the modified differential equation of the discrete travelling wave equation (6.23).

for $T = 2\pi$, $\sigma = \kappa = 0.5$, where,

y_1 is the solution of $\ddot{y} = f(y)$

y_2 is the solution of $\ddot{y} = f(y) + \mu_2 f_3(y, \dot{y})$

y_3 is the solution of $\ddot{y} = f(y) + \mu_2 f_3(y, \dot{y}) + \mu_4 f_5(y, \dot{y})$.

Not much can be seen in Figure 6.10, because the curves all seem close together. To get a better idea of what is going on we need to find the error of each of the truncated solutions.

We can check the error of the modified differential equations at each truncation index for $\sigma = \kappa$ to see if it is consistent with the order of the method—recall that we have the leapfrog method when $\sigma = \kappa$. The error is measured by taking the difference between the numerical solution and each truncation y_1 , y_2 and y_3 . The error for each of these truncations is given in Figure 6.11. As more terms are kept in the modified equation we see that the error is decreasing as expected.

We can also plot the resonances of the numerical solution from Chapter 5 and that of the modified equation on the same axes. This is given in Figure 6.12

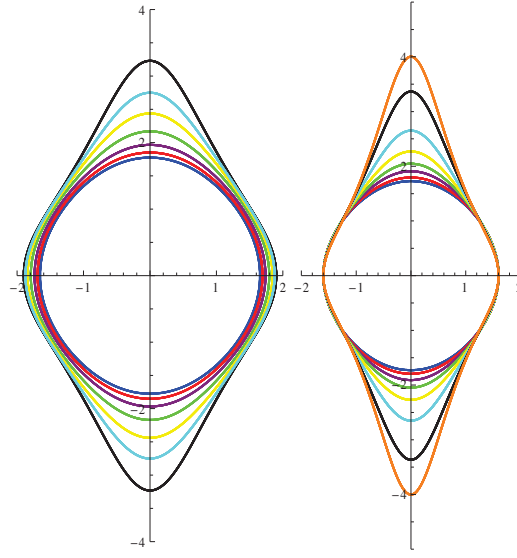


Figure 6.9: **Left:** Orbits of fixed period $T = 2\pi$, for increasing $\kappa = \sigma$. The blue orbit has very small value of $\sigma = 0$ and the black orbit has a large value of $\sigma = 1.5$. The curves in between these have increasing values of σ from the blue orbit to the black orbit.

Right: Orbits of fixed amplitude equal to 1.6, for increasing $\kappa = \sigma$. The blue orbit has very small value of $\sigma = 0$ and the orange orbit has a large value of $\sigma = 1.8$. The curves in between these have increasing values of σ from the blue orbit to the orange orbit.

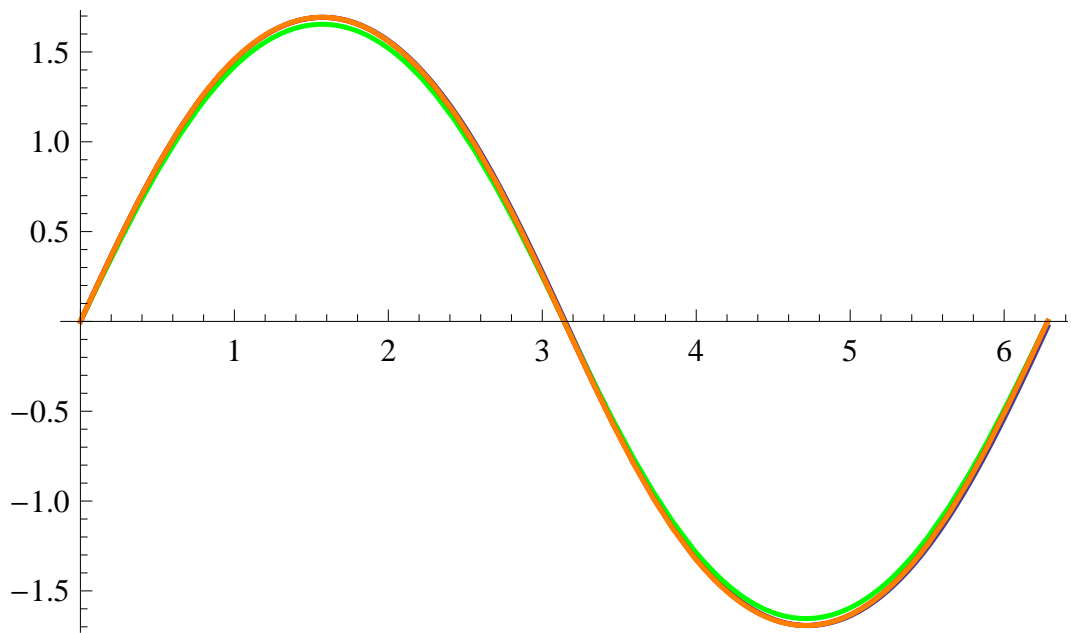


Figure 6.10: Truncated solutions of the modified differential equation for the discrete travelling wave equation: y_1 is the green curve, y_2 , the red curve, and y_3 the orange curve. The numerical solution is given by the blue curve.

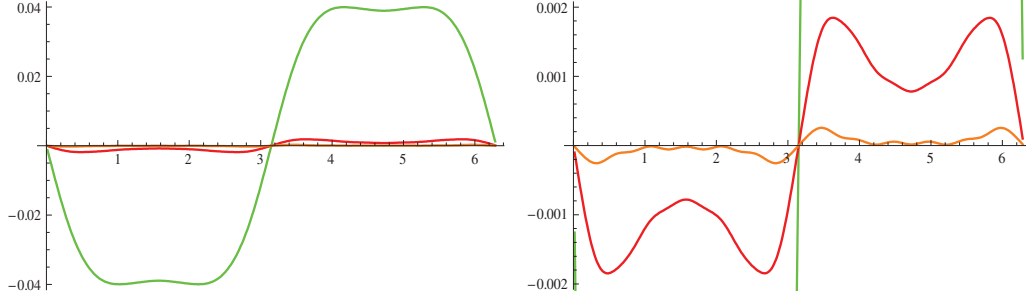


Figure 6.11: On the left we show the error (the difference between the numerical solution and the solution of the modified equation) of the three truncations of the modified equation for the discrete travelling wave equation: y_1 -green, y_2 -red, y_3 -orange. On the right is a zoom of the graph on the left.

for a rational ratio of $\frac{\sigma}{\kappa}$ on the left and an irrational one on the right. The red line is the resonances of the MDE and the blue line the resonances of the numerical solution. We see that the MDE contains no resonances and so can conclude that for the 4th order truncation a smooth solution is always produced.

For a fixed value of T , and c already fixed, we can vary the parameters σ and κ and plot the resonances on a contour plot. This is given in Figure 6.13 where the value of σ is given on the x -axis and the value of κ is given on the y -axis. The size of the resonances are measured by taking the 2-norm of the difference between the numerical solution of the modified differential equation and the numerical solution of the discrete travelling wave equation (5.3). The lighter the shading the bigger the resonances are. As expected for small values of σ and κ the resonances are very small and get larger as the values of these parameters increase.

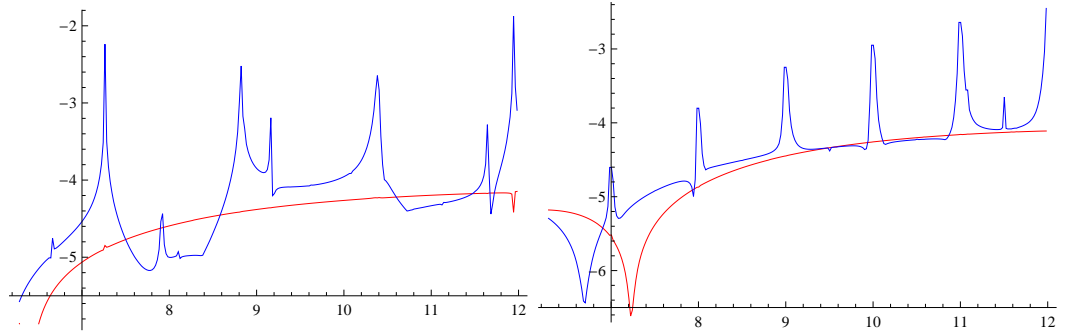


Figure 6.12: Resonances of the numerical solution from Chapter 5 given by the blue curve. Resonances of the modified differential equation for the discrete travelling wave equation given by the red curve.

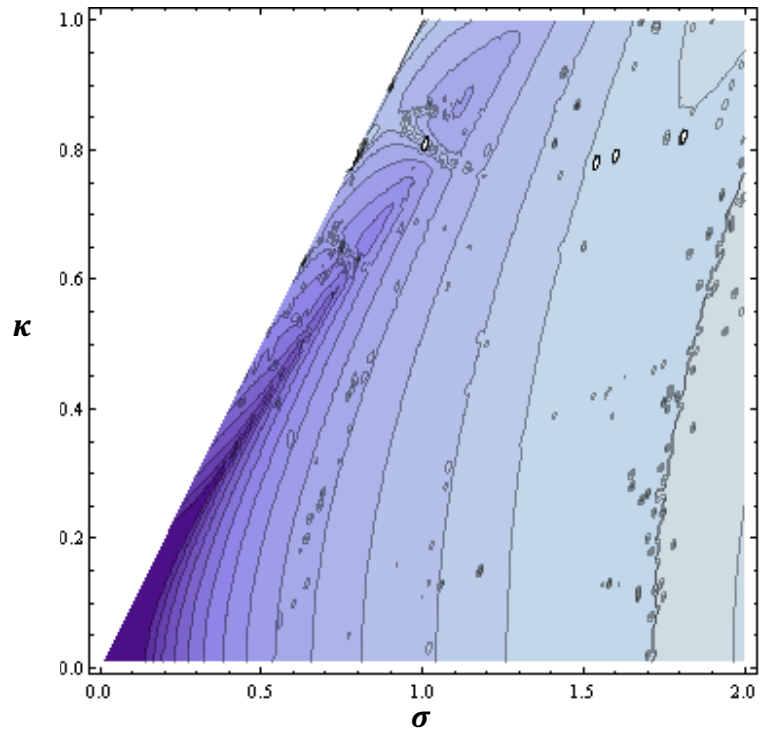


Figure 6.13: Contour plot of the resonances for $T = 2\pi$ and $c = 1.3$. The lighter the shading the bigger the resonances are.

6.6.2 The Modified Hamiltonian of the Discrete Travelling Wave Equation

In this section we derive the modified Hamiltonian of the discrete travelling wave equation. We give reference to a proof that can be followed, but give our own method of finding the modified Hamiltonian.

Theorem 6.6.2. *For the discrete travelling wave equation (6.15) (or (6.23)), there exists a series of the form*

$$\tilde{H}(y, \dot{y}) = H(y, \dot{y}) + h^2 H_3(y, \dot{y}) + h^4 H_5(y, \dot{y}) + \dots$$

where H is the Hamiltonian of the original 2nd order ODE (6.22) and h is a placeholder for separating terms of different orders.

Proof. The modified Hamiltonian of the discrete travelling wave equation (6.15) can be found by following the proof given in [37] for Theorem 6.4.2. Or it can be found by our method as follows:

We have the second order modified differential equation (6.24) and split it into a first order system,

$$\dot{y} = p \tag{6.30}$$

$$\dot{p} = f(y) + h^2 f_3(y, p) + h^4 f_5(y, p) + \dots, \tag{6.31}$$

where $f(y) = \frac{-V'(y)}{c^2 - 1}$.

We assume that the system can be written as

$$\begin{bmatrix} \dot{y} \\ \dot{p} \end{bmatrix} = \begin{bmatrix} 0 & \tilde{K} \\ -\tilde{K} & 0 \end{bmatrix} \nabla \tilde{H} \tag{6.32}$$

where \tilde{K} is a series with unknowns K_3, K_5, \dots ,

$$\tilde{K} = 1 + h^2 K_3 + h^4 K_5 + \dots$$

and \tilde{H} is a modified Hamiltonian,

$$\tilde{H} = H + h^2 H_3 + h^4 H_5 + \dots$$

Expanding out the first row of (6.32) we get

$$\begin{aligned}
\dot{y} &= \tilde{K} \frac{\partial \tilde{H}}{\partial p} = (1 + h^2 K_3 + h^4 K_5 + \dots) \frac{\partial}{\partial p} (H + h^2 H_3 + h^4 H_5 + \dots) \\
&= (1 + h^2 K_3 + h^4 K_5 + \dots) (p + h^2 \frac{\partial H_3}{\partial p} + h^4 \frac{\partial H_5}{\partial p} + \dots) \\
&= p + h^2 \left(\frac{\partial H_3}{\partial p} + p K_3 \right) + h^4 \left(\frac{\partial H_5}{\partial p} + K_3 \frac{\partial H_3}{\partial p} + p K_5 \right) + \dots .
\end{aligned}$$

Since $\dot{y} = p$ from (6.30) then the above equation gives

$$\frac{\partial H_3}{\partial p} + p K_3 = 0, \quad \frac{\partial H_5}{\partial p} + K_3 \frac{\partial H_3}{\partial p} + p K_5 = 0 \quad (6.33)$$

$$\Rightarrow K_3 = -\frac{1}{p} \frac{\partial H_3}{\partial p}. \quad (6.34)$$

Similarly, expanding the second row of (6.32) we get

$$\begin{aligned}
\dot{p} &= -\tilde{K} \frac{\partial \tilde{H}}{\partial y} = f(y) + h^2 \left(K_3 f(y) - \frac{\partial H_3}{\partial y} \right) \\
&\quad + h^4 \left(K_5 f(y) - K_3 \frac{\partial H_3}{\partial y} - \frac{\partial H_5}{\partial y} \right) + \dots .
\end{aligned}$$

Matching this equation with (6.31) we get

$$K_3 f(y) - \frac{\partial H_3}{\partial y} = f_3(y, p), \quad K_5 f(y) - K_3 \frac{\partial H_3}{\partial y} - \frac{\partial H_5}{\partial y} = f_5(y, p) \quad (6.35)$$

$$\Rightarrow K_3 f(y) - \frac{\partial H_3}{\partial y} = f_3(y, p). \quad (6.36)$$

Substituting K_3 from (6.34) into (6.36) we get

$$-\frac{1}{p} \frac{\partial H_3}{\partial p} f(y) - \frac{\partial H_3}{\partial y} = f_3(y, p)$$

where $f_3(y, p) = \mu_2(p^2 f''(y) + f'(y)f(y))$ and was given in (1.3).

So we have

$$-\frac{1}{p} \frac{\partial H_3}{\partial p} f(y) - \frac{\partial H_3}{\partial y} = \mu_2 (p^2 f''(y) + f'(y)f(y)), \quad (6.37)$$

and from this we conclude that H_3 has the form

$$H_3 = \alpha f^2(y) + \beta f'(y)p^2.$$

From this we get

$$\frac{\partial H_3}{\partial p} = 2\beta p f'(y), \quad \frac{\partial H_3}{\partial y} = 2\alpha f'(y)f(y) + \beta f''(y)p^2.$$

Substituting these into the left hand side of (6.37) we get

$$-\frac{2}{p}\beta p f'(y)f(y) - (2\alpha f'(y)f(y) + \beta f''(y)p^2) = \mu_2(p^2 f''(y) + f'(y)f(y)).$$

Finally, matching coefficients of like terms we get

$$\alpha = \frac{1}{2}\mu_2, \quad \beta = -\mu_2.$$

So

$$H_3 = \frac{1}{2}\mu_2 f^2(y) - \mu_2 f'(y)p^2.$$

We can find H_5 in a similar way. We use the second equations in (6.33) and (6.35) and substitute what we now know, K_3 , $\frac{\partial H_3}{\partial p}$, and $\frac{\partial H_3}{\partial y}$ into them. The equation from (6.33) can now be rearranged to give an equation for K_5 , which can also be substituted into the equation from (6.35). This equation is slightly more difficult than the previous one, but we can still make a guess for H_5 then take the partial derivatives and match coefficients of like terms giving

$$H_5 = \mu_4 f(y)^2 f'(y) + \frac{1}{2}(\mu_2^2 - 3\mu_4) f'(y)^2 p^2 - 2\mu_4 f(y) f''(y) p^2 - \mu_4 p^4 f^{(3)}(y).$$

And therefore the modified Hamiltonian truncated at order h^4 is

$$\begin{aligned} \tilde{H} = H + h^2 & \left(\frac{1}{2}\mu_2 f^2(y) - \mu_2 f'(y) \dot{y}^2 \right) + h^4 \left(\mu_4 f^2(y) f'(y) \right. \\ & \left. + \frac{1}{2}(\mu_2^2 - 3\mu_4) f'(y)^2 \dot{y}^2 - 2\mu_4 f(y) f''(y) \dot{y}^2 - \mu_4 \dot{y}^4 f^{(3)}(y) \right) \end{aligned}$$

where $\dot{y} = p$. □

The phase portrait with the above Hamiltonian can now be plotted for different values of σ and κ and is given in Figure 6.14. On the left for small values of σ and κ the modified Hamiltonian shows that the discrete travelling wave equation gives heteroclinic and periodic travelling wave solutions as does the exact solution. As σ and κ increase the modified Hamiltonian gets distorted

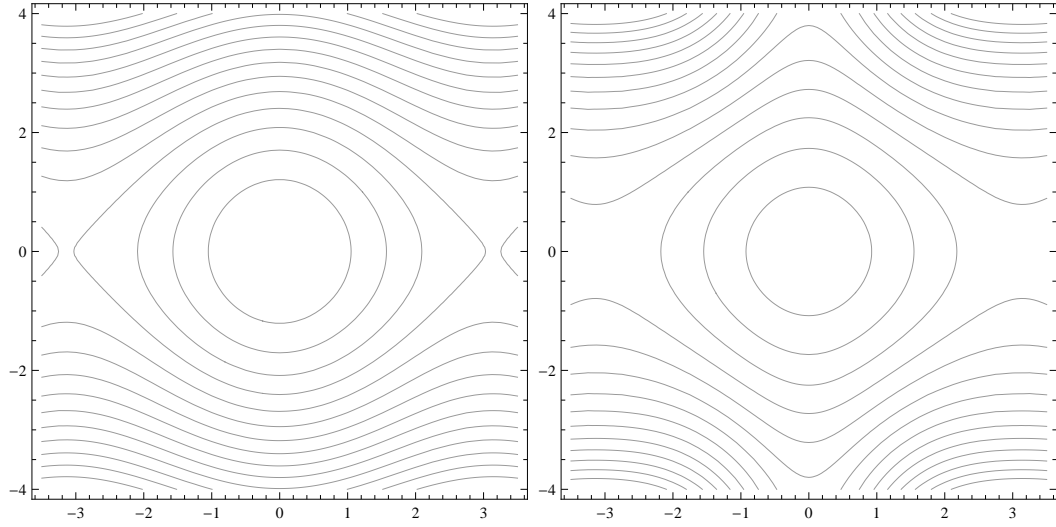


Figure 6.14: On the left is the modified Hamiltonian with small values of σ and κ and on the right the modified Hamiltonian with large values of σ and κ .

as expected, but it still shows that the discrete travelling wave equation still gives the right qualitative behaviour.

Before going further, we discuss some of the implications of Theorem 6.6.1. Backward error analysis is a powerful tool for analysing our problem. For ODEs in the ordinary case backward error analysis reduces $(n+1)$ -dimensional map to n dimensions. So we get a reduction of the dimension by one. This reduction of the dimension by one allows conclusions such as the existence of one modified integral, the energy. But for our problem our method is the discrete travelling wave equation (6.15) which is an infinite-dimensional map, discussed in Section 4.1.1. This next theorem will show just how powerful backward error analysis is for us.

Theorem 6.6.3. *The modified differential equation (6.38) for the discrete travelling wave equation, is a second order ODE, which can be rewritten in the form,*

$$\dot{\mathbf{z}} = \tilde{\mathbf{J}}^{-1}(\mathbf{z}) \nabla \tilde{H}(\mathbf{z}),$$

since we know the modified equation has a modified Hamiltonian. Here, $\dot{\mathbf{z}} \in \mathbb{R}^2$,

$\tilde{\mathbf{J}}^{-1}$ is some 2×2 symplectic structure matrix which depends on the variables in \mathbf{z} , and $\widetilde{H}(\mathbf{z})$ is the modified Hamiltonian.

We mentioned earlier that Chartier, Faou, and Murua [16] were the first to prove that conjugate to symplectic methods preserve modified quadratic first integrals. Symmetric multistep methods are conjugate to symplectic and so is the discrete travelling wave equation since it is equivalent to a symmetric multistep method. Therefore, $\tilde{\mathbf{J}}^{-1}$ is a symplectic structure matrix and (6.32) is a Poisson system.

By use of backward error analysis we get an equation of the form

$$\ddot{y} = \tilde{f}(y, \dot{y}, \sigma, \kappa) \quad (6.38)$$

where σ and κ are parameters.

That is, BEA has reduced an infinite-dimensional map to a two-dimensional ODE, a far more spectacular reduction than that of the ordinary case. This is even more striking in view of the fact that there is no accepted BEA for fully discrete PDEs in general. This allows us to plot solutions of the modified equation and the modified Hamiltonian giving us all the information we need.

Thus we see that backward error analysis is exceptionally powerful for this problem, reducing the difficult, intractable functional equation (6.15) to a simple planar Hamiltonian ODE. Furthermore, by comparing the phase portraits of the original system in Figure 5.1 and the modified system in Figures 6.14 and 6.8, we get that any orbits that are structurally stable, that is any orbits that are also present up to small perturbations in nearby Hamiltonian systems, are preserved. This includes periodic and heteroclinic travelling waves for the sine-Gordon equation Figure 5.1, although this result is not specific to the sine-Gordon equation or its integrability and holds (generically) for any potential. This preservation holds in the sense of backward error analysis, that is up to any power of the time and space step sizes.

This situation in the ODE case, analysing the preservation of phase portraits by symplectic integrators, has been considered in [67] using the language of topological equivalence:

Definition 6.6.1. $H \in C^k(M, \mathbb{R})$, $k \geq 2$, is a Morse function if its critical points $\{x: dH(x) = 0\}$ are isolated, nondegenerate (that is $H''(x)$ is nonsingular), and if each level set of H contains at most one critical point. Two functions H and $\tilde{H} \in C^k(M, \mathbb{R})$ are topologically equivalent if there are homeomorphisms Φ, Ψ such that $\Psi \circ \tilde{H} = H \circ \Phi$.

The level sets of two topologically equivalent functions are topologically equivalent, although they may have a different shape (determined by Φ) and the level sets may have different values (determined by Ψ).

Definition 6.6.2. A symplectic integrator for the Hamiltonian H is topologically stable for any step τ on the compact set D if its modified Hamiltonian \tilde{H} is topologically equivalent to H on D .

Theorem 6.6.4. [76] Let H be a C^k Morse function, and let \tilde{H} be sufficiently close to H in the C^k topology (defined by the ball $B(\varepsilon) = \{H \in C^k(M, \mathbb{R}): |D^\alpha H(x)| < \varepsilon, \forall x \in M, \forall |\alpha| \leq k\}$). Then \tilde{H} is topologically equivalent to H .

Corollary 6.6.1. [67] If the Hamiltonian H is a Morse function on a compact set, then any symplectic integrator is topologically stable for all sufficiently small time steps.

Theorem 6.6.5. [67] If H is C^k on a compact set, with all critical points nondegenerate, and if for each pair of critical points of H with equal values the corresponding critical points of \tilde{H} have equal values for all sufficiently small time steps, then for all sufficiently small time steps the symplectic integrator is topologically stable.

This paper [67] goes on to describe integrators for which these conditions hold.

Thus we can expect, for example, that if a travelling wave corresponds to a topologically unstable orbit of the travelling wave equation, then it will not be preserved by typically multisymplectic integrators. This, however, is an exceptional case, and even in higher dimensions we can expect that typical

travelling waves, whose existence is due to preserved features of the travelling wave equation like dimension and linear symmetries, will be preserved by multisymplectic integrators.

Although the numerical examples given above suggest that the modified vector field is a very good approximation to the travelling waves, which in direct numerical calculations do appear to exist, of course this is no substitute for a rigorous proof of their existence. This could be a very difficult process involving KAM theory and/or variational techniques and is beyond the scope of this thesis. Instead, we regard the backward error analysis as suggesting the mechanism by which travelling waves can be preserved and as a guide to the development of good numerical methods.

6.7 Backward Error Analysis for Multisymplectic Integrations of Multi-Hamiltonian PDEs

Our results so far are for one multisymplectic integrator applied to one type of PDE, the nonlinear wave equation, in the form given. We would like to say something more general for multisymplectic integrators applied to multi-Hamiltonian PDEs. To do this we need to see if BEA can be applied directly to a multi-Hamiltonian PDE (2.8) for a multisymplectic integrator. Instead of beginning with the nonlinear wave equation in its multi-Hamiltonian form, we begin with the nonlinear Schrödinger equation. The analysis for the nonlinear Schrödinger equation is much more straightforward than that of the nonlinear wave equation.

We use the nonlinear Schrödinger equation,

$$i\psi_t + \psi_{xx} + 2|\psi|^2\psi = 0, \quad \psi \in \mathbb{C}.$$

Since $\psi \in \mathbb{C}$ we begin by letting $\psi = p + iq$, which gives

$$i(p_t + iq_t) + p_{xx} + iq_{xx} + 2(p^2 + q^2)(p + iq) = 0.$$

Now, to turn it into a first order system we let $p_x = v$ and $q_x = w$ to get

$$-q_t + v_x + 2(p^2 + q^2)p + i(p_t + w_x + 2(p^2 + q^2)q) = 0.$$

Next, we split the equation into real and imaginary parts to get the four-dimensional 1st order system,

$$\begin{aligned} p_x &= v \\ q_x &= w \\ -q_t + v_x &= -2(p^2 + q^2)p \\ p_t + w_x &= -2(p^2 + q^2)q. \end{aligned}$$

The multi-Hamiltonian form is

$$z = \begin{bmatrix} p \\ q \\ v \\ w \end{bmatrix}, \quad \mathbf{K} = \begin{bmatrix} 0 & -1 & 0 & 0 \\ 1 & 0 & 0 & 0 \\ 0 & 0 & 0 & 0 \\ 0 & 0 & 0 & 0 \end{bmatrix}, \quad \mathbf{L} = \begin{bmatrix} 0 & 0 & 1 & 0 \\ 0 & 0 & 0 & 1 \\ -1 & 0 & 0 & 0 \\ 0 & -1 & 0 & 0 \end{bmatrix}$$

and $S = -\frac{1}{2}(p^2 + q^2) - \frac{1}{2}(v^2 + w^2)$.

Substituting travelling wave coordinates into the multi-Hamiltonian PDE of the nonlinear Schrödinger equation we get

$$(\mathbf{L} - c\mathbf{K})\dot{\varphi}(\xi) = \nabla S(\varphi(\xi)) \tag{6.39}$$

where

$$(\mathbf{L} - c\mathbf{K}) = \begin{bmatrix} 0 & c & 1 & 0 \\ -c & 0 & 0 & 1 \\ -1 & 0 & 0 & 0 \\ 0 & -1 & 0 & 0 \end{bmatrix}, \quad (\mathbf{L} - c\mathbf{K})^{-1} = \begin{bmatrix} 0 & 0 & -1 & 0 \\ 0 & 0 & 0 & -1 \\ 1 & 0 & 0 & c \\ 0 & 1 & -c & 0 \end{bmatrix}, \quad \varphi = \begin{bmatrix} \varphi_1 \\ \varphi_2 \\ \varphi_3 \\ \varphi_4 \end{bmatrix},$$

and $S = -\frac{1}{2}(\varphi_1^2 + \varphi_2^2) - \frac{1}{2}(\varphi_3^2 + \varphi_4^2)$.

Notice that after substituting travelling wave coordinates we reduce our skew-symmetric matrices \mathbf{K} and \mathbf{L} into one matrix $\mathbf{L} - c\mathbf{K}$ which is also skew-symmetric. Also notice that $\mathbf{L} - c\mathbf{K}$ is invertible. This is key to a step further on.

For our nonlinear wave problem we applied the leapfrog discretisation then substituted travelling wave coordinates so we do this in the same order too for this first order system. But, since there is no general leapfrog discretisation of a multi-Hamiltonian PDE, we use the Preissman box scheme for this example. The Preissman box scheme was introduced in Section 2.5.1. We discretise the multi-Hamiltonian PDE using the Preissman box scheme

$$(\mathbf{K}D_tM_x + \mathbf{L}D_xM_t)z_i^n = \nabla S(M_tM_xz_i^n), \quad (6.40)$$

where for the Preissman box scheme D_t , D_x , M_t , and M_x are given by (2.20) and (2.21).

The discretisation given by (6.40) can be considered as a general multisymplectic discretisation of a multi-Hamiltonian PDE where the discrete approximations D_tM_x and D_xM_t are defined in a way that produces a multisymplectic integrator. Note that the averages M_x and M_t may or may not exist in other multisymplectic integrators.

In matrix form (6.40), for the nonlinear Schrödinger equation, becomes

$$\begin{bmatrix} 0 & -D_tM_x & D_xM_t & 0 \\ D_tM_x & 0 & 0 & D_xM_t \\ -D_xM_t & 0 & 0 & 0 \\ 0 & -D_xM_t & 0 & 0 \end{bmatrix} z_i^n = \nabla S(M_tD_xz_i^n).$$

Substituting travelling wave coordinates into the finite difference and average operators (2.20) and (2.21), we get the difference equations

$$\begin{aligned} D_\xi^\kappa \varphi(\xi) &= -\frac{c(\varphi(\xi) - \varphi(\xi - \kappa))}{\kappa}, & D_\xi^\sigma \varphi(\xi) &= \frac{\varphi(\xi + \sigma) - \varphi(\xi)}{\sigma}, \\ M_\xi^\kappa \varphi(\xi) &= \frac{(\varphi(\xi) + \varphi(\xi - \kappa))}{2}, & M_\xi^\sigma \varphi(\xi) &= \frac{\varphi(\xi) + \varphi(\xi + \sigma)}{\sigma} \end{aligned}$$

so that upon substituting travelling wave coordinates in the discretisation (6.40) we get the system of difference equations,

$$(\mathbf{K}D_\xi^\kappa M_\xi^\sigma + \mathbf{L}D_\xi^\sigma M_\xi^\kappa)\varphi(\xi) = \nabla S(M_\xi^\kappa M_\xi^\sigma \varphi(\xi)),$$

or in matrix form,

$$\begin{bmatrix} 0 & -D_\xi^\kappa M_\xi^\sigma & D_\xi^\sigma M_\xi^\kappa & 0 \\ D_\xi^\kappa M_\xi^\sigma & 0 & 0 & D_\xi^\sigma M_\xi^\kappa \\ -D_\xi^\sigma M_\xi^\kappa & 0 & 0 & 0 \\ 0 & -D_\xi^\sigma M_\xi^\kappa & 0 & 0 \end{bmatrix} \varphi(\xi) = \nabla S(M_\xi^\kappa M_\xi^\sigma \varphi).$$

Applying the D operator, the time derivative, to both sides and moving the matrix on the left hand side to the right hand side we get,

$$\dot{\varphi}(\xi) = D \begin{bmatrix} 0 & 0 & -\frac{1}{D_\xi^\sigma M_\xi^\kappa} & 0 \\ 0 & 0 & 0 & -\frac{1}{D_\xi^\sigma M_\xi^\kappa} \\ \frac{1}{D_\xi^\sigma M_\xi^\kappa} & 0 & 0 & -\frac{D_\xi^\kappa M_\xi^\sigma}{(D_\xi^\kappa M_\xi^\sigma)^2} \\ 0 & \frac{1}{D_\xi^\sigma M_\xi^\kappa} & \frac{D_\xi^\kappa M_\xi^\sigma}{(D_\xi^\kappa M_\xi^\sigma)^2} & 0 \end{bmatrix} \nabla S(M_\xi^\kappa M_\xi^\sigma \varphi(\xi)).$$

This last step was possible because $\mathbf{L} - c\mathbf{K}$ is invertible.

Now, the matrix can be expanded in a Taylor series, then the whole right hand side can be expanded in a series and the proof that the modified equation exists follows from the proof of Theorem 6.4.1.

Next, we go back to the nonlinear wave equation and put it into its multi-Hamiltonian form as was done in Section 2.3. Recall, that for the nonlinear wave equation we get,

$$\mathbf{K}\mathbf{z}_t + \mathbf{L}\mathbf{z}_x = \nabla S(\mathbf{z})$$

where,

$$\mathbf{z} = \begin{bmatrix} u \\ v \\ w \end{bmatrix}, \quad \mathbf{K} = \begin{bmatrix} 0 & 1 & 0 \\ -1 & 0 & 0 \\ 0 & 0 & 0 \end{bmatrix}, \quad \mathbf{L} = \begin{bmatrix} 0 & 0 & -1 \\ 0 & 0 & 0 \\ 1 & 0 & 0 \end{bmatrix},$$

and $S(\mathbf{z}) = -V(u) + \frac{1}{2}(w^2 - v^2)$.

Hence, for the continuous case we have, (after substituting travelling wave coordinates),

$$(\mathbf{L} - c\mathbf{K}) = \begin{bmatrix} 0 & -c & -1 \\ c & 0 & 0 \\ 1 & 0 & 0 \end{bmatrix}, \quad \varphi = \begin{bmatrix} \varphi_1 \\ \varphi_2 \\ \varphi_3 \end{bmatrix}, \quad (6.41)$$

and $S(\varphi) = -V(\varphi_1) + \frac{1}{2}(\varphi_3^2 - \varphi_2^2)$.

Notice that we have a 3-dimensional problem in this first order formulation, but our ODE in the original formulation was 2-dimensional.

We want to go back to using the leapfrog discretisation for the nonlinear wave equation in multi-Hamiltonian form, as this was the discretisation we applied to the nonlinear wave equation in its original form in the previous two Chapters. The following formulation for leapfrog method applied to the nonlinear wave equation in its multi-Hamiltonian form can be checked by applying the discretisation then eliminating the variables. The result is the leapfrog method applied to the nonlinear wave equation in its original form.

Note, that this is also equivalent to applying the Euler Box scheme then eliminating the variables.

The multi-Hamiltonian discretisation (6.40) for the leapfrog discretisation of the nonlinear wave equation becomes,

$$(\mathbf{K}D_t + \mathbf{L}D_x)z_i^n = \nabla S(z_i^n) \quad (6.42)$$

where for the leapfrog method,

$$D_t z_i^n = \frac{z_i^{n+\frac{1}{2}} - z_i^{n-\frac{1}{2}}}{\Delta t}, \quad D_x z_i^n = \frac{z_{i+\frac{1}{2}}^n - z_{i-\frac{1}{2}}^n}{\Delta x}. \quad (6.43)$$

We can do a quick check that this discretisation is correct by finding $D_t(D_t z_i^n)$ and $D_x(D_x z_i^n)$ and get

$$D_t(D_t z_i^n) = \frac{z_i^{n+1} - z_i^n - z_i^n + z_i^{n-1}}{(\Delta t)^2} = \frac{z_i^{n+1} - 2z_i^n + z_i^{n-1}}{(\Delta t)^2},$$

which is the second order discretisation for the leapfrog method that we used in Section 4.1.

In matrix form (6.42) becomes

$$\begin{bmatrix} 0 & D_t & -D_x \\ -D_t & 0 & 0 \\ D_x & 0 & 0 \end{bmatrix} z_i^n = \nabla S(z_i^n).$$

Substituting travelling wave coordinates into the discretisations (6.43) we get the difference equations,

$$D_\xi^\kappa \varphi(\xi) = -\frac{c(\varphi(\xi + \frac{1}{2}\kappa) - \varphi(\xi - \frac{1}{2}\kappa))}{\kappa}, \quad D_\xi^\sigma \varphi(\xi) = \frac{\varphi(\xi + \frac{1}{2}\sigma) - \varphi(\xi - \frac{1}{2}\sigma)}{\sigma}, \quad (6.44)$$

so that upon substituting travelling wave coordinates in the discretisation (6.42) we get the system of difference equations,

$$(\mathbf{K}D_\xi^\kappa + \mathbf{L}D_\xi^\sigma)\varphi(\xi) = \nabla S(\varphi(\xi)), \quad (6.45)$$

or in matrix form,

$$\begin{bmatrix} 0 & D_\xi^\kappa & -D_\xi^\sigma \\ -D_\xi^\kappa & 0 & 0 \\ D_\xi^\sigma & 0 & 0 \end{bmatrix} \varphi(\xi) = \nabla S(\varphi).$$

It would be nice if the system of difference equations (6.45) was a direct analogue of the continuous system of equations (6.39). We notice that the difference $D_\xi^\kappa \varphi(\xi)$ in (6.44) has a $-c$ term that does not occur in $D_\xi^\sigma \varphi(\xi)$. We generalise these differences so that for any parameter γ we have

$$D_\xi^\gamma \varphi(\xi) = \frac{\varphi(\xi + \frac{1}{2}\gamma) - \varphi(\xi - \frac{1}{2}\gamma)}{\gamma}, \quad (6.46)$$

so that (6.45) becomes

$$(\mathbf{L}D_\xi^\sigma - c\mathbf{K}D_\xi^\kappa)\varphi(\xi) = \nabla S(\varphi(\xi)),$$

and in matrix form,

$$\begin{bmatrix} 0 & -cD_\xi^\kappa & -D_\xi^\sigma \\ cD_\xi^\kappa & 0 & 0 \\ D_\xi^\sigma & 0 & 0 \end{bmatrix} \varphi(\xi) = \nabla S(\varphi(\xi)), \quad (6.47)$$

where $D_\xi^\kappa \varphi(\xi)$ and $D_\xi^\sigma \varphi(\xi)$ are defined by (6.46).

When we did backward error analysis for the nonlinear wave equation in the usual form given, we expanded the left and right sides of the discrete

travelling wave equation in a Taylor series and put these expansions in terms of exponential functions. Then we moved everything except the variable φ to the right hand side. In our first order formulation we encounter a problem doing this because the matrix $(\mathbf{L}D_\xi^\sigma - c\mathbf{K}D_\xi^\kappa)$ is singular and hence cannot be moved to the right hand side after expansion.

Notice also that the matrix $(\mathbf{L} - c\mathbf{K})$ for the continuous case is also singular and so for any multi-Hamiltonian PDE in which $(\mathbf{L} - c\mathbf{K})$ is singular the discrete version of the matrix will also be singular and therefore a slightly different method of applying backward error analysis will need to be used. This method is shown below for the nonlinear wave equation. On the other hand if $(\mathbf{L} - c\mathbf{K})$ is nonsingular then we saw from the previous example of the nonlinear Schrödinger equation how backward error analysis can be applied directly to a multi-Hamiltonian PDE and that the proof that there exists a modified equation follows from the proofs we gave of Theorem 6.4.1.

In the case where $(\mathbf{L} - c\mathbf{K})$ is not invertible a change of coordinates is most likely needed. Before making a change of coordinates check the the matrix $(\mathbf{L} - c\mathbf{K})$ does not contain a row of zeros. If there is a row of zeros then a variable can be eliminated. Eliminate a variable for each row of zeros that exist. This should reduce the dimension of the problem back to the same dimension as the ODE in the original formulation and if the reduced matrix is now invertible then backward error analysis can be applied directly as in the nonlinear Schrödinger example.

If the reduced matrix is not invertible or the original matrix is not invertible then $(\mathbf{L} - c\mathbf{K})$ will have to be put in Darboux normal form. The columns of the change of coordinates matrix are formed from the eigenvectors of the matrix $(\mathbf{L} - c\mathbf{K})$. This will produce a row of zeros which will allow the dimension to be reduced by 1 leaving the remaining matrix invertible. Backward error analysis can be then carried out on this coordinate system then changed back to the original coordinates at the end. We go through this procedure in detail for the nonlinear wave equation as a multi-Hamiltonian PDE (6.39).

Firstly, we go through the continuous case where $(\mathbf{L} - c\mathbf{K})$ is given in (6.41).

We form the matrix \mathbf{A} by letting the eigenvectors of $(\mathbf{L} - c\mathbf{K})$ be the columns of \mathbf{A} ,

$$\mathbf{A} = \begin{bmatrix} 0 & (c^2 + 1)^{\frac{1}{2}} & 0 \\ -c & 0 & 1 \\ -1 & 0 & -c \end{bmatrix}. \quad (6.48)$$

Now, let $\varphi(\xi) = \mathbf{A}\hat{\varphi}(\xi)$ where \mathbf{A} is given by (6.48) and substitute this into (6.39) to get,

$$\begin{aligned} (\mathbf{L} - c\mathbf{K})\mathbf{A}\hat{\varphi}(\xi) &= \nabla S(\mathbf{A}\hat{\varphi}(\xi)) \\ \Rightarrow \mathbf{A}^T(\mathbf{L} - c\mathbf{K})\mathbf{A}\hat{\varphi}(\xi) &= \mathbf{A}^T \nabla S(\mathbf{A}\hat{\varphi}(\xi)) \\ &= \nabla T(\hat{\varphi}(\xi)) \end{aligned} \quad (6.49)$$

where,

$$\mathbf{A}^T(\mathbf{L} - c\mathbf{K})\mathbf{A} = (c^2 + 1)^{\frac{3}{2}} \begin{bmatrix} 0 & -1 & 0 \\ 1 & 0 & 0 \\ 0 & 0 & 0 \end{bmatrix}.$$

Or, by writing out the matrices on both sides of (6.49) in full we get,

$$(c^2 + 1)^{\frac{3}{2}} \begin{bmatrix} 0 & -1 & 0 \\ 1 & 0 & 0 \\ 0 & 0 & 0 \end{bmatrix} \hat{\varphi} = \begin{bmatrix} 2c\hat{\varphi}_3 - (c^2 - 1)\hat{\varphi}_1 \\ -(c^2 + 1)^{\frac{1}{2}}V'((c^2 + 1)^{\frac{1}{2}}\hat{\varphi}_2) \\ 2c\hat{\varphi}_1 + (c^2 - 1)\hat{\varphi}_3 \end{bmatrix}.$$

The variable $\hat{\varphi}_3(\xi)$ can now be eliminated to get the 2-dimensional system,

$$\begin{bmatrix} \hat{\varphi}_1 \\ \hat{\varphi}_2 \end{bmatrix} = \begin{bmatrix} -(c^2 + 1)^{-1}V'((c^2 + 1)^{\frac{1}{2}}\hat{\varphi}_2) \\ (c^2 + 1)^{\frac{1}{2}}(c^2 - 1)^{-1}\hat{\varphi}_1 \end{bmatrix}.$$

This system can be transformed back to the original coordinates by taking $\varphi(\xi) = \mathbf{A}^{-1}\hat{\varphi}(\xi)$ then solving for φ_3 we get, $\varphi_3 = -\frac{1}{c}\varphi_2$. So the first order Hamiltonian system in original coordinates becomes

$$\begin{bmatrix} \dot{\varphi}_1(\xi) \\ \dot{\varphi}_2(\xi) \end{bmatrix} = \begin{bmatrix} -\frac{1}{c}\varphi_2(\xi) \\ c(c^2 - 1)^{-1}V'(\varphi_1(\xi)) \end{bmatrix}. \quad (6.50)$$

If we let

$$\mathbf{f}(\hat{\varphi}) = \begin{bmatrix} -(c^2 + 1)^{-1} V' \left((c^2 + 1)^{\frac{1}{2}} \hat{\varphi}_2 \right) \\ (c^2 + 1)^{\frac{1}{2}} (c^2 - 1)^{-1} \hat{\varphi}_1 \end{bmatrix},$$

then we look for a modified equation of the form,

$$\hat{\varphi} = \mathbf{f}(\hat{\varphi}) + h^2 \mathbf{f}_3(\hat{\varphi}) + h^4 \mathbf{f}_5(\hat{\varphi}) + \dots$$

where $\mathbf{f}_3(\hat{\varphi})$, $\mathbf{f}_5(\hat{\varphi})$, \dots are 2-dimensional vector functions to be determined.

For the discrete case, we have the matrix $(\mathbf{L}D_\xi^\sigma - c\mathbf{K}D_\xi^\kappa)$ given in (6.47) and let $\varphi(\xi) = \mathbf{A}\hat{\varphi}(\xi)$ where,

$$\mathbf{A} = \begin{bmatrix} 0 & (c^2(D_\xi^\kappa)^2 + (D_\xi^\sigma)^2) & 0 \\ -cD_\xi^\kappa & 0 & D_\xi^\sigma \\ -D_\xi^\sigma & 0 & -cD_\xi^\kappa \end{bmatrix}.$$

Then,

$$\mathbf{A}^T(\mathbf{L}D_\xi^\sigma - c\mathbf{K}D_\xi^\kappa)\mathbf{A}\hat{\varphi}(\xi) = \mathbf{A}^T \nabla S(\mathbf{A}\hat{\varphi}(\xi))$$

becomes

$$(c^2(D_\xi^\kappa)^2 + (D_\xi^\sigma)^2)^{\frac{3}{2}} \begin{bmatrix} 0 & -1 & 0 \\ 1 & 0 & 0 \\ 0 & 0 & 0 \end{bmatrix} \begin{bmatrix} \hat{\varphi}_1 \\ \hat{\varphi}_2 \\ \hat{\varphi}_3 \end{bmatrix} = \begin{bmatrix} \hat{\varphi}_1((D_\xi^\sigma)^2 - c^2(D_\xi^\kappa)^2) + 2c\hat{\varphi}_3 D_\xi^\kappa D_\xi^\sigma \\ -(c^2(D_\xi^\kappa)^2 + (D_\xi^\sigma)^2)^{\frac{1}{2}} V'((c^2(D_\xi^\kappa)^2 + (D_\xi^\sigma)^2)^{\frac{1}{2}} \hat{\varphi}_2) \\ 2cD_\xi^\kappa D_\xi^\sigma \hat{\varphi}_1 + \hat{\varphi}_3(c^2(D_\xi^\kappa)^2 - (D_\xi^\sigma)^2) \end{bmatrix}.$$

Eliminating $\hat{\varphi}_3$, rearranging and applying the time derivative D to both sides we get the 2-dimensional discrete system

$$\begin{bmatrix} \hat{\varphi}_1 \\ \hat{\varphi}_2 \end{bmatrix} = D \begin{bmatrix} -(c^2(D_\xi^\kappa)^2 + (D_\xi^\sigma)^2)^{-1} V'((c^2(D_\xi^\kappa)^2 + (D_\xi^\sigma)^2)^{\frac{1}{2}} \hat{\varphi}_2) \\ (c^2(D_\xi^\kappa)^2 + (D_\xi^\sigma)^2)^{\frac{1}{2}} (c^2(D_\xi^\kappa)^2 - (D_\xi^\sigma)^2)^{-1} \hat{\varphi}_1 \end{bmatrix}.$$

The Taylor series of the right hand side can now be taken to begin the backward error analysis and find the modified equations as described earlier.

The Hamiltonian can now be found and the phase portrait plotted. This is given in Figure 6.15, where we see that the travelling wave solutions are

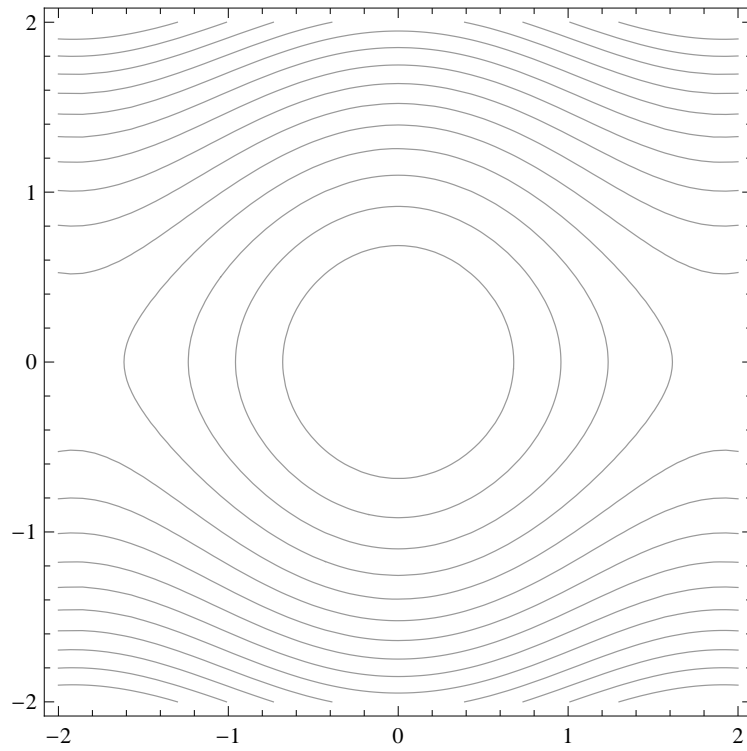


Figure 6.15: Modified Hamiltonian of the 1st order nonlinear wave system with change of coordinates.

preserved. The Hamiltonian could also be changed back to the original coordinates with the same result.

After using this method of putting the matrix $(\mathbf{L}D_\xi^\sigma - c\mathbf{K}D_\xi^\kappa)$ into Darboux normal form it was found that there was a simpler way to apply backward error analysis to the multi-Hamiltonian PDE for the nonlinear wave equation. First we look at the continuous system (6.39) and write the system out in full,

$$\begin{aligned} -c\dot{\varphi}_2 - \dot{\varphi}_3 &= -V'(\varphi_1) \\ c\dot{\varphi}_1 &= -\varphi_2 \\ \dot{\varphi}_1 &= \varphi_3. \end{aligned}$$

Notice, that the last two equations in the system both contain $\dot{\varphi}_1$, which allows us to eliminate φ_3 to get the 2-dimensional system,

$$\dot{\varphi} = \begin{bmatrix} -\frac{1}{c}\varphi_2 \\ c(c^2 - 1)^{-1}V'(\varphi_1) \end{bmatrix} = f(\varphi).$$

Notice, that this equation is the same as (6.50), which we got from putting the first order system in Darboux normal form then changing the coordinates back once the dimension of the system was reduced. Hence, this new reduction is much easier and faster to perform than the change of coordinates. It is the study of travelling waves that allows us to eliminate one of the variables and reduce the dimension to the same as the study for the nonlinear wave equation in its original form.

For the discrete case, we also write the discrete system (6.47) out in full to get

$$\begin{aligned} -cD_\xi^\kappa\varphi_2 - D_\xi^\sigma\varphi_3 &= -V'(\varphi_1) \\ cD_\xi^\kappa\varphi_1 &= -\varphi_2 \\ D_\xi^\sigma\varphi_1 &= \varphi_3. \end{aligned}$$

We can now eliminate φ_3 , rearrange the equation and apply the time derivative D to both sides to give the discrete system

$$\dot{\varphi} = D \begin{bmatrix} 0 & (cD_\xi^\kappa)^{-1} \\ -cD_\xi^\kappa(c^2(D_\xi^\kappa)^2 - (D_\xi^\sigma)^2)^{-1} & 0 \end{bmatrix} \begin{bmatrix} -V'(\varphi_1) \\ -\varphi_2 \end{bmatrix}.$$

The 2×2 matrix on the right hand side can now be expanded in a Taylor series, then the whole right hand side expanded in a Taylor series. The modified equation, and hence the modified Hamiltonian, can then be found and the phase portraits of the modified Hamiltonian plotted. This is plotted in Figure 6.16 for different values of σ and κ . Both solutions gives periodic travelling waves and heteroclinic travelling waves, the same as the original problem, but the solution on the right, for higher values of σ and κ , gives a more distorted view of the original solution.

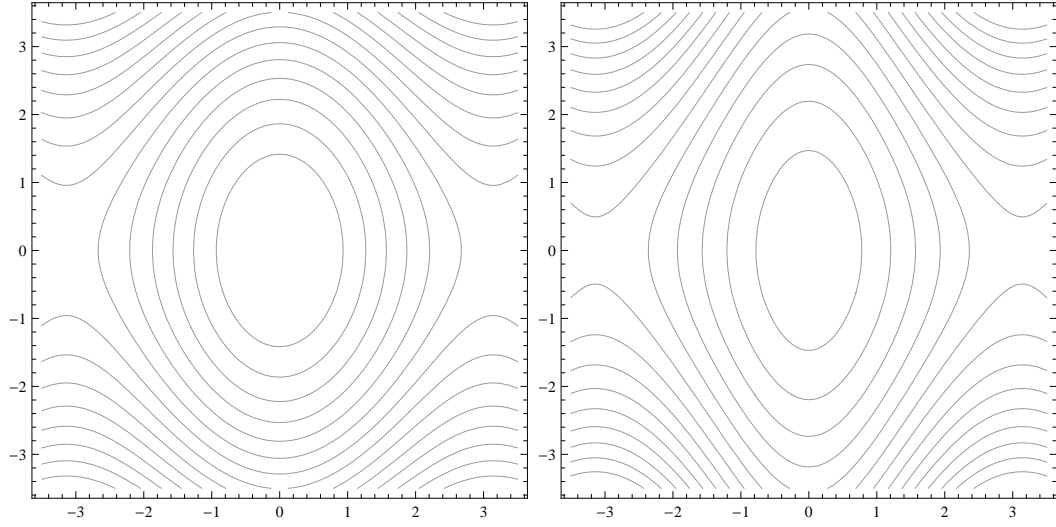


Figure 6.16: Modified Hamiltonians of the leapfrog method applied to the nonlinear wave equation as a 1st order system for small σ and κ on the left and large σ and κ on the right.

This backward error analysis was also done for the Preissman box scheme applied to the nonlinear wave equation in a multi-Hamiltonian form. The modified Hamiltonian for the Preissman box scheme is given in Figure 6.17 and shows similar results to that of the leapfrog method, the travelling waves are preserved.

It can be seen that the ideas and methods developed in this thesis also apply to higher-dimensional wave equations and the preservation of travelling waves by multisymplectic integrators.

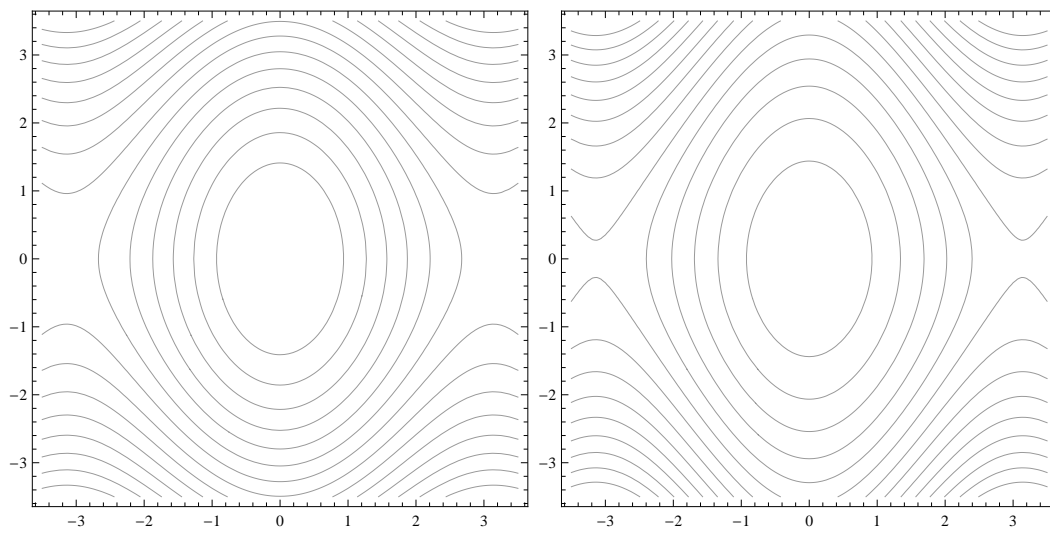


Figure 6.17: Modified Hamiltonians of the Preissman box scheme applied to the nonlinear wave equation as a 1st order system for small σ and κ on the left and large σ and κ on the right.

Chapter 7

Summary and Conclusions

The main question of this thesis was: Do multisymplectic integrators give better preservation of the dynamics than non-multisymplectic methods? We chose to look at this question through the preservation of travelling wave solutions. Most of the research previously done on the behaviour of multisymplectic integrators only considers the propagation of a solitary wave or the collision of two or three solitons. We attempt to look at the family of travelling wave solutions.

We choose the nonlinear wave equation as our test problem and show that for a particular nonlinearity it possesses two types of travelling waves, heteroclinic and periodic. All our nonlinearities, for the nonlinear wave equation, in this thesis possess these two types of travelling wave solutions. We choose the leapfrog method as our main multisymplectic integrator, which results in what we call the discrete travelling wave equation.

We show that the discrete travelling wave equation is only finite-dimensional for $\frac{\sigma}{\kappa}$ rational and for $\frac{\sigma}{\kappa}$ irrational it is infinite-dimensional. This makes the discrete travelling wave equation very difficult to solve. Boundary conditions are imposed on the discrete travelling wave equation corresponding to each type of orbit in the phase portrait.

We attempt to overcome the difficulty of solving the discrete travelling wave equation by using simplified nonlinearities. We begin with the McKean

nonlinearity which is piecewise constant with a discontinuity. The phase portrait shows that the solution has heteroclinic and periodic travelling waves. Solving the continuous travelling wave ODE of the nonlinear wave equation with McKean nonlinearity for heteroclinic waves we get an explicit solution in terms of an infinite integral. This infinite integral is evaluated using residue theory resulting in a heteroclinic travelling wave.

We give an example showing that even symmetric methods for symmetric PDEs need not preserve travelling wave solutions. Symmetric methods only preserve symmetric travelling waves.

Our goal is to study preservation of discrete travelling waves, so we discretise the nonlinear wave equation with McKean nonlinearity with the leapfrog method. The discrete travelling wave with this simplified nonlinearity gives an explicit solution in terms of an infinite integral, which can be solved using residue theory. We solve this for the 3 cases, $c = 0$, $\sigma = \kappa$ and $\sigma = 2\kappa$.

For $c = 0$ we get the denominator of the infinite integral gives the zero $s = 0$ and a complex conjugate pair lying on the imaginary axis. The periodic images of the roots on the imaginary axis are also zeros. The solution is the shape of a heteroclinic wave, which is smooth at the ends, but has a piecewise constant middle section.

For $\sigma = \kappa$ the discrete travelling wave equation is equivalent to applying the leapfrog method in time directly to the travelling wave ODE. We get the same results as those for $c = 0$, but also see that as c increases the solution becomes steeper.

For $\sigma = 2\kappa$ the solution is slightly more complicated. The denominator of the infinite integral gives the same zeros as those described for $c = 0$, but also has two additional zeros plus their periodic images. These are real roots. The result of solving the infinite integral is an explicit solution in terms of hypergeometric functions. The solution contains wiggles at each end of the solution as well as a piecewise constant middle section.

We summarise the results for the McKean nonlinearity:

- The wiggles at the tails of the solution are from the real poles

- The exponential part of the solution comes from the imaginary poles
- The solutions have the general shape of a solitary wave corresponding to a heteroclinic orbit, but contain wiggles
- The solutions are piecewise constant including the wiggles
- The wiggles are $O(\kappa^2)$, (or $O(\sigma^2)$ for $c = 0$)

These results are better than what a non-multisymplectic integrator would produce or even the results of a symmetric method applied to a symmetric PDE. Heteroclinic travelling waves are not symmetric, so are not preserved by symmetric methods.

Next, we move onto looking at the discrete periodic waves of the discrete travelling wave equation with McKean nonlinearity. To look for discrete periodic solutions we apply the discrete Fourier series, which gives an explicit formula in terms of Fourier series. To analyse this we need to take a finite truncation of this solution, which gives us only a numerical analysis.

We found that the discrete periodic solutions sometimes had large wiggles for both rational and irrational values of $\frac{\sigma}{\kappa}$ and conclude that no true periodic travelling wave solutions exist for the discrete travelling wave equation with McKean nonlinearity.

The McKean nonlinearity worked well in McKean's study of nerve conduction, but did not work so well for our problem. One reason for this may be due to the fact that McKean's model is dissipative, whereas our problem is non-dissipative. The discontinuity could also have been part of the problem, so next we look at a piecewise linear nonlinearity, the sawtooth function, that does not have a discontinuity.

The phase portrait with the sawtooth nonlinearity once again shows the continuous solution possesses heteroclinic and periodic travelling waves, but only periodic travelling wave solutions are looked at. The heteroclinic orbit can be approached by taking the period $T \rightarrow \infty$. The second order travelling wave ODE with sawtooth nonlinearity is solved analytically for periodic waves by splitting the nonlinearity into 5 parts and solving each part separately.

The discrete periodic solutions are found using a discrete Fourier series. These solutions seem to match those of the corresponding analytic solution. It would have been nice to have been able to measure the difference in the analytic and discrete solutions for the same parameters, but the method of finding the analytic solution made this difficult. We conclude that discrete periodic travelling waves exist for the sawtooth nonlinearity.

We finally move on to a smooth nonlinearity of the nonlinear wave equation. This nonlinearity gives the sine-Gordon equation in which the travelling wave ODE has a phase portrait indicating that heteroclinic and periodic travelling wave solutions exist. We only study the preservation of the periodic travelling waves.

We describe our pseudospectral Newton continuation method that we use to numerically solve the discrete travelling wave equation for the discretisation of the sine-Gordon equation. This method involves using a Fourier series for the linear part of the discrete travelling wave equation and the Newton method for the nonlinear part. We fix c so that the only parameters which need to be controlled are σ , κ and T . The period T is varied through the continuation part of our method.

Our pseudospectral Newton method produces two types of solution. One type of solution appears to be smooth, but the other type has wiggles in the solution. These wiggles are known as resonances and we give a method for measuring the size of them.

Newton's method converges quadratically for all solutions except at some large resonances. We were able to check our numerical simulation against the case $\sigma = \kappa$ as this gives the leapfrog method of the sine-Gordon equation. For both types of solutions our method for $\sigma = \kappa$ agrees with the leapfrog method.

After studying many combinations of the parameters, $\frac{\sigma}{\kappa}$ rational and irrational, we summarise the following main results:

- For $\frac{\sigma}{\kappa} \in \mathbb{Z}$ a resonance will occur if $\frac{T}{2\kappa} \in \mathbb{Z}$
- There seems to be some relationship between the resonances and the parameters for all $\frac{\sigma}{\kappa} \in \mathbb{Q}$, but we were unable to find this relationship

- As the period $T \rightarrow \infty$ travelling wave solutions exist for all values of $\frac{\sigma}{\kappa}$ and do not contain any resonances. We could not find any explanation for this behaviour
- κ has a greater influence on the size and position of the resonances than σ

In Chapter 6 we studied the preservation of travelling wave solutions through BEA of multistep methods. We achieve this by showing that the discrete travelling wave equation is equivalent to a symmetric multistep method when $\frac{\sigma}{\kappa}$ is rational. Normally, for multistep methods, the parasitic modified differential equation needs to be studied in addition to the principal modified equation. If the method gives parasitic solutions these will not show up in the study of the principal modified equation. Our problem is a boundary value problem, rather than an initial value problem in the normal case, in which we restrict solutions to (periodic) travelling waves. This damps out any parasitic solutions so we can fully analyse the discrete travelling wave equation through the principal modified equation by itself.

We found the 1st characteristic polynomial of the discrete travelling wave equation and made a conjecture on the number of pairs of roots of the polynomial which lie on the unit circle, (and those which lie inside and outside the unit circle). This conjecture and the paper by Quinlan [77] lead us back to predicting when the resonances would occur, but we ended up dropping this idea in favour of the more successful backward error analysis.

Since we can think of the discrete travelling wave equation as a symmetric multistep method when $\frac{\sigma}{\kappa}$ is rational we can use the proofs that modified equations and modified Hamiltonians exist for multistep methods to find the modified equation and modified Hamiltonian of the discrete travelling wave equation. We prove that these modified equations exist, not only for $\frac{\sigma}{\kappa}$ rational, but also for $\frac{\sigma}{\kappa}$ irrational. The resulting modified equations are 2-dimensional and always produce a smooth solution. We give a numerical validation of BEA which includes comparing our solutions of the modified equation to the

numerical solutions we obtained in Chapter 5. This was done for 3 truncations of the solution of the modified equation for a fixed set of parameters. The difference between the numerical solution from Chapter 5 and the solution of each truncation of the modified differential equation was then plotted. As expected, the modified equation gets closer to the numerical solution at each increasing truncation index.

We use our own method to prove that a modified Hamiltonian of the discrete travelling wave equation exists and conclude the discrete travelling wave equation (for the multisymplectic leapfrog method applied to the sine-Gordon equation) preserves travelling wave solutions.

It is now that we see how powerful BEA analysis is for our problem. In the ordinary sense of BEA an $(n+1)$ -dimensional map is reduced to n dimensions. This reduction of dimension by one allows conclusions such as the existence of one modified integral, the energy. But for us, BEA reduces an infinite-dimensional map to a 2-dimensional ODE, a far more spectacular reduction. This is even more striking in view of the fact that there is no accepted BEA for fully discrete PDEs in general. That is, BEA reduces the difficult intractable functional equation, we call the discrete travelling wave equation, to a simple planar Hamiltonian ODE.

By comparing the orbits of the phase portraits of the original system and the modified system we got that any orbits that are structurally stable are preserved. This includes heteroclinic and periodic waves for the sine-Gordon equation, but the result is not specific to the sine-Gordon equation, or its integrability, and holds for any potential of the nonlinear wave equation.

We expect that typical travelling waves, whose existence is due to preserved features of the travelling wave equation, like dimension and linear symmetries, will be preserved by multisymplectic integrators.

In this thesis, we do not give rigorous proofs of the existence of travelling waves of multisymplectic integrators but regard BEA as suggesting a mechanism by which travelling waves can be preserved.

To make more general conclusions on the preservation of travelling waves

for multisymplectic integrations of multi-Hamiltonian PDEs, we applied BEA analysis directly to these discrete systems. We used the Preissman box scheme applied to the 1st order nonlinear Schrödinger equation and the leapfrog method applied to the 1st order nonlinear wave equation to make the following conclusions:

- If $(\mathbf{L} - c\mathbf{K})$ is invertible, BEA analysis can be directly applied to a multisymplectic integration of a multi-Hamiltonian PDE, to show that the modified differential equation exists.
- If $(\mathbf{L} - c\mathbf{K})$ is not invertible, then a change of coordinates or an elimination of variables is needed before BEA can be applied to show that the modified differential equation exists.

The ideas and methods developed in this thesis also apply to higher-dimensional wave equations and the preservation of travelling waves by multisymplectic integrators.

Bibliography

- [1] D. Arapura, *Introduction to Differential Forms*, unpublished lecture notes, 2010.
- [2] U.M. Ascher, R.I. McLachlan, *Multisymplectic Box Schemes and the Korteweg-de Vries Equation*, Appl. Numer. Math., **48** (2004), 255–269.
- [3] U.M. Ascher, R.I. McLachlan, *On Symplectic and Multisymplectic Schemes for the KdV Equation*, Journal of Scientific Computing **25**, 83–103, 2005.
- [4] E. Barth, B. Leimkuhler, *Symplectic Methods for Conservative Multibody Systems*, In Integration Algorithms and Classical Mechanics (Toronto, ON, 1993), American Mathematical Society, Providence, RI, pp. 25–43.
- [5] O.M. Braun, Y.S. Kivshar, *The Frenkel–Kontorova Model*, Springer-Verlag, Berlin Heidelberg, 2010.
- [6] T.J. Bridges, G. Derks, *Unstable eigenvalues and the linearization about solitary waves and fronts with symmetry*, Proc. R. Soc. Lond. A, **455** (1999), 2427–2469.
- [7] T.J. Bridges, S. Reich, *Multi-Symplectic Integrators: Numerical Schemes for Hamiltonian PDEs that Conserve Symplecticity*, J. Phys. A: Math. Gen., **284**, (2001) 184–193 .
- [8] T.J. Bridges, G. Derks, *Linear Instability of Solitary Wave Solutions of the Kawahara Equation and its Generalizations*, SIAM J. Math. Anal., **33** (2002), 1356–1378.
- [9] T.J. Bridges, S. Reich, *Numerical Methods for Hamiltonian PDEs*, J. Phys. A **39**, (2006) 5287–5320.

- [10] C.J. Budd, A. Iserles, *Geometric Integration: Numerical Solution of Differential Equations on Manifolds*, Phil. Trans. Roy. Soc. A **357** (1999), 945–956.
- [11] J.C. Butcher, *The Numerical Analysis of Ordinary Differential Equations*, John Wiley & Sons, 1987.
- [12] J.C. Butcher, *Numerical Methods for Ordinary Differential Equations*, John Wiley & Sons, 2008.
- [13] J.W. Cahn, J. Mallet-Paret, and E.S. Van Vleck, *Traveling Wave Solutions for Systems of ODEs on a Two-Dimensional Spatial Lattice*, SIAM J. Appl. Math. **59** (1999), 455–493.
- [14] J. Cai, *A New Explicit Multisymplectic Scheme for the Regularized Long-Wave Equation*, Journal of Mathematical Physics, **50** (2009), 013535.
- [15] J. Cai, Y. Wang, Z. Qiao, *Multisymplectic Preissman Scheme for the Time-Domain Maxwell's Equations*, Journal of Mathematical Physics, **50** (2009), 033510.
- [16] P. Chartier, E. Faou, A. Murua, *An algebraic approach to invariant preserving integrators: the case of quadratic and Hamiltonian invariants*, Numer. Math. **103**(4) (2006), 575–590.
- [17] J. Chen, M. Qin, Y. Tang, *Symplectic and Multi-Symplectic Methods for the Nonlinear Schrödinger Equation*, Computers and Mathematics with Applications, **43**, (2002) 1095–1106.
- [18] S. Chow, J. Mallet-Paret, *Pattern Formation and Spatial Chaos in Lattice Dynamical Systems—Part I*, IEEE Transaction on Circuits and Systems I: Fundamental Theory and Applications **42** (1995), 746–751.
- [19] S. Chow, W. Shen, *Dynamics in a Discrete Nagumo Equation: Spatial Topological Chaos*, SIAM Journal on Applied Mathematics, **55** (1995), 1764–1781.
- [20] P. Console, E. Hairer, *Long-Term Stability of Symmetric Partitioned Linear Multistep Methods*, In: Current challenges in stability issues for numerical differential equations. C.I.M.E. Summer School, Lecture Notes, pp. 1–36, 2011.

- [21] M. Dahlby, B. Owren, *A general framework for deriving integral preserving numerical methods for PDEs*, SIAM J. Sci. Comput. **33**(5) (2011), 2318–2340.
- [22] G. Dahlquist, *Convergence and Stability in the Numerical Integration of Ordinary Differential Equations*, Math. Scand. **4** (1956), 33–53.
- [23] A. Dullweber, B. Leimkuhler, R.I. McLachlan, *Split-Hamiltonian Methods for Rigid Body Molecular Dynamics*, J. Chem. Phys.. **107**(5), (1997) 5840–5851.
- [24] T. Eirola, *Aspects of backward error analysis of numerical ODE's*, J. Comp. Appl. Math. **45** (1993), 65–73.
- [25] C. Elmer, E. Van Vleck, *Computation of traveling waves for spatially discrete bistable reaction-diffusion equations*, Applied Numerical Mathematics **20** (1996), 157–169.
- [26] C.E. Elmer, E.S. Van Vleck, *Traveling Wave Solutions for Bistable Differential–Difference Equations with Periodic Diffusion*, SIAM J. Appl. Math., **61**(5) (2001), 1648–1679.
- [27] M. Fečkan, V.M. Rothos, *Travelling waves in Hamiltonian systems on 2D lattices with nearest neighbour interactions*, Nonlinearity **20** (2007), 319–341.
- [28] K. Feng, *Formal power series and numerical algorithms for dynamical systems*, in Proceedings of international conference on scientific computation, Series on Appl. Math. 1, 1991, 28–35.
- [29] J. Frank, B.E. Moore, S. Reich, *Linear PDEs and Numerical Methods that Preserve a Multi-Symplectic Conservation Law* SIAM J. Sci. Comput., **28**(1), (2006), 260–277.
- [30] J. de Frutos, J.M. Sanz-Serna, *Accuracy and Conservation Properties in Numerical Integration: The Case of the Korteweg–de Vries Equations*, Numerische Mathematik **75** (1997), 421–445.
- [31] O. Gonzalez, *Time Integration and Discrete Hamiltonian Systems*, Journal of Nonlinear Science **6** (1996), 449–467.

- [32] M.J. Gotay, J. Isenberg, R. Montgomery, J.E. Marsden, J. Śniatycki, P.B. Yasskin, *Momentum Maps and Classical Relativistic Fields. Part I: Covariant Field Theory*, Arxiv preprint physics/9801019v2, 2004.
- [33] D.F. Griffiths, J.M. Sanz-Serna, *On the scope of the method of modified equations*, SIAM J. Sci. Stat. Comput. **7** (1986), 994–1008.
- [34] E. Hairer, *Backward Error Analysis for Multistep Methods*, Numer. Math. **84** (1999), 199–232.
- [35] E. Hairer, *Conjugate-Symplecticity of Linear Multistep methods*, Journal of Computational Mathematics **26** (2008), 657–659.
- [36] E. Hairer, S.P. Nørsett, G. Wanner, *Solving Ordinary Differential Equations I. Nonstiff Problems, 2nd Edition*, Springer Series in Computational Mathematics **8**, Springer Berlin, 1993.
- [37] E. Hairer, C. Lubich, G. Wanner, *Geometric Numerical Integration: Structure-Preserving Algorithms for Ordinary Differential Equations*, Springer Series in Computational Mathematics **31**, Springer Berlin, 2002.
- [38] E. Hairer, C. Lubich, G. Wanner, *Geometric Numerical Integration Illustrated by the Störmer–Verlet Method*, Acta Numerica, **12** (2003), 399–450.
- [39] E. Hairer, C. Lubich, *Symmetric Multistep Methods Over Long Times*, Numer. Math. **97** (2004), 699–723.
- [40] A.C. Hansen, *A Theoretical Framework for Backward Error Analysis on Manifolds*, J. Geom. Mech., **3** (2011), 81–111.
- [41] A.L. Hodgkin, A.F. Huxley, *A Quantitative Description of Membrane Current and its Application to Conduction and Excitation in Nerve*, J. Physiol., **117** (1952), 500–544.
- [42] J.P. Holloway, *On Numerical Methods for Hamiltonian PDEs and a Collocation Method for the Vlasov-Maxwell Equations*, J. Comput. Phys. **129**(1) (1996), 121–133.
- [43] J.L. Hong, Y. Liu, G. Sun, *The Multi-Symplecticity of Partitioned Runge–Kutta Methods for Hamiltonian PDEs*, Math. Comp. **75** (2005), 167–181.

- [44] G. Iooss, *Travelling waves in the Fermi–Pasta–Ulam lattice*, Nonlinearity, **13** (2000), 849–866.
- [45] G. Iooss, K. Kirchgässner, *Travelling Waves in a Chain of Coupled Nonlinear Oscillators*, Commun. Math. Phys. **211** (2000), 439–464.
- [46] A. Iserles, A. Zanna, *A Scalpel, Not a Sledgehammer: Qualitative Approach to Numerical Mathematics*, DAMTP 1996/NA07, University of Cambridge, 1996.
- [47] A.L. Islas, D.A. Karpeev, C.M. Schober, *Geometric Integrators for the Nonlinear Schrödinger Equation*, Journal of Computational Physics **173** (2001), 116–148 .
- [48] E.M. Izhikevich, R. FitzHugh, *FitzHugh–Nagumo model*, Scholarpedia 1, 2006, 1349.
- [49] G. James, Y. Sire, *Center Manifold Theory in the Context of Infinite One-Dimensional Lattices*, in *The Fermi–Pasta–Ulam Problem* pp. 207–238, Springer, 2008.
- [50] B. Jiang, Y. Wang, J. Cai, *A New Multisymplectic Scheme for Generalised Kadomtsev–Petviashvili Equation*, Journal of Mathematical Physics **47** (2006), 83503.
- [51] U. Kirchgraber, *Multi-Step Methods are Essentially One-Step Methods*, Numer. Math. **48** (1986), 85–90.
- [52] J.D. Lambert, I.A. Watson, *Symmetric Multistep Methods for Periodic Initial Value Problems*, J. Inst. Maths. Applies. **18** (1976), 189–202.
- [53] B. Leimkuhler, S. Reich, *Simulating Hamiltonian Dynamics*, Cambridge University Press, Cambridge, 2004.
- [54] J. Li, Z. Liu, *Smooth and non-smooth traveling waves in a nonlinearly dispersive equation*, Applied Mathematical Modelling **25** (2000), 41–56.
- [55] H. Liu, K. Zhang, *Multi-Symplectic Runge–Kutta-Type Methods for Hamiltonian Wave Equations*, IMA Journal of Numerical Analysis **26**(2) (2006), 252–271.

- [56] J. Mallet-Paret, *Spatial Patterns, Spatial Chaos, and Travelling Waves in Lattice Differential Equations*, Lefschetz Center for Dynamical Systems and Center for Control Sciences, Division of Applied Mathematics, Brown University, 1996.
- [57] J. Mallet-Paret, W. Shen, *Traveling Waves in Lattice Dynamical Systems*, Journal of Differential Equations, **149** (1998), 248–29.
- [58] D.W. Markiewicz, *Survey on Symplectic Integrators*, preprint, University of California at Berkeley, 1999.
- [59] J.E. Marsden, G.W. Patrick, S. Shkoller, *Multisymplectic Geometry, Variational Integrators, and Nonlinear PDEs*, Communications in Mathematical Physics **199**(2) (1998), 351–395.
- [60] J.E. Marsden, S. Shkoller, *Multisymplectic Geometry, Covariant Hamiltonians and Water Waves*, Math. Proc. Camb. Phil. Soc. **125** (1999), 553–575.
- [61] M.P. McKean, *Nagumo’s Equation*, Adv. Math. **4** (1970), 209–223.
- [62] R.I. McLachlan, *Symplectic Integration of Hamiltonian Wave Equations*, Numer. Math. **66** (1994), 465–492.
- [63] R.I. McLachlan, *Composition Methods in the Presence of Small Parameters*, BIT Numerical Mathematics **35**(2) (2003), 258–268.
- [64] R.I. McLachlan, G.R.W. Quispel, G.S. Turner, *Numerical Integrators that Preserve Symmetries and Reversing Symmetries*, SIAM Journal of Numerical Analysis **35** (1998), 586–599.
- [65] R.I. McLachlan, G.R.W. Quispel, N. Robidoux, *Geometric Integration Using Discrete Gradients*, Phil. Trans. Roy. Soc. A **357** (1999), 1021–1046.
- [66] R.I. McLachlan, R. Quispel, *Six Lectures on the Geometric Integration of ODEs*, in Foundations of Computational Mathematics pages 155–210, ed. R. DeVore, A. Iserles, E. Süli, Cambridge University Press, Cambridge, 2001.
- [67] R. I. McLachlan, M. Perlmutter, and G. R. W. Quispel, *On the nonlinear stability of symplectic integrators*, BIT **44** (2004), 99–117.

- [68] R.I. McLachlan, G. R. W. Quispel, *Geometric Integrators For ODEs*, J. Phys. A **39**(19) (2006), 5251–5286.
- [69] R.I. McLachlan, Y. Sun, P.S.P Tse, *Linear Stability of Partitioned Runge–Kutta Methods*, SIAM J. Numer. Anal. **49**(1) (2011), 232–263.
- [70] P.C. Meek, J. Norbury, *Nonlinear Moving Boundary Problems and a Keller Box Scheme*, SIAM Journal on Numerical Analysis **21**(5) (1984), 883–893 .
- [71] B.E. Moore, S. Reich, *Backward Error Analysis for Multi-Symplectic Integration Methods*, Numerische Mathematik **95**(4) (2003), 625–652.
- [72] B.E. Moore, S. Reich, *Multi-Symplectic Integration Methods for Hamiltonian PDEs*, Future Generation Computer Systems **19**(21) (2003), 395–402.
- [73] K.W. Morton, D.F. Mayers, *Numerical Solution of Partial Differential Equations, Second Edition*, Cambridge University Press, Cambridge, 2005.
- [74] A.A. Pankov, K. Pflüger, *Travelling waves in lattice dynamical systems*, Mathematical Methods in the Applied Sciences **23**(14) (2000), 1223–1235.
- [75] J.B. Perot, V. Subramanian, *A Discrete Calculus Analysis of the Keller Box Scheme and a Generalisation of the Method to Arbitrary Meshes*, Journal of Computational Physics, **226** (2007), 494–508.
- [76] A du Plessis and T Wall, *The Geometry of Topological Stability*, Clarendon, Oxford, 1995.
- [77] G.D. Quinlan, *Resonances and instabilities in Symmetric Multistep Methods*, Report, 1999, available on <http://arxiv.org/abs/astro-ph/9901136>.
- [78] G.D. Quinlan, S. Tremaine, *Symmetric Multistep Methods for the Numerical Integration of Planetary Orbits*, Astron. J. **100** (1990), 1694–1700.

- [79] G.R.W. Quispel, G.S. Turner, *Discrete Gradient Methods for Solving ODE's Numerically While Preserving a First Integral*, J. Phys. A **29**(13) (1996), L341–L349.
- [80] G.R.W. Quispel, C. Dyt, *Solving ODE's Numerically While Preserving Symmetries, Hamiltonian Structure, Phase Space Volume, or First Integrals*, Proc. 15th IMACS World Congress, vol. 2 pp. 601–607, 1997.
- [81] S. Reich, *Backward error analysis for numerical integrators*, SIAM J. Numer. Anal. **36** (1999), 475–491.
- [82] S. Reich, *Multi-Symplectic Runge–Kutta Collocation Methods for Hamiltonian Wave Equations*, J. Comput. Phys. **157** (2000), 473–499.
- [83] B.N. Ryland, *Multisymplectic Integration*, Ph.D. Thesis, Massey University, 2007.
- [84] B.N. Ryland, R.I. McLachlan, *On Multisymplecticity of Partitioned Runge–Kutta Methods*, SIAM J. Sci. Comput. **84**(6) (2007), 847–869.
- [85] J.M. Sanz-Serna, *Symplectic integrators for Hamiltonian problems: an overview*, Acta Numerica **1** (1992), 243–286.
- [86] J.M. Sanz-Serna, M.P. Calvo, *Numerical Hamiltonian Problems*, Chapman & Hall, 1994.
- [87] R.D. Skeel, G. Zhang, T. Schlick, *A Family of Symplectic Integrators: Stability, Accuracy, and Molecular Dynamics Applications*, SIAM J. Sci. Comput. **18**(1) (1997), 203–222.
- [88] D. Smets, M. Willem, *Solitary Waves with Prescribed Speed on Infinite Lattices*, Journal of Functional Analysis **149**, (1997), 266–275.
- [89] A. Stanoyevitch, *Introduction to Numerical Ordinary and Partial Differential Equations Using MATLAB*, John Wiley & Sons, 2005.
- [90] J. Sun, M. Qin, *Multi-symplectic methods for the coupled 1D Nonlinear Schrödinger System*, Computer Physics Communications **155** (2003), 221–235.
- [91] A. Tabatabaei, E. Shakour, M. Dehghan, *Some Implicit Methods for the Numerical Solution of Burgers' Equation*, Applied Mathematics and Computation **191** (2007), 560–570.

- [92] A.P. Veselov, *Integrable Discrete-Time Systems and Difference Operators*, Funct. Anal. Appl. **22** (1988), 83–93.
- [93] A.P. Veselov, *Integrable Lagrangian Correspondences and the Factorization of Matrix Polynomials*, Funct. Anal. Appl. **25** (1991), 112–122.
- [94] T. Wang, L. Zhang, F. Chen, *Numerical Analysis of a Multi-symplectic Scheme for a Strongly Coupled Schrödinger System*, Applied Mathematics and Computation **203** (2008), 413–431.
- [95] Y. Wang, M. Qin, *Multisymplectic Schemes for the Nonlinear Klein-Gordon Equation*, Mathematical and Computer Modeling **36** (2002), 963–977.
- [96] Y. Wang, M. Qin, *Multisymplectic structure and Multisymplectic Scheme for the Nonlinear Wave Equation*, Acta Mathematicae Applicatae Sinica **18**(1) (2002), 169–176.
- [97] J.H. Wilkinson, *Error Analysis of floating-point computation*, Numer. Math. **2** (1960), 319–340.
- [98] H. Yoshida, *Construction of Higher Order Symplectic Integrators*, Physics Letters A **150**(5) (1990), 262–268.
- [99] H. Yoshida, *Recent progress in the theory and application of symplectic integrators*, Celestial Mech. Dynam. Astronom. **56** (1993), 27–43.
- [100] P.F. Zhao, M.Z. Qin, *Approximations for KdV Equation as a Hamiltonian System*, Int. J. Comput. Math. Appl. **39** (2000), 1–11.
- [101] Y. Zhou, Q. Liu, W. Zhang, *Bifurcation of travelling wave solutions for the $(2 + 1)$ -dimensional Broer–Kau–Kupershmidt equation*, Applied Mathematics and Computation **204** (2008), 210–215.
- [102] D.G. Zill, M.R. Cullen, *Differential Equations with Boundary-Value Problems*, 2009, Cengage.